Universidade do Minho
Escola de Engenharia

Manuel Ernesto Suazo-Uribe

Assessment of Small-Diameter and Minimally Processed Round Logs of the Invasive Species *Acacia dealbata* Link for Structural Applications

March 2026

Assessment of Small-Diameter and Minimally Processed Round Logs of the Invasive Species *Acacia dealbata* Link for Structural Applications
Manuel Ernesto Suazo-Uribe
UMinho | 2026

Universidade do Minho
Escola de Engenharia

Manuel Ernesto Suazo-Uribe

Assessment of Small-Diameter and Minimally Processed Round Logs of the Invasive Species *Acacia dealbata* Link for Structural Applications

Thesis Doctoral
Doctoral Programme of Civil Engineering

Supervision
Professor Doctor Jorge M. Branco
Professor Doctor José L. Louzada

March 2026

Copyright and Terms of Use for Third Party Work

This dissertation reports on academic work that can be used by third parties as long as the internationally accepted standards and good practices are respected concerning copyright and related rights.

This work can thereafter be used under the terms established in the license below.

Readers needing authorization conditions not provided for in the indicated licensing should contact the author through the RepositóriUM of the University of Minho.

License granted to users of this work



Attribution-ShareAlike
CC BY-SA
https://creativecommons.org/licenses/by-sa/4.0/

Acknowledgments

Many. Fellow PhD students at the University of Minho: Alejandro, Juan 1 and 2, Zabhi, Aiuba, Arthur, Daniel... To the people of Portilame enterprise on Portugal for letting me work in their facilities, and especially to Marco Oliveira, who supported me during difficult times. To Tomás Azevedo and the ICNF rangers at the Peneda-Gerês National Park in northern Portugal, for their diligence and enormous kindness. To many anonymous, kind, and diligent Portuguese people who lent me a hand at times.

My colleagues at the University of Bío Bío in Chile Alexander Opazo, Linette Salvo, Claudio Montero, and Víctor Rosales shared their wisdom in difficult times. Also to those who were there with a listening ear and encouragement: Franco, Alan, Lore, and Ginnia and to my friends Horacio, the forester, and Pablo, a friend who always teaches.

Finally, I would like to thank my family: my dear mother, Maite; my sister, Marce; my brother, Gigio; and, of course, my children, Pedro and Elisa, and my wife Barbara, who have been with me through the good and bad times of this adventure.

Statement of Integrity

I hereby declare having conducted this academic work with integrity. I confirm that I have not used plagiarism or any form of undue use of information or falsification of results along the process leading to its elaboration.

I further declare that I have fully acknowledged the Code of Ethical Conduct of the University of Minho.

Resumo

Esta tese investiga a caracterização física e mecânica de toros de madeira roliça de pequeno diâmetro de *Acacia dealbata* Link, uma espécie invasora em Portugal, com o objetivo de avaliar o seu potencial para aplicações estruturais. O estudo aborda o duplo desafio de promover uma gestão florestal sustentável e valorizar os subprodutos resultantes do controlo de espécies invasoras, em conformidade com os princípios da economia circular.

As campanhas experimentais foram realizadas com toros provenientes do Parque Nacional da Peneda-Gerês, no norte de Portugal, totalizando 45 exemplares com diâmetros entre 90 e 143 mm, recolhidos em duas épocas de abate: primavera (17 toros, 2,0 m) e inverno (28 toros, 2,4 m). A caracterização mecânica foi efetuada através de ensaios destrutivos e não destrutivos, incluindo métodos de propagação de ondas de tensão longitudinais, vibração transversal e resistência à perfuração. Para validar os resultados, foram também realizados ensaios destrutivos em provetes pequenos e isentos de defeitos.

Observaram-se diferenças consistentes entre os toros colhidos na primavera e os colhidos no inverno, sugerindo uma relação entre a época de abate e as propriedades físico-mecânicas da espécie. Verificaram-se correlações significativas entre os módulos de elasticidade dinâmicos e estáticos, confirmando a capacidade preditiva dos métodos não destrutivos para a classificação mecânica da madeira roliça. As análises complementares dos parâmetros de classificação visual revelaram uma influência limitada no desempenho mecânico, embora se mantenham úteis na pré-seleção em campo.

Adicionalmente, foram avaliadas técnicas específicas de pré-tratamento — como o entalhe longitudinal e o perfuramento central — com vista a mitigar o fendilhamento induzido pela secagem, tendo-se obtido resultados positivos na redução das fendas nas extremidades dos toros. No geral, a *Acacia dealbata* apresentou valores de densidade e rigidez de moderados a elevados, comparáveis aos de outras folhosas utilizadas na construção, confirmando a sua viabilidade técnica para aplicações estruturais de baixa exigência.

Estes resultados evidenciam o potencial de integrar o controlo de espécies invasoras com o uso sustentável de materiais, contribuindo assim para o desenvolvimento de estratégias construtivas ecoeficientes e práticas de gestão florestal baseadas na economia circular.

Palavras-chave *Acacia dealbata*, controlo de fissuras na madeira, efeitos sazonais, madeira pequena redonda.

Abstract

This thesis investigates the physical and mechanical characterization of small-diameter roundwood logs of *Acacia dealbata* Link, an invasive species in Portugal, to evaluate their potential for structural applications. The study addresses the dual challenge of promoting sustainable forest management and valorizing by-products derived from invasive-species control, in alignment with circular-economy principles.

Experimental campaigns were carried out on logs harvested from the Peneda–Gerês National Park, northern Portugal, comprising a total of 45 logs (90–143 mm in diameter) collected across two harvesting seasons: spring (17 logs, 2.0 m) and autumn (28 logs, 2.4 m). Mechanical characterization was performed through both destructive and non-destructive testing, including longitudinal stress-wave propagation, transverse vibration, and drilling-resistance techniques. To validate the results, additional destructive tests were conducted on small, defect-free specimens.

Consistent differences were observed between logs harvested in spring and those harvested in autumn, suggesting a relationship between harvest season and the physical-mechanical properties of the species. Significant correlations were found between dynamic and static moduli of elasticity, confirming the predictive capacity of non-destructive methods for mechanical grading of roundwood. Complementary analyses of visual-grading parameters revealed a limited influence on mechanical performance compared with dynamic indicators, although visual assessment remains useful for preliminary field preselection.

In addition, specific pre-treatment techniques—such as longitudinal kerfing and central hollowing—were evaluated to mitigate drying-induced cracking, yielding positive results in reducing end-log splits. Overall, *Acacia dealbata* exhibited moderate to high density and stiffness values comparable to those of other hardwoods used in construction, confirming its technical feasibility for low-demand structural applications.

These findings highlight the potential to integrate invasive-species control with sustainable material utilization, thereby contributing to eco-efficient construction strategies and circular forest-management practices.

Keywords *Acacia dealbata*, seasonal effects, small round wood, timber cracking control.

...es como descifrar signos sin ser sabio competente,
volver a ser de repente tan frágil como un segundo,
volver a sentir profundo como un niño frente a Dios...

($Violeta\ Parra$, chilean singer-songwriter)

Contents

1 Introduction 1

1.1 Small Diameter Round Wood (*srw*) . . . 2
1.2 Uses and Limitations . . . 4
1.3 Use of *Acacia dealbata* Logs from the Portuguese Forest . . . 6
1.4 Objectives . . . 7
1.5 Motivation . . . 8
1.6 Document Structure . . . 8

2 Utilization of By-Products from Portugal Forests: small-diameter roundwood (*srw*) of Invasive Species *Acacia dealbata*. 10

2.1 The Importance of Forests . . . 10
2.2 By-Products from the Forest Management . . . 12
2.2.1 General By-Products from the Forest . . . 13
2.2.2 Uses of Low-Processed Small-Diameter Roundwood . . . 14
2.3 The Challenge of Invasive Species Control . . . 17
2.4 The Case of Invasive Species *Acacia dealbata* in Portugal . . . 18
2.4.1 Portugal's Forests . . . 19
2.4.2 Species *Acacia dealbata* in Portugal . . . 20
2.5 Chapter conclusions . . . 26

3 Mechanical Characterisation of small-diameter roundwood (*srw*) of *Acacia dealbata* Link 27

3.1 Mechanical Performance of *srw* Logs with Minimal Processing . . . 27
3.2 Factors Affecting the Mechanical Performance of Logs . . . 29
3.2.1 Juvenile Wood . . . 29
3.2.2 Density . . . 32
3.2.3 Moisture Content . . . 33
3.2.4 Temperature . . . 34
3.2.5 Cracking Formation . . . 35
3.3 Mechanical Characterisation of Wood Logs . . . 37
3.3.1 Full-Size Destructive Testing . . . 37
3.3.2 Free-Defect Small Specimen Testing . . . 38
3.3.3 *Acacia dealbata* Reference Characterization . . . 39
3.4 Experimental Campaign to Determine the Mechanical Properties of *Acacia dealbata* Logs from Peneda–Gerês National Park, Northern Portugal. . . . 39
3.4.1 Collection of Logs . . . 40
3.4.2 Determination of Moisture Content (MC) and Density (ρ) . . . 45
3.4.3 Destructive Testing on Full-size Logs . . . 50
3.4.4 Analysis of Results on Full-size Logs . . . 60

3.4.5 Destructive Testing on Free-defect Small Samples . . . 70
3.4.6 Analysis of Results on Free-defect Small Samples . . . 73
3.4.7 Comparison Between Full-Size Logs and Defect-Free Small Specimens . . . 77
3.5 Chapter conclusions . . . 82

4 Prediction of the Physical and Mechanical Properties of *Acacia dealbata* Logs Using Non-Destructive Techniques 83
4.1 Non-Destructive Techniques . . . 83
4.2 Visual Grading . . . 83
4.3 Influence of Visual Characteristics on Mechanical Performance . . . 87
4.3.1 Knots . . . 87
4.3.2 Sweep . . . 87
4.3.3 Grain Angle . . . 88
4.4 Non Destructive Methods . . . 88
4.4.1 Acoustic Methods . . . 88
4.4.2 Resistance Drilling . . . 90
4.5 Visual Grading and Mechanical Properties . . . 92
4.5.1 Ovality . . . 92
4.5.2 Tapered . . . 92
4.5.3 Sweep . . . 92
4.5.4 Knots all/central, KS . . . 93
4.5.5 Cracks . . . 93
4.5.6 Allowable characteristics . . . 94
4.5.7 Visual Characteristics and Mechanical Properties of *Acacia dealbata* Logs . . . 94
4.5.8 Evaluation of Ranta-Maunus Visual Grading as a Pre-selection Tool . . . 104
4.6 Experimental Campaign to Predict the Mechanical Performance of *Acacia dealbata* Logs Using Non-Destructive Techniques . . . 107
4.6.1 Transversal Vibration Testing . . . 107
4.6.2 Longitudinal Stress Wave Testing . . . 109
4.6.3 Resistance Drilling Testing . . . 111
4.6.4 Results of NDT for Physical-Mechanical Properties Prediction of Logs . . . 112
4.6.5 Regression Models . . . 117
4.7 Chapter conclusions . . . 123

5 Formation and Control of End Cracks in *Acacia dealbata* Logs During Drying 124
5.1 Crack Formation . . . 124
5.1.1 Drying Stress . . . 125
5.1.2 Growth Stresses . . . 126
5.1.3 Internal and External Factors in Crack Formation . . . 126
5.2 Description and Measurement . . . 128

5.3 Cracking Control 130
5.3.1 Pretreatments 130
5.3.2 Air-Drying Considerations 131
5.3.3 Techniques to Reduce Tangential Stresses in Logs 131
5.4 Experimental campaign, article *Assessing Treatments to Mitigate End-Face Cracking in Air-Dried Acacia dealbata Logs* 133

6 Conclusions **135**
6.0.1 Context of the Study 135
6.0.2 Physical and Mechanical Characterization of Full-Size Logs 135
6.0.3 Evaluation through Visual Grading and Non-Destructive Techniques (NDT) . . . 136
6.0.4 Control of Cracking and Air Drying 136
6.0.5 General Implications 137
6.1 Future Developments 137

Appendix **139**

References **167**

List of Figures

1 Use of roundwood in different structural systems: (a) the Toyoson Stonemason Museum by Yasufumi Kijima with beams forming a reciprocal frame, Japan (1993) [4]; (b) the roof of Doncaster's Earth Centre forming a 3D truss, England (2000) [5]. 1

2 Different processing levels, according to Bukauskas et al.[6] 2

3 Applications in structures and development of tools for the Use of small-diameter logs: (a) Logs used as top and bottom chords of beams in a roof structure, forming bidirectional Vierendeel beams [39]; (b) A bridge utilising small-diameter logs arranged diagonally to form a Warren-type truss [6]; (c) A point-cloud of an unprocessed wood log and its final representation as an image for the use of non-standardized timber [40]. 5

4 Different techniques to control crack formation: (a) A central hollow along the entire length of the piece [48]; (b) Use of kerfs (2) approximately 1 cm deep on opposite sides along the entire length of the log (our research image); (c) Diagram illustrating the use of metal wires surrounding the end of a log to prevent crack formation [52]. 6

5 Forest map of Europe from European Environment Agency, 2001 [67] 11

6 European Primary Forest Database version 2.0 (EPFD v2.0), according to Sabatini et al. [70]. Note of authors: Both points and polygons were magnified to improve visibility. . . 12

7 *srw* potential applications, based on Dramm (1999)[97] and Ramage et al. (2017) [1]. * Glued Laminated Timber (GLT) and Cross Laminated Timber (CLT). 15

8 Actual *srw* applications: (a) hybrid structural wall (Wu et al. [102]); (b) I beam with small diameter trunks (Gorman et al [105]); A commercial product of small-diameter hollow logs from New Zealand (Batchelar [47]). 16

9 Distribution map of forest uses and species in the Portuguese mainland. Source: 6th National Forest Inventory - ICNF [53]. Ocupação principal: (1) Pinheiro-bravo; (2) Pinheiro-manso; (3) Outras resinosas; (4) Sobreiro; (5) Azinheira; (6) Carvalhos; (7) Castanheiro; (8) Eucaliptus; (9) Acácias; (10) Alfarrobeira; (11) Outras folhosas; (12) Cortes únicos/Ardidos; (13) Matos e Pastagens; (14) Agricultura; (15) Urbano-improductivos; (16) Inacessiveis. Note: each point is a field sample. 20

10 The figure is a visual summary of the colonization process of *Acacia dealbata* Link since its introduction (past), its interaction with biotic and abiotic agents (present) and its final stage of consolidation (future). The base image was extracted and adapted from "*Here to stay. recent advances and perspectives about acacia invasion in mediterranean areas*" by Souza-Alonso et al. [59]. 22

11 *Acacia dealbata* Link: (a) Isolated tree, (b) branch and bipinnate leaves, and (c) pod and seed (all these images are from [149]). (d) Image of *Acacia dealbata* stands with its characteristic yellow flower (March 2021) from Serra da Estrela (Portugal) by Raposo et al [60]. The authors of the image highlight that the stands develop along the line of water courses. 25

12 Anatomy of *Acacia dealbata* Link.(a) View of a typical section (1 m from the ground) from a tree in the Peneda-Gerês National Park. Microscopic view of samples from southern Chile: (b)-(c), Tn = transversal section; (d)-(e), Tg= tangential to the rings section; and (f)-(g), Rd= radial section through the rings. Images provided by Linette Salvo-Sepúlveda. 26

13 Reaction wood formation in an inclined stem. (a) Tension wood in angiosperm (hardwood). (b) Compression wood in gymnosperm (softwood). Image from "*Tree growth stress and related problems*" [158] based on the Illustration of H. Yamamoto. 29

14 Corewood or Juvenile wood (JW) distinctive characteristics, according Moore and Cown [44]. 30

15 Diagram to explain the reduction of mature wood (MW) and the relative increase of juvenile wood (JW) by the sawing process (based on Baxter [111]). 31

16 Schematic relationships between density and various variables: (a) strength; (b) compression strain; and (c) moisture content. According Blass et al [23]. 32

17 Relationship between moisture content (MC) and different wood strengths (adapted from Wood Handbook [162]). 33

18 Immediate effect of temperature at various moisture content levels (0%, 12%, and 18%) relative to the value at 20°C for clear, defect-free wood: (a) MOE parallel to the grain, (b) MOR. The graph is a composite of results from several studies. Variability in reported trends is illustrated by the width of the bands. From Wood Handbook [162]. 34

19 (a) Variation of the moisture gradient in *Acacia dealbata* logs inside a climate chamber at a temperature of 20°C (±0.5°C) and relative humidity of 60% (±5%), measurements at the centre of the log each week at three depths: mc1= outwood; mc2 = ± 20 mm; mc3 = close to pith. (b) Formation of cracks at the end of the log after 5 weeks. 35

20 (a) The red circle indicates the location of Peneda-Gerês National Park in northern Portugal; (b) a view of mimosa (*Acacia dealbata*) colonized areas by Peneda-Gerês National Park, and the polygon outlines an area colonized, characterized by distinct slight colouration; (c) a typical view of a high-density mimosa stand, along with ICNF rangers harvesting logs; (d) a close-up of a mimosa specimen illustrates the natural misalignment of the tree shaft. 40

21 Design of experimental campaign for the mechanical characterization of *Acacia dealbata* logs. *Non-destructive* testing during the first phase (November 2022–July 2023) included visual characterization for qualitative classification (Ranta Maunus [25]) and longitudinal stress wave and transverse vibration tests on samples with moisture content (MC) >12%, followed by oven-dried samples with MC = 12%. *Destructive* testing in the second phase (August 2023–July 2024) involved bending, parallel compression, and drill penetration resistance tests on full-scale logs and bending and parallel compression tests on free-defect small specimens. 42

22 Moisture content (MC) determination methods. (a) Weighing and (b) oven-drying of log slices, and (c) use of an electrical resistance moisture meter for full-scale logs. 45
23 Linear correlation between two methods for determining moisture content: oven-drying method vs. electrical resistance moisture meter. 46
24 Correlation between the moisture content (MC) obtained from the mean of three measurements using a calibrated electrical resistance meter (according to Equation 2) and the MC determined by the oven-drying method from disc samples extracted near the fracture zone. 47
25 (a) Components of the immersion procedure for determining the volume of irregular bodies, as outlined in ASTM D2395 - mode II [164], (b) tare of the water-filled container and securing of the sample in the support frame, and (c) immersion of the sample and data capture. 49
26 Relationship between the density of the full-size log ($\rho_{fb,12}$) adjusted to 12% MC and density based on the immersion method (ρ_{12}). 50
27 Graphical definition of the apparent diameter (d_{app}). 51
28 (a) Indication of sections measured on each log during the experiments: Sections S1, S2, S3, S4, and S5 were measured. (b) Perimeter measurements (for d_{app}) were taken using an adjustable measuring tape (1), while (c) diameter measurements (for d_{nom}) were obtained using an orthogonal steel piece (2), a carpenter's square (3), and a rigid measuring tape (4). 51
29 Preparation of samples for destructive testing. Conditioning of the logs in a climatic chamber: (a) for the 2nd and (b) the 1st group of bending tests, and for the (c) parallel compression tests. 52
30 (a) Bending testing setup with geometrical definition according to EN 14251:2003 [18]; (b) Image of the test to determine the local modulus of elasticity (E_{local}). The support conditions, the couple of concrete load-heads, and the ruler screwed at both ends over the log neutral line (centring to 5 d_{nom}) with one of the two LVDT devices to measure the deflection in the central section are observed; (c) Detail of support device and (d) of concrete loading-head with fibres, coust to each log. 54
31 Parallel to the grain compression test setup. (a) Geometrical definition according to EN 14251:2003 [18]; (b) Test image with the loading device and a couple of LVDT devices to measure axial deformation. 56
32 Figures a, b, c, and d: Failures by tension at the lower edge; Figures e, f, g, and h: Failures initiated by compression crushing at the upper edge, culminating in brittle tensile fracture at the lower edge (the log number is indicated in the upper right corner). 62
33 All images: Examples of splintering failures affecting a larger area of the lower edge in tension (the log number is indicated in the upper right corner). 63

34 Failure modes under parallel compression: (a) Specimen exhibiting the highest ovality; (b) and (c) failure occurring in the concave region of a highly curved log (log 11); (d) and (e) typical shear failure observed in logs with lower curvature (logs 20 and 6). 63
35 (a) Stress–strain curves for 17 *Acacia dealbata* Link logs harvested in spring (1st group) and (b) 28 logs harvested in autumn (2nd group). 64
36 Histograms of destructive test results: logs 1–33 correspond to the 1st group, and logs 35–65 to the 2nd group. Unfilled bars represent outliers excluded from the statistical analysis. Reference values from other studies are shown at the far right [15, 136, 137]. (a) Local modulus of elasticity (E_{local}, blue) and global modulus of elasticity (E_{global}, red); crosshairs indicate density values adjusted to 12% moisture content (MC), according to EN 384:2016+A2:2022. (b) Bending strength (f_m) and corresponding MC for each log. . 65
37 Relationships between moisture content (MC) and mechanical properties from destructive tests, separated by group (1st and 2nd): (a) E_{local} (triangles) and E_{global} (circles); (b) Bending strength (f_m); (c) Ductility index (μ). 67
38 Stress–strain curves of full-size logs: (a) Curves corresponding to logs with ovality exceeding the limit proposed by R-M (≤ 20% for Grade B). The dashed line represents the curve of the specimen with the lowest maximum load, included for reference; (b) Curves of logs exhibiting sweep greater than 10 mm/m. The dashed line indicates the curve of the specimen with the highest maximum load, also shown for reference. 69
39 Small clear sample preparation. (a) Sawing of logs to form 25.25 mm^2 strips; (b) conditioning of small clear samples in the climatic chamber; (c) tray for drying in an oven of fragments of 25.25.25 mm^3 from bending test samples. 71
40 Bending test setup of small clear samples. (a) Geometrical definition according to NCh 987.of86 [199]; (b) Image of the test with the two sliding supports (1), the central LVDT device (2) and (3) the solid steel loading head according to the standard. 72
41 Parallel compression of small clear samples. (a), (b) View the set-up with a couple of samples before testing. 73
42 Bending force-displacement curves for free-defect small samples from 6 trees harvested in (a) spring (1st group) and 10 trees harvested in (b) autumn (2nd group). 74
43 Bending failure modes of free-defect small samples: (a) embedding failure; (b) typical brittle bending fracture; (c) and (d) splintering tension failure; and (e) slope fibre failure. . 74
44 Parallel compressive force-displacement curves for free-defect small samples from 6 trees harvested in (a) spring (1st group) and 8 trees harvested in (b) autumn (2nd group). 75
45 Parallel compressive failure modes of free-defect small samples: (a) shear failure in the middle; (b) failure associated with checks; (c) and (d) sapwood side failure. 76

46 Box-plot comparing density adjusted according to EN 384:2016+A2:2022 (for moisture content, MC) and excluding outliers. The orange and grey colours without contours represent the full-size logs, while the white and grey colours with bold outlines correspond to the free-defect small samples. Dots on the left side of each box represent MC, with crosses indicating the lowest, middle, and highest values. 78
47 Box-plot comparing the Modulus of Elasticity adjusted according to EN 384:2016+A2:2022 (for MC) and excluding outliers. The orange and grey colours without contours represent the full-size logs for local modulus (E_{local}) and global modulus (E_{global}). In contrast, the white and grey colours with bold outlines correspond to the free-defect small samples. Dots on the left side of each box represent MC, with crosses indicating the lowest, middle, and highest values. 79
48 Box-plot comparing bending strengths, excluding outliers. The orange and grey colours without contours represent the full-size logs, while the white and grey boxes with bold outlines correspond to the free-defect small samples. Dots on the left side of each box represent MC, with crosses indicating the lowest, middle, and highest values. 80
49 Box-plot comparing parallel compressive strengths, excluding outliers. The orange and grey boxes without outlines represent the full-size logs, while the white and grey boxes with bold outlines correspond to the free-defect small samples. 80

50 (a) Correlation between bending strength and MOE (softwood). (b) Correlation between bending strength and knot area ratio (softwood). (c) Correlation between bending strength and a combination of several grading parameters. Image from Blaß and Sandhaas & [23]. 86
51 Schematic comparison of tensile and compressive strengths as a function of fibre angle relative to load, for small defect-free specimens of Douglas fir (*Pseudotsuga menziesii*) at MC = 12%. Adapted from Dinwoodie [140]. 88
52 Graphical definition of the parameters used to determine knot percentage, $Knot, all, cen$: including d_{knot} (knot diameter) and $d_{section-knot}$ (sectional diameter of log). 93
53 Relationship between the reference values of R-M and those of this study, for the visual characteristics of logs tested in (a) bending and (b) in parallel compression. 96
54 Relationship between Sweep and: (a) bending strength, (b) parallel compression, (c) local and (d) global modulus of elasticity, for 1st (spring) and 2nd (autumn) group. . . . 97
55 Relationship between different Sweep ranges in mm/m, and (a) local and global Modulus of Elasticity, and (b) parallel compression strength (note: The uncolored boxes correspond to the results of the defect-free samples). 98
56 Knotness of the (a) central zone, $Knot, cen$, and of (b) the whole log, $Knot, all$, in relation to the Local Modulus of Elasticity , E_{local}. 99
57 Knotness of the (a) central zone, $Knot, central$, and (b) the whole log, $Knot, all$, in relation to the bending strength, f_m; (c) Knotness in relation to the parallel compression strength, f_m 100

58 Typical brittle failure adjacent to the log knot subjected to bending (log 1 and 2): parallel and perpendicular tension. 101
59 All images: Horizontal shear failure modes (the log number is indicated in the upper right corner). 103
60 Logs with fibre deviation (the log number is indicated in the upper left corner). 104
61 Grading of logs, A or B, according to the allowed values of R-M for each visual characteristic (see table 10). TOTAL considers the threshold of the most unfavorable classification. 105
62 Comparison between grade A and B according to R-M for different physical-mechanical properties: dynamic Elasticity modulus for (a) longitudinal stress wave and (b) transversal vibration, static Elasticity modulus (c) local and (d) global, (e) bending strength and (f) density. 106
63 Transverse vibration testing. (a) Spring supports and 2-meter-long plastic wires, (b) accelerometer model PCB 393B12, (c) accelerometer model PCB 352B, (d) data acquisition cards, and (e) test setup showing the five accelerometers (1), wire supports (2), data acquisition system (3), and laptop (4). Note the geometric arrangement for free-free boundary conditions. 109
64 Longitudinal stress wave testing. (a) The test setup shows hammer model 086D20 (1) and accelerometer model PCB 352B (2), and the input-output points are marked on the log ends; (b) Devices: hammer (1), accelerometer (2), data acquisition card (3), laptop (4), and connection wires (5); and (c) Fourier amplitude spectrum showing the resonance frequency of the first longitudinal stress wave (f_{lsw}). 110
65 (a) Use of the Resistance drilling tool (Resistograph) on the central area of a log before the bending test; (b) result graph of resistance to drill penetration in %; (c) Indication of the sections of the log where the test is applied: A, B and C. 112
66 Boxplot comparing dynamic ($E_{dyn,lsw}$ and $E_{dyn,tv}$) and static (E_{local} and E_{global}) elastic moduli. "1st" refers to the spring harvest, "2nd" to the autumn harvest, and "all" to the combined dataset. 115
67 Relationship between drilling resistant (R_m) and density (ρ_{12}) considering (a) all specimens, and (b) separated into the 1st and 2nd groups. 118
68 Model 3: regression model with full-body density ρ_{fb} and Resistograph resistance R_m as predictors, and density at 12% MC, ρ_{12} as the response variable. 119
69 (a) Model 6: relationship between dynamic modulus of elasticity $E_{dyn,lsw}$ and local modulus of elasticity E_{local} in the 1st group. (b) Model 9: relationship between dynamic modulus of elasticity $E_{dyn,tv}$ and local modulus of elasticity E_{local} in the 2nd group. . . . 120
70 (a) Model 11: relationship between dynamic modulus of elasticity $E_{dyn,tv}$ and global modulus of elasticity E_{global} for all specimens.(b) Model 12: relationship between dynamic modulus of elasticity $E_{dyn,lsw}$ and global modulus of elasticity E_{global} in the 1st group. 121

71 Model 16: relationship between wave velocity v and bending strength f_m in the 1st group.(b) Model 17: relationship between dynamic modulus of elasticity $E_{dyn,lsw}$ and bending strength f_m in the 2nd group. 122

72 Examples of crack formation in wood. (a–c) Crack types according to Yin and Liu [242]: (a) surface checks, (b) internal checks, and (c) end checks. (d) Surface checks at the end of a log in service; (e) End splitting in a log due to the predominance of growth stresses; (f) Collapse in kiln-dried roundels (courtesy of Professor J.L. Louzada). 125

73 Schematic representation of moisture gradient and crack formation during drying [36]. . 126

74 Examples of cracking measurement techniques in small samples: (a) Quantification of checking and shrinkage in *Eucalyptus nitens* wood wedges using open-source R-based image analysis algorithms [251]; (b) Analysis of deformation and fracture processes in Douglas-fir slice using vertical and horizontal deformation measurements with a video camera on a polar reference system (c) [253]. 129

75 Examples of investigations employing techniques to reduce tangential stresses in logs. (a) Application of the kerfing technique on the lower part of a log in service [264]. (b) "Promoting" effect of kerfing (reagent colouration indicates treatment absorption levels) [265]. (c) Detail of the incision technique applied to a solid piece [268]. (d) Formation of larger cracks due to the interconnection of multiple incisions [238]. (e) Reduction in resistance to point loads in centrally hollowed logs [50]. (f) Partial central hollows of two diameters (16 mm and 30 mm) in *Acacia dealbata* logs [237]. 132

76 Preliminary results of an experimental campaign with air-dried logs. (a) Experimental design: 30 *Acacia dealbata* logs cut into three segments, the two control ends and the central one with one or two perpendicular cuts. (b) Preliminary view of log 25 dried for 14 months with the same cut on both sides: untreated (b-1 and b-2) and treated (b-3 and b-4). (c) View of the stack. 134

List of Tables

1 Standards referenced for mechanical testing of timber and roundwood (adapted from Bukauskas et al.[6]). . . . 38
2 Summary of the main mechanical properties inferred in the experimental campaign. . . . 44
3 Correlations between destructive test results. . . . 68
4 Mechanical properties and strength classes (to properties definitions see table 2). . . . 69
5 Means comparison (t-test) between the 1st and 2nd groups of full-size logs for different mechanical properties 70
6 Statistical summary for mechanical properties and density of free-defect small samples (1st and 2nd groups). . . . 76
7 Pearson correlation coefficients between density ($\rho_{small,12}$), modulus of elasticity (E_{small}) and bending strength ($f_{small,m}$) for 1st (spring) and 2nd (autumn) harvest groups of free-defect small samples. . . . 77
8 Means comparison (t-test) between the 1st and 2nd groups of free-defect small samples for different mechanical properties 78

9 Standards related to visual strength grading and qualitative classification of round timber. 85
10 Allowable visual characteristics values grading to Ranta-Maunus. [25] 94
11 Visual characteristics of bending specimens. . . . 95
12 Visual characteristics of parallel compression specimens. . . . 95
13 Comparison of means between groups A and B including U values and significance level. 105
14 Descriptive statistics with results of dynamic and static tests and resistograph on full-scale logs(1st and 2nd groups). . . . 114
15 Correlation results for various mechanical properties. . . . 116
16 Linear regression models for density, ρ_{12}. . . . 118
17 Linear regression models for local modulus of elasticity, E_{local}. . . . 119
18 Linear regression models for global modulus of Elasticity, E_{global}. . . . 120
19 Linear regression models for bending strength, f_m. . . . 121

20 A: Reproduction of the questionnaire administered to Mr. Henrique José Morais Fernandes Reis, Head of the Northern Coastal Forestry Management Division of the Portuguese ICNF, concerning specific aspects of the *Acacia dealbata* invasion in the Peneda–Gerês National Park, northern Portugal. . . . 139
21 B: Results for each specimen obtained from static bending tests, including nominal (d_{nom}) and apparent (d_{app}) diameter, oven-dry moisture content (MC), density adjusted to 12% moisture content (ρ_{12}), local modulus of elasticity (E_{local}), global modulus of elasticity (E_{global}), and bending strength (f_m). . . . 144
22 C: Summary of results obtained from static bending tests, including MC, ρ_{12}, E_{local}, E_{global}, and f_m. . . . 146

23 D: Results for each specimen and summary obtained from compression parallel tests, including moisture content (MC), density adjusted to 12% moisture content (ρ_{12}), compression parallel modulus of elasticity ($E_{c,0}$) and compression parallel strength ($f_{c,0}$). The remaining columns expose visual characteristics of the samples: Apparent diameter, Sweep, and Knottness. 147
24 E: Visual characteristics of each specimen and corresponding grading according to the Ranta-Maunus system (A: superior grade, B: intermediate grade, R: reject), evaluated for each individual parameter and globally. The assessed parameters include Ovality, Tapered, Sweep, Knots (all and central), and the Knot sum (KS). Note: For completeness, the KS factor was included, although the logs were unaffected, as indicated by the Ranta–Maunus classification. 148
25 F: Summary of visual characteristics, including Ovality, Tapered, Sweep, Knots (all and central), and Knotness sum (KS). The last columns present the mean values of nominal diameter (d_{nom}), apparent diameter (d_{app}), and length for each group. 150
26 G: Results for each specimen obtained from Non-destructive test longitudinal stress wave (lsw) for MC > 12 %. Parameters include the MC obtained with the electrical resistance meter, Velocity (Vel), Density for full-body (ρ_{fb}), and the corresponding dynamic modulus of Elasticity ($E_{dyn,lsw}$) and its respective values, adjusted to 12 % of MC. 151
27 H: Summary of results obtained from Non-destructive test longitudinal stress wave (lsw) tests for MC > 12 %. Including MC, Velocity, Density and dynamic modulus of elastic and its respective values, adjusted to 12 % of MC. 153
28 I: Results for each specimen obtained from Non-destructive test longitudinal stress wave (lsw) for MC = 12 %. Parameters include the MC obtained with the electrical resistance meter, Velocity (Vel), Density for full-body (ρ_{fb}), and the corresponding dynamic modulus of Elasticity ($E_{dyn,lsw}$) and its respective values, adjusted to 12 % of MC. 154
29 J: Summary of results obtained from Non-destructive test longitudinal stress wave (lsw) tests for MC = 12 %. Including MC, Velocity, Density and dynamic modulus of elastic and its respective values, adjusted to 12 % of MC. 156
30 K: Results for each specimen obtained from Non-destructive test transversal vibration (tv) for MC > 12 %. Parameters include the MC ⊣ obtained with the electrical resistance meter, first vibration mode (f_1), mass, length, moment of inertia and modulus of Elasticity ($E_{dyn,lsw}$) with it respective value, adjusted to 12 % of MC. 157
31 L: Summary of results obtained from Non-destructive test transversal vibration (tv) for MC > 12 %. Including MC, first vibration mode (f_1), mass, length, moment of inertia and modulus of Elasticity ($E_{dyn,lsw}$) with it respective value, adjusted to 12 % of MC. . . 159
32 M: Results for each specimen obtained from Non-destructive test transversal vibration (tv) for MC = 12 %. Parameters include the MC obtained with the electrical resistance meter, first vibration mode (f), mass, length, moment of inertia and modulus of Elasticity ($E_{dyn,lsw}$) with it respective value, adjusted to 12 % of MC. 160

33 N: Summary of results obtained from Non-destructive test transversal vibration (tv) for MC = 12 %. Including MC, first vibration mode (f), mass, length, moment of inertia and modulus of Elasticity ($E_{dyn,lsw}$) with it respective value, adjusted to 12 % of MC. 161
34 O: Results for each specimen obtained from Resistograph tests performed on sections A, B, and C, including the corresponding mean value (R_m). 162
35 P: Summary of Resistograph Results tests and its mean values (R_m). 163
36 Q: Descriptive statistics of end-face crack measurements across each concentric ring (from pith: r_1, r_2, r_3, r_4, and r_p, corresponding to the log perimeter) after the air-drying campaign. Parameters include the relative crack ratio (c_r), defined as the percentage of the total crack length over each ring, and the number of cracks (n_r). Reported statistics comprise the mean, standard error (S.Error), standard deviation (SD), maximum (Max), minimum (Min), and count (Count). 164
37 R: Comparative performance of relative cracking (c_r) on the peripheral ring, r_p (a), and ring 2, more central, r_2 (b). The boxplots comparing untreated (samples in black/white), R, with their respective other treated faces, K-2k, K-3k, H-16 mm, and H-30 mm (in gray). In the top left corner, the significance level for the t-test is indicated, with * = p < 0.05; ** = p < 0.001; ns = not significant. The cross on each box indicates the mean value. . 165
38 S: Comparative performance of the number of cracks ($n°_r$) on the peripheral ring, r_p (a), and ring 2, more central, r_2 (b). The boxplots comparing untreated (samples in black/white), R, with their respective other treated faces, K-2k, K-3k, H-16 mm, and H-30 mm (in gray). In the top left corner, the significance level for the t-test is indicated, with * = p < 0.05; ** = p < 0.001; ns = not significant. The cross on each box indicates the mean value. 166

lrw large round wood. 2

srw small round wood. xi, 2, 4, 5, 8, 14–17, 26–28, 39, 92, 124

1st First log samples harvested in spring. xiii–xviii, 43, 52, 53, 60, 61, 64–68, 70, 73–82, 94–97, 99, 102, 104–107, 109, 110, 112, 114–122, 144

2nd Second log samples harvested in autumn. xiii–xviii, 43, 47, 52, 53, 60, 61, 64–68, 70, 73–82, 94–97, 99, 102, 104–110, 112, 114–122, 144

CLT Cross Laminated Timber. xi, 1, 2, 14, 15

cov Coefficient of variation. 68, 76, 77, 95, 114, 115

DT Destructive testing. 43, 45, 46, 70, 113–115

EMC Equilibrium Moisture Content. 33, 125, 130

EWPs Engineering Wood Products. 2, 14, 27

FSP Fibre Saturation Point. 4, 33, 43, 66, 83, 89, 108

GLT Glued Laminated Timber. xi, 1, 2, 14, 15

IAPs Invasive Alien Plants. 17, 18

ICNF Instituto da Conservação da Natureza e das Florestas. xi, xii, xviii, 19–21, 39–41, 139

JW juvenile wood. xii, 29–31

lsw Longitudinal stress wave testing. 41, 50, 89, 90, 113, 123

LVDT Linear Variable Differential Transformer (electromechanical transducer). xiii, xiv, 53, 54, 56, 60, 72

MC Moisture Content. xii–xvi, xviii–xx, 3, 4, 33–36, 39, 41–43, 45–48, 50, 52, 55, 61, 64–67, 70, 71, 74, 76–80, 82, 83, 88, 89, 96, 107–113, 118–120, 125, 126, 130, 131, 144, 146, 147, 151, 153, 154, 156, 157, 159–161

MG Moisture Gradient. 35, 126

MOE Modulus of Elasticity. xii, xv, 6, 7, 30–34, 38, 39, 55, 64, 77, 84, 86, 87, 89, 90, 101, 113, 114, 120, 122

MOR Modulus of Rupture. xii, 30, 31, 34, 64, 66, 86, 101

MW mature wood. xii, 29–31

NDT Non-destructive testing. 32, 41, 43, 45, 48, 50, 52, 70, 89, 112–115, 123

R-M Reference to Ranta Maunus report. xiv–xvi, 68, 69, 94–96, 98, 99, 101, 102, 104–107

SD Standard Deviation. xx, 39, 41, 47, 49, 60, 61, 64, 66, 73, 76, 95, 107–110, 114, 117, 164

tv Transversal vibration testing. 41, 50, 89, 113, 123

Chapter 1

Introduction

The term ”round wood” lacks a universal definition. The most basic interpretation refers to the timber in the initial processing stage after it is harvested from the forest. At this stage, the wood is known as ”round wood” and is transported from the forest to a sawmill for further processing, including removal of the bark and correction of surface defects [1].

The use of round wood, or ”round timber,” in construction dates back to the earliest human-made structures. The simplicity of construction techniques and the availability of abundant forest resources facilitated the development of diverse structures using round wood in various parts of the world. Notable examples of ancient high-performance structures include the 11th-century Chinese bridges [2, 3] and, more recently, the wooden log trestle rail bridges in North America. Beyond these historical precedents, the current environmental crisis has elevated timber construction, including round wood, as a preferred alternative to materials with higher environmental impacts, such as reinforced concrete or steel. Some contemporary examples can be seen in Figure 1, with applications in two different structural systems, a reciprocal frame (a) and a 3d truss structure (b).



Figure 1: Use of roundwood in different structural systems: (a) the Toyoson Stonemason Museum by Yasufumi Kijima with beams forming a reciprocal frame, Japan (1993) [4]; (b) the roof of Doncaster’s Earth Centre forming a 3D truss, England (2000) [5].

Round wood construction has garnered particular interest today for several reasons [6]. Environmentally, round wood requires minimal processing, significantly reducing the environmental impact associated with sawing. Additionally, as an adhesive-free structural product, round wood has an environmentally advantageous position, especially when compared to GLT elements, CLT panels, particleboards or fibreboards.

1.1 Small Diameter Round Wood (*srw*)

Forest management practices, such as forest thinning, offer the opportunity to develop a specialised roundwood construction industry using small diameter roundwood (*srw* hereafter). Some of these residual logs, after a grading process to select the highest-quality specimens, represent a valuable surplus resource distinct from wood-based products for engineering applications, pulp for paper production, or biomass products. Utilising these excess resources *srw* not only encourages the growth of larger trees with higher commercial potential but also mitigates the accumulation of hazardous fuel loads in fire prone forests a critical concern in the context of global warming [7].

Stern [8] distinguishes between large-diameter round wood (*lrw*) and small-diameter round wood (*srw*). *lrw* includes logs, bolts, poles, posts, and other structural members with diameters of 5 inches (127 mm) or larger. In contrast, *srw* refers to smaller diameter members and products. Wolfe [7] further defines *srw* as wood ranging in diameter from 100 to 225 mm (4 to 9 inches), with physical properties suitable for structural applications, provided it meets minimum requirements for straightness, knot size, grain angle, and the presence and size of defects. Bukauskas et al. [6] propose the broader concept of "whole timber," encompassing a wide range of round wood elements. These range from minimally processed elements (with bark intact) to more refined round wood elements featuring special profiling, such as tongue and groove. Intermediate forms include debarked elements, those with varying degrees of peeling to achieve a cylindrical or conical shape, and even hollow-core elements (Figure 2).

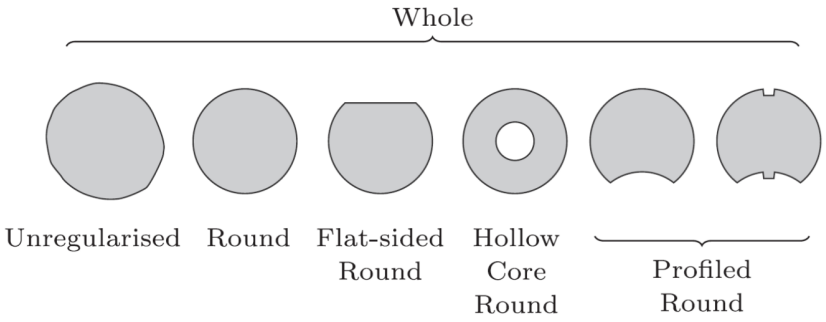

Figure 2: Different processing levels, according to Bukauskas et al.[6]

From a mechanical properties perspective, *srw* structures exhibit significantly lower performance compared to engineered wood products (EWPs) such as CLT or GLT. However, considering its environmental benefits and the substantial increase in demand for forestry byproducts [9], the use of *srw* in structures with less demanding structural requirements offers several advantages.

In its natural state, a tree functions as a cantilevered beam anchored to the ground, supporting its self-weight as it grows, along with potential horizontal wind loads. Consequently, trees develop strength and stiffness in response to this loading pattern [10]. A tree's mechanical strength is maximal at its base and gradually decreases with height, a characteristic reflected in its tapered shape. Furthermore, within the cross-section of the tree, bending capacity increases as it moves away from the centroid, where the pith is located. The natural tapered shape of a tree not only optimises its structural form but also minimises the

impact of knots. While knots represent weak points in the saw timber, in a tree, they are surrounded by continuous woody tissue [11, 12]. Indeed, Vega et al. [13] demonstrate that peeling and processing logs of chestnut (*Castanea sativa*) wood into a cylindrical form reduces part of the stronger cross-section. It exposes a higher relative percentage of juvenile wood, weaker than mature wood, resulting in a significant decrease in modulus of elasticity and density.

Non-destructive techniques offer the potential for preselecting *srw* in the early stages of processing, using relatively simple procedures that cause minimal damage to the pieces. This can be particularly advantageous when working with residual *srw* from forest thinning or overcrowded forest control [14]. As Larson et al.[11] demonstrate, well-sorted logs can have higher economic value, thereby facilitating the development of a supply chain for such forest by-products. Furthermore, various studies have shown high and significant correlations between destructive and non-destructive tests, supporting the use of predictive models for the physical-mechanical performance of standing trees, logs, sawn timber, and other wood-derived by-products [14, 15, 16, 17]. However, the mechanical characterisation and grading of *srw* present challenges. A tree exhibits significant variability in its physical and mechanical properties, not only between species but also among individual trees of the same species, within the same site, and even within different parts of the tree. Mechanical characterization of logs requires standardized destructive tests such as EN 14251 [18] and ASTM D1036-99 [19], which differ from tests for regular and rectangular sawn timber. In addition to external factors affecting wood, such as moisture content (MC), visual characteristics that influence mechanical performance must also be considered, including taper, ovality, curvature, and the presence of knots, among others.

The first and oldest non-destructive preselection and grading method is the visual one, which was initially based on transmitted local traditions and experiences. Detailed grading protocols were later standardized in the United States [20, 21] and in Europe [22]. However, over time, the wide variety of species and building traditions have complicated the applicability of many of these protocols. Furthermore, grading is inherently an individual process, dependent on the grader, and thus, to some extent, a subjective method [23]. Another issue with visual grading is under-grading, which often results in overly conservative values, leading to high rejection rates and the underutilization of the material [13]. Additionally, visual grading does not provide valuable objective data, such as density or modulus of elasticity—properties that are directly related to strength. However, for small-diameter logs, an initial pre-selection based on visual characteristics at the harvest site enables the identification of the most geometrically suitable specimens by assessing aspect ratios such as ovality and sweep. Furthermore, some studies have also demonstrated that combining certain visual classification parameters with more robust methods can enhance the predictability of multivariate models [24]. Although no visual grading protocol is infallible, some have yielded better results. For example, Ranta-Maunus [25], in a comprehensive study of thinned logs from northern European conifers (Norway Spruce and Scots Pine), proposed allowable values based solely on visual characteristics such as ovality, taper, and cracking, among others, to pre-grade small-diameter logs. This grading method classified the logs into two grades, without associated mechanical properties. Some authors, such as Morgado et al. [26] and Fernández-Golfín et al. [27], have evaluated and used these limit values as a reference, obtaining consistent results.

Currently, numerous well-established non-destructive techniques allow for the inference of physico-mechanical properties of different materials, including wood [28]. For example, acoustic methods are commonly used to evaluate the stiffness of standing trees and logs from various species. These methods analyze stress waves propagating through the material, which are intrinsically related to its physical and mechanical properties, such as the dynamic modulus of elasticity [29]. Another variant of the acoustic method involves studying transverse vibrations. In a system consisting of a beam with defined boundary conditions, low-energy impacts or ambient vibrations can excite the system, allowing for the measurement of the natural frequency of the first transverse vibration mode, [30, 31]. Then, by applying analytical formulas derived from Euler-Bernoulli beam theory, the dynamic modulus of elasticity can be determined. In addition to these methods, various other non-destructive techniques are available for determining properties like density or assessing the condition of existing structures [32]. For instance, devices that measure resistance to needle penetration, such as the resistograph or Pilodyn, are used with consistent results [33, 34]. Some studies have also demonstrated that the combined use of these techniques can enhance statistical models that predict the mechanical performance of elements [35].

As a hygroscopic material, the physical properties of wood are influenced by changes in moisture content (MC) [36]. Experimentally, MC has been observed to be closely related to the physical and mechanical properties of wood [37]. From the fibre saturation point to an equilibrium MC of 12%, an inverse relationship is observed between MC and strength and stiffness, while density decreases proportionally with moisture loss. At the dynamic level, the acoustic velocity decreases as MC increases, and further reduction in velocity is observed above the fibre saturation point (FSP) [38].

1.2 Uses and Limitations

Wood is an optimal material for various structural applications due to its high strength-to-weight ratio, which facilitates prefabrication and assembly processes. The use of small-diameter (*srw*), minimally processed logs in structural applications has been extensively explored in several studies, highlighting their numerous advantages. For instance, the pioneering work of Burton, Dickson, and Harris [39] capitalises on the ease of bending of small-diameter green wood (Figure 3a), enabling its use in forming effective structural elements such as tensioned stay beams and compression-based arch shells for roofing. Bukauskas [6] demonstrates the versatility of minimally processed logs in a wide range of applications, including highly efficient structural forms such as flat and spatial trusses (Figure 3b). Furthermore, logs can be used in combination with other materials, such as in the design of flat trusses reinforced with log strands and internal steel bars, or in mixed concrete structures incorporating permanent formwork slabs based on logs. Also, other studies have introduced new technologies that overcome certain limitations inherent to natural materials, such as the use of photogrammetry (Figure 3c) to control geometric irregularities for the application of computer-aided design and manufacturing (CAD-CAM) methods in the fabrication of complex structural components [40, 41, 42, 43].



Figure 3: Applications in structures and development of tools for the Use of small-diameter logs: (a) Logs used as top and bottom chords of beams in a roof structure, forming bidirectional Vierendeel beams [39]; (b) A bridge utilising small-diameter logs arranged diagonally to form a Warren-type truss [6]; (c) A point-cloud of an unprocessed wood log and its final representation as an image for the use of non-standardized timber [40].

One significant challenge with a minimally processed product like small-diameter round wood (*srw*) is the variability and unpredictability of its mechanical properties [7]. Due to the minimal processing, the visual characteristics of the logs—such as knottiness, sweep, ovality, and taper—affect their physical-mechanical performance and must be considered when evaluating their potential as a product for structural use [26]. Moreover, *srw* often contains a substantial amount of juvenile wood, characterised by lower density, which results in reduced strength and stiffness and greater longitudinal shrinkage. This makes *srw* more susceptible to drying defects such as cracking on the weaker tangential plane [44]. Managing these effects during construction and service life is crucial, requiring careful storage and handling, as well as awareness of the equilibrium moisture content relative to the environment to minimise hygroscopic effects like swelling and shrinkage [23].

The formation of cracks (checking and splitting) in the tangential plane is triggered by the difference in drying rates between the exterior and interior of the wood, which generates surface tangential stresses and shrinkage, leading to cracking [23, 45]. Various strategies have been developed to address this issue [46]. In New Zealand, for example, hollowing *srw* along its cross-section has been employed with *Pinus radiata* species [47]. This technique modifies the drying process, reducing its negative effects (checking and splitting) by decreasing moisture gradients, which in turn lowers external tangential stresses [48] (see Figure 4a). Other advantages include reduced drying time—the most energy-intensive stage in timber production—improved penetration of wood durability treatments, and reduced weight of the elements, leading to lower energy costs for transport. Research has examined the mechanical behaviour of hollow elements compared to massive ones. Yeo et al. [49] demonstrated that, despite the reduction in cross-sectional area, compressive strength parallel to the fibre did not differ significantly between specimens, which the authors attribute to the removal of juvenile wood, normally having lesser resistance than mature one. Although the study did not address internal cracking or microcracking, failures were observed to begin in areas where surface drying cracks had formed. However, in compression perpendicular to the grain, the hollow elements exhibited unexpected failure modes at lower load levels than anticipated. This

behaviour reflects a low tangential strength of the hollow round sections, causing transverse flattening [50]. Other pretreatment techniques to control the effects of drying also show promising results. Traditional woodworking methods, such as the Se-wari technique in Japan, involve making small, controlled saw cuts parallel to the grain, which helps alleviate tangential stresses [49]. Similarly, the technique of sawing a kerfing of a certain depth along the length of the piece helps dissipate surface tension caused by drying and reduces cracking [49] (see Figure 4b). Studies on exposed posts with double kerfing have demonstrated a significant reduction in crack size [51].

Cracks can impact the performance of log end connections, a critical factor for the effective transmission of structural loads. Consequently, other approaches focus on confining the end zone of the log to prevent crack formation, using methods such as galvanised steel wire weaving [52] (see Figure 4c) or annular groove connections [47].

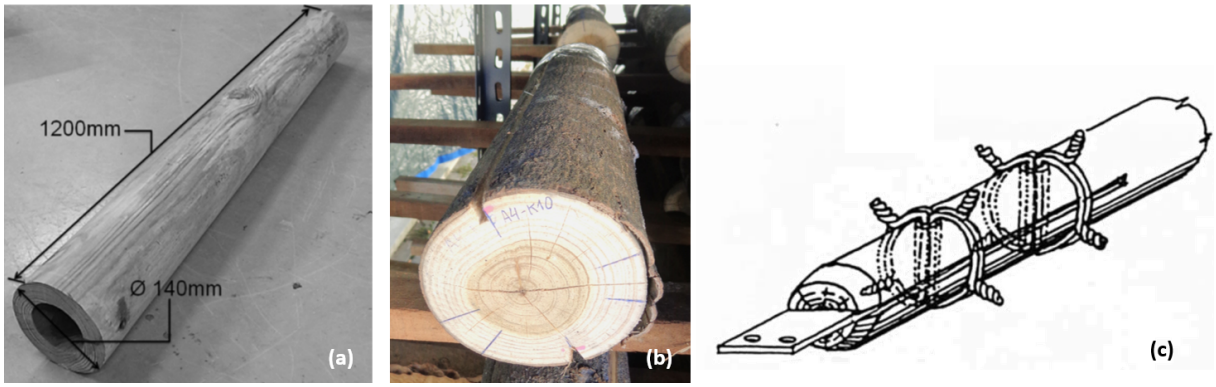

Figure 4: Different techniques to control crack formation: (a) A central hollow along the entire length of the piece [48]; (b) Use of kerfs (2) approximately 1 cm deep on opposite sides along the entire length of the log (our research image); (c) Diagram illustrating the use of metal wires surrounding the end of a log to prevent crack formation [52].

1.3 Use of *Acacia dealbata* Logs from the Portuguese Forest

According to the VI National Forest Inventory (2015), approximately 5.7×10^3 ha of the continental Portuguese forest were deforested areas with unidentified species, likely overtaken by invasive species [53]. Furthermore, the inventory indicates that the *Acacia* genus occupies 8.4×10^3 ha of this area. This genus has demonstrated remarkable performance in applications beyond its traditional use as firewood or fuel. Although studies on the physical properties of Acacia species are still limited, the results are promising, especially considering that some authors advocate for the use of hardwoods to meet the growing global demand for wood resources [54].

In a study by Martins et al. [55], the average density of *Acacia melanoxylon* from Portugal was reported at 647 kg/m^3, with an average modulus of elasticity (MOE) of 13.9×10^3 MPa and a bending strength of 65 MPa, demonstrated its potential for structural applications. In Chile, a technical report by the Chilean Forestry Institute, Pinilla et al. [56], indicates that *Acacia dealbata* exhibits superior physical properties compared to the reference species *Pinus radiata*. The report reveals average density values of 495 kg/m^3,

an MOE of 11.5×10^3 MPa, and a bending strength of 65.7 MPa for *Acacia dealbata*, all of which surpass the corresponding values for *Pinus radiata*.

From a forest management perspective, the removal of invasive species aligns with traditional criteria for clearing and control, which involves extracting significant amounts of forest residues that can be used in applications beyond their primary purposes. The species studied in this research is *Acacia dealbata*, a hardwood species recognised as the first invasive species in Europe within the plant life form category, according to Nentwig et al. [57]. Native to Australia, it was deliberately introduced to Portugal in the mid-19th century to face a significant deforestation, particularly in litoral and mountainous regions such as the Serra da Estrela and Serra do Gerês [58]. Its successful spread is attributed to several factors, including its aggressive colonisation capacity, rapid growth rate, adaptability to environmental disturbances such as wildfires, and high floral density—factors extensively explored in the literature [59, 60, 61, 62, 63]. Consequently, the potential use of these forest residues could be even more significant and environmentally relevant, particularly considering arguments from some authors who point out that direct control strategies for highly invasive species, like *Acacia dealbata*, are insufficient to halt their spread in a sustainable and economically viable way [64]. As a result, economically and environmentally valorising the forest residues from its control, based on an understanding of its physical and mechanical properties, could offer an alternative approach by integrating the species into value chains that help offset the associated costs.

1.4 Objectives

Given the considerations outlined above and an opportunity to utilise a material with potential for construction, several research questions arise. Based on this background, what are the physical and mechanical performances of *Acacia dealbata* logs for structural applications? Do non-destructive grading methods provide reliable mechanical characterisation to support a grading protocol? Are pretreatment techniques effective in controlling the cracking effects of drying?

The general objective of this thesis is to physically and mechanically analyse and evaluate small roundwood elements made from the invasive species *Acacia dealbata* for structural applications. The specific objectives are:

1. To establish a general mechanical characterisation protocol for small-diameter roundwood as a residual by-product of forest management;

2. To evaluate the reliability of non-destructive methods for the mechanical pregrading of small-diameter roundwood;

3. To assess various techniques for mitigating crack formation during the drying process of unprocessed roundwood logs.

1.5 Motivation

I have three personal motivations for pursuing this investigation. The first is practical, rooted in the simple fact that the planet is home to vast forested areas, which should ideally increase for our survival. Consequently, the by-products of forest management—such as Small Diameter Round Wood (*srw*)—will be available as a resource that deserves our attention throughout the life cycle of these forests. In this sense, the potential utility of this work could have a global impact.

The second motivation relates to the study of round wood, which represents a return to wood as an elemental raw material for construction. I find this particularly intriguing at a time when technological advancements—despite bringing unprecedented well-being to humanity—can sometimes overshadow the most fundamental knowledge of nature. In my view, nature remains an inexhaustible source of new understanding.

The third motivation is aesthetics, rooted in my belief as an architect that incorporating raw natural objects into architecture signals a different relationship between architecture and construction and between art and the world. This approach is not about embracing a 'rustic' aesthetic for its own sake, but about integrating natural objects as functional components of a larger structural system. This reflects the *zeitgeist*, a movement away from a romanticized vision of nature towards a deeper understanding that we are an integral part of it.

1.6 Document Structure

Each chapter of this thesis begins with a brief literature review, followed by an experimental section (except for Chapters 1 and 2), and concludes with a summary of findings. *Chapter 1* introduces and defines the research problem, presenting the general and specific objectives together with the motivation behind this study. *Chapter 2* contextualizes and discusses the potential use of a residual material—*Acacia dealbata* logs—derived from the control of an invasive species, for structural applications. *Chapter 3* presents the empirical study aimed at mechanically characterizing *A. dealbata* logs collected from the Peneda–Gerês National Park in northern Portugal, including both full-size logs and small defect-free specimens, to assess their potential applicability in structural uses. *Chapter 4* analyses the relationship between visual characteristics and mechanical properties by evaluating a visual grading method (Ranta-Maunus) and subsequently describes the empirical study applying several non-destructive techniques—longitudinal stress wave, transverse vibration, and resistance drilling—establishing correlations with destructive methods and developing linear regression models linking both approaches. *Chapter 5* focuses on the control of cracking during air drying, exploring techniques such as kerfing and central hollowing to reduce cracking formation in end logs. Finally, the document concludes with general conclusions (*Chapter 6*), appendices (*Chapter 7*), and references.

The overall structure of the thesis was influenced by two main trends consolidated toward the end of the research process. On the one hand, the influence of visual characteristics proved to be relatively marginal compared with the impact of the results derived from non-destructive testing. This justified presenting

the analysis of visual characteristics and their relationship with mechanical properties separately from the destructive tests, which are discussed in the subsequent chapter. On the other hand, the repeated and consistent observation of differences between logs harvested in spring and those harvested in autumn required a more detailed analysis of the destructive tests performed on defect-free specimens.

This document was initially written in Spanish, with the use of specific English terminology. It was later translated into English using automatic translation tools and subsequently refined with AI-assisted editing. The final English version was manually revised and improved by the author to ensure linguistic accuracy and consistency in the final written form.

Chapter 2

Utilization of By-Products from Portugal Forests: small-diameter roundwood (*srw*) of Invasive Species *Acacia dealbata*.

This chapter contextualises the significance of studying small, minimally processed logs of the invasive species *Acacia dealbata* in the Portuguese protected forests. Within the global context of increasing demand for environmentally sustainable products, it addresses the role of forests and the emerging utilisation of by products from their management particularly small-diameter round logs as potential resources for construction applications. The discussion then examines the economic and environmental rationale for valorising invasive species such as *Acacia dealbata*, framing their exploitation as a strategy to support control measures within the principles of a circular economy. Finally, the analysis focuses on the Portuguese context, highlighting the threats and opportunities posed by this species to the protected forest areas.

2.1 The Importance of Forests

Forests serve not only as a primary source of construction wood, but also as a foundation for environmental, social, and economic stability. Ramage et al. [1] analyse the interplay of environmental, social, and economic factors within forestland management, highlighting the global role of forests in environmental equilibrium through carbon capture and storage. Forests managed sustainably and used as sources for certified timber in construction contribute to environmental sustainability by effectively sequestering carbon, which benefits global climate stability.

From a social perspective, forests enhance the well-being of the community when properly balanced between economic and environmental needs. For example, a sustainable mix of monoculture plantations for economic use and diverse primary forests for recreation, culture, and ecosystem preservation is essential for long-term social benefit. Economically, wood stands out among construction materials due to its renewability. Unlike materials such as steel or reinforced concrete, whose production demands the depletion of finite resources, wood requires that topsoil remain intact, allowing seedlings to regenerate and forests to be continuously nurtured before harvesting [1]. Its energy requirements for growth, largely derived from solar energy, are minimal compared to the larger environmental footprint of conventional materials such as concrete [65] or steel [66].

European forests, particularly those in high-precipitation areas (see Figure 5), further demonstrate ecological resilience. These forests access deep water tables that are unreachable to most vegetation and adapt well to severe conditions, such as those in mountainous regions. This adaptability minimizes their impact on food security, as they do not compete with agricultural land.

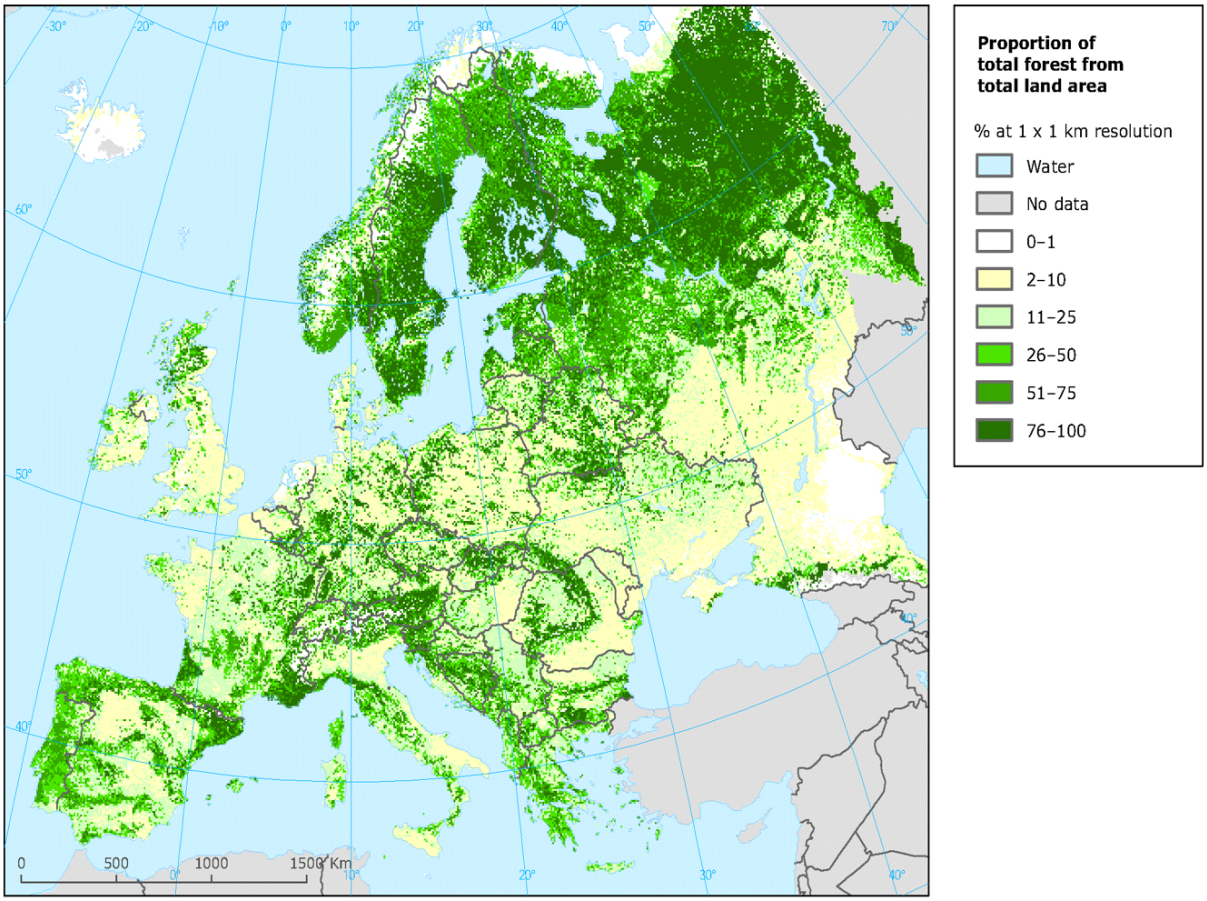

Figure 5: Forest map of Europe from European Environment Agency, 2001 [67]

According to the definitions of the FAO [68], forests fall into two major categories: primary and planted. Primary forests, close to the concept of native or unmanaged forests, consist of diverse, multi-species ecosystems with minimal human intervention. These forests exhibit complex and biodiverse natural ecosystems with limited human influence, primarily in relation to regeneration activities. In contrast, planted forests, often referred to as managed forests, are predominantly monocultures of exotic species designed for intensive, single-purpose exploitation, mainly aimed at wood and wood-based product production.

Although Sathre and González-García [69] demonstrated that specialized forestry machinery in planted forests incurs certain environmental burdens, both types of forests can contribute to the mitigation of climate change. Native forests play a crucial environmental role as habitats for biodiversity, permanent carbon sinks, and protectors of water quality, while helping to moderate temperatures and provide models for the management of forests close to nature (see Figure 6). These forests also hold intrinsic cultural and identity value for the communities that sustain them [70].

Well-managed forest plantations, on the other hand, are instrumental in wood supply and allow carbon sequestration through wood-based products like utensils, furniture, and construction materials. Both types of forest management contribute significantly to carbon capture. In the case of Chile, Droppelmann et al.[71] report that the cost-efficiency of carbon sequestration per ton of CO_2 in managed forests is lower when comparing similar production levels in wood yield or permanent carbon sinks. This best cost-

effectiveness is partly due to the higher reforestation costs with native species and the slower growth rates of native species compared to exotics, which offer quicker returns on initial investment. However, Droppelmann et al. [71] emphasise a strong consensus within forest engineering on the importance of native forest recovery to counteract degradation, improve productivity and increase the value of landowners.

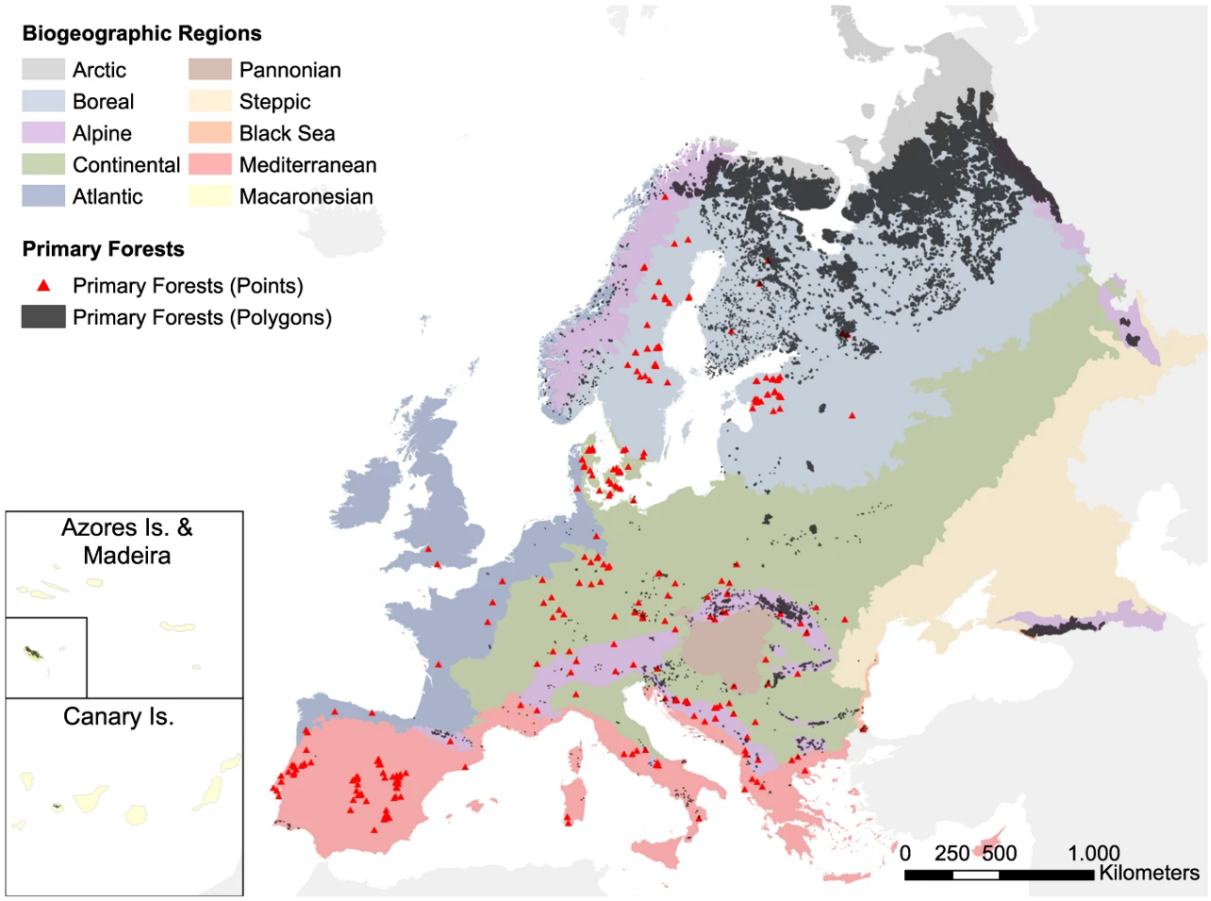

Figure 6: European Primary Forest Database version 2.0 (EPFD v2.0), according to Sabatini et al. [70]. Note of authors: Both points and polygons were magnified to improve visibility.

2.2 By-Products from the Forest Management

Global demand for wood in construction has risen significantly due to its environmental performance [9]. To mitigate overexploitation risks and promote sustainable forest management, a growing emphasis is on valuing the by-products of wood production [72]. An important resource for these by-products arises from forest management itself. Beyond the primary wood supply chain, forest residues offer considerable potential for various applications. For example, in plantations, selective cutting or thinning generates substantial wood from removed logs to improve the growth of higher-quality trees by optimising their access to essential resources such as water, nutrients, and sunlight. In densely populated stands, selective cutting may also reduce wildfire risks [73]. Recent studies also explore the physical-mechanical quality of fire-damaged wood, with some researchers proposing using invasive species with practical applications, including construction, to offset control costs [64].

Effective forest management often entails intensive selective thinning practices to remove less suitable trees [74]. This practice supports the growth of high-potential specimens, as well-managed thinning can improve the density, heartwood-to-sapwood ratio, and other wood properties [75]. Studies have shown that intensive thinning can significantly increase tree diameter by providing more space and sunlight to selected trees [74] while positively impacting wood quality and economic returns [76]. Additionally, intensive thinning can enhance carbon sequestration [77] and mitigate drought effects [78].

Increasingly severe and frequent wildfires due to climate change have elevated the global need for fire protection measures [61]. Droughts heighten forest fuel potential, and competing land uses (e.g., agriculture, settlements) combined with inadequate forest management can trigger fires. Poorly managed plantations and overpopulated natural forests are particularly fire-prone [73, 79]. As Wolfe [7] suggested, reducing forest fuel loads by thinning overstocked trees is essential in fire-prone areas. Fire susceptibility varies by species; for instance, ponderosa pine proved more fire-resistant than firs in the 2000 U.S. fires [73], while exotic species like *Acacia dealbata* and *Eucalyptus globulus* in Chile were found to be highly flammable compared to native *Cryptocarya alba* and *Quillaja saponaria* [61]. Some recommend prioritizing fire control in managing invasive species, as certain species can aggressively colonize burned areas [80, 81].

Fire-damaged forests offer another source of wood for potential by-products. Although research on this topic is limited, studies have examined the effects of fire on the mechanical properties of wood from burned forests [82]. Preliminary findings, mainly on conifers [83, 84, 85], suggest that despite the reductive effects of combustion, there is generally no significant reduction in the physical-mechanical properties of wood. Additionally, research has explored using fire-damaged wood in MDF [86] or OSB panel manufacturing [87]. Consequently, a substantial volume of available material, such as forest residues, shrubs, branches, bark, and logs, offers opportunities for added value. While primary use as firewood is widespread, increasing the economic value of these resources benefits local communities and supports sustainable forest management [1, 73, 88]. Although many harvested logs have lower timber potential (e.g., with misalignment or excessive branching), some demonstrate suitable physical-mechanical properties for new applications with economic potential. For example, Underhill et al. [89] noted that during a secondary thinning after 10–15 years, around 300 trees per hectare with diameters between 150 and 300 mm are harvested, sizes that could be competitive in the construction market.

2.2.1 General By-Products from the Forest

Forest residues and by-products from plantations and protected forests present diverse applications across various fields. These residues, which include branches, bark, sawdust, and small-diameter logs with potential for timber or structural material, have gained increasing attention from researchers in recent years. Santos, Anjos, and Simões [90] demonstrated the potential of pulp from *Acacia dealbata* and *Acacia melanoxylon* in papermaking, with slightly superior performance to *Eucalyptus globulus* for pulp and paper production. In a more recent study aimed at valorizing invasive Acacia species, Neiva et al. (2024) include other species (*Acacia longifolia*, *Acacia mearnsii* De Wild, and *Acacia saligna* Labill),

again demonstrating the applicability of these species in this field and suggesting species combinations to improve performance. Additionally, biomass is being explored as a source of energy, commonly called "wood fuel" [1]. Nunes et al. [91] evaluated the high potential of *Acacia dealbata* waste as bioenergy. They proposed a biomass application model using protected Portuguese forests, which face serious threats from the species' aggressiveness [79]. However, an analysis of *Acacia dealbata* components revealed certain limitations for direct certification as pellets, suggesting a mixed-use with other higher-performance species to enable economic valorization of the species for exploitation and control [92].

Some small-diameter logs exhibit timber-suitable shapes and sizes for construction applications, although examples of using invasive species for this purpose are limited. In Portugal, Martins et al. [55] utilized invasive hardwood *Acacia melanoxylon* timber for Glued Laminated Timber (GLT), achieving superior performance to softwoods. In Chile, Ananias et al. [93] reported good results in kiln drying *Acacia dealbata* and *Acacia melanoxylon* boards, with low levels of cracking and warping. A technical report by the Chilean Forestry Institute highlighted competitive physical-mechanical properties of *Acacia dealbata* for construction applications [56]. Research has also been conducted on thinning-derived logs from overpopulated forest areas prone to fires. For example, Levan-Green and Livingston [94] note that for Engineering Wood Products (EWPs) such as GLT or Cross Laminated Timber (CLT), lower-grade woods can be used in areas of lower structural importance, a potentially viable application. Using boards from overstocked young *Pinus ponderosa* forests, Hernandez et al. [95] achieved competitive results for GLT beams. Liao et al. [96] studied the feasibility of manufacturing CLT using fast-grown, small-diameter Eucalyptus lumber. Similarly, Underhill et al. [89] used hardwood veneers from forest thinning in Australia to produce laminated veneer plate.

In a preliminary study on the feasibility of utilizing large volumes of timber from overstocked North American forests, Dramm [97] noted that adapting sawmills to process smaller logs is essential for economically viable production. However, these initial investments impact final product quality and influence market prices [94]. For an overview of the potential applications of small-diameter logs in construction, Figure 7 provides a chart based on Dramm's proposal [97], which differentiates products by quality. The following section will elaborate on applications for small-diameter logs requiring minimal or no processing.

2.2.2 Uses of Low-Processed Small-Diameter Roundwood

Small-diameter roundwood (*srw*) logs, derived from forest management practices, represent a valuable resource for construction. Despite this potential, research on the physical-mechanical performance of *srw* is considerably limited compared to the extensive studies on sawn timber with rectangular cross-sections [98]. Conversely, some researchers have identified the opportunity to utilize *srw* as an available, eco-friendly, and cost-effective material. For instance, Bukauskas et al. [6] conducted a comprehensive review of the state of the art surrounding "whole timber", i.e., minimally processed wood logs, to encourage increased *srw* utilization.

To define the scope, Stern [8] classified large-diameter roundwood (*lrw*) as logs with diameters equal to or greater than 5 inches (127mm) and small-diameter roundwood (*srw*) as logs with diameters under 5

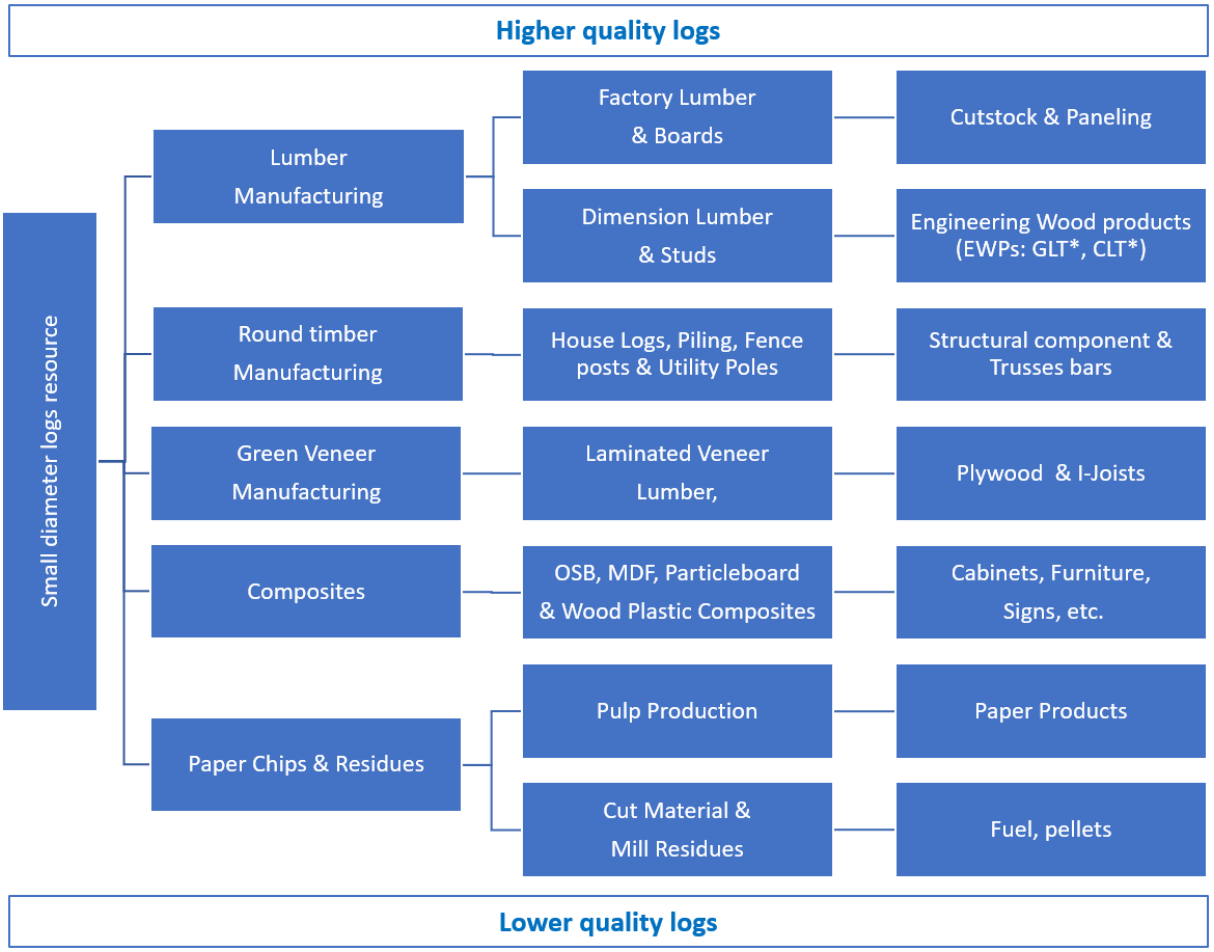

Figure 7: *srw* potential applications, based on Dramm (1999)[97] and Ramage et al. (2017) [1]. * Glued Laminated Timber (GLT) and Cross Laminated Timber (CLT).

inches originating from thinning operations. This limited cross-section restricts their yield but aligns with their use as structural elements with minimal processing. However, *srw* logs may display considerable misalignment and defects such as knots, tapered, irregular cross-sections, and ovality, impacting their performance. Given their young age (under 20 years), these logs also contain a high percentage of juvenile wood, or "corewood" [44], which, due to anatomical characteristics, generally exhibits inferior mechanical performance compared to mature or "outwood" [11]. These factors can affect the log's resistance, increasing susceptibility to severe cracking during drying. The small diameter may also limit their mechanical performance when structural adjustments, such as notches or central holes, are made [98, 50]. Logs may also suffer from reaction wood formation due to environmental stressors, as in sloped and windy areas, which can compromise mechanical performance [23].

Despite these challenges, the high availability of small-diameter logs presents an opportunity to selectively use high-quality specimens. An adequately graded *srw* log, peeled or partially shaped into a cylindrical form with consistent cross-section and internal quality, would be suitable for construction applications. The circular shape also offers mechanical advantages, as trimming a log into a rectangular cross-section can result in the loss of mature wood, reducing the amount of load-bearing material, especially in the outer wood, where stresses are highest. The circle is also a more efficient shape for distributing

load across the cross-sectional area [99]. Some studies also show that minimal processing for such logs can be advantageous, as it preserves the mature wood's outer layer without weakening knot-surrounding areas [11, 12].

Historic examples of *srw* used in soil stabilisation include the foundation piles of Venice, Italy [100]. Modern studies, such as Numata et al. [101], demonstrate its applicability in soil stabilisation using multiple piles to reduce liquefaction damage during earthquakes. Other foundation applications involve hollow logs driven into cohesive soils, relying on a combination of end-bearing and skin friction resistance [47]. Several experimental prototypes and structures incorporate *srw* at various levels, from simple elements to complex systems [6]. For example, *srw* wall framing using U-shaped nails and structural OSB plates (Figure 8-a) achieves compression resistance comparable to conventional timber walls [102, 103]. Another example is a highly efficient I-beam designed [104] by sawing to optimise log use (80% of section area as seen in Figure 8-b).

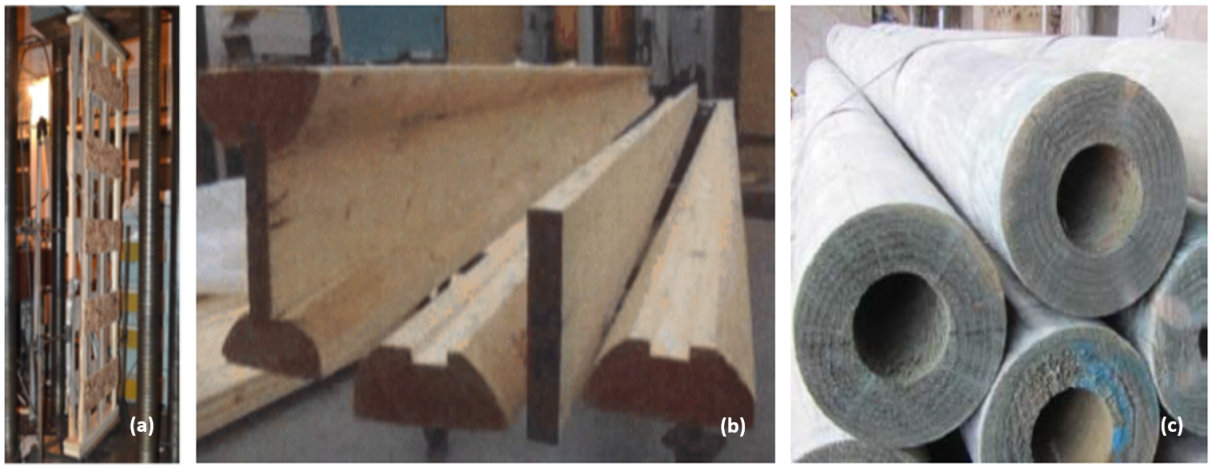

Figure 8: Actual *srw* applications: (a) hybrid structural wall (Wu et al. [102]); (b) I beam with small diameter trunks (Gorman et al [105]); A commercial product of small-diameter hollow logs from New Zealand (Batchelar [47]).

Research has demonstrated that logs from thinning can achieve satisfactory mechanical performance. For example, Vega et al. [13] reported positive results with small chestnut trees (*Castanea sativa* Mill.), and Llana et al. [15] obtained comparable findings with thinned hardwood logs sourced from Ireland (Alder (*Alnus glutinosa* (L.) Gaertn.), European ash (*Fraxinus excelsior* L.), European birch (*Betula pendula* Roth. and *Betula pubescens* Ehrh.), and Sycamore (*Acer pseudoplatanus* L.).

In the construction sector, *srw* has been investigated for a range of applications. Burton, Dickson, and Harris [39], working in England in the late 1990s, empirically demonstrated its suitability for diverse structural typologies. Their work also catalysed further research into related topics, including wood protection strategies, construction processes, and structural connection systems.

In commercial contexts, New Zealand markets standardised *Pinus radiata* poles in two formats: (i) peeled and machined to a constant diameter, and (ii) so-called "Uglies" which retain their natural conical taper, thereby increasing strength by approximately 6%. These products are employed in construction, retaining systems, power transmission, and telecommunications [106]. Small-diameter hollow poles re-

move a portion of the juvenile wood, accelerating drying, reducing weight, and enhancing preservative treatment through complete penetration. Structural performance is further improved by the incorporation of post-tensioned steel rods, which enhance overall stability (Figure 8-c). Notable applications include telecommunication towers and foundation piles [47].

Recent technological developments have expanded the potential of *srw* in architecture and engineering. Contemporary approaches [107, 108] employ advanced tools to address the inherent irregularities of raw logs, such as photogrammetry for geometric control and CAD–CAM systems for the precise fabrication of structural elements. Steinmetz et al. [109] examined the use of rustic logs as floor joists in different configuration patterns, integrating parametric design and robotic construction. Similarly, Fereday et al. [110] explored speculative design strategies using Sweet Chestnut log segments, developing several prototype structures.

Overall, roundwood represents an abundant and cost-effective byproduct of forest management, requiring minimal processing while offering proven mechanical properties with potential for further optimization. As noted by Amelia Baxter in The Future of Structural Roundwood: *"Traditional wood product markets that once supported these... more than 700 million acres of private and public forests in the U.S. (about 10% of which are severely undermanaged), such as lumber and pulp, are depressed. The long-term decline of the housing and paper industries exacerbates the oversupply and requires new, diversified markets within the forest products industry..."*[111].

2.3 The Challenge of Invasive Species Control

The United Nations Sustainable Development Goal 15 aims to "protect, restore and promote sustainable use of terrestrial ecosystems, sustainably manage forests, combat desertification, halt and reverse land degradation, and halt biodiversity loss". This goal has driven global and local initiatives in recent years to address the challenge posed by invasive alien plants (IAPs), particularly in natural forests, which are crucial biodiversity reservoirs. For instance, studies examining the impact of *Acacia dealbata* on native ecosystems, such as the *Quercus robur* forests in northern Iberia, have shown that Acacia invasion reduces species richness, alters native seed banks, and hinders regeneration—even after IAPs removal [112]. Additionally, various IAPs have been observed to modify ecosystem characteristics, leading to biodiversity reduction and alterations in soil physicochemical properties [59, 60, 113, 114]. However, achieving these objectives—promoting healthy forest ecosystems while preserving biodiversity—remains a complex challenge. Pötzelsberger et al. [115] review the multifaceted nature of non-native species in European forests, highlighting both the environmental risks associated with invasiveness and the potential opportunities for future management, among others. They conclude that a more rational and evidence-based approach is essential, drawing on accumulated knowledge and recent advances in forest science.

Controlling Invasive Alien Plants (IAPs) is particularly demanding due to their high potential for reinvasion, the large spatial extent of affected areas, and the substantial costs of intervention [116]. Effective management requires a thorough understanding of species' colonisation patterns and invasion dynamics. For example, controlled burning has been employed to regulate overstocked forests [94] or to deplete

soil seed banks [116]. Nevertheless, this method can have unintended consequences; for instance, it may stimulate the germination of heat-resistant seeds such as those of *Acacia dealbata*, thereby favouring invasive species over native flora and ultimately reducing overall species richness [80].

Control methods for IAPs primarily include biological agents, physical removal, and chemical applications [64]. In a Portuguese case study involving differents stakeholders, mechanical methods were identified as environmentally preferable but costly and energy-intensive; chemical control was noted for its speed but also for its environmental risks; and biological control outcomes varied by species. Promising results in strategic IAPs approach for the *Acacia dealbata* control include employing inhibitory shrubs [117] and/or focusing control efforts upstream of water courses to limit gravitational spread [60].

Despite efforts, IAPs spread rates especially in natural parks indicate that control strategies remain insufficient [60, 114]. Alternative approaches prioritize native species protection, suggesting less ambitious but more economically and socially sustainable IAPs control [59, 91]. Along this line, Lorenzo and Morais [64] argue that current IAPs control strategies yield only short-term results and that traditional methods have become impractical for large areas. They advocate for extended, cost-intensive control efforts with a medium to long term focus, aligning with circular economy principles and Sustainable Development Goals 12 (responsible consumption and production) and 15 [64]. Therefore, some researchers advocate for economic evaluation of IAPs waste among *Acacia dealbata* use [58] recognizing the limited effectiveness of current strategies.

In the context of utilizing invasive species for value-added applications, Lorenzo and Morais [64] compile a comprehensive review of the scientific literature, analyzing various potential applications of invasive alien plant (IAPs) waste. However, authors [64] and other researchers emphasize the importance of not overlooking the boundary conditions that limit this approach. Legal restrictions, such as the European Regulation (EU) No. 1143/2014, which prohibits IAPs cultivation and prioritizes prevention, early detection, and rapid eradication, limit the scope of these strategies [118]. National regulations, such as Portuguese Decree-Law No. 92/2019 [119] and Spanish Royal Decree 630/2013 [120], reinforce these limitations. To succeed, control strategies also require a strong long-term management plan and must incorporate methods that minimize reinvasion risk and include post-management monitoring [79]. Further, sustainable IAPs control must involve localizing product consumption in the affected territories to retain benefits within affected territories and reduce transportation-associated impacts [91].

2.4 The Case of Invasive Species *Acacia dealbata* in Portugal

In Portugal, the demand for wood and the valorisation of forest resources are influenced by alignment with European and international environmental policies. The Portugal Market Report 2023 [121] identifies several key policy frameworks shaping forest management and the forest products sector, including the Climate Basis Law (Law No. 98/2021), the Roadmap for Carbon Neutrality 2050 (Government Order No. 107/2019), the National Integrated Energy and Climate Plan 2030 (Government Order No. 53/2020), and the Climate Change Adaptation Action Program (Government Order No. 130/2019). These national initiatives support broader European strategies, such as the 2018 update of the EU Bioeconomy Strategy,

the European Green Deal, and the United Nations 2030 Agenda for Sustainable Development.

A number of these policies directly address the utilisation and valorisation of forest management residues. They emphasise the promotion of circular use for both wood and non-wood forest products, the expansion of the bioeconomy through afforestation, the implementation of efficient forestry practices and ecosystem services, the protection and restoration of biodiversity, and the adoption of circular economy principles. Other policy measures target the control of pests, diseases, and invasive species, as well as the prevention of their spread. Additionally, several initiatives encourage research, development, and innovation to strengthen scientific and technological capacity in the forestry sector.

2.4.1 Portugal's Forests

According to the 2021 Forest Profile of the Instituto da Conservação da Natureza e das Florestas (ICNF), forest areas in Portugal, including temporarily deforested lands (e.g., logging, burning, or regeneration zones), cover approximately 3,305 × 10^3 ha, representing 36% of the country's total area. As of 2015, the predominant species group corresponds to hardwoods, occupying 2,055 × 10^3 ha (64% of the forest area), primarily composed of Eucalyptus species covering 845 × 10^3 ha. Meanwhile, coniferous species occupy 745 × 10^3 ha (23%), with Pinheiro-Bravo (*Pinus pinaster*) comprising the majority at 713 × 10^3 ha. The remaining area consists of mixed forests.

Figure 9 from the ICNF [53] illustrates the species distribution across the Portuguese territory. Native species predominantly constitute the continental forests, with holm oaks and cork oaks representing approximately 349 × 10^3 ha and 720 × 10^3 ha, respectively, amounting to 31% of the total forest area. The remainder of the forest area is mainly composed of species with more limited distributions, including chestnuts, carobs, acacias, strawberry trees, poplars, riparian species, and other resinous species.

The forest sector holds substantial economic importance for Portugal. According to the Portugal Market Report 2023 [121], forest-based industries including forestry, wood processing, paper, and cork production generate over 72 × 10^3 jobs, accounting for 2.4% of national employment. Macroeconomically, the sector contributes 0.5% to Portugal's Gross Added Value (GVA), positioning it eighth in Europe for GVA's relative economic weight. When normalized per forested hectare, Portugal ranks fourth in Europe with a GVA of €273/ha, comparable to Austria and Italy and surpassing Finland, France, and Sweden, underscoring the sector's economic significance [122].

A breakdown of Portugal's 2022 forest product [122] outputs shows cork production at 27.5%, pulpwood at 41.4%, saw timber at 18.3%, and miscellaneous products at 12.8%. Although cork production has recently declined due to climate factors, its high demand has increased prices and trade surpluses. The relative importance of sawn wood, primarily from *Pinus pinaster*, has decreased due to a limited number of mature trees, driving up prices and imports. Pulpwood, largely derived from eucalyptus and used in pulp, fiberboards and particleboard, represents a significant volume, though domestic production remains insufficient for industry demands, necessitating imports. Energy wood, including pellets, briquettes, and firewood, has gained in value amid the international boycott of Russian oil and gas and the search for alternative energy sources, such as biomass [122].

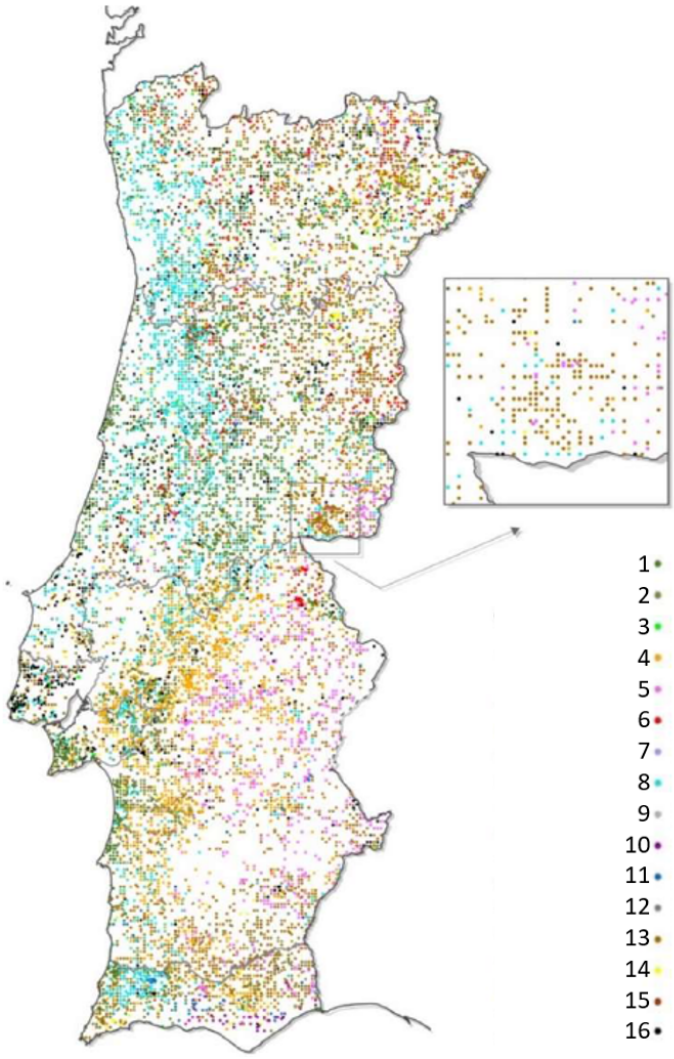

Uso/ocupação do solo	# pontos
Floresta	**7967**
Pinheiro-bravo	1899
Pinheiro-manso	611
Outras resinosas	102
Eucaliptos	1823
Sobreiro	1662
Azinheira	815
Carvalhos	436
Castanheiro	137
Acácias	120
Alfarrobeira	41
Outras folhosas	171
Povoamentos ardidos	74
Cortes únicos	76
Matos e Pastagens	**3388**
Matos	1575
Matos altos	246
Matos ardidos	36
Pastagem regadio	128
Pastagem sequeiro	1403
Agricultura	**252**
Improdutivos	**18**
Urbano	**22**
Pontos inacessíveis	698
Total	**12345**

Figure 9: Distribution map of forest uses and species in the Portuguese mainland. Source: 6th National Forest Inventory - ICNF [53]. Ocupação principal: (1) Pinheiro-bravo; (2) Pinheiro-manso; (3) Outras resinosas; (4) Sobreiro; (5) Azinheira; (6) Carvalhos; (7) Castanheiro; (8) Eucaliptus; (9) Acácias; (10) Alfarrobeira; (11) Outras folhosas; (12) Cortes únicos/Ardidos; (13) Matos e Pastagens; (14) Agricultura; (15) Urbano-improductivos; (16) Inacessiveis. Note: each point is a field sample.

The profitability of Portugal's forestry sector increases with product value addition. Although the balance of trade for raw forest materials, such as unprocessed wood and natural cork, shows a deficit of €393.1 million (2023), products with added value shift this trend positively. Cork-based products (e.g., stoppers, insulation, footwear, decor) and paper/cardboard yield substantial trade surpluses of €1,032.8 million and €940.2 million, respectively. By contrast, although small in volume, processed wood products for construction show a trade deficit favouring imports.

2.4.2 Species *Acacia dealbata* in Portugal

Acacia dealbata was introduced into Portugal in the late 19th century, primarily for ornamental purposes and for erosion control on degraded or overexploited soils [58, 62]. Over the past three decades, the extent of land occupied by Acacia species in mainland Portugal has expanded dramatically, increasing

from 2.7×10^3 ha in 1995 to 8.4×10^3 ha in 2015 equivalent to approximately 0.3% of the national forest area according to the most recent National Forest Inventory [53, 92]. This rapid expansion, particularly of *Acacia dealbata* Link, has encroached upon the country's limited primary forests (see Figure 6), posing a significant threat to biodiversity and to the ecological integrity of areas designated under the European network of protected natural sites. Indeed, Sabatini et al. [70] report that primary forests in Portugal cover only about 15.8×10^3 ha, representing a mere 0.5% of the total forest area.

Raposo et al. [60] assessed the invasive potential of this species within the Serra da Estrela Natural Park, using spatiotemporal data from orthophoto maps. They project a potential spread of *Acacia dealbata* by 2039, from 5.4 ha to 43.3 ha, corresponding to an Invasiveness Rate of 807%, if no preventive actions are taken. To estimate the potential invasion range of the species, Monteiro et al. [114] examined a core area of 5.4×10^3 ha within the Peneda Gerês National Park (total area: 70.29×10^3 ha [123]), using very high resolution (VHR) satellite imagery in combination with species distribution models (SDM). Their findings indicate that *Acacia dealbata* could potentially occupy up to two-thirds of the study area, with approximately 62.5% of this potential already colonised. More recent estimates provided by Henrique Reis, Head of the North Coast Forest Management Division of the ICNF (see Appendix A and 20), suggest that the current reference area of *Acacia dealbata* occupancy is approximately 1.35×10^3 ha equivalent to about 2% of the total park area.

Several factors explain the successful spread of *Acacia dealbata* across the Iberian Peninsula. Vieites-Blanco and González-Prieto [81] overlaid distribution maps of relevant physical attributes (burned area, soil pH, frost days per year, precipitation) with the areas occupied by invasive *Acacia* species. Although coarse, their data suggests that increasing fire incidents promote the expansion of *Acacia dealbata* and *Acacia melanoxylon*, as evidenced by the increase in these species on burned areas a finding corroborated by other studies. Other anthropogenic disturbances, such as expanding agricultural areas, also facilitate new colonization [124]. These species are well suited to acidic soils with pH values below 5.5. Although inconclusive, the species' spread appears correlated with climate factors; *Acacia dealbata* is less likely to expand in areas with frequent frost days, while it tends to thrive in the rainiest regions of the Iberian Peninsula.

Numerous researchers have identified attributes associated with *Acacia dealbata* that contribute to its invasive success in Portugal: High growth rate in poor and acidic soils [81]; Ability to exploit environmental disturbances like fires [62]; Adaptive and phenotypic plasticity to different environmental conditions [62]; Fire tolerance and vegetative regeneration capacity after cutting or burning [62, 60]; Production of a large quantity of hard-coated seeds (up to 62,000 seeds per square meter) that survive fires and can germinate post-disturbance [60]; Absence of natural predators [81]; High flower density, which attracts pollinators, and capacity for self-pollination [63, 60]; Allelopathic potential, where it releases substances that inhibit the growth of other plants as native ones [62, 125]. Figure 10, adapted from Souza-Alonso et al. [59], visually summarizes the primary processes triggered by the invasion of *Acacia dealbata*.

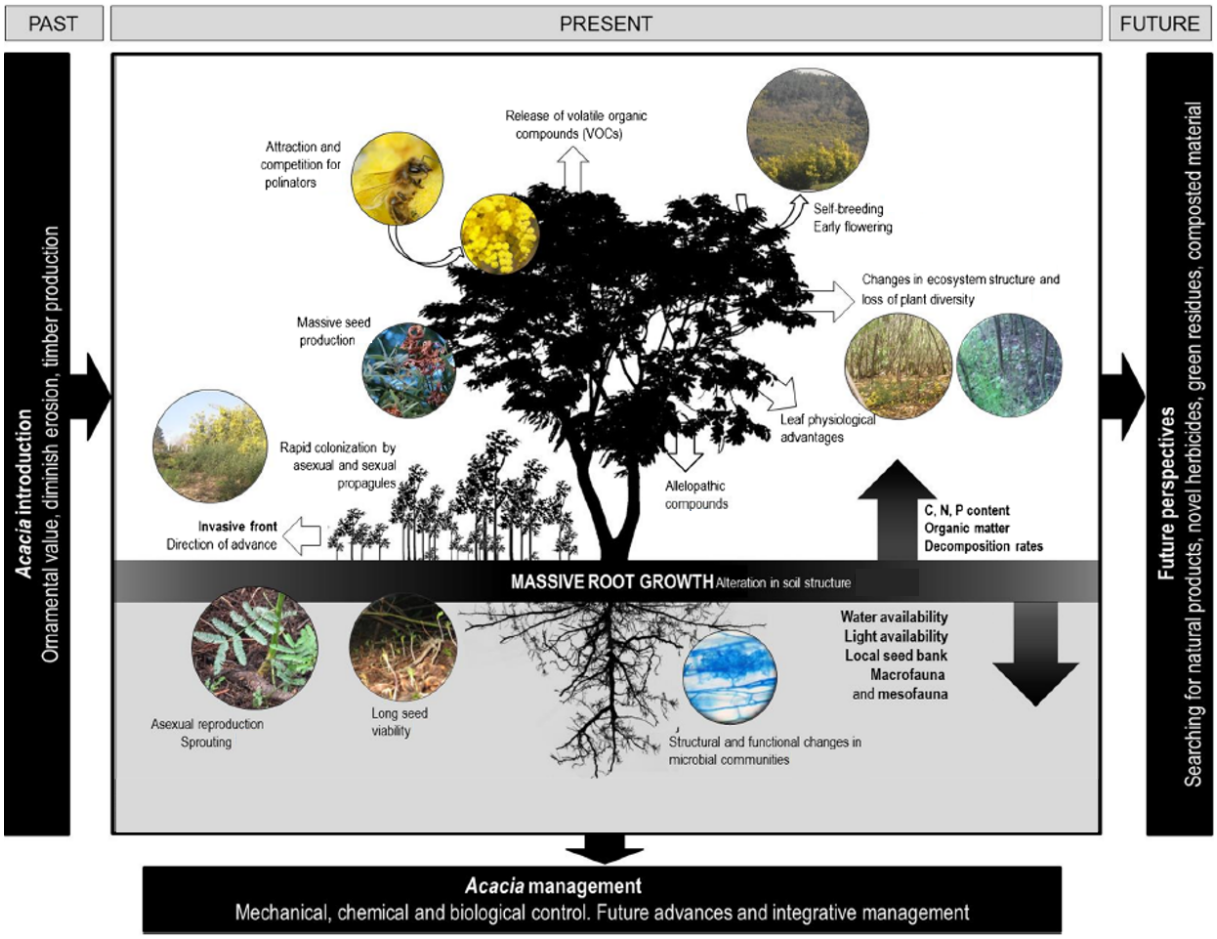

Figure 10: The figure is a visual summary of the colonization process of *Acacia dealbata* Link since its introduction (past), its interaction with biotic and abiotic agents (present) and its final stage of consolidation (future). The base image was extracted and adapted from "*Here to stay. recent advances and perspectives about acacia invasion in mediterranean areas*" by Souza-Alonso et al. [59].

2.4.2.1 Control Methods and Economic Valuation

Controlling genus *Acacia* species in northern Iberian has yielded inconclusive results [81]. Mechanical, chemical, and biological techniques have shown only partial and limited success. Chemical control using herbicides like Triclopyr, combined with cutting and bark stripping, is among the most commonly employed methods for control and eradication, though its applicability remains limited. Furthermore, these control efforts should ideally be complemented by soil restoration, preferably with native species sharing attributes similar to those of the invasive ones.

In the context of *Acacia dealbata* management within the Peneda–Gerês National Park, Henrique Reis (See Appendix A and 20) reports that the control strategy prioritises the removal of isolated specimens. This approach has proven to be the most effective, as it requires less effort and offers a higher success rate; in many cases, these individuals have not yet produced seeds. The second priority is the intervention in small, localised areas, followed by work in larger infested zones, proceeding from the periphery towards the centre. Control methods are primarily mechanical, supplemented in some cases by shading using other plant species. The main implementation challenges include a shortage of human resources, the

complex topography of the terrain—particularly in areas near residential properties—which greatly hinders field operations, and the occurrence of frequent wildfires, which tend to favour the spread of *Acacia dealbata* over native species.

There are no comprehensive studies evaluating the economic profitability of harvesting *Acacia dealbata* logs. Nunes et al. [79] provide cost estimates for clearing juvenile specimens (less than 20 years old) to assess their potential use as biomass. Reported costs range from 10 €/t to 60 €/t, encompassing felling and branch removal, retrieval and extraction, and transport operations (including loading and unloading). These costs are highly dependent on operational conditions, such as the size of the intervention area, slope gradient (often in proximity to inhabited areas), the possibility of employing heavy machinery, the availability of access routes, and the presence of other vegetation types that necessitate careful separation.

Given that current biomass market returns approximately 15 €/t cover only a fraction of these expenses, Nunes et al. [79] propose that careful planning and an optimised logistical framework, ensuring a regular supply of biomass, could potentially double the market price. Profitability could also be enhanced by increasing the added value of forest by-products, thereby integrating them into a more complex and diversified value chain.

2.4.2.2 By-Products of *Acacia dealbata* Species

The valorisation of *Acacia dealbata* through its by-products (e.g., flowers, seeds, bark) presents economic potential across multiple sectors. Lorenzo et al. [126] examined the use of *Acacia dealbata* flowers as a bioherbicide, demonstrating its effectiveness in enhancing wheat crop growth while contributing to the reduction of seed dispersal. The species also exhibits allelochemical properties that, although inhibitory to native plants, can be advantageous for weed control [127]. In the field of animal nutrition, Uushona [128] investigated the incorporation of flour derived from *Acacia mearnsii* and *Acacia dealbata* leaves into ruminant diets. In the chemical and biomedical domain, Correia et al. [129] reported antimicrobial properties in leaf and branch extracts of *Acacia dealbata*, with bactericidal activity against selected pathogens.

In industrial applications, Teixeira et al. [129] demonstrated that *Acacia dealbata* bark can significantly reduce the environmental impact of cotton dyeing processes by lowering CO_2-equivalent emissions compared to conventional methods [130]. Similarly, Ranesi et al. [131] evaluated the incorporation of *Acacia dealbata* bark residues into plaster mortars, obtaining promising results for interior cladding in construction.

Despite these researches, the use of small-diameter *Acacia dealbata* roundwood for structural applications is unexplored in Portugal. Research on logs for structural use has been conducted in Portugal, such as the work of Morgado et al. with Maritime Pine logs [26, 132, 133]; in Brazil Zangiacomo et al. with *Pinus elliottii* and *Eucalyptus citriodora* logs [134, 135]; and in Germany, different researchers had studied Green oak (*Quercus petraea*) low-processing logs [136, 137, 138]. In recent years, there has been growing interest in promoting hardwood species for construction, driven by the global increase in wood demand. As with Eucalyptus in Portugal, certain hardwoods are abundant in Europe. Merz et al. [54] analyse and promote the construction sector uses of hardwood species existing in Europe, including Oak, Ash, Maple, Birch, Beech , Chestnut, Eucalyptus and Poplar. At the same time, other studies have

explicitly focused on their performance in structural connections using hardwood [139]. Hardwoods typically exhibit superior physical and mechanical properties compared to Softwoods [140]; however, their use poses several challenges, including higher processing costs due to greater hardness, greater variability between species and individual specimens, and lower sawn timber yield per tree [54]. For *Acacia dealbata* in particular, it is essential to recognise that utilisation strategies must be subordinate to its control as an invasive species, especially in protected natural areas.

In Chile, the Forestry Institute assessed the physical and mechanical properties of *Acacia dealbata* boards sourced from the south-central region, confirming their technical viability for construction applications [56]. However, this Chilean approach prioritised support for small-scale local timber producers and did not address the significant environmental concerns associated with the species' invasiveness. While a similar strategy might offer economic opportunities in Portugal, the arguments presented here suggest that management efforts should prioritise the control and eradication of *Acacia dealbata* rather than its purely economic exploitation. This would entail classifying the species as a renewable resource only under particular conditions or, paradoxically, as a non-renewable resource.

2.4.2.3 Characterisation of the *Acacia dealbata* Species

The genus *Acacia* s.l. comprises approximately 1300 species [141] within the Mimosoideae subfamily (Fabaceae family). Distributed across various ecosystems worldwide, *Acacia* species exhibit similar characteristics and behaviours [142]. They are highly adaptable to rainy areas, can thrive in diverse soil types, and produce resilient, long-lived seeds with high germinability. The seeds can disperse over large distances through biotic and abiotic means and often re-sprout or germinate in vacant niches e.g., after forest fires posing a threat to native species by disrupting pre-existing ecological networks. This quality defines *Acacia* as an invasive plant, i.e., "able to spread and suppress native plants" [142], differentiating it from other introduced plants considered "casual" or "naturalized" in exotic environments.

While genus *Acacia* originated in southeastern Australia (New South Wales) [142, 143], certain species, such as *Acacia dealbata* Link, have expanded globally to places like New Zealand, Madagascar, South Africa, and Chile [144]. In Europe, it is found along the northern Mediterranean coast of Italy [145, 146] and in Iberian northern Spain [112, 113] and Portugal, where it is considered a highly invasive species, triggering specific legislation in these countries addresses its control and management. It is known by various common names, such as mimosa, aromo, and French Acacia [147]. In English, it is also called silver green wattle, silver wattle, sydney black wattle, and wattle bark, and acacie blanchatre and mimosa argente in French [148]. Notably, *Acacia dealbata* ranks sixth among the "100 worst" alien species in Europe, as developed by Nentwig et al. [57] ranking, demonstrating its substantial economic and environmental impact as the top-ranking plant on a list of 486 invasive species, including among others mammals, fishes, birds and plants.



Figure 11: *Acacia dealbata* Link: (a) Isolated tree, (b) branch and bipinnate leaves, and (c) pod and seed (all these images are from [149]). (d) Image of *Acacia dealbata* stands with its characteristic yellow flower (March 2021) from Serra da Estrela (Portugal) by Raposo et al [60]. The authors of the image highlight that the stands develop along the line of water courses.

A mature tree of *Acacia dealbata* has a greyish trunk reaching between 4 and 20 meters in height (Figure 11a). Its bipinnate leaves measure 10–20 cm in length, with some displaying a silvery hue (Figure 11-b). During winter, *Acacia dealbata* produces conspicuous yellow flowers arranged in dense panicles, which bloom from January to March in Portugal (Figure 11d). The species bears dry, hard legumes between 4 and 10 cm long, flattened and slightly narrowed between the seeds (Figure 11c). It reproduces vegetatively through re-sprouting after cutting or fires and through seeds, forming a persistent seed bank germinating rapidly following disturbances like fires [141].

There is limited anatomical research on *Acacia dealbata*. Macro- and meso-anatomical observations of cross-sections collected from Portugal's Peneda-Gerês National Park reveal general characteristics (Figure 12a): clear differentiation between heartwood and sapwood, with growth rings that are indistinct, either diffuse or semi-diffuse, affecting the discernibility between earlywood (spring) and latewood (winter). Microscopic studies of samples from Portugal and Curitiba, Brazil [147] describe several features. At the conductive and storage level, rays and pores are visible to the naked eye. The rays are frequent and unstratified, while the pores are medium-sized and diffusely distributed. Vessels (for conduction) are large and sparse, occupying approximately 12.2% of the cross-sectional area. The libriform fibres, which provide strength, are non-septate with small, simple pits, making up roughly two-thirds of the wood volume. These observations align with Figure 12b,c,d,e,f,g which shows images of samples from southern Chile. A similar micro-anatomical description for Australian temperate climate *Acacia* species has been noted by Warwick et al [143].

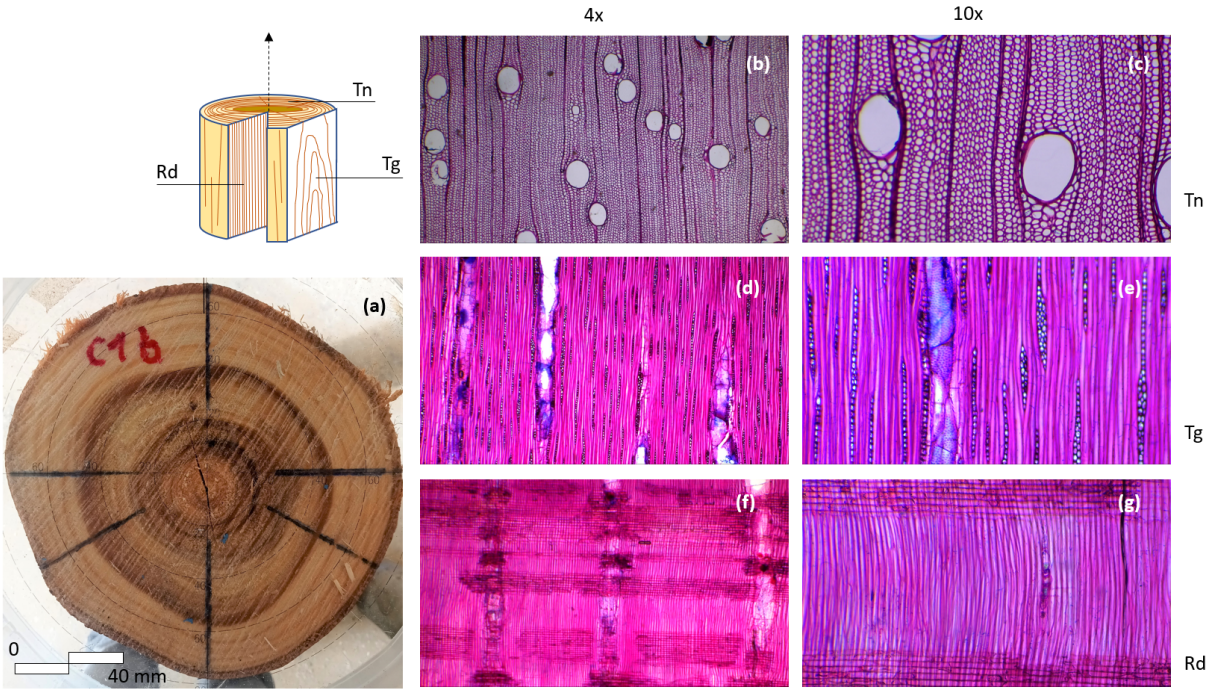

Figure 12: Anatomy of *Acacia dealbata* Link.(a) View of a typical section (1 m from the ground) from a tree in the Peneda-Gerês National Park. Microscopic view of samples from southern Chile: (b)-(c), Tn = transversal section; (d)-(e), Tg= tangential to the rings section; and (f)-(g), Rd= radial section through the rings. Images provided by Linette Salvo-Sepúlveda.

2.5 Chapter conclusions

Forest management by-products, including small-diameter roundwood (*srw*), represent an available yet underutilized resource. Beyond their potential applications in various sectors, evidence suggests that when carefully selected and minimally processed, *srw* can achieve competitive performance in specific construction uses—such as shelters, lookout points, small structures, or observation towers. These advantages are complemented by other benefits, including the reduction of forest fuel loads, alignment with thinning objectives, and the creation of opportunities to develop value chains at the rural level.

In the Portuguese context, however, the rapid expansion of the invasive species *Acacia dealbata* within protected areas poses a dual challenge. The ecological impacts of this species, the legal restrictions on its spread, and the high risk of reinvasion imply that any potential use must remain strictly subordinated to control and restoration objectives. Conversely, targeted valorization could help offset control costs while diversifying the supply of sustainable wood-based products in a context of growing market demand. This is achievable by channeling part of the extracted biomass into higher value-added products, provided that interventions are ecologically sound, time-limited, and integrated within sustainable management strategies.

These considerations support the research lines addressed in the following chapters of this study: the establishment of technical and logistical criteria for the pre-selection of *Acacia dealbata* logs suitable for structural applications, and the development of grading, drying, and minimal-processing protocols aimed at mitigating defects inherent to juvenile wood and the drying process.

Chapter 3

Mechanical Characterisation of small-diameter roundwood (*srw*) of *Acacia dealbata* Link

The study of residual logs derived from young trees without silvicultural management remains limited. While some research has examined the physical and mechanical properties of *Acacia dealbata* in Chile [56] and *Acacia melanoxylon* in Portugal [55], these studies predominantly focus on sawnwood production, and therefore, they address larger-diameter roundwood. In contrast, the mechanical characterisation of juvenile (15–20 years), small-diameter logs (<150 mm) with potential applications in structural systems is sparse.

To address this gap, the present study presents and analyses the results of destructive tests conducted on representative samples of low-processed logs derived from the control of the invasive species under investigation (*Acacia dealbata*). The first part of this study characterises the physical-mechanical behaviour of the species, providing support for its potential use in structural applications with characteristic values of reference. A subsequent comparative analysis is conducted with small, defect-free samples to substantiate the initial findings and to clarify emerging issues, such as the influence of the harvest season.

3.1 Mechanical Performance of *srw* Logs with Minimal Processing

Although research has been conducted on the use of small round wood (*srw*) as raw material for engineered wood products [95], *srw* logs derived from thinning operations generally exhibit limited sawn timber yield. For this reason, their optimal application lies in structural uses requiring minimal processing [25]. Studies on the physical mechanical performance of logs in general and *srw* in particular remain considerably more scarce when compared with the extensive literature on sawn timber of rectangular section, which is the dominant raw material for engineered wood products (EWPs). Nevertheless, in light of the significant increase in global demand for timber in the construction sector [9], the valorisation of residual materials derived from forest management has gained momentum in scientific research, driven mainly by economic and environmental imperatives [6, 136, 137, 32].

Several authors have demonstrated that silvicultural conditions, whether in natural or plantation forests, influence the mechanical performance of wood. Simic et al. [150] confirmed that stand density has a strong effect on timber properties. In *Sitka spruce* plantations, lower stand densities (<1850 stems $\times ha^{-1}$) increase total harvest volume, whereas higher densities (>3100 stems $\times ha^{-1}$) enhance the mechanical properties of logs and boards. Similarly, Rais et al. [151] investigated the influence of planting density on the tensile strength of *Douglas-fir* boards. They found significant differences across three regimes (1000, 2000, and 4000 trees $\times ha^{-1}$), with higher planting densities producing superior characteristic values. The same author also demonstrated that greater stand density reduces knot frequency in *Douglas-fir* boards [152].

From a mechanical perspective, trees in their natural form are highly adapted structures for withstanding loads arising from self-weight and environmental forces such as wind. Their conical stem resembles a cantilever beam model [10], while anatomically, trees are composed of resistant tissues tracheids in

softwoods and libriform fibres in hardwoods that are organised to distribute structural capacity according to loading demands during growth [23, 140]. Consequently, the physical–mechanical properties of a tree can vary considerably, not only between different individuals within the same stand or species but also within a single tree, depending on its environment. For example, Langum et al. [153] reported that in *srw* of *Douglas-fir* and *Western hemlock*, strength and stiffness decrease linearly with tree height (less resistance at greater height) and radially from outerwood toward the pith (lower strength near the pith), i.e., juvenile wood has less mechanical resistance than mature wood. However, Fischer et al. [154] noted that longitudinal variation in wood density is not fully consistent across species, as it ultimately depends on site-specific growing conditions.

With respect to load-bearing efficiency, the circular cross-section of logs presents certain advantages. Unlike rectangular sections, a circle has an infinite number of axes of equal resistance around its centroid. In contrast, rectangular sections exhibit either two equivalent moments of inertia (I) in square sections or distinct strong/weak axes in rectangular sections. Wolfe and Murphy [155] provided an analytical comparison of circular and rectangular sections, demonstrating the expected reduction in mechanical capacity of the latter when sawn from round logs. Moreover, bending stresses are reduced more severely in rectangular sections because resistance increases with the distance of fibers from the centroid. The section modulus ($S = I / y_{max}$) of circular logs is between 1.5 and 3.0 times higher than that of comparable rectangular sections. At the same time, the moment of inertia (I) - a key parameter for a stiffness controlled design - ranges from 1.8 to 3.1 times higher. Nevertheless, deviations from stem straightness can occur due to slope, wind exposure, or asymmetric crown development. These environmental influences can induce ovality in the stem cross-section at zones of greatest stress [156], or curvature in the stem axis, resulting in a deformation commonly referred to as “crook” [157]. In highly stressed regions, trees may also develop reaction wood (see Figure 13), an adaptive tissue formed to restore stem verticality [23]. In hardwoods this is known as tension wood, while in softwoods it is referred to as compression wood [158]. Reaction wood is associated with denser but more brittle tissue in softwood, which complicates processing. Growth stresses may be released after felling, manifesting as cracks. According to Gril et al. [158], this phenomenon is particularly pronounced in young, fast-growing hardwood species, such as *Populus* spp., *Acacia* spp., and *Eucalyptus* spp.

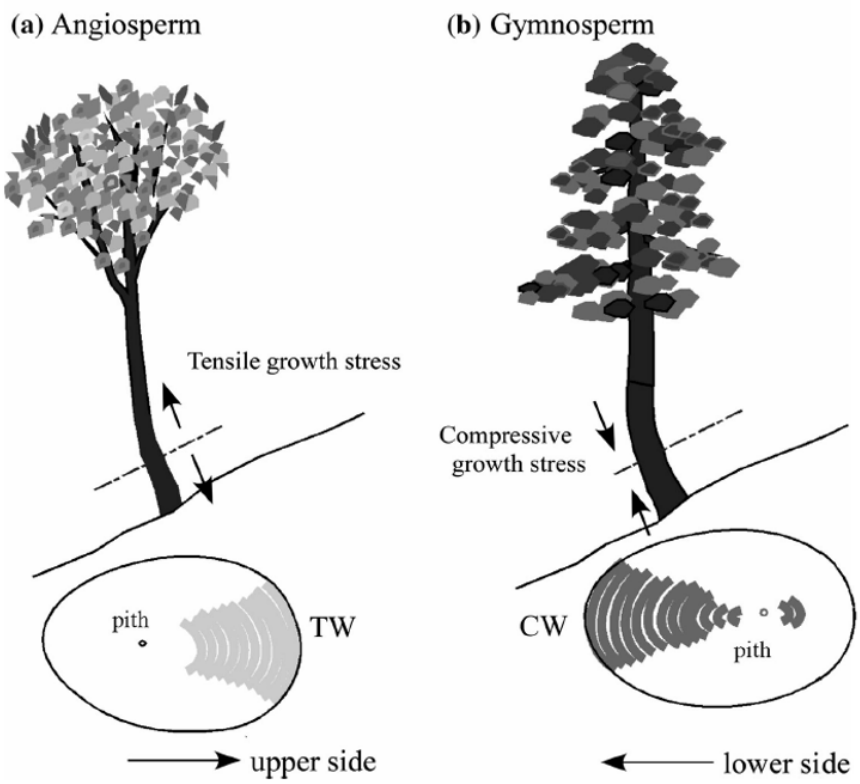

Figure 13: Reaction wood formation in an inclined stem. (a) Tension wood in angiosperm (hardwood). (b) Compression wood in gymnosperm (softwood). Image from "*Tree growth stress and related problems*" [158] based on the Illustration of H. Yamamoto.

Another growth-related defect is the spiral grain, in which successive growth layers develop at an angle relative to the longitudinal stem axis. The spiral grain reduces mechanical strength, increases susceptibility to swelling and shrinkage under fluctuations in moisture, and causes greater distortion during drying. In logs, this can lead to end-rotation between extremities, while in sawn timber it complicates machining operations [23]. Dinwoodie [140] observed that grain angle markedly reduces wood stiffness, with the modulus of elasticity declining significantly between 0° and 30–40° relative to the specimen axis.

3.2 Factors Affecting the Mechanical Performance of Logs

3.2.1 Juvenile Wood

Low-processed logs that contain a high proportion of juvenile wood (JW) exhibit a number of inherent irregularities, including pronounced ovality, taper, growth-induced curvature, and a limited proportion of mature wood (MW). In general terms, JW refers to the wood formed closest to the pith, in contrast to MW, which develops toward the periphery of the stem [159]. To avoid direct association with chronological age, some authors instead adopt the terms corewood and outwood, which more accurately reflect the radial location of the tissue within the tree [44]. The number of growth rings marking the transition from JW to MW is not universally defined and varies according to species, position along the stem, and other factors.

However, several studies approximate this transition at around 20 growth rings [11, 159].

The anatomical and mechanical characteristics of JW differ markedly from those of MW [44, 95]. At the microanatomical level, JW typically presents shorter and narrower cells with thinner cell walls, as well as a larger microfibril angle in the S2 layer. This angle varies across species, being greater in softwoods such as pines (40°–50°) than in hardwoods such as eucalyptus, poplar, and birch (25°–35°). At the macroanatomical level, JW is characterized by a higher spiral grain angle generally reaching a maximum in the innermost rings and decreasing toward the periphery as well as a higher incidence of reaction wood (Figure 14).

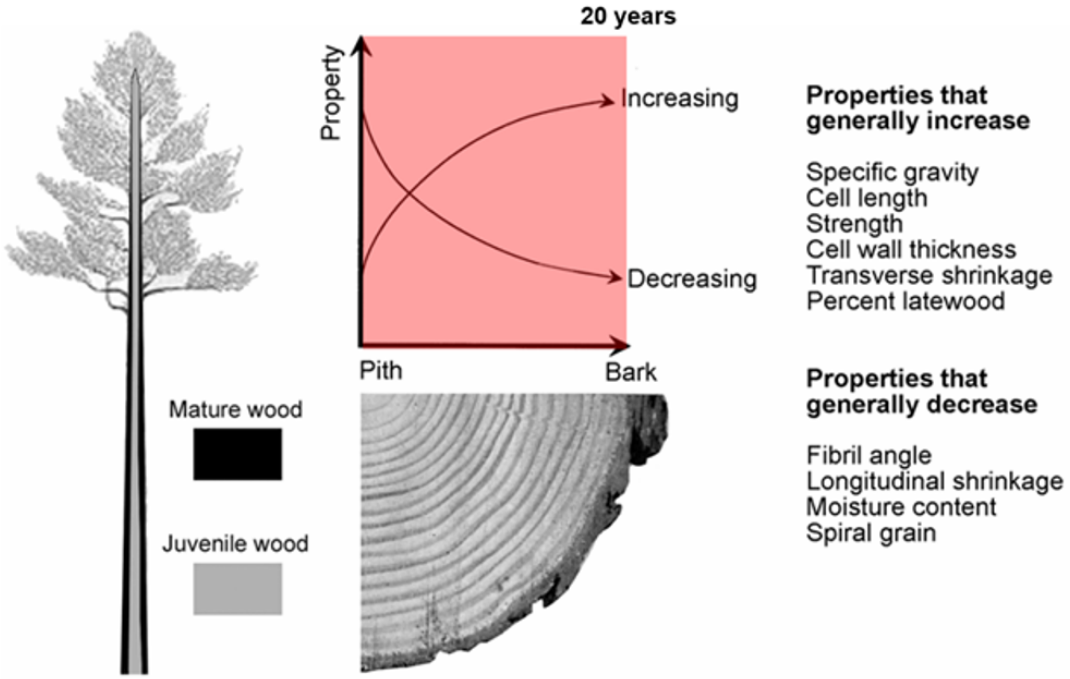

Figure 14: Corewood or Juvenile wood (JW) distinctive characteristics, according Moore and Cown [44].

These features directly influence the physical-mechanical properties of the the logs. JW is generally associated with lower density, reduced modulus of elasticity (MOE) and modulus of rupture (MOR), and greater longitudinal shrinkage, which in turn leads to a higher tendency to distort during drying. Spiral grain and reaction wood further reduce stiffness and increase susceptibility to internal cracking. Larson et al. [11], for example, demonstrated a clear reduction in MOR in *Ponderosa pine* logs containing a higher proportion of JW.

One common strategy to improve the appearance and workability of rustic logs is machining them into cylindrical form. However, this process often removes a proportion of the peripheral mature wood, thereby increasing the relative proportion of structurally weaker JW [44] (See Figure 15). While machining to a constant section may not strongly affect grain angle at the surface, it does expose JW, knots, and reaction wood, which act as local zones of weakness. Green et al. [12] investigated the influence of machining on the mechanical properties of small-diameter logs. They reported that adjusting *Douglas-fir* and *Ponderosa pine* logs to a constant diameter reduced MOR by 8–12% and MOE by 15–33%, primarily due to the removal of mature wood. Similarly, Vega et al. [13] observed that increasing the proportion

of JW in *Castanea sativa* logs (from 20% to 80%) significantly reduced MOE and density in a consistent pattern. However, the authors noted that MOR did not follow a clear trend, likely due to the confounding effects of knots and grain deviations.

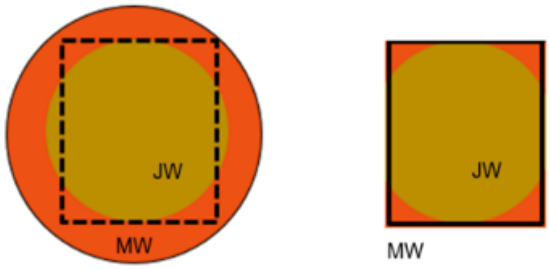

Figure 15: Diagram to explain the reduction of mature wood (MW) and the relative increase of juvenile wood (JW) by the sawing process (based on Baxter [111]).

Consequently, one strategy to mitigate the adverse effects of JW is to preserve the natural stem shape by maintaining a low level of processing. In small-diameter logs, the juvenile core is typically surrounded by a sheath of mature wood, particularly in the basal section of the stem (Figure 15), which partially offsets the mechanical drawbacks of JW and provides additional strength [155]. Moreover, retaining natural outgrowth fibres helps reduce the detrimental impact of certain defects, such as grain deviation and knots, which, in sawn wood, are well known to affect mechanical performance and lower strength [160]. This effect arises because such "defects" are naturally integrated into the growth of the tree. In unprocessed, tapered logs, the grain follows the external curvature of the stem, remaining parallel to the surface and continuously enclosing knots. In contrast, when timber is sawn, knots are exposed and the associated grain deviation terminates abruptly at steep angles relative to the cut surface. This discontinuity introduces stress concentration points that substantially weaken rectangular sections, as demonstrated by Derikvand et al. [17]. The resulting strength reduction is primarily expressed as increased variability due to premature failures occurring at these localized zones of grain interruption.

Several studies have confirmed that the mechanical performance of minimally processed logs surpasses that of machined or sawn counterparts derived from the same stem. Sandoz [161] reported mechanical strength increases exceeding 30% when comparing debarked rustic spruce logs with square-sectioned counterparts, attributing the difference to the natural optimization of the growing tree. Similarly, Ranta-Maunus [25] demonstrated that the bending strength of small-diameter round timber from northern European conifers is often higher than that of sawn timber obtained from the same logs. Conversely, Larson et al. [11] observed that mechanically reshaping *Ponderosa pine* logs into perfect cylinders resulted in the removal of a substantial proportion of mature wood particularly in the basal zones which corresponded to reductions of 20.3% in the MOR and 10.0% in the MOE.

3.2.2 Density

Density, defined as the ratio of mass (or weight) to volume, is always expressed for wood at a specific moisture content. According to the Wood Handbook [162], density represents one of the most critical physical properties for wood characterisation. Reported values of density are typically expressed as averages; however, like most wood properties, density is highly variable and species-specific [140]. Intra- and inter-tree variability is considerable: density differences may be observed between earlywood and latewood, heartwood and sapwood, pith and outerwood, the basal and upper stem regions, as well as among trees of the same species within a single stand, between sites and species [140].

From an anatomical perspective, density reflects the proportion of voids within the cellular tissue. In softwoods, it is primarily determined by the relative proportions of earlywood and latewood and the thickness of the cell walls: a greater proportion of latewood typically results in higher density, whereas a dominance of earlywood leads to lower density. In hardwoods, density is influenced not only by fiber cell-wall thickness but also by the volumetric proportion of vessels and parenchyma (tissues with lower density), reflecting their more complex anatomical structure [162].

Density is also closely linked to the mechanical properties of wood. Dinwoodie [140] highlights that correlations between density and the MOE are generally strong, often with correlation coefficients exceeding $R^2 = 0.8$. For species-level assessments, the Wood Handbook [162] recommends linear correlation analyses between density and mechanical properties. Schematic relationships between density and selected mechanical parameters are illustrated in Figure 16. Accurate determination of volume, and therefore density, becomes particularly challenging in irregular bodies such as minimally processed logs. Advanced techniques, such as laser scanning, provide precise measurements [163]. Simpler methods include taking multiple-section measurements along the specimen or applying the water displacement or immersion method (as described in the ASTM D2395-17, 2013 [164]), which is particularly suitable for smaller specimens, such as log slices.

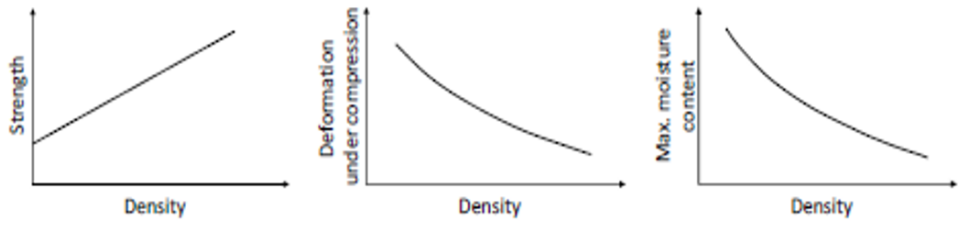

Figure 16: Schematic relationships between density and various variables: (a) strength; (b) compression strain; and (c) moisture content. According Blass et al [23].

In addition, various semi-destructive and non-destructive testing (NDT) methods have been shown to correlate favourably with density. For example, Sharapov et al. [165] reported coefficients of determination (R^2) ranging from 0.60 to 0.89 when using a resistograph on multiple species, including Scots pine, beech, oak, and lime. Similarly, Faggiano et al. [35] achieved $R^2 = 0.6$ by combining resistograph data with ultrasonic testing and a sclerometric hammer in chestnut (*Castanea sativa* Mill.) specimens recovered from historic structures.

3.2.3 Moisture Content

The influence of moisture content (MC) on the physical and mechanical behaviour of wood has been extensively investigated and documented [23, 162, 140, 36, 159]. At high MC levels, permanent loads can increase creep, and above 20% MC wood becomes highly susceptible to fungal attack.

Freshly felled trees contain large amounts of water essential for physiological activity—typically ranging from 60% to 200% of oven-dry mass [140]. Once felled, moisture loss begins as a result of temperature and relative humidity conditions, triggering a process of internal water transport within the cellular structure. The initial drying phase involves the evaporation of free water from cell lumina. When this phase is complete, only bound water remains within the cell walls. The threshold between these two stages is referred to as the fiber saturation point (FSP), which generally lies between 25% and 30% MC depending on species. Below the FSP, water loss continues within the cell walls until the wood reaches equilibrium moisture content (EMC), a balance with the surrounding environment.

The range of MC between the FSP (≈30–25%) and approximately 8% is particularly critical for mechanical performance. Within this interval, an inverse and approximately linear relationship is generally observed between MC and mechanical properties, although the slope varies depending on the species (Figure 17). Above the FSP, mechanical properties remain essentially constant. Dinwoodie [140] notes that timber at 12% MC exhibits a higher MOE compared with green wood. Arriaga et al. [159] further explain that bending stiffness is not significantly altered because the gain in MOE is counterbalanced by the reduction in moment of inertia (I) associated with shrinkage during drying.

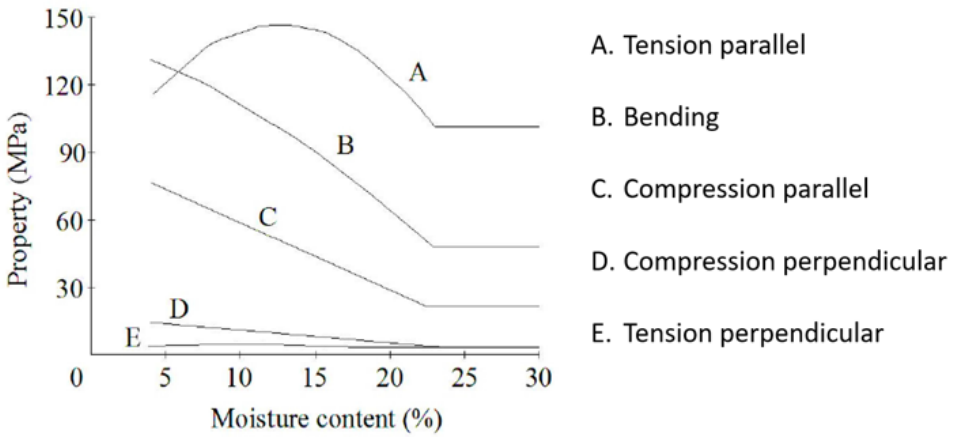

Figure 17: Relationship between moisture content (MC) and different wood strengths (adapted from Wood Handbook [162]).

The relationship between MC and strength is less pronounced when defects such as knots or grain deviations are present, as these tend to dominate failure behaviour. In such cases, the beneficial effect of reducing MC diminishes with increasing knot size or grain angle [140]. Conversely, in high-quality, defect-free wood, reducing MC can significantly increase strength. For example, Ido et al. [166] compared sugi (*Cryptomeria japonica*) piles at green condition (MC = 75.8%) and after air-drying (MC = 17.6%), observing a consistent, though modest, increase in bending strength.

Ido et al. [166] also highlighted a size effect in the influence of MC: the relative increase in strength when drying from green to air-dry conditions is more pronounced in smaller specimens. The effect is largest in small clear samples, smaller in boards, and further reduced in square or round timber. This trend was confirmed by comparisons across round timber of different diameters (12–14 cm, 16–20 cm, and 18–22 cm), where smaller diameters exhibited proportionally greater increases in strength with decreasing MC.

Moisture Content is most reliably determined using the oven-drying method, standardized in ISO 3130 [167]. This procedure involves extracting a representative sample, immediately recording its mass, and oven-drying it at 103 °C ± 2 °C until a constant mass is reached. The dry mass is then used to calculate MC as the percentage of water relative to oven-dry mass [36]. Alternative methods are widely employed in practice, including electrical resistance meters (suitable for MC > 6%) and dielectric devices that measure surface properties to estimate MC up to a penetration depth of approximately 35 mm [36].

3.2.4 Temperature

The mechanical performance of wood is significantly influenced by temperature (Figure 18). At elevated temperatures, the MOE and MOR of clear, defect-free specimens decrease, while cooling generally enhances these properties [162, 23]. Dinwoodie [140] further observed that the effect of temperature is amplified when moisture content (MC) is considered as an interacting variable. For example, when temperature increases from 20 °C to 60 °C, specimens at 12% MC exhibit a 15% reduction in MOE, whereas specimens at 20% MC show a 25% reduction. This effect also tends to be more pronounced in hardwoods than in softwoods.

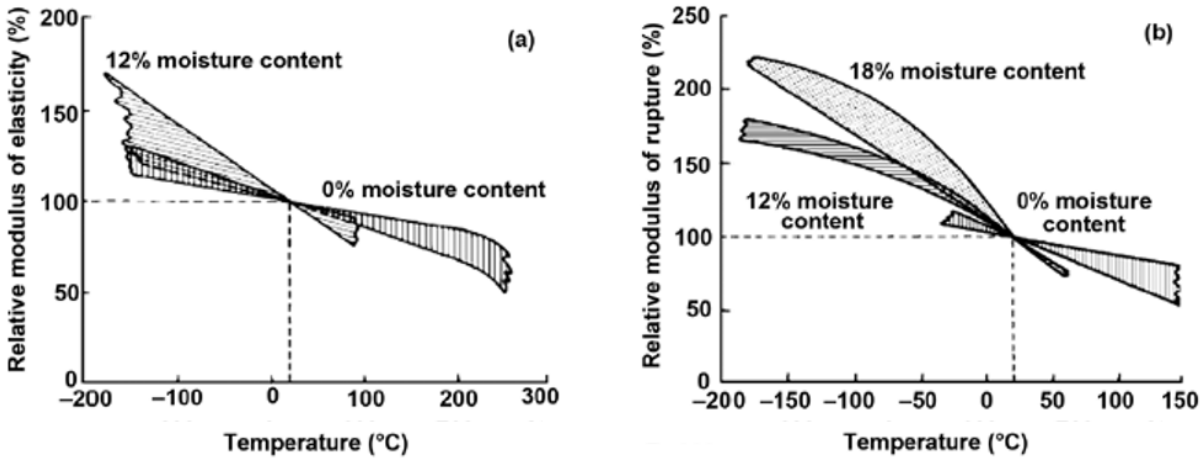

Figure 18: Immediate effect of temperature at various moisture content levels (0%, 12%, and 18%) relative to the value at 20°C for clear, defect-free wood: (a) MOE parallel to the grain, (b) MOR. The graph is a composite of results from several studies. Variability in reported trends is illustrated by the width of the bands. From Wood Handbook [162].

In the context of fire safety design, reliable prediction of temperature-dependent strength reduction is essential. Garcia-Castillo et al. [168] proposed a probabilistic model to estimate reduction factors for

structural timber exposed to elevated temperatures. Their review of state of the art studies on timber under parallel to grain tension and compression at temperatures ranging from 20 °C to 300 °C highlights the role of multiple variables, including MC, density, and specimen size. While the correlation between MC and strength was reaffirmed, the influence of other factors—such as density and scale effects—remains less clearly defined.

3.2.5 Cracking Formation

Moisture transport during drying causes the expansion and contraction of wood tissue, leading to dimensional variations. In larger elements such as logs, this phenomenon is often accompanied by uneven internal moisture distribution, which generates moisture gradients (MG) across both the cross-section and longitudinal axis. As drying progresses, these gradients induce internal stresses that can ultimately lead to the formation of cracks.

Figure 19a illustrates the temporal variation of the MG in the central section of an 80 cm length *Acacia dealbata* log. During the first week, the outwood moisture content (MC) decreased rapidly from approximately 37% to around 20%, then continued to decline more gradually toward values near 15%. In contrast, the reduction near the pith was slower and more progressive. For nearly three weeks, the differential in MC between the outer and inner regions of the log ranged from 10% to 15%. This imbalance generates differential stresses: wood near the pith, retaining higher MC, tends to expand, whereas the drier outwood contracts.

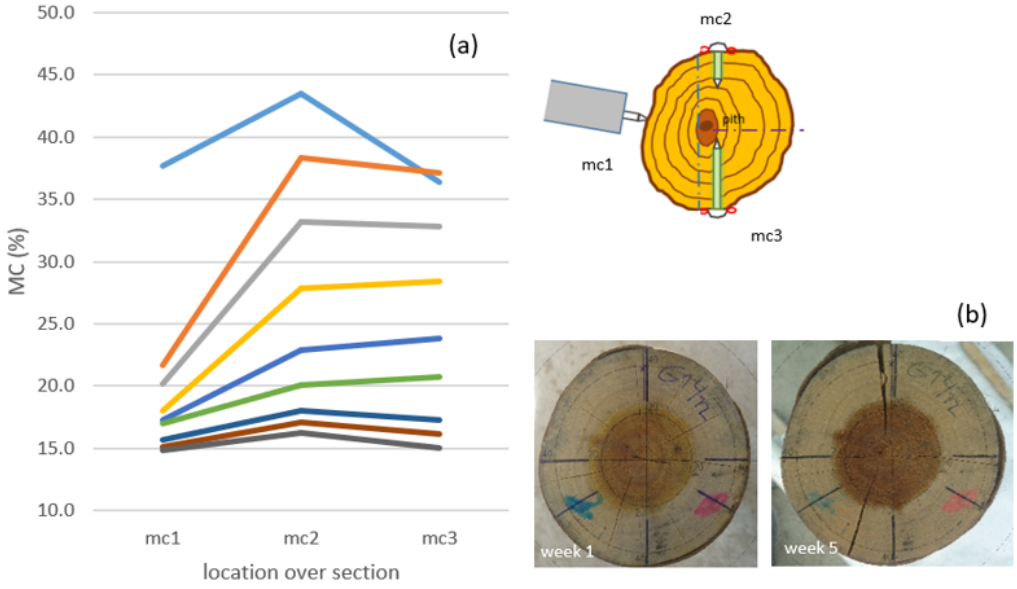

Figure 19: (a) Variation of the moisture gradient in *Acacia dealbata* logs inside a climate chamber at a temperature of 20°C (±0.5°C) and relative humidity of 60% (±5%), measurements at the centre of the log each week at three depths: mc1= outwood; mc2 = ± 20 mm; mc3 = close to pith. (b) Formation of cracks at the end of the log after 5 weeks.

When drying stresses in the contracting zones exceed the tensile strength capacity of the wood—particularly in the tangential plane—cracking occurs. Figure 19b shows the end faces of *Acacia dealbata* logs

after four weeks of controlled drying in a hygrothermal chamber, where checking patterns typical of this process can be observed. These drying-induced cracks occur in addition to those arising from growth stresses, jointly compromising the mechanical integrity of the logs.

Research explicitly addressing the relationship between drying-induced cracking and the mechanical performance of full-size logs remains limited. However, some studies on rectangular timber members provide insights. Esteban et al. [169] investigated longitudinal cracks in Scots pine beams with cross-sections of 100.120 mm² and 100.150 mm². Although cracked areas occupied 45% or more of the shear resistant zone in the mid height region, no significant correlations with bending or shear failure modes were identified. In contrast, Mergny et al. [170], studying 71 Oak beams with cross-sections of 100.100 mm² and 180.180 mm², concluded—through analytical and numerical analysis—that horizontal radial cracks were particularly detrimental, reducing bending stiffness by 5% to 25%.

Further evidence is provided by Zhang et al.[171], who examined horizontal cracks in Scots pine beams with cross-sections of 80 × 110 mm² and 133 × 130 mm². Their results indicated that when crack depth exceeded 25% of beam width, the dominant failure mode shifted from pure bending to combined bending and shear, driven by horizontal sliding in the central third. This shift was accompanied by marked reductions in strength, stiffness, and ductility relative to uncracked beams.

Several authors have highlighted the importance of studying end-cracking in logs, as it directly affects the performance of structural connections [25, 172]. For example, Chahade and Schober [173] investigated bonded-in threaded rods anchored with polymer concrete in predrilled log holes. They observed tensile failure patterns strongly associated with the presence of radial end fractures. Their results emphasize that such cracks must be identified and controlled, recommending a maximum of four perpendicular radial cracks. Additionally, they recommend avoiding heartwood in the central bore, as it alters strength properties, and excluding this connection type from applications in service class 3 conditions (MC > 20%).

Another critical factor influencing the mechanical performance of round timber relates to the subtraction of load-bearing material during joint fabrication. In log to log connections, cutbacks for coupling must be minimized. Green et al. [12] recommend limiting such reductions to 30% of the log radius, corresponding to only a 10% loss of cross-sectional area. However, knowledge of longitudinal (σ) and transverse (τ) stress distribution in circular sections remains limited. Dewey et al. [98] analyzed stress implications of notching at log supports, showing that local reductions in section can significantly alter stress flow and failure mechanisms. Similarly, Villasante et al. [174] studied continuous cuts along round sections to create flat surfaces, which facilitate connections but also modify bending behavior.

To mitigate cracking caused by drying stresses, some researchers have proposed hollowing logs, thereby reducing internal moisture gradients. Lim et al. [50] tested this technique for highway guardrail applications and found that small-diameter hollow sections retained comparable bending performance to solid logs. However, subsequent experiments on center-drilled round specimens subjected to point bending revealed inconsistent outcomes: strength values were lower than expected, and failures were dominated by tangential cracking. These findings underscore the inherently low tangential strength of completely hollowed sections, raising concerns about the practical applicability of this technique.

3.3 Mechanical Characterisation of Wood Logs

The grading of timber is a critical aspect in timber engineering, as it directly influences structural safety, serviceability, and the efficient use of forest resources. To address this issue, several standards have been established for the characterization and mechanical grading of logs and sawn timber intended for structural applications.

As described by Bukauskas et al. [6], there are three principal approaches for determining the mechanical properties of timber elements, which may be applied either independently or in combination:

1. Visual strength grading: Characteristic values are assigned according to standardized visual grading rules or through certified grading agencies. In this approach, the wood species and its geographical origin must be explicitly included in the grading guidelines, and the pieces must satisfy the minimum requirements specified therein.

2. Destructive testing of representative samples: A statistically adequate number of specimens representative of the material population is subjected to destructive testing under controlled laboratory conditions. The results are then used to infer characteristic values applicable to the remaining material.

3. Non-destructive evaluation: In this approach, a predictive model is first developed using non-destructive testing (NDT) or evaluation techniques applied to a representative subset of specimens. The resulting model is then used to classify the entire population of logs or sawn pieces intended for structural use.

This chapter focuses on the second approach, which, although not statistically robust due to logistical constraints, provides essential data for addressing the current lack of information on the mechanical behaviour of a poorly studied species. These results serve as a foundation for comparison with the first and third approaches, which are discussed in the following chapter.

3.3.1 Full-Size Destructive Testing

To obtain reliable and safe characteristic strength values, destructive testing of full-size elements remains the reference method for structural characterization. Such testing allows direct measurement of the relevant mechanical properties of logs under controlled laboratory conditions and provides statistically sound datasets for determining characteristic values.

Internationally, a range of reference standards exists for testing structural timber elements across different cross-sections. In addition to general timber-testing standards, there are specific protocols designed for the evaluation of roundwood members. Table 1 (adapted from Bukauskas et al.[6]) summarizes several of the most relevant standards for full-size destructive testing, excluding the visual grading standards that are addressed in the following chapter.

Table 1: Standards referenced for mechanical testing of timber and roundwood (adapted from Bukauskas et al.[6]).

Source	Number	Year	Name
ASTM	D198	2022	Standard Test Methods of Static Tests of Lumber in Structural Sizes
ASTM	D1036	2017	Standard Test Methods of Static Tests of Wood Poles
EN	14251	2014	Structural Round Timber – Test Methods

The American standard ASTM D198 (updated in 2022) [175] specifies test methods for determining bending, compressive, tensile, and torsional strength and stiffness of timber members of any cross-section, including round and irregular sections. In addition, ASTM D1036 [19] establishes procedures for evaluating utility poles used in supporting overhead lines, employing a cantilever bending setup. This standard also references ASTM D143 [176] for the testing of small, defect-free specimens extracted from the butt section of poles. On the European side, EN 14251 [18] provides specific procedures for determining bending and parallel to grain compressive strength, as well as the corresponding MOE, in roundwood members [6]. Beyond testing standards, several normative documents address the design of structures using roundwood [6]. At the North American level, these include ASTM D2899 - 2001 (*Standard Practice for Establishing Allowable Stresses for Round Timber Piles*,) [177]; ICC 400-2017 (*Standard on the Design and Construction of Log Structures*) [178], published by the International Code Council; and ANSI/AWC, 2018 (*National Design Specification (NDS)* for Wood Construction) [179], which contains a dedicated chapter on round timber poles and piles. In the Southern Hemisphere, the New Zealand standard NZS 3603:1993 (*Timber Structures*) provides strength adjustment factors for mechanically peeled (debarked) logs [180]. Furthermore, the joint Australian-New–New Zealand standard AS/NZS 7000:2016 (*Overhead Line Design*) [181] incorporates provisions for strength adjustments in mechanically rounded utility poles.

3.3.2 Free-Defect Small Specimen Testing

Until the 1970s, working stresses were commonly determined using small, free-defect specimens. These tests were less costly and provided standardized values by excluding natural defects such as knots, grain deviations, or age related irregularities. The resulting values were subsequently adjusted downward through correction factors accounting for load duration, moisture content, section dimensions, material quality, and safety factors [182].

However, subsequent research has demonstrated that the mechanical properties derived from small, clear specimens do not necessarily correspond to those obtained from full-size structural elements. As noted by Argüelles et al. [182], although such tests are valuable for the scientific investigation of species-specific characteristics, they are insufficient for determining design values applicable to real structural members, whose mechanical performance is influenced by the presence of natural defects. Nevertheless, standards based on small, clear specimens remain relevant for research purposes, particularly for establishing baseline reference data for lesser-known species [183, 184], such as *Acacia dealbata*. Among the most widely adopted protocols is ASTM D143-94, which forms the basis of the Chilean standards NCh 987: 2018 for bending [185] and NCh 973: 2018 for compression parallel to the grain [186]. At the

international level, ISO 13061-6:2014 [187] has been established by the International Organisation for Standardisation (ISO).

3.3.3 *Acacia dealbata* Reference Characterization

To date, no studies have been reported on the mechanical performance of small roundwood (*srw*) logs of *Acacia dealbata* in Portugal. However, research exists on sawn timber of this species in Chile. Padilla-Reyes et al. [188] investigated sawn boards from 15 year old *Acacia dealbata* plantations using Chilean standards based on the allowable stress method, where values are adjusted to the 5th percentile. Their results showed strength and stiffness values exceeding those of *Pinus radiata*, the reference species in Chile. Visual classification into two grades was consistent with the results of destructive testing. At 12% moisture content, allowable stresses were 17.6 and 14.8 MPa in bending strength (60.0% and 34.1% higher than *Pinus radiata* grade GS, respectively), and 17.6 and 17.5 MPa in compression parallel to the grain (9.2% and 8.3% higher, respectively). The MOE (MOE), adjusted to 12% MC, was 11.0 GPa for Grade 1 and 10.1 GPa for Grade 2, while mean densities were 508 kg/m³ and 504 kg/m³, respectively.

In Portugal, studies exist on another species of the same genus, *Acacia melanoxylon*. Martins and Knapic [189] characterized 40 sawn specimens (50 × 120 × 2900 mm³) sourced from mainland Portugal. The mean values, adjusted to 12% MC and determined in accordance with EN 384:2016+A2:2022, were: bending strength 69.3 MPa (SD = 21.6), MOE 14.4 GPa (SD = 2.1), and density 701 kg/m³ (SD= 72.2).

3.4 Experimental Campaign to Determine the Mechanical Properties of *Acacia dealbata* Logs from Peneda–Gerês National Park, Northern Portugal.

The experimental campaigns described and analysed in this Chapter (Chapter 3) and in the subsequent Chapter 4 were carried out using samples collected from the Peneda–Gerês National Park, located in northern Portugal (see Figure 20a). As outlined in the previous chapter, the extensive colonization of *Acacia dealbata* throughout large areas of the park has been identified by several authors as a serious threat to the conservation of its natural heritage [81, 113, 114] (see Figure 20b). All specimens were harvested in collaboration with rangers from the Portuguese Instituto da Conservação da Natureza e das Florestas (ICNF), following an on site preselection process. According to the head ranger, stands originated after a major wildfire that occurred approximately fifteen years ago.

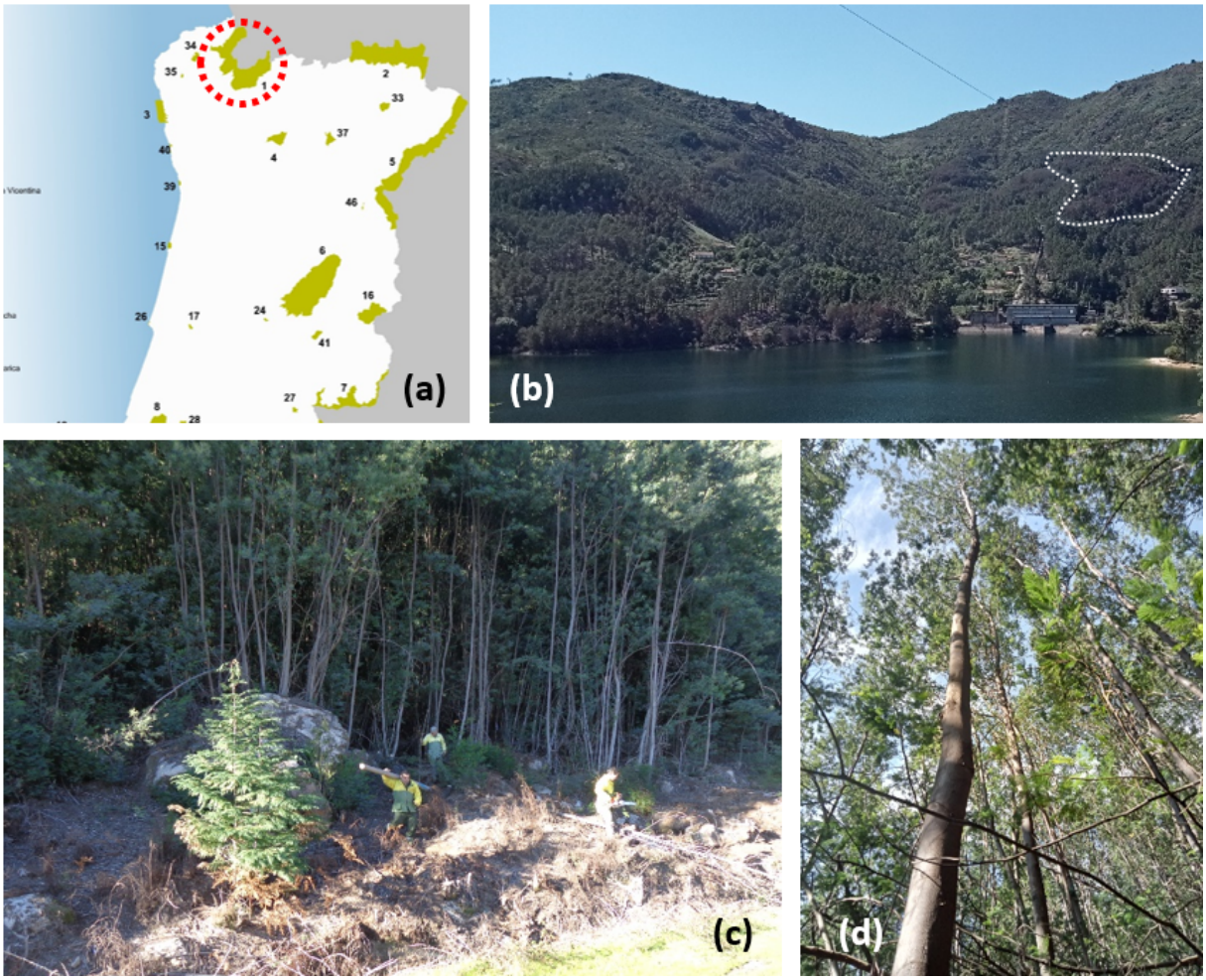

Figure 20: (a) The red circle indicates the location of Peneda-Gerês National Park in northern Portugal; (b) a view of mimosa (*Acacia dealbata*) colonized areas by Peneda-Gerês National Park, and the polygon outlines an area colonized, characterized by distinct slight colouration; (c) a typical view of a high-density mimosa stand, along with ICNF rangers harvesting logs; (d) a close-up of a mimosa specimen illustrates the natural misalignment of the tree shaft.

3.4.1 Collection of Logs

In the whole experimental campaign, two collections were made: the first in spring 2022 (late May) and the second in autumn 2022 (early December). The stands recommended by the ICNF rangers were chosen within the park and less than 5 km from the Gerês village. All selected stands were very dense (8 to 9 trees per square meter), predominantly composed of Acacias, with young approximately 15–20 years old specimens of varying diameters (see Figure 20c), frequently established on sloping terrain with limited accessibility. In the forest, each tree was selected. For that its straightness, defects, and diameters were reviewed in two orthogonal views using a tree diameter gauge at breast height (dbh) for final selection. The selected trees were marked for felling with spray paint. The most straight and regular specimens were chosen, with diameters ranging from 100 to 150 mm and no significant defects. The diameter and length were determined by an aspect ratio: 18 times the diameter for the smaller logs and 20 times for the larger ones, to facilitate subsequent destructive bending tests. Finding specimens meeting these require-

ments was difficult, especially regarding straightness (see Figure 20d). The felling involved a chainsaw cut approximately 300 mm from the ground. After the tree fell, the branches were removed and cut to the desired length.

3.4.1.1 First Collection

On May 27, 2022, 34 logs were collected from stands with abundant *Acacia dealbata* populations. With the support of ICNF rangers, the logs were cut to lengths close to 2000 mm and identified at the base. Simultaneously, slices approximately 30 mm thick were cut from the base of each log, identified with their respective tree, and stored in plastic bags to minimise moisture loss. Each slice was weighed to determine the tree's moisture content at the time of cutting, yielding 70.90 % (SD = 5.78 %) MC according to the oven-drying method. In some cases, several logs were cut from the same tree: 2 or 3. Immediately after cutting, the logs were transported directly to the Civil Engineering Laboratory (University of Minho, Guimarães), where they were stacked in a location protected from rain and direct sunlight, with 20 mm spacing between them and 20 mm battens for height separation. The logs were kept in these conditions until the first general measurements (perimeter and moisture content with an electrical meter device) and NDT were carried out.

3.4.1.2 Second Collection

On December 2, 2022, a second collection of 61 logs was carried out with the assistance of ICNF rangers. Unlike the previous collection, only one log per tree was collected. The trees were harvested to a length of approximately 2500 mm and then transported to the ICNF offices and storage facilities. Here, all logs were trimmed at both ends to a length of 2400 mm, with slices 20 to 30 mm thick extracted from both ends for moisture measurement. The MC was 46.61 % (SD = 6.25 %) according to the oven-drying method. The logs were then divided into two groups of 30 and 31 specimens. The first 30 were prepared and stacked in ICNF facilities for later experimental campaigns. The remaining 31 specimens were transported to the Civil Engineering Laboratory, where they were stacked inside the IBS (Institute of Science and Innovation for Bio-Sustainability Laboratory, University of Minho) building for general measurements (perimeter and moisture content with an electrical meter device) and initial non-destructive tests.

3.4.1.3 Design and Execution of the Experimental Campaign

The experimental campaign's design (Figure 21) was based on logistical capabilities and the availability of equipment and tools. It was proposed to be divided into two parts to determine the mechanical characteristics of *Acacia dealbata* logs (Chapter 3) and evaluate the reliability of some non-destructive techniques (Chapter 4).

Non-destructive tests (NDT) were conducted, including a visual characterisation to select the final samples and two dynamic tests: longitudinal stress wave (lsw) and transverse vibration (tv). The visual characterisation was conducted in the Civil Engineering Laboratory in January 2023. According to this, a total of 45 specimens were selected, comprising 17 from the first collection and 28 from the second.

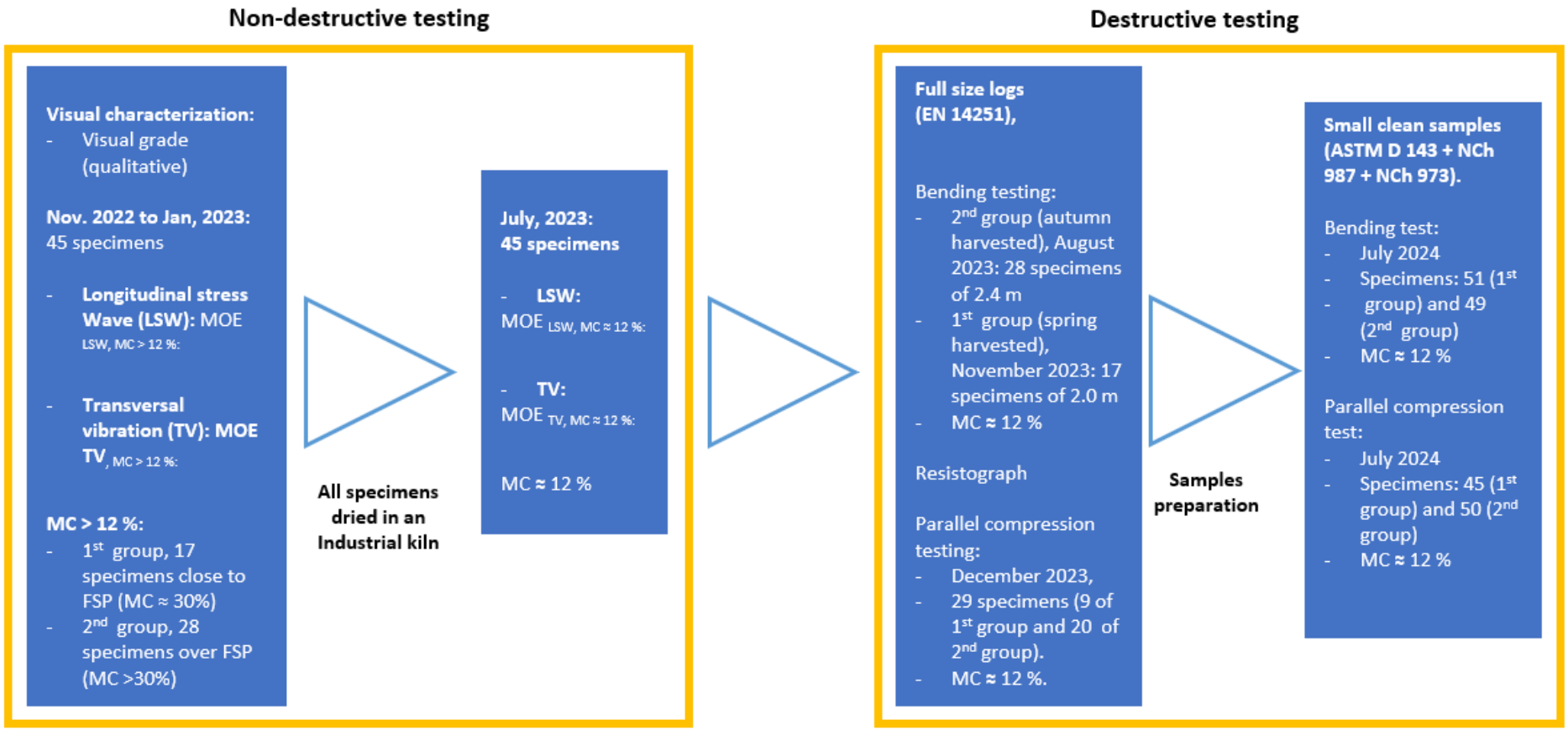

Figure 21: Design of experimental campaign for the mechanical characterization of *Acacia dealbata* logs. *Non-destructive* testing during the first phase (November 2022–July 2023) included visual characterization for qualitative classification (Ranta Maunus [25]) and longitudinal stress wave and transverse vibration tests on samples with moisture content (MC) >12%, followed by oven-dried samples with MC = 12%. *Destructive* testing in the second phase (August 2023–July 2024) involved bending, parallel compression, and drill penetration resistance tests on full-scale logs and bending and parallel compression tests on free-defect small specimens.

Two dynamic tests were performed in two rounds to study the influence of MC on the dynamic properties of the logs [190].

The first round of NDT was conducted with a moisture content above 12%, therefore green MC. But due to the collections being made in different seasons and the varying time between harvesting and stacking, different moisture contents were obtained. If we use a reference value corresponding to the fibre saturation point (FSP), which is close to 30% of MC, two groups were formed. One with a moisture content above 30% (corresponding to the second collection or 2nd) and the other below 30% (the first collection or 1st). Due to this and the availability of instruments, the tests were conducted between August 2022 and January 2023 for the 1st collection and between January and March 2023 for the 2nd collection.

The second round of NDT was conducted in July 2023, after all the logs (from both groups, 1st and 2nd) were dried in an industrial kiln in Oporto using a drying program specifically designed for eucalyptus, with great physical and anatomical similarity to *Acacia dealbata* wood, achieving a moisture content of approximately 12%. The results of the dynamic tests were used to determine the dynamic modulus of elasticity, E_{dyn}, for both non-destructive techniques.

The destructive tests (DT) were conducted on full-scale log samples and small, defect-free specimens, all conditioned to a MC of approximately 12%. Prior to testing, all samples were stored in a climate-controlled chamber at 20°C (± 0.5°C) and 60% (± 5%) relative humidity until achieving a constant weight, with weight measurements taken every 6 hours in accordance with the reference standards.

The bending tests on full-scale logs were performed between August and November 2023, while the parallel compression tests, using shorter specimens from either remaining logs or residual material from the bending tests, were carried out in December 2023. Before the bending tests, penetration resistance measurements were obtained for all logs using a Resistance drilling tool to determine the drill penetration resistance (R_m). Based on EN 384:2016+A2:2022, the mechanical properties and characteristic values for these samples were calculated.

To prepare the small defect-free specimens, logs remaining from the visual sorting process were utilised, ensuring that samples from both harvest periods were included. These specimens with a nominal cross-sectional area of 25 × 25 mm were subsequently subjected to bending and compression tests parallel to the grain, conducted in July 2024.

Table 2 provides an overview of the mechanical properties evaluated in this study, based on the complete set of tests performed.

Table 2: Summary of the main mechanical properties inferred in the experimental campaign.

Acronym	Test	unit	MC	Size	
$E_{dyn,lsw}$	Dynamic modulus of elasticity for longitudinal stress wave	GPa	> 12% ≈ 12%	full	NDT
$E_{dyn,tv}$	Dynamic modulus of elasticity for transversal vibration	GPa	> 12% ≈ 12%	full	NDT
E_{local}	Static local modulus of elasticity	GPa	≈ 12%	full	DT
E_{global}	Static global modulus of elasticity	GPa	≈ 12%	full	DT
$E_{0,k}$	Characteristic static local modulus of elasticity	GPa	≈ 12%	full	Analytic
$E_{90,mean}$	Mean modulus of elasticity perpendicular to the grain	GPa	≈ 12%	full	Analytic
G_{mean}	Mean shear modulus	GPa	≈ 12%	full	Analytic
f_m	Bending strength	MPa	≈ 12%	full	DT
$f_{m,k}$	Characteristic bending strength	MPa	≈ 12%	full	Analytic
$f_{c,0}$	Parallel to the grain compression strength	MPa	≈ 12%	full	DT
$f_{c,0,k}$	Characteristic parallel to the grain compression strength	MPa	≈ 12%	full	DT/Analytic
$f_{c,90,k}$	Characteristic perpendicular to the grain compression strength	MPa	≈ 12%	full	Analytic
$f_{t,0,k}$	Characteristic parallel to grain tension strength	MPa	≈ 12%	full	Analytic
$f_{t,90,k}$	Characteristic perpendicular to grain tension strength	MPa	≈ 12%	full	Analytic
$f_{v,k}$	Characteristic shear strength	MPa	≈ 12%	full	Analytic
f_{small}	Bending strength in small specimens	MPa	≈ 12%	small	DT
$f_{small,c,0}$	Parallel to the grain compression strength in small specimens	MPa	≈ 12%	small	DT
$\rho_{fb,12}$	Density in full-body log	kg/m^3	≈ 12%	full	DT
ρ_{12}	Density	kg/m^3	≈ 12%	slice	DT
ρ_{mean}	Mean density	kg/m^3	≈ 12%	full	Analytic
$\rho_{small,12}$	Density in free-defect small samples	kg/m^3	≈ 12%	small	DT
$\rho_{k,12}$	Characteristic density	kg/m^3	≈ 12%	slice	Analytic
R_m	Resistance to drilling penetration	%	≈ 12%	full	NDT

NDT: non-destructive testing; DT: Destructive testing; Analytic: It was analytically derived from the experimental data.

3.4.1.4 Statistical analysis

All analyses begin with a descriptive statistical assessment of the data. Inferential comparisons between two groups were conducted using independent-samples t-tests, while comparisons involving more than two groups were analysed using analysis of variance and Tukey post hoc tests (ANOVA-Tukey). The selection of statistical tests was guided by the verification of relevant assumptions and the robustness of the data.

The correlations between the variables were evaluated using the Pearson correlation coefficient (r) for parametric data or the Spearman rank correlation coefficient (s) for non-parametric samples, with interpretation based on the guidelines provided by Mukaka [191]. Statistical significance was evaluated

at a 95% confidence level ($p < 0.05$), with more stringent thresholds indicated where applicable. All analyses were performed using the Real Statistics add-in for Microsoft Excel 2021, with data validation and consistency checks conducted through supplementary AI-assisted tools.

3.4.2 Determination of Moisture Content (MC) and Density (ρ)

3.4.2.1 Moisture Content

Two methods were employed to determine the moisture content (MC) of the specimens. The oven-drying method, in accordance with ISO 13061-1:2014 [187], was applied to small specimens (slices and small clear samples) and for full-size samples, a calibrated electrical resistance device was used.



Figure 22: Moisture content (MC) determination methods. (a) Weighing and (b) oven-drying of log slices, and (c) use of an electrical resistance moisture meter for full-scale logs.

The weight of each small specimen was determined using an electronic balance with an accuracy of 1 g (Figure 22a). Subsequently, the specimens were oven-dried at 103 ± 2 °C until a constant mass was achieved (Figure 22b). The moisture content (MC) of each specimen was then calculated according to Equation 1, which relates the oven-dry mass ($m_{MC,dry}$) to the initial mass (m_{MC}):

$$\text{MC} = \frac{m_{MC} - m_{MC,dry}}{m_{MC,dry}} \times 100\% \quad (1)$$

The electrical resistance method was used to determine the MC of full-scale logs during NDT, both before and after kiln drying, and prior to DT in order to correlate both methods. A Protimeter Survey-Master® BLD5365 moisture meter was employed, ensuring a penetration depth of approximately 3 mm (See Figure 22c). Following the manufacturer's specifications and previous studies [36], readings were restricted to a range between 5% and 30% MC. Measurements were taken in three central longitudinal sections one quarter, one-half, and three-quarters of the log length (corresponding to sections S2, S3, and S4 in Figure 28) and the mean value was used for analysis.

Calibration of the electrical resistance device was performed using disc slices obtained from the bottom end of the logs collected during the first harvest. To achieve saturation, the slices were submerged in water overnight. After excess surface water was removed, they were conditioned in a climate chamber

maintained at a constant temperature of (20 ± 0.5) °C and relative humidity (RH) of (60 ± 5)%. Inside the chamber, periodic mass and moisture readings were taken at five positions on each disc: two perpendicular pairs of points across the heartwood and sapwood, and one central point in the sapwood. Measurements were initially recorded every two hours, with the interval extended as values stabilized, and terminated once a constant mass was achieved. The oven-drying procedure defined by ISO 13061-1:2014 [187] was then applied to determine the reference dry mass, and the corresponding equation 1 was used to compute the MC.

Equation 2 describes the linear regression model developed to estimate the MC in full-size logs from electrical resistance readings, while Figure 23 presents the correlation between the results obtained from both methods. Values above 30% of MC from the hygrometer were discarded. $MC_{equipment}$ corresponds to MC meter record and MC_{adjust} is the MC value adjusted:

$$MC_{adjust} = 0.6612(MC_{equipment}) + 0.915 \quad (2)$$

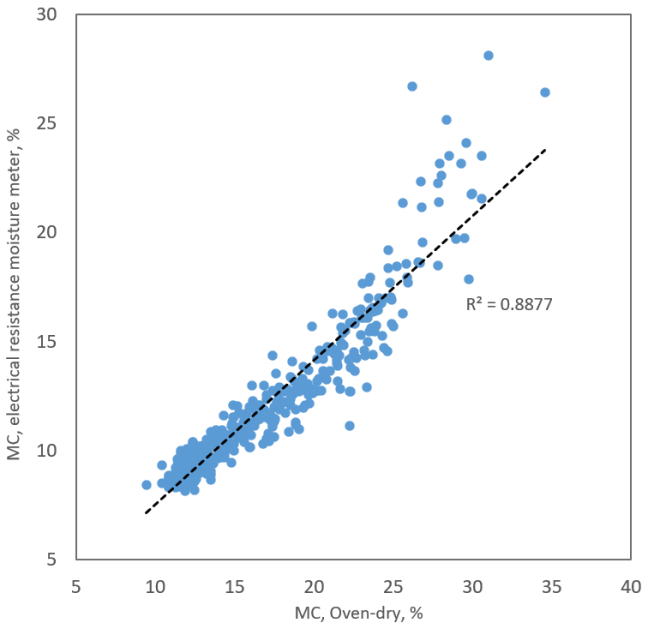

Figure 23: Linear correlation between two methods for determining moisture content: oven-drying method vs. electrical resistance moisture meter.

The MC values obtained from both methods (oven-dry and electrical resistance) were subsequently used to adjust the mechanical test results to the reference moisture content of 12%, in accordance with EN 384:2016+A2:2022 [192].

3.4.2.2 Results of Moisture Content Measurement

As previously discussed, for the DT phase, two independent methods were employed to determine the (MC) to examine their relationship and to propose a reliable approach for MC estimation. The first method consisted of electrical resistance measurements calibrated according to Equation 2 ($MC_{electrical,all}$), while the second involved the oven-drying method ($MC_{oven\text{-}dry,all}$) according equation 1 applied to a slice sample

removed immediately after destructive testing, taken from a zone adjacent to the fracture. Figure 24 illustrates the relationship between the two methods for the 43 tested specimens (excluding outlier values), along with the corresponding coefficient of determination (R^2), showing statistically significant correlations ($p < 0.00$) and indicating a hight linear relationship between them. Despite this correlation, t-tests revealed significant differences between the mean values obtained from both methods. The oven-dry method yielded higher moisture contents, with a mean $MC_{oven-dry,all}$ = 15.35 % (SD = 3.08 %), compared with $MC_{electrical,all}$ = 11.96 % (SD = 1.91 %).

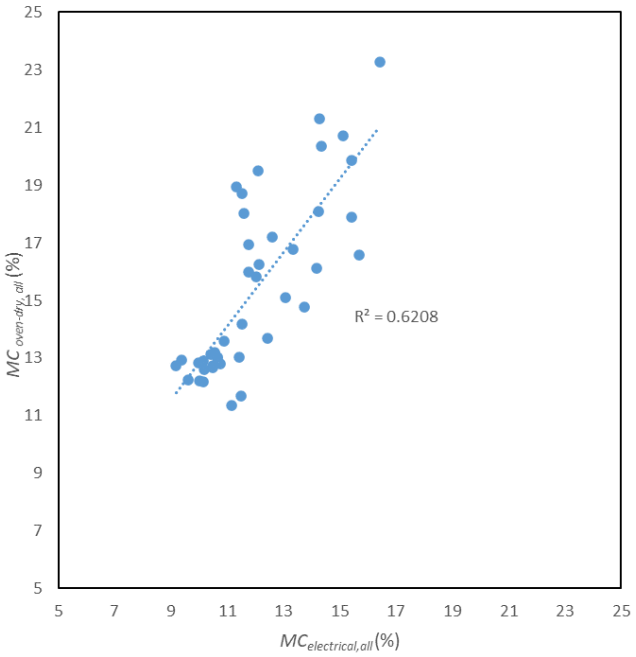

Figure 24: Correlation between the moisture content (MC) obtained from the mean of three measurements using a calibrated electrical resistance meter (according to Equation 2) and the MC determined by the oven-drying method from disc samples extracted near the fracture zone.

This discrepancy can be partly attributed to instrument limitations. The electrical resistance moisture meter measures only the moisture in the permeable sapwood zone, which typically exhibits lower water content. Conversely, the oven-drying method accounts for the entire cross-section of the specimen, including the heartwood, which is less permeable and tends to retain more bound water during drying. This pattern was consistent across both groups of specimens; however, the 2nd group (harvested in autumn) displayed higher overall MC values. This behaviour may be explained by the presence of bark, which retained moisture within the log and was detected by the instrument.

When comparing the oven-dry MC data with the mean values obtained from the uncalibrated electrical resistance readings using a t-test, no significant differences were observed. On this basis, a new predictive model for MC estimation was developed, derived from the mean of the three uncalibrated measurements after excluding outliers and values close 30 % MC. The resulting model, expressed in Equation 3, represents a simple linear regression that enables the estimation of moisture content from electrical resistance measurements for full-size logs.

$$MC_{ADJUST} = 0.8412\,(MC_{electrical}) + 1.2961 \quad (3)$$

In this equation, $MC_{electrical}$ corresponds to the mean value of the three uncalibrated electrical resistance readings, while MC_{ADJUST} refers to the moisture content adjusted according to the calibration regression model. This relationship replaces Equation 2 used in NDT and presents a coefficient of determination of R^2 = 0.62, based on a sample size of n = 43.

3.4.2.3 Density

The determination of density for a specific MC is based on the ratio between mass (m) and volume (v):

$$\rho_{MC} = \frac{m}{v} \quad (4)$$

Due to the geometric irregularity of the material, two methods were employed to measure volume and density:

1. *Full-body volume measurement by the geometric method* (ρ_{fb}): For determining the density of the whole logs, after weighing using an electronic scale, the volume was calculated by measuring the length and averaging the five apparent diameters (d_{app}) to determine a mean area (See Figure 27).

2. *Volume measurement of extracted slices cut samples using the immersion method*: Three slices were taken from the bottom, middle, and top of each log. For measuring the density of slices, after being weighed and stored in polyethene bags, the volume was determined according to ASTM D2395, 9.2.2.2, Mode II [164] (Figure 25a), which describes an immersion method for irregular bodies. To that, a frame was constructed, where a slender screw was attached to secure the sample, allowing it to be submerged in a container filled with distilled water, ensuring the sample was fully submerged and did not touch the sides (Figure 25b,c).

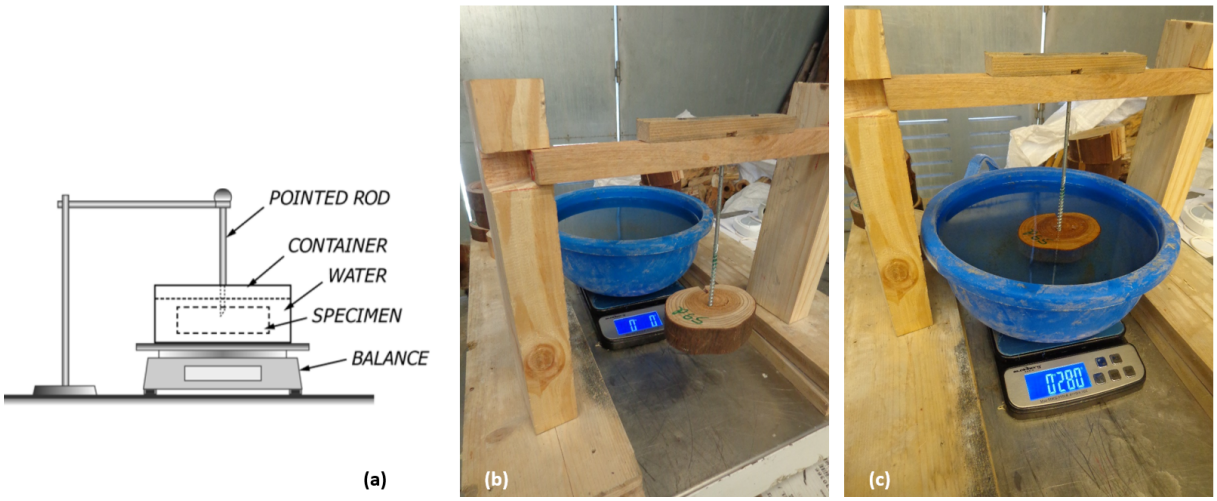

Figure 25: (a) Components of the immersion procedure for determining the volume of irregular bodies, as outlined in ASTM D2395 - mode II [164], (b) tare of the water-filled container and securing of the sample in the support frame, and (c) immersion of the sample and data capture.

For both methods, density values for moisture contents between 10% and 18% (ρ_{MC}) were adjusted according to EN 384:2016+A2:2022 [192] using equation:

$$\rho_{12/fb,12} = \rho_{MC}(1 - 0.005(MC - 12\%)) \tag{5}$$

3.4.2.4 Results of Density Measurement

Regarding the relationship between the two density measurement methods, the scatterplot in Figure 26 illustrates their correlation and the corresponding coefficient of determination. A high and statistically significant relationship was observed between the two methods ($p < 0.00$). Despite this strong correlation, significant differences were found between the mean values obtained by each method: the full-body method yielded a mean density of 646.36 kg/m³ (SD = 91.04), while the immersion method produced a mean density of 692.80 kg/m³ (SD = 97.84), representing an approximately 6.7 % higher value for the immersion technique.

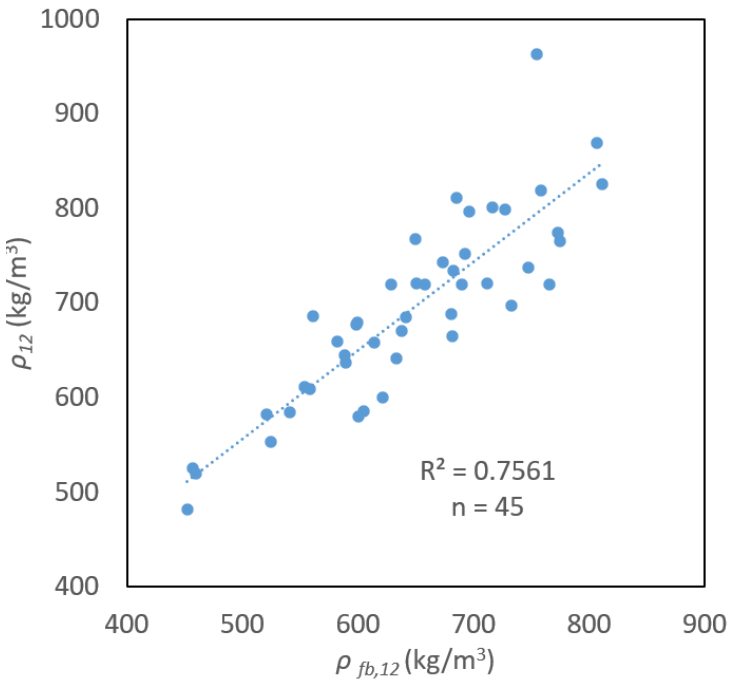

Figure 26: Relationship between the density of the full-size log ($\rho_{fb,12}$) adjusted to 12% MC and density based on the immersion method (ρ_{12}).

To reconcile these differences, a simple linear regression model (Equation 6) is proposed to estimate the density at 12 % moisture content (ρ_{12}) from full-body log measurements ($\rho_{fb,12}$), following the methodology described above.

$$\rho_{12} = 0.9348\,(\rho_{fb,12}) + 88.561 \tag{6}$$

3.4.3 Destructive Testing on Full-size Logs

3.4.3.1 Diameter Definitions

Due to the geometric irregularity of the logs, several specific diameters are distinguished according to the type of test and analysis:

- d_{app}, Apparent diameter: EN 14251 [18] by Test methods for Structural round timber, defines it as "the diameter of a circle with the same circumference as the actual circumference at the measurement section" (Figure 27). In the destructive tests, d_{app} was used to determine the local Modulus of Elasticity, E_{local}, specifically the smallest value d_1 (average between S2 and S3 in Figure 28) and the largest value, d_2 (average between S3 and S4 in Figure 28). In the NDT, it was used to determine the volume (and density, ρ) in the lsw tests and to calculate the inertia, I, in the tv testing.

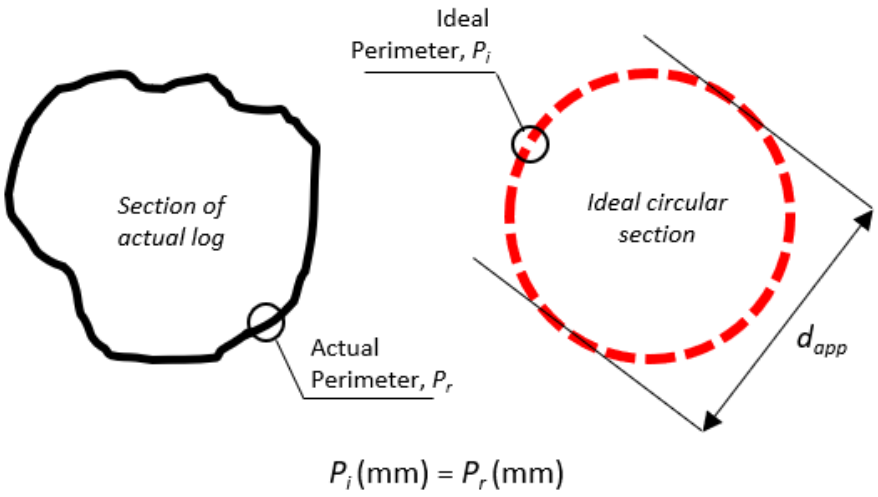

Figure 27: Graphical definition of the apparent diameter (d_{app}).

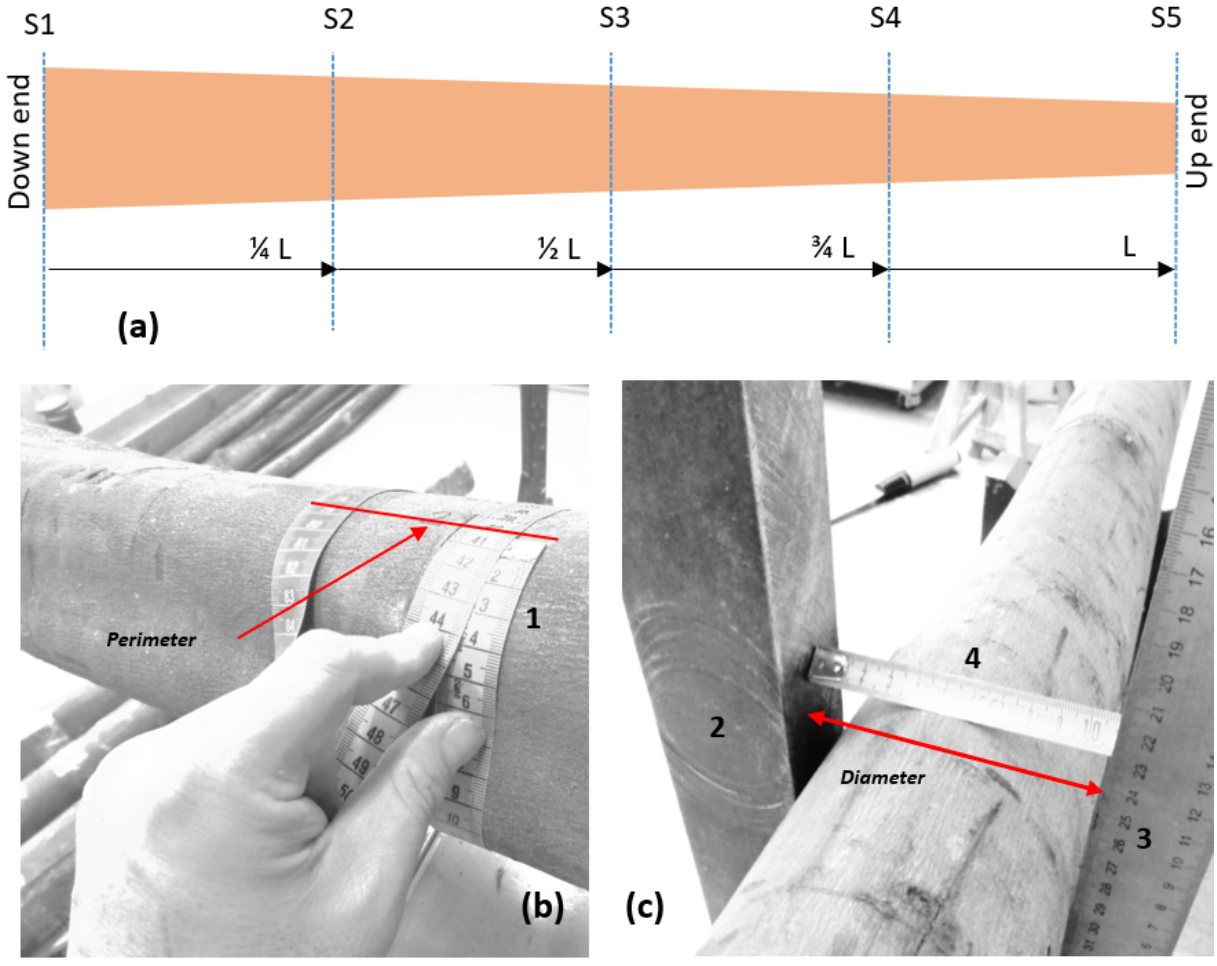

Figure 28: (a) Indication of sections measured on each log during the experiments: Sections S1, S2, S3, S4, and S5 were measured. (b) Perimeter measurements (for d_{app}) were taken using an adjustable measuring tape (1), while (c) diameter measurements (for d_{nom}) were obtained using an orthogonal steel piece (2), a carpenter's square (3), and a rigid measuring tape (4).

- d_{nom}, Nominal diameter: EN 14251 [18] defines it conditionally based on ovality: If ovality ≥ 5%, the largest apparent diameter, d_{app} should be used, S1 in Figure 28. If ovality < 5%, the largest minimum diameter of the log should be used, that is, in section S5 in Figure 28. This definition was used for the visual characterisation of the logs and for the geometric definition of the setup for the destructive tests.

Other specific diameter definitions are described later according to the configuration of each test.

3.4.3.2 Samples preparation

After completing all Non-destructive testing (NDT), the kiln-dried logs, with an approximate moisture content (MC) of 12%, were stored in a climate chamber at a temperature of 20°C (±0.5°C) and relative humidity of 60% (±5%) until a constant weight was achieved, measured at 6 hour interval (see Figure 29a,b,c). Although the standard requires bark-free logs for bending tests, the 28 logs from the 2nd group (autumn), measuring 2.4 m in length, had bark firmly adhered to them due to the lack of specialised tools and high bonding. However, the 17 logs, measuring 2.0 m in length, from the 1st group (spring) were bark-free after kiln drying, likely due to the longer air-drying period.



Figure 29: Preparation of samples for destructive testing. Conditioning of the logs in a climatic chamber: (a) for the 2nd and (b) the 1st group of bending tests, and for the (c) parallel compression tests.

3.4.3.3 Determination of moisture content and density

To determine the density, wood slices approximately 75 mm thick were extracted from sections near the failure zone. Each slice was immediately weighed and sealed in polyethylene bags to prevent moisture loss. The volume of each slice was then determined using the water immersion method. For moisture content (MC) determination, both methods previously described were employed: (i) an electrical resistance moisture meter, using the average of three readings adjusted according to Equation 2 (for compression parallel to the grain, MC was measured only within the central two-thirds of the specimen), and (ii) the oven-drying method, in which the slices were dried to a constant mass in order to determine their dry weight and calculate MC according to Equation 1.

3.4.3.4 Bending testing

All tests were performed in accordance with EN 14251:2003 [18] at the Civil Engineering Laboratory. The load cell used for the bending tests had a capacity of 600 kN, while that for compression tests had a capacity of 2500 kN. Due to equipment availability, the bending tests were conducted on two separate occasions: at the end of August and beginning of September 2023, 28 logs (2.4 m in length) from the 2nd collection (autumn) were tested, and in mid-November 2023, 17 logs (2.0 m in length) from the 1st collection (spring) were tested. Before each bending test, resistograph measurements were performed. All compression parallel-to-grain tests were carried out in early December 2023.

Figure 30a presents the bending test configuration, showing the main parameters used. Due to the irregular geometry of the logs, each specimen required a specific setup with minimal variations. The specimens were verified to meet the required slenderness ratios using the nominal diameter (d_{nom}), maintaining a span of $18d_{nom}$, and applying symmetrically centred loads. The natural curvature of each log was aligned with the direction of loading. Specific steel support fixtures and loading heads were fabricated for these tests (see Figure 30). Solid steel supports were designed to hold the logs in place during testing (see Figure 30b,c). To prevent indentation and ensure a uniform stress distribution, high-strength concrete loading heads (100×100 mm^2), reinforced with steel fibres, were cast in custom moulds for each log (see Figure 30b,d).

The loading protocol in bending included two tests: one to determine the local modulus of elasticity (E_{local}) in the central span of the log, and another to determine the global modulus of elasticity (E_{global}) and the ultimate bending strength (f_m).

To determine E_{local}, a preliminary test was performed on two residual logs to estimate the load below the proportional limit and refine the testing protocol. The final procedure consisted of three loading–unloading cycles at a constant displacement rate of 0.132 mm/s, up to a maximum deflection of 12 mm. To measure deformation in the central span, L-shaped aluminium profiles were centred and screwed along the neutral axis on both sides of the specimen, covering the central third of the span (as shown in Figure 30a). High-precision LVDTs were mounted on these profiles at a gauge length of $5d_{nom}$. For the calculation of the coefficient c in Equation 9, the calibrated local span (l_l) was defined as $5d_{nom}$. The minimum and maximum apparent diameters within this span were designated as d_1 and d_2, respectively. These values were obtained by averaging measurements taken in sections S2 and S3 for d_2, and in S3 and S4 for d_1, corresponding to approximately $3/8$ of the log length from the supports. The minimum moment of inertia (I_l) was calculated using the minimum apparent diameter (d_1) (see Figure 30a).

To determine the global modulus of elasticity (E_{global}) and bending strength (f_m), a single lower-precision LVDT was used to record the midspan deflection relative to the supports and to determine the failure load. The testing protocol consisted of a single loading cycle up to a deflection of 120 mm or until failure, at a constant displacement rate of 0.36 mm/s. The moment of inertia, or the second moment of area, was determined using the mean of five apparent diameters (d_{app}) measured along each log (see Figure 27 and 28).

Before each test, checks and splits were recorded for each specimen, distinguishing between radial

checks and diametrical splits. Each crack type was described in terms of the percentage of log length and position relative to the load direction on the section: vertical, horizontal, and diagonal.

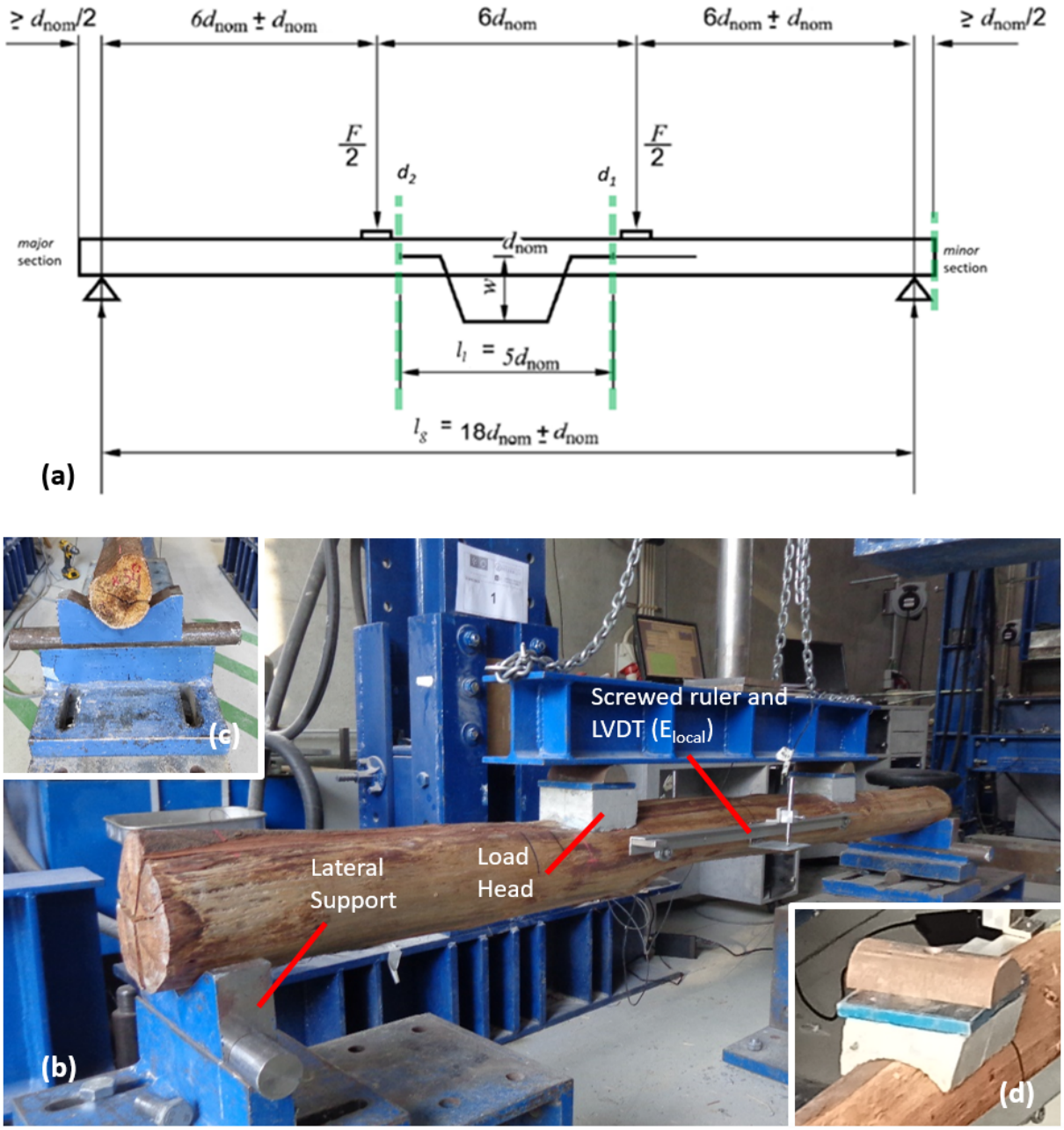

Figure 30: (a) Bending testing setup with geometrical definition according to EN 14251:2003 [18]; (b) Image of the test to determine the local modulus of elasticity (E_{local}). The support conditions, the couple of concrete load-heads, and the ruler screwed at both ends over the log neutral line (centring to 5 d_{nom}) with one of the two LVDT devices to measure the deflection in the central section are observed; (c) Detail of support device and (d) of concrete loading-head with fibres, coust to each log.

The equation gives the static local modulus de elasticity, E_{local}, in GPa is:

$$E_{local} = \frac{\Delta M}{\Delta w_l} \frac{c^4}{6I_1} \left[-\frac{1}{(c + l_1/2)^2} - \frac{D}{2} + \frac{1}{c^2} \right] \quad (7)$$

$$D = \left(\frac{1}{c^2} - \frac{1}{(c + l_l)^2} \right) \tag{8}$$

$$c = \frac{l_l d_1}{(d_2 - d_1)} \tag{9}$$

$$I_l = \frac{1}{4} \pi r^4 \tag{10}$$

Where ΔM is the increment of bending moment on the straight line portion of the load–deformation curve, expressed in Nmm; Δw_l is the increment of displacement on the same straight line portion of the load deformation curve, in mm; d_1 is the smallest apparent diameter along the gauge length (see Figure 30a), in mm; d_2 is the largest apparent diameter along the gauge length (see Figure30a), in mm; I_l is the smallest second moment of area (the d_1 section was used, see Figure 30a) along the gauge length, in mm^4; and l_l is the local gauge length (Figure 30a), in mm.

According EN 408 [193], the global modulus of elasticity in bending parallel to the grain, E_{global} in GPa is determined by :

$$E_{global} = \frac{\Delta F}{\Delta w_g} \frac{{l_e}^3}{12 I} \left[\frac{3a}{4 l_e} - \left(\frac{a}{l_e} \right)^3 \right] \tag{11}$$

Where ΔF is the increment of load on the straight line portion of the load deformation curve, expressed in N; Δw_g is the increment of displacement on the same straight-line portion of the load–deformation curve, in mm; l_e is the span distance (see Figure 30a), in mm; a is the distance between the loading position and the support, in mm; and I is the second moment of area corresponding to the mean apparent diameter (d_{app}), expressed in mm^4. Moreover, according to EN 384:2016+A2:2022 [192], the MOE corresponding to MC between $8\,\%$ and $18\,\%$ shall be adjusted using the following expression:

$$E_{local/global} = E_{MC}(1 + 0.01(MC - 12\%)) \tag{12}$$

The bending strength f_m in MPa is given by the equation:

$$f_m = \frac{16 F_{max} a}{\pi d_h d_v^2} \tag{13}$$

where F_{max} is the maximum total load applied by both loading heads, expressed in N; a is the distance between the loading position and the support, in mm; d_v is the diameter measured in the direction of the load at mid-span, in mm; and d_h is the diameter measured perpendicular to the load direction at mid-span, in mm.

3.4.3.5 Parallel to the grain compression testing

Most samples used in compression tests came from previously discarded logs after visual classification. Sections with minimal misalignment were selected to reduce second order effects. Some remaining sam-

ples from the bending tests were also used. The samples were cut with a fixed table saw to ensure flatness and parallelism between both end's faces. The length of each sample was set at six times the nominal diameter (d_{nom}), as previously defined in section 3.2.3.f. Care was taken to apply the load concentrically and to reduce the risk of failure by bending, including a spherical seated loading head at the lower end (Figure 31).

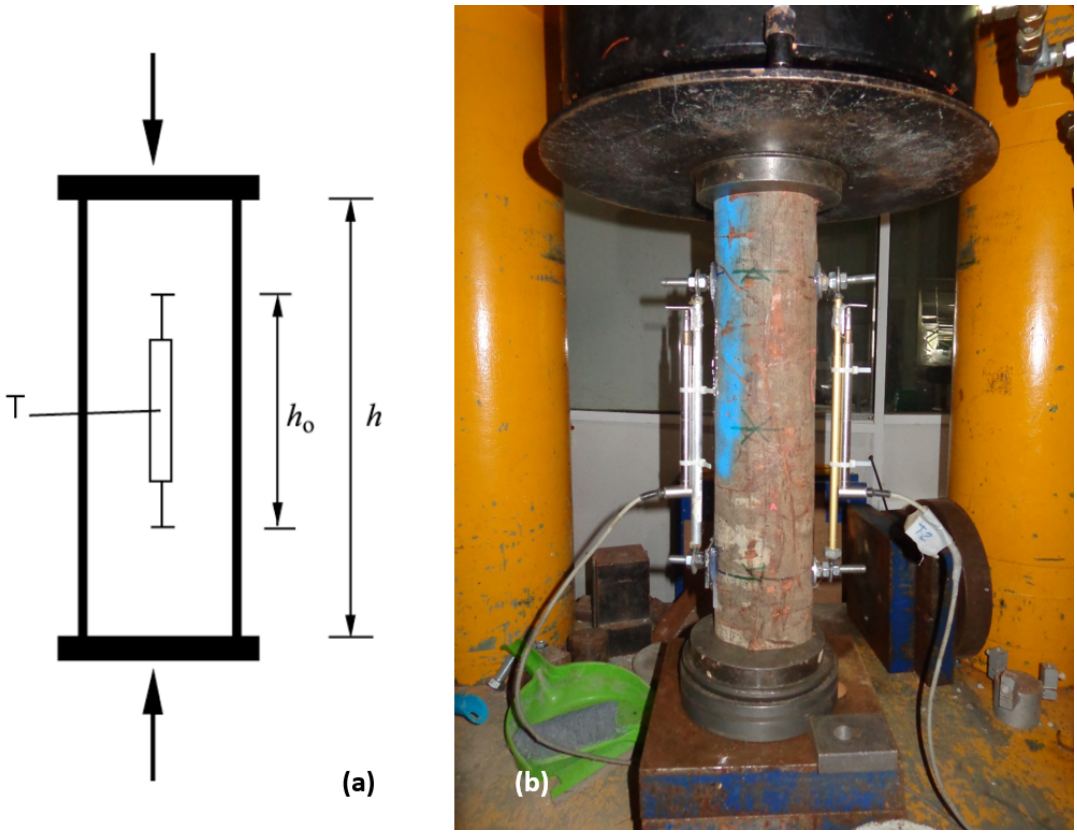

Figure 31: Parallel to the grain compression test setup. (a) Geometrical definition according to EN 14251:2003 [18]; (b) Test image with the loading device and a couple of LVDT devices to measure axial deformation.

The parallel to the grain compression modulus of elasticity $E_{c,0}$ is given by the equation, in GPa:

$$E_{c,0} = \frac{h_0 (F_2 - F_1)}{A (w_2 - w_1)} \tag{14}$$

Where $(F_2 - F_1)$ is the increment of load on the straight-line portion of the load–deformation curve, expressed in N; $(w_2 - w_1)$ is the mean increment of deformation corresponding to $(F_2 - F_1)$, in mm; h_0 is the gauge length, in mm; and A is the cross-sectional area near the location of failure, expressed in mm^2.

The parallel to the grain compression strength $f_{c,0}$ in MPa is given by the equation:

$$f_{c,0} = \frac{4F_{max}}{\pi d_2 d_1} \tag{15}$$

Where F_{max} is the maximum load, expressed in N; and d_1 and d_2 are two diameters perpendicular to

each other, measured close to the fracture, in mm.

3.4.3.6 Determination of characteristic values of mechanical properties and density

The procedures outlined in EN 384:2016+A2:2022 [192] were followed. Given that the number of sub-samples was 2, with 17 and 28 specimens respectively, the procedure described in EN 14358:2016 [194] was adopted, based on a parametric approach for each property and density.

Determination of characteristic modulus of elasticity values. For stiffness related properties (E_{local} and $E_{c,0}$), in GPa, the following expressions considering normally distributed data were used:

$$\bar{y} = \frac{1}{n}\sum_{i=1}^{n} m_i \tag{16}$$

$$s_y = \max\left\{\sqrt{\frac{1}{n-1}\sum_{i=1}^{n}(m_i - \bar{y})^2},\ 0.05\bar{y}\right\} \tag{17}$$

where $\bar{y}$ is the sample mean, s_y is the sample standard deviation, m_i is the value of the property, and n is the number of specimens.

The characteristic mean value of the property (m_{mean}) is given by:

$$m_{\text{mean}} = \bar{y} - k_s(n)\, s_y \tag{18}$$

where the factor $k_s(n)$ is defined as:

$$k_s(n) = \frac{0.78}{n^{0.53}} \tag{19}$$

The characteristic modulus of elasticity $E_{0,\text{mean}}$ for each grade was calculated according to:

$$E_{0,\text{mean}} = \min\left\{1.1\,\bar{E}_{i,\text{min}},\ \frac{\sum_{i=1}^{n_s} n_i \bar{E}_i}{n}\right\} \cdot \frac{k_n}{0.95} \tag{20}$$

where $\bar{E}_i$ is the mean modulus of elasticity of sub-sample i (equation 18), $\bar{E}_{i,\text{min}}$ is the lowest mean modulus of elasticity among sub-samples, n_s is the number of sub-samples, n_i is the number of specimens in sub-sample i, and n is the total number of specimens. The factor k_n is an adjustment factor accounting for the number of sub-samples, taken as $k_n = 0.91$ for two sub-samples.

Determination of characteristic strength values. In the case of bending strength ($f_{m,0}$), two adjustments values were applied, k_h and k_l.

For depth less than 150 mm, and characteristic density less than or equal to 700 kg/m3, bending strength shall be adjusted to 150 mm depth by dividing by the factor kh from equation:

$$k_h = \min\left\{\left(\frac{150}{h}\right)^{0.2},\ 1\right\} \tag{21}$$

where:

h is the depth in mm.

Where the bending test arrangement is within the boundaries in EN 408, but with span l different of 18 h and/or distance between inner load points, a_f different of 6 h, then the bending strength shall be adjusted by dividing by the factor k_l according equation:

$$k_l = \left[\frac{48h}{l_{et}}\right]^{0.2} \tag{22}$$

$$l_{et} = l + 5a_f \tag{23}$$

Where l_{et} are the effective test length in mm, l are the span within the test arrangement, a_f are the distance between the two inner loading points, and the a_f and l are the values taken from the test.

To determine strength properties ($f_{m,0}$ and $f_{c,0}$), the following expressions were used, assuming a logarithmically normally distribution:

$$\bar{y} = \frac{1}{n}\sum_{i=1}^{n} \ln m_i \tag{24}$$

$$s_y = \max\left\{\sqrt{\frac{1}{n-1}\sum_{i=1}^{n}\left(\ln m_i - \bar{y}\right)^2},\ 0.05\right\} \tag{25}$$

where $\bar{y}$ is the mean value of the logarithmic data (Eq. 24), s_y is the corresponding standard deviation (Eq. 25), $\ln m_i$ is the natural logarithm of the property value, and n is the number of specimens.

The characteristic value of the property (m_k) is given by:

$$m_k = \exp\left(\bar{y} - k_s(n)\, s_y\right) \tag{26}$$

where the factor $k_s(n)$ is defined as:

$$k_s(n) = \frac{6.5n + 6}{3.7n - 3} \tag{27}$$

The characteristic strength value (f_k) for each grade is calculated as:

$$f_k = \min\left\{f_{05,i,\min},\ \frac{\sum_{i=1}^{n_s} n_i f_{05,i}}{n}\right\} \cdot k_n \tag{28}$$

where $f_{05,i}$ is the 5th percentile strength of sub-sample i, $f_{05,i,\min}$ is the lowest 5th percentile strength among sub-samples, n_s is the number of sub-samples, n_i is the number of specimens in sub-sample i, and n is the total number of specimens. The factor k_n accounts for the number of sub-samples and was

taken as $k_n = 0.80$ for two sub-samples.

Determination of characteristic density values. The characteristic value of density (ρ_k, kg m^{-3}) was determined using the expressions defined in Eqs. (16) and (17), where $\bar{y}$ is the sample mean, s_y is the sample standard deviation, m_i is the value of the property, and n is the number of specimens.

The characteristic value of the sample is given by:

$$m_k = \bar{y} - k_s(n)\, s_y \tag{29}$$

where the factor $k_s(n)$ is determined according to Eq. (19).

The characteristic density value (ρ_k) for each grade was calculated as:

$$\rho_k = \min\left\{1.1\rho_{05,i,\text{min}},\ \frac{\sum_{i=1}^{ns} n_i \rho_{05,i}}{n}\right\} \cdot k_n \tag{30}$$

where $\rho_{05,i}$ is the 5th percentile density of sub-sample i, $\rho_{05,i,\text{min}}$ is the lowest 5th percentile density among sub-samples, n_s is the number of sub-samples, n_i is the number of specimens in sub-sample i, and n is the total number of specimens. The factor k_n accounts for the number of sub-samples and was taken as $k_n = 0.91$ for two sub-samples.

Finally, specific mechanical properties were derived analytically using the empirical expressions proposed in EN 384:2016+A2:2022 [192] for hardwood species according table 2 definitions:

$$f_{t,0,k} = 0.6\, f_{m,k} \tag{31}$$

$$f_{t,90,k} = 0.6 \tag{32}$$

$$f_{c,0,k} = 4.3\, f_{m,k}^{0.5} \tag{33}$$

$$f_{c,90,k} = 0.010\, \rho_k \tag{34}$$

$$f_{v,k} = \begin{cases} 3.0 + 0.03\, f_{m,k} & f_{m,k} \leq 60\,\text{MPa} \\ 5.0 & f_{m,k} > 60\,\text{MPa} \end{cases} \tag{35}$$

$$E_{0,k} = 0.84\, E_{0,\text{mean}} \tag{36}$$

$$E_{90,\text{mean}} = \frac{E_{0,\text{mean}}}{15} \tag{37}$$

$$G_{\text{mean}} = \frac{E_{0,\text{mean}}}{16} \tag{38}$$

$$\rho_{\text{mean}} = 1.2\,\rho_k \tag{39}$$

3.4.4 Analysis of Results on Full-size Logs

Low and statistically no-significant correlations were found between the visual characteristics and the mechanical properties (see Section 4.6.4.c). Consequently, the influence of visual characteristics on mechanical performance will be analysed in detail in Chapter 4, in connection with the visual grading approach proposed by Ranta-Maunus [25], which is used in this study as a reference for the pre-selection of logs. Although no significant differences were observed in nominal or apparent diameters between the sample groups from both harvesting campaigns, the differences in specimen length 2.0 m for the 1st group (spring harvested) and 2.4 m for the 2nd (autumn harvested) required adapting the distance between the loading head and the lateral supports (a in Equations 11 and 13) to the geometry of each log. The logs from the 1st group were adjusted to a span between 5 and 6 times the nominal diameter (d_{nom}), while those from the 2nd group were adjusted to $6d_{nom}$, as illustrated in Figure 30.

To minimize the influence of environmental conditions during testing, each sample was removed from the hygrothermal chamber only minutes before its respective test. Temperature and relative humidity measurements were not taken during the trials. As reference values, for the 1st group (spring), and according to our records in the open field, temperatures of 11.70 °C (SD = 3.4 °C) were observed, with a relative humidity of 86 % (SD = 14.0%). For the logs of the 2nd group (autumn), an average temperature of 19° C was observed [195].

For the final bending tests aimed at determining the global modulus of elasticity (E_{global}) and bending strength (f_m), the mean duration to reach the maximum load (F_{max}) varied between the two groups. Due to logistical constraints, the first series of tests was performed on the 2nd group (autumn-harvested logs), during which the testing protocol was calibrated. This explains the longer average test duration recorded for this group 383.5 s (SD = 124.1 s) which exceeded the recommended standard of 300 $\pm$ 120 s [18]. However, the variability progressively decreased as the testing procedure was refined. In contrast, the 1st group (spring-harvested logs) exhibited an average test duration of 306.6 s (SD = 50.3 s), which was in accordance with the prescribed standard.

3.4.4.1 Failure Modes: Bending

Post-test inspection of the bending specimens confirmed that no indentation damage was observed at the interfaces between the fibre-reinforced concrete loading heads and the corresponding load application points on the logs. Most of the logs failed in the region of maximum tensile stress, except two specimens from the 2nd group, which did not fracture due to LVDT malfunction during testing. The most common failure mode was pure tension, characterised by the detachment and brittle fracture of a lower segment of the log, observed in 59% of specimens from the 1st group and 46% from the 2nd group (Figure 32 a–d). The second most frequent failure mode involved partial fracture initiated by the formation of one or more compression lines approximately perpendicular to the log in its upper-central region (Figure 32 e–h),

followed by a clear tensile fracture in the lower zone. This occurred in 47% of the 1st group and 23% of the 2nd group. Additionally, some specimens from the 2nd group exhibited splintering tension failures, where splintering of the lower area preceded a brittle tensile fracture (Figure 33 a-d). In specimens from both groups, failures related to longitudinal shear and deviations in grain angle were observed. These aspects are qualitatively analysed in greater detail in the visual characterization section (Figures 59 and 60).

3.4.4.2 Failure Modes: Parallel to the grain Compression

A total of 29 specimens were tested, comprising 9 specimens from 8 logs in the 1st group and 20 specimens from 10 logs in the 2nd group. No statistically significant differences were identified between the two groups concerning visual characteristics or mechanical strength parameters; therefore, the data from both groups were analysed collectively.

Two preliminary tests were conducted to establish the loading protocol. To ensure concentric load application and prevent secondary bending, each specimen was mounted on a spherical seat at the base. The compressive load was applied at a constant rate calibrated to induce failure within the timeframe specified by the standard (300 ± 120 s). The mean time to failure was 227 s (SD = 73 s), with 8 of the 29 specimens failing below the lower limit of 180 s and only 1 specimen exceeding the upper limit of 420 s. Following each test, a segment near the failure zone was extracted to determine moisture content (MC) and density. The MC, determined by the oven-drying method, averaged 16.07% (SD = 4.77%). The mean density, obtained via the immersion method, was 599.29 kg/m^3 (SD = 75.33 kg/m^3) a value approximately 15.6% lower than that measured in the bending tests.

Due to geometric irregularities and the presence of multiple defects including sweep, knots, and pre-existing cracks failure patterns in parallel compression varied significantly. In logs with pronounced sweep, failure typically initiated in the central region on the concave side, often accompanied by localised crushing of compressed fibres along one plane (Figure 34b, c). In logs with less sweep, failure was more frequently observed in the upper or lower third, often originating in knot zones or near cracks. These failures followed a shear plane oriented at approximately 45° (Figure 34d, e).

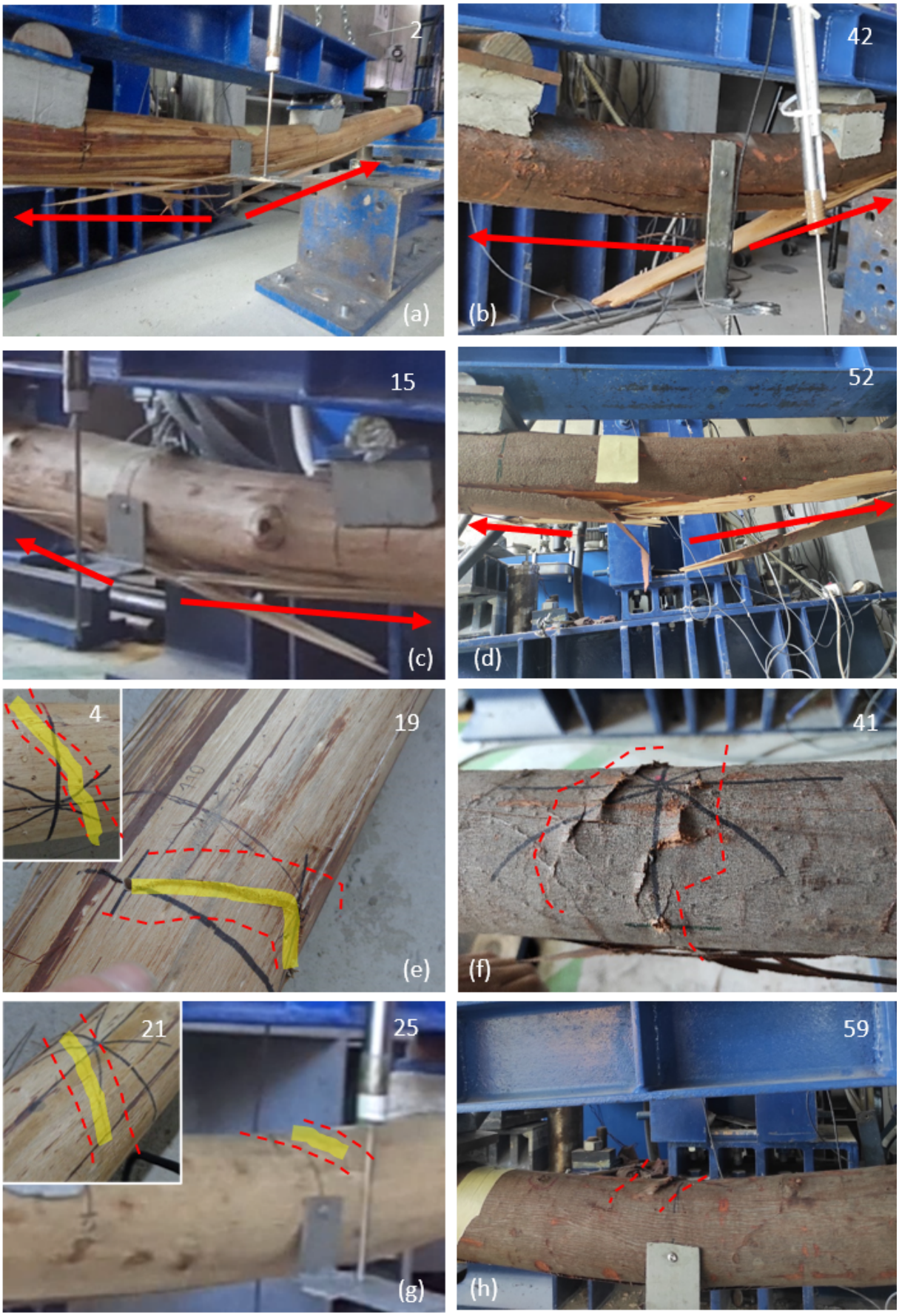

Figure 32: Figures a, b, c, and d: Failures by tension at the lower edge; Figures e, f, g, and h: Failures initiated by compression crushing at the upper edge, culminating in brittle tensile fracture at the lower edge (the log number is indicated in the upper right corner).

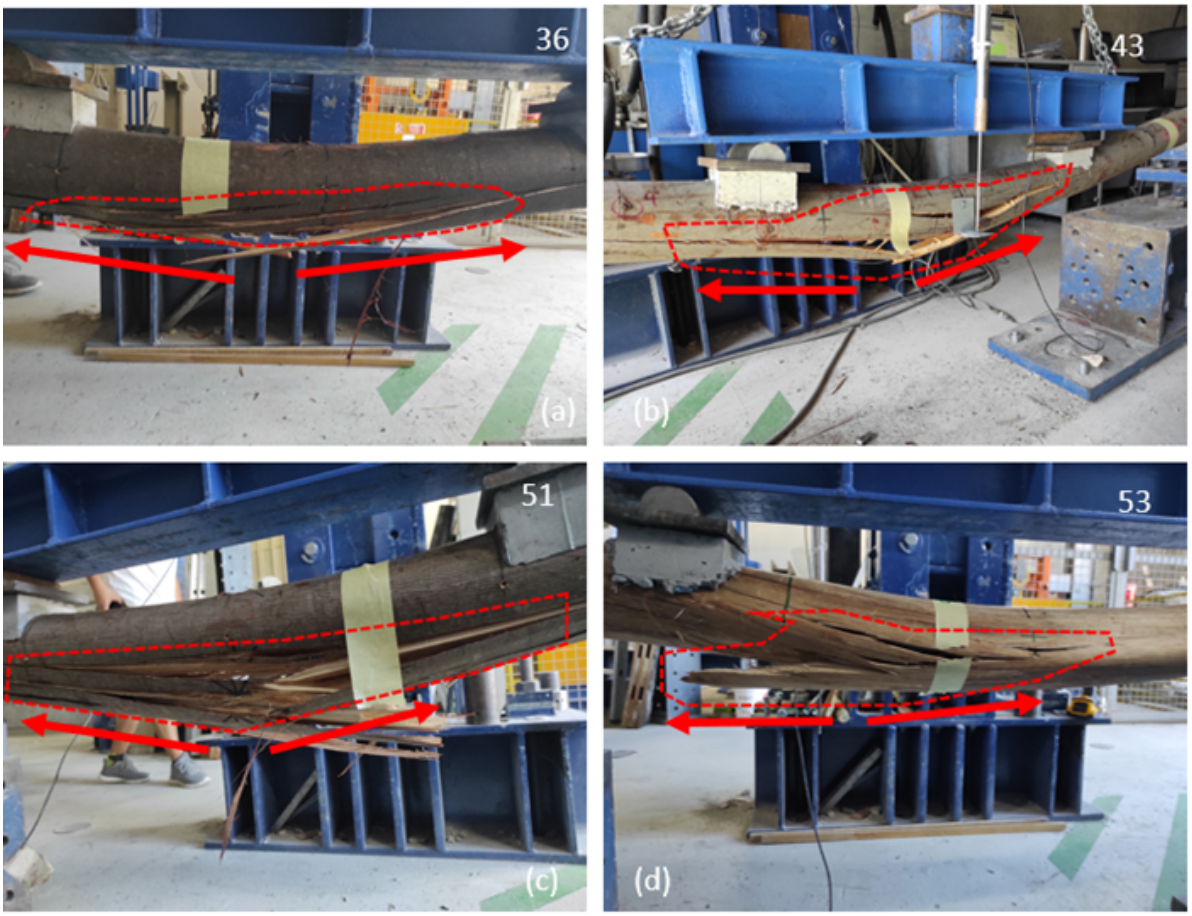

Figure 33: All images: Examples of splintering failures affecting a larger area of the lower edge in tension (the log number is indicated in the upper right corner).

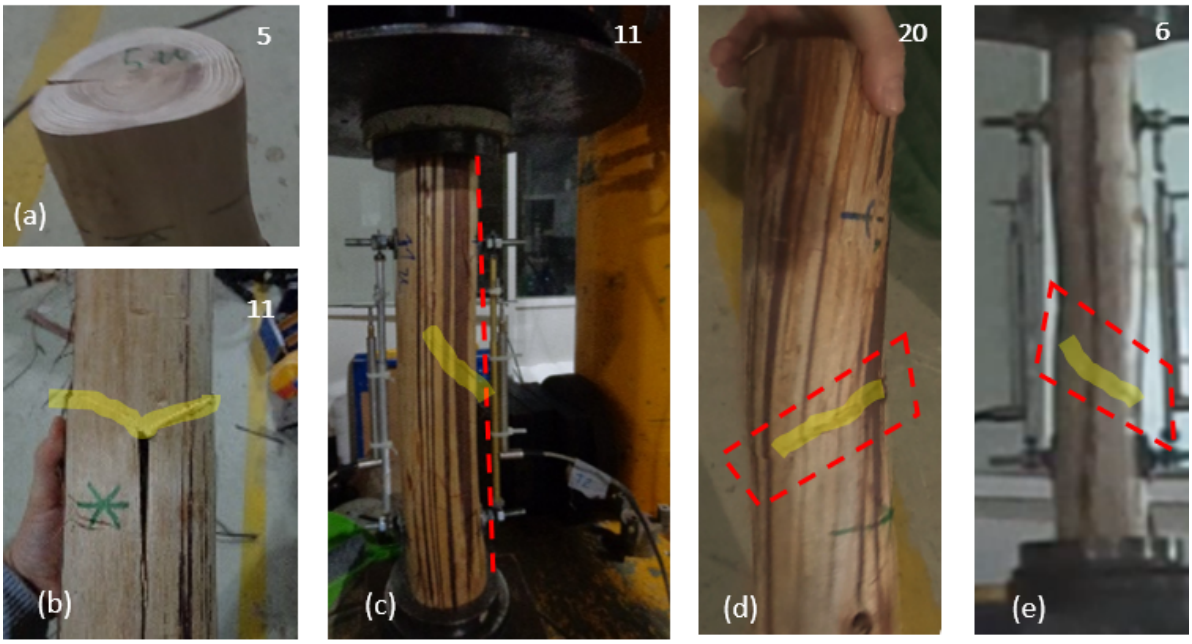

Figure 34: Failure modes under parallel compression: (a) Specimen exhibiting the highest ovality; (b) and (c) failure occurring in the concave region of a highly curved log (log 11); (d) and (e) typical shear failure observed in logs with lower curvature (logs 20 and 6).

3.4.4.3 Mechanical Characterisation of Full-Size Logs

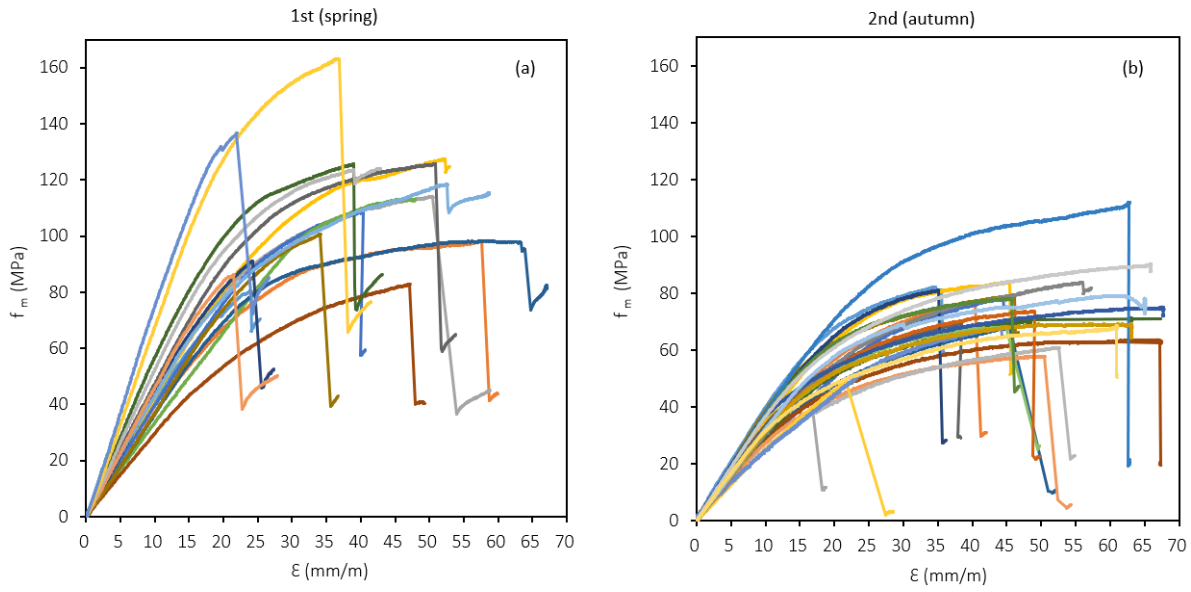

Figure 35: (a) Stress–strain curves for 17 *Acacia dealbata* Link logs harvested in spring (1st group) and (b) 28 logs harvested in autumn (2nd group).

Figure 35 presents the stress–strain curves for the logs tested in bending (all data review appendix B and C, table 21 and 22). The curves reveal notable differences between the two groups, with the 1st group demonstrating higher maximum loads and steeper initial slopes. Although most curves exhibit post-elastic behaviour, this was more pronounced in the 2nd group. Defining pseudo-ductility (μ) as the ratio between ultimate deformation (w_u) and yield deformation (w_y), the average values were 1.9 (SD = 0.4) for the 1st group and 2.5 (SD = 0.6) for the 2nd, indicating greater ductility in the latter.

Figure 36 provides histograms of all results from the destructive tests and compares them with reference values reported for other low-processed hardwood species [15, 136, 137]. Figure 36a displays the adjusted values of local and global Modulus of Elasticity ($E_{local-global}$), along with density (ρ_{12}) and bending strength (f_m), all normalised to 12% moisture content (MC) by the EN 384:2016+A2:2022 standard [192]. Figure 36b shows the unadjusted bending strength values and the corresponding MC of each log, as measured at the time of testing following the kiln-drying protocol.

In the comparative histogram analysis, both E_{local} and E_{global} of the *Acacia dealbata* logs exceeded those of all reference hardwood species. Specifically, the mean E_{local} values for the 1st and 2nd groups were 23.6% and 12.1% higher, respectively, than those reported for Oak the hardwood species with the highest modulus (both MOE and MOR) in the referenced literature. In terms of average density, the values also surpassed those of Alder (by 29.4%), Ash (4.2%), Birch (13.5%), and Sycamore (20.2%), while remaining only 3.9% below Oak. A similar trend was observed for bending strength. The 2nd group alone exhibited mean f_m values that were 31.6% higher than Oak, 35.4% above alder, 28.3% above Ash, and 44.8% and 44.9% higher than Birch and Sycamore, respectively.

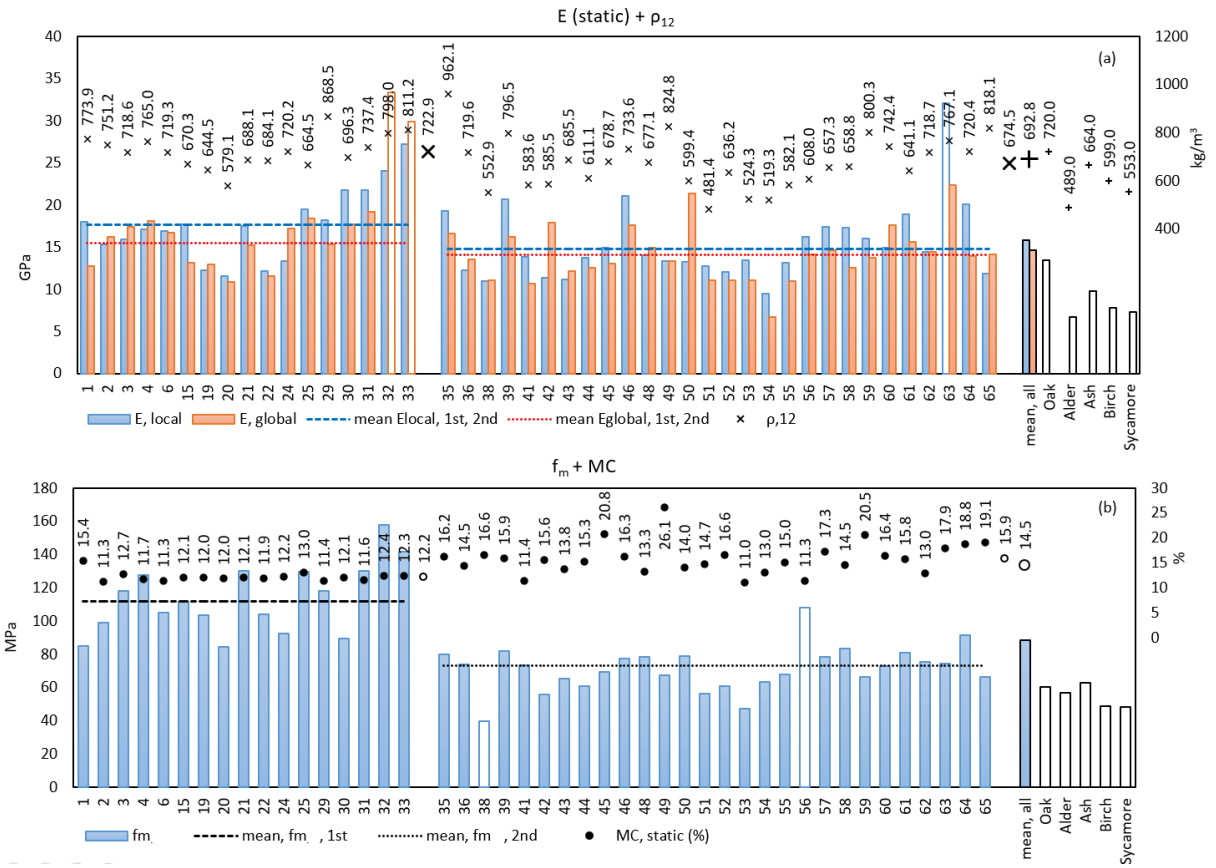

Figure 36: Histograms of destructive test results: logs 1–33 correspond to the 1st group, and logs 35–65 to the 2nd group. Unfilled bars represent outliers excluded from the statistical analysis. Reference values from other studies are shown at the far right [15, 136, 137]. (a) Local modulus of elasticity (E_{local}, blue) and global modulus of elasticity (E_{global}, red); crosshairs indicate density values adjusted to 12% moisture content (MC), according to EN 384:2016+A2:2022. (b) Bending strength (f_m) and corresponding MC for each log.

When comparing the two groups, 1st (spring) and 2nd (autumn), particular attention should be given to the behaviour of E_{local} relative to the other parameters. The E_{local} values are directly comparable between groups for two main reasons. First, this parameter is derived using Equation 7, which is based on the apparent diameter (d_1). As we will discuss in Section 4.5.1, no significant differences were found between the mean values of d_1 for the two groups; therefore, statistical comparability is maintained. Second, the loading configuration ensures that shear deformations do not influence midspan deflections, effectively isolating the pure bending response. Furthermore, the moisture corrections applied according to EN 384:2016+A2:2022 (Equation 12) further minimise residual variability. Conversely, as noted in the literature review, E_{global} and f_m are more likely to be affected by geometric irregularities, natural defects, and moisture content (MC), and thus should be interpreted with greater caution.

Considering these factors, the 1st group achieved significantly higher stiffness and strength values. The histograms illustrate the full data distribution, with hollow bars indicating outliers excluded from the calculation of mean values. Both groups exhibited E_{local} values exceeding their corresponding E_{global} values—by 12.6% in the 1st group and 4.3% in the 2nd which aligns with the theoretical expectation that shear effects do not influence E_{local} in the 1st group. The E_{global} of the 1st group was 16.5% higher than

that of the 2nd group, although this difference was not statistically significant.

One potential factor influencing E_{global} is the difference in log length between groups. Zangiácomo [134] reported that for logs of *Pinus elliottii*, *Pinus caribaea* var. caribaea, and *Eucalyptus*, an increase in the length-to-diameter (l/d) ratio led to a decrease in the modulus of elasticity, albeit to varying degrees depending on the species. In the present study, due to length differences (2.0 m for the 1st group and 2.4 m for the 2nd), the values of the lateral support span (a) were not constant. As a result, the l/d ratio ranged from 16 to 18 for the 1st group and was consistently around 18 for the 2nd group. This may partly explain the higher E_{global} in the 1st group, even though the difference was not statistically significant. Additionally, the position of the section relative to the applied load may influence outcomes due to irregular cross-sectional geometry. Christoforo et al. [196] recommend testing logs in multiple orientations for more accurate modulus determination, particularly in irregular sections. However, in this study, all tests were conducted following the natural curvature of each log, which in most cases coincided with the section of smallest diameter—thus yielding conservative estimates. At the level of bending strength (f_m), the difference between the two groups was highly significant ($p < 0.001$), with the 1st group exhibiting values 34.5% higher than those of the 2nd. A plausible explanation for this disparity relates to the moisture content (MC), which—unlike other physical or mechanical parameters—is not typically corrected by adjustment factors in the case of bending strength. However, as with other wood properties, bending strength tends to increase as the MC decreases below the fiber saturation point (FSP), approximately 30%. Several authors have documented the influence of MC on the mechanical performance of wood. Arriaga et al.[159], citing the *Wood Handbook* [197], indicate that the modulus of rupture (MOR) increases by approximately 4% for each 1% reduction in MC below the FSP. For a narrower range (12% to 16% MC), Dinwoodie [140] reports a 3.3% variation in MOR for *Pinus sylvestris* timber.

Ido et al. [166] also highlight two factors that, in the context of the present study, could act in opposite directions. On the one hand, the effect of MC on bending strength is smaller in round timber than in small, defect-free rectangular specimens. On the other hand, the presence of significant defects—particularly knots can diminish the sensitivity of the material to moisture variations. In the present study, as previously discussed, knot prevalence was more pronounced in the 1st group, where 23.5% of the logs exceeded the most restrictive threshold proposed by Ranta-Maunus (i.e., 30% of the diameter). Nevertheless, considering the values proposed by Arriaga et al. [159] and the MC distributions observed in both groups, the expected increases in bending strength attributable solely to moisture content are limited. For the 1st group, with a mean MC of 12.21% (SD = 0.95%), the estimated strength increase would be less than 1%. In contrast, the 2nd group exhibited an average MC of 15.88% (SD = 3.22%), which could theoretically result in a 10–15% reduction in strength. Thus, even after accounting for moisture-related effects, a substantial and statistically significant difference in bending strength remains between the two groups.

Figure 37 presents the relationship between mechanical properties (excluding outliers) and moisture content (MC). The elastic moduli (E_{local} and E_{global}) were adjusted to a reference MC of 12% by EN 384:2016+A2:2022, which had a more pronounced effect on the 2nd group (Figure 37a). The correction resulted in smaller percentage differences in the final values of the elastic moduli for the 2nd group, with

adjustments of 6.5% for E_{local} and 6.8% for E_{global}. In contrast, the 1st group showed differences of less than 1%, indicating limited influence of MC adjustment due to their narrower MC range.

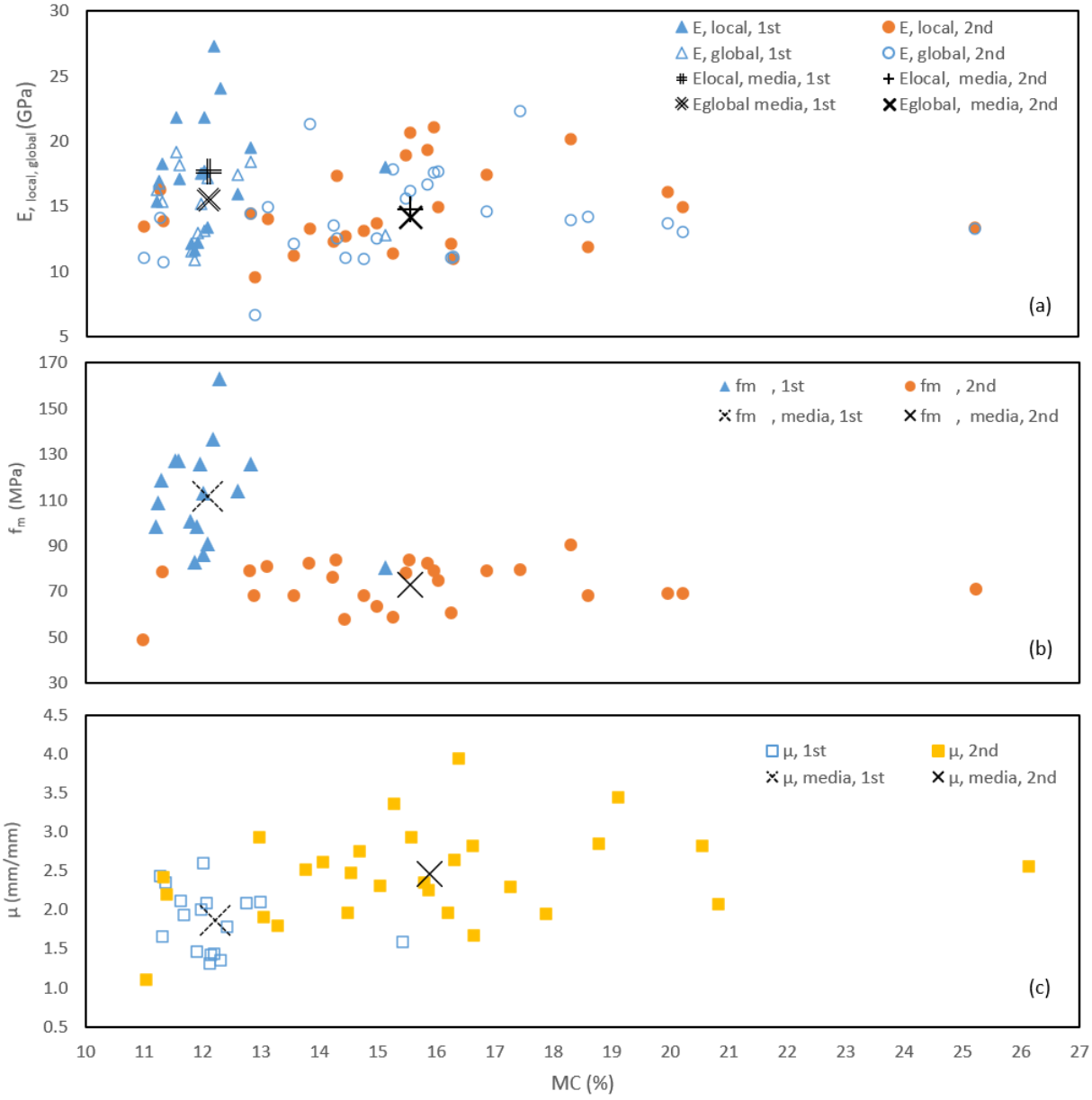

Figure 37: Relationships between moisture content (MC) and mechanical properties from destructive tests, separated by group (1st and 2nd): (a) E_{local} (triangles) and E_{global} (circles); (b) Bending strength (f_m); (c) Ductility index (μ).

Regarding bending strength, a clearer trend is observed (Figure 37b). In the 1st group, lower MC dispersion around values close to 12% is associated with the highest but more variable strength values, reflecting the inherent heterogeneity of the logs. In the 2nd group, greater dispersion in MC is observed alongside lower variability in strength values, possibly indicating a moderating effect of moisture on mechanical behavior. Figure 37c illustrates the relationship between ductility and MC. A higher and more dispersed MC correlates with more pronounced post-elastic behavior, which aligns with the findings of Kherais et al. [37], who linked ductile or semi-ductile responses to elevated MC.

Table 3 presents the correlation matrix among the mechanical properties obtained from the destructive tests. Across all specimens, the static density (ρ_{12}) exhibited a low but positive and statistically significant correlation with the mechanical parameters, with the strongest relationship observed with E_{local} (r = 0.51, p < 0.001). It should be noted that these correlations are considerably lower than those reported in the reference literature. In contrast, the correlations between the mechanical properties themselves (f_m, E_{local}, and E_{global}) were higher than those involving density for all groups. This behaviour can be attributed to the variability of the mechanical test results. As shown in Table 22 (Appendix C), the coefficients of variation (cov) for all logs are close to or greater than 30%, whereas the cov for density is 14.1%.

Table 3: Correlations between destructive test results.

		f_m	E_{global}	E_{local}
ρ_{12}	all	0.41 **	0.48 ***	0.51 ***
	1st	0.46 ^{ns}	0.54 *	0.57 *
	2nd	0.37 ^{ns}	0.46 *	0.45 *
E_{local}	all	0.52 ***	0.71 ***	-
	1st	0.65 **	0.81 ***	-
	2nd	0.48 **	0.63 ***	-
E_{global}	all	0.63 ***	-	-
	1st	0.77 ***	-	-
	2nd	0.37 ^{ns}	-	-

ns: no significance level; * p < 0.05 ; ** p < 0.01; *** p < 0.001

When analysed by group, the 1st group exhibited a moderate positive correlation between density and E_{local}, while the 2nd group remained within a low-correlation range. This trend of stronger correlations in the 1st group is particularly evident in the relationship between E_{local} and E_{global}, which was high and statistically significant across all samples (r = 0.81 for the 1st group). The correlation between E_{local} and bending strength (f_m) was moderately positive, whereas E_{global} and f_m were highly and positively correlated (r = 0.77), indicating that E_{global} is a more reliable predictor of bending performance.

Finally, to illustrate the parallel compression results, Figure 38 presents representative stress–strain curves selected based on specific visual characteristics (all data review appendix D table 23). Figure 38a shows specimens exhibiting ovality greater than the limit proposed by Ranta Maunus [25] (>20%) as shown in Figure 34a. The segmented curve denotes the lowest performance among all tests in the ovality R-M threshold. These specimens exhibited abrupt stiffness loss following peak load, which would be indicative of buckling about the weak axis. In contrast, Figure 38b displays a stress-strain graph for curved specimens with sweep values exceeding 10 mm/m, a threshold according to Ranta-Maunus (See table 10). These specimens generally demonstrated a smoother curve and more ductile behaviour.

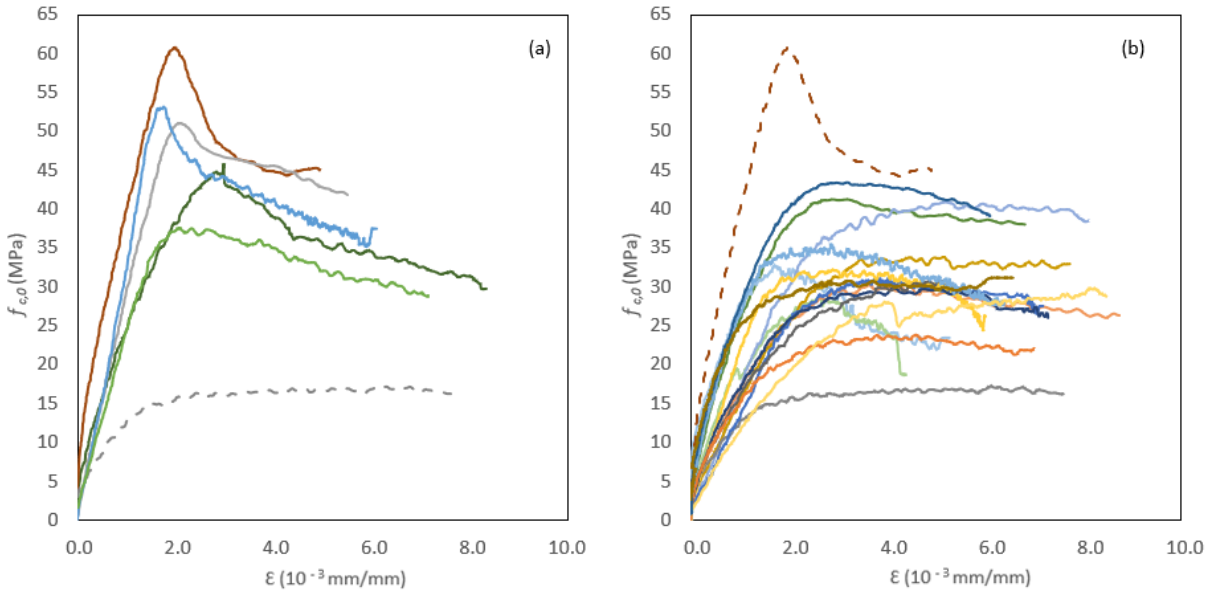

Figure 38: Stress–strain curves of full-size logs: (a) Curves corresponding to logs with ovality exceeding the limit proposed by R-M (≤ 20% for Grade B). The dashed line represents the curve of the specimen with the lowest maximum load, included for reference; (b) Curves of logs exhibiting sweep greater than 10 mm/m. The dashed line indicates the curve of the specimen with the highest maximum load, also shown for reference.

Table 4: Mechanical properties and strength classes (to properties definitions see table 2).

	1st				2nd				all				
	Mean[(1)]	Char.$_{,k}$[(2)]	S.C.[(3)]	n°	Mean[(1)]	Char.$_{,k}$[(2)]	S.C.[(3)]	n°	Mean[(1)]	Char.$_{,k}$[(2)]	S.C.[(3)]	n°	Source
Stiffness properties in GPa													
$E_{0,k}$	17.67	16.93	D60	17	14.68	13.59	D50	28	15.84	14.25	D50	45	Testing
$E_{90,\text{mean}}$	1.13				0.91				1.06				EN 384
G_{mean}	1.06				0.85				0.99				EN 384
Strength properties in MPa													
$f_{m,0}$	111.66	70.71	D70	17	73.16	53.41	D50	26	88.38	48.20	D45	43	Testing
$f_{c,0}$	39.43	25.22	D35	9[(4)]	36.49	18.57	D18	20[(4)]	37.40	16.51	un[(5)]	29[(4)]	Testing
$f_{t,0,k}$									28.92				EN 384
$f_{t,90,k}$									0.60				EN 384
$f_{c,0,k}$									29.85				EN 384
$f_{c,90,k}$									4.69				EN 384
$f_{v,k}$									4.45				EN 384
Density in kg/m^3													
ρ_{12}	723.01	588.45	D45	17	674.50	470.99	un[(5)]	28	692.83	468.98	un[(5)]	45	Testing
ρ_{mean}	706.14				565.19				562.78				EN 384

(1) Mean value adjusted according to EN 384:2016+A2:2022 [192].
(2) Characteristic value according to EN 384:2016+A2:2023 and EN 14358:2016 [194].
(3) Strength class according to EN 338:2016 [198].
(4) Some specimens correspond to the same tree.
(5) Unclassifiable according to EN 338:2016.

To assess the suitability of the logs for structural applications, the samples were classified according to

the European standard EN 384:2016+A2:2022 [192]/ EN 14358:2016 [194] and summarized in Table 4. Outliers were removed, and strength classes were assigned according to EN 338:2016 [198], based on density, modulus of elasticity, bending and compressive strength parallel to the grain. For bending modulus of elasticity, only E_{local} was considered. Given that the p-values for group comparisons approached significance thresholds, the characterisation summarises the resulting strength class assignments, indicating the number of valid specimens per category.

These results are consistent with preliminary findings from an earlier phase of the study (Suazo-Uribe et al. [190]), which assigned strength classes based on NDT. The characteristic elasticity modulus ($E_{0,k}$) values supported classifications ranging from D50 to D60, while characteristic density ($\rho_{k,12}$) yielded lower class assignments, typically around D40, and was unclassifiable (uc) for some specimens in the 2nd group.

Table 5: Means comparison (t-test) between the 1st and 2nd groups of full-size logs for different mechanical properties

	ρ_{12}	E_{local}	E_{global}	$f_{m^{(1)}}$	$E_{c,0}$	$f_{c,0}$
t-statistic	1.64	2.59	1.42	6.87	1.07	1.29
p-value	ns	*	ns	***	ns	ns

ns: no significance level; * p < 0.05 ; ** p < 0.01; *** p < 0.001;(1) Unequal Variance

When the results are analysed by harvest season, both DT and NDT [190] revealed statistically significant differences in mechanical performance between the two harvest groups. Table 5 presents the results of independent sample t-tests for the main mechanical properties obtained through destructive testing, excluding outliers. No significant differences were found in density (ρ_{12}), E_{global}, or compressive properties ($E_{c,0}$, $f_{c,0}$). However, significant differences were detected in E_{local} (marginally significant) and f_m (highly significant). The reasons for this disparity remain unclear. Suazo-Uribe et al.[190] proposed several hypotheses, including the influence of harvest timing, log length differences, and the presence of bark in the 2nd group—factors likely associated with greater variation in moisture content (MC).

3.4.5 Destructive Testing on Free-defect Small Samples

3.4.5.1 Samples Preparation

The small, clear samples were primarily obtained from discarded logs following visual classification, with a smaller portion derived from remnants of samples previously tested on a full scale. Since the diameters of the logs were smaller than 150 mm, the secondary method for geometric definitions, as outlined in ASTM D 143-94 [176] and NCh987.Of86 [199] standards were chosen.

The logs were sawn in a specialized timber construction facility into strips with a 25.25 mm² cross-sectional area (Figure 39 (a)). The final length was adjusted to 410 mm for the bending tests, with the test distance marked at 360 mm on each piece. The strips were further cut to 100 mm for the compression tests to ensure flat, parallel cuts at both ends using a fixed cutting disc. Two sample groups were extracted for bending and compression testing: one from the spring group, consisting of 51/45 specimens from 6 trees, and the other from the autumn group, consisting of 49/50 specimens from 10/8 trees, respectively.



Figure 39: Small clear sample preparation. (a) Sawing of logs to form 25.25 mm^2 strips; (b) conditioning of small clear samples in the climatic chamber; (c) tray for drying in an oven of fragments of 25.25.25 mm^3 from bending test samples.

3.4.5.2 Determination of Moisture Content and Density

Before testing, all samples were weighed using an electronic scale and measured with a digital calliper. Two length measurements and three cross-sectional measurements (height and width) were taken for the bending tests. After each bending test, a 25 mm length specimen was extracted from the area near the failure zone (Figure39 (c)), weighed, and then stored in a drying oven at 103 °C following the specified standard [167] for the oven-drying method. The procedure for compression tests was similar, with the entire sample volume considered, taking two cross-sectional measurements of height and width at both ends of each specimen. These values were used to determine each sample's density and moisture content during the tests. Following EN 384:2016+A2:2022 standards [192], adjustments were made to the density, $\rho_{small,12}$, parallel compression strength, $f_{c,0}$ and modulus of elasticity, E_{small} values using MC values got with oven drying method.

Additionally, visual characteristics were recorded for each specimen. Over each end, the percentage of heartwood and the angle of the tangential plane to the growth rings according to the load were determined, averaging both sets of values. The fibre slope on both sides of the piece was also measured along its length.

3.4.5.3 Bending and Parallel Compression Testing

The testing protocols were based on ASTM D 143-94 [176] and NCh987.Of86 [199] standards for bending, and NCh973.Of86 [200] for parallel compression. The tests were conducted at the civil engineering laboratory in July 2024 using 25 kN servo-actuator. Before testing, the samples, adjusted to the appropriate geometry, were stored in a climate chamber at a temperature of 20°C (±0.5°C) and relative humidity of 60% (±5%) until a constant weight was reached (Figure39(b)).

The static bending test protocol (Figure 40) consisted of applying a point load at the centre of the span at a constant rate of 2.5 mm/min, measuring deflections with a precision greater than 0.01 mm. Care

was taken to ensure that the cross-section of each sample was oriented with the load applied in the radial plane and with the pith at the top. The bending modulus of elasticity for small clear samples, E_{small} is given by the equation:

$$E_{small} = \frac{F_{pl}}{\delta_{pl}} \frac{L^3}{4bh^3} \tag{40}$$

Where F_{pl} is the load at the proportionality limit, expressed in N; δ_{pl} is the deflection at the proportionality limit, in mm; L is the span length between supports, in mm; b is the width of the specimen, in mm; and h is the height of the specimen, in mm.

The bending strenght for small clear samples, $f_{small,m}$ is given by the equation:

$$f_{small,m} = \frac{3F_{max}L}{2bh^2} \tag{41}$$

Where, F_{max} is the maximum load in N.

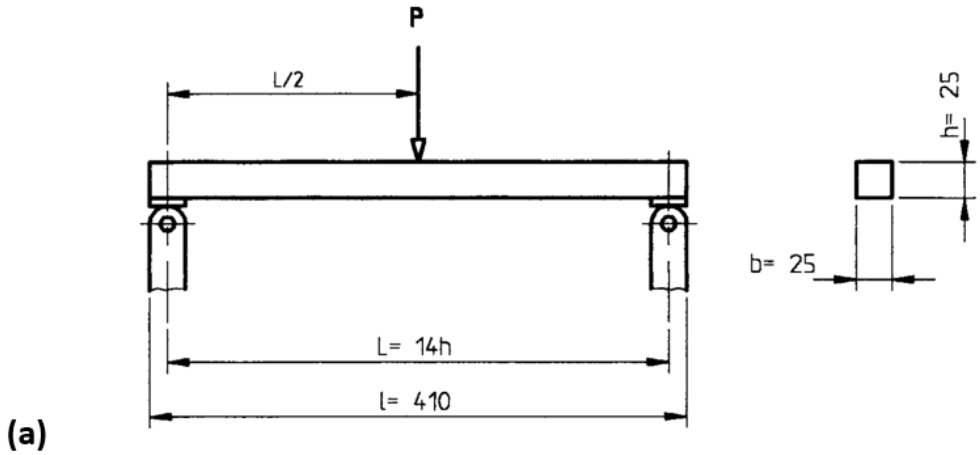

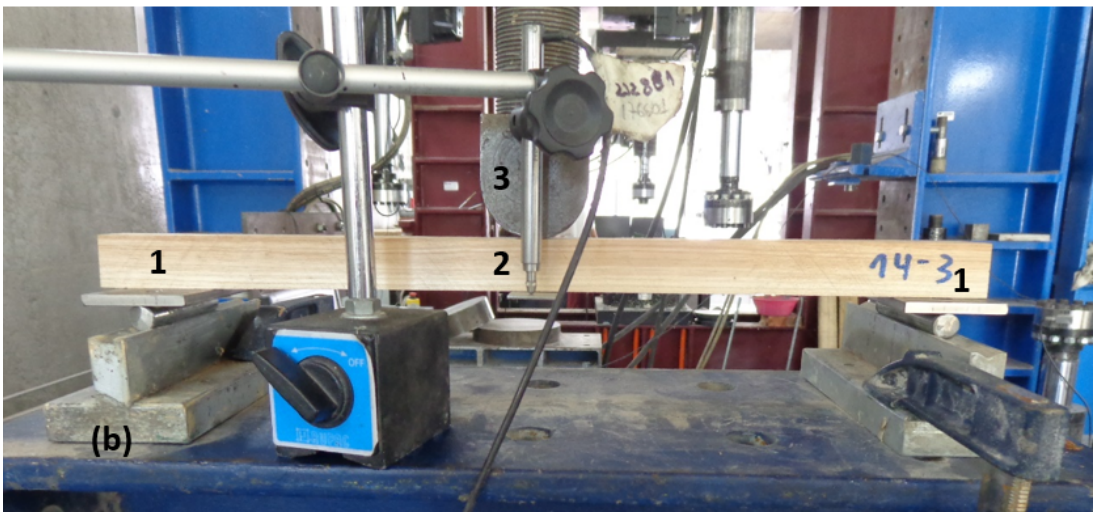

Figure 40: Bending test setup of small clear samples. (a) Geometrical definition according to NCh 987.of86 [199]; (b) Image of the test with the two sliding supports (1), the central LVDT device (2) and (3) the solid steel loading head according to the standard.

For the parallel compression test (Figure 41), a point load was applied along the axis of the specimen at a constant rate of 0.6 mm/min, with deformations measured to a precision greater than 0.002 mm. The lower head was designed with a ball joint to ensure uniform load distribution across the specimen. The parallel compression strength for small clear samples, $f_{small,c,0}$ is given by the equation:

$$f_{small,c,0} = \frac{F_{max,c}}{wt} \tag{42}$$

Where $F_{max,c}$ is the maximum load in parallel compression, expressed in N; w is the average of the measured widths, in mm; and t is the average of the measured thicknesses, in mm.

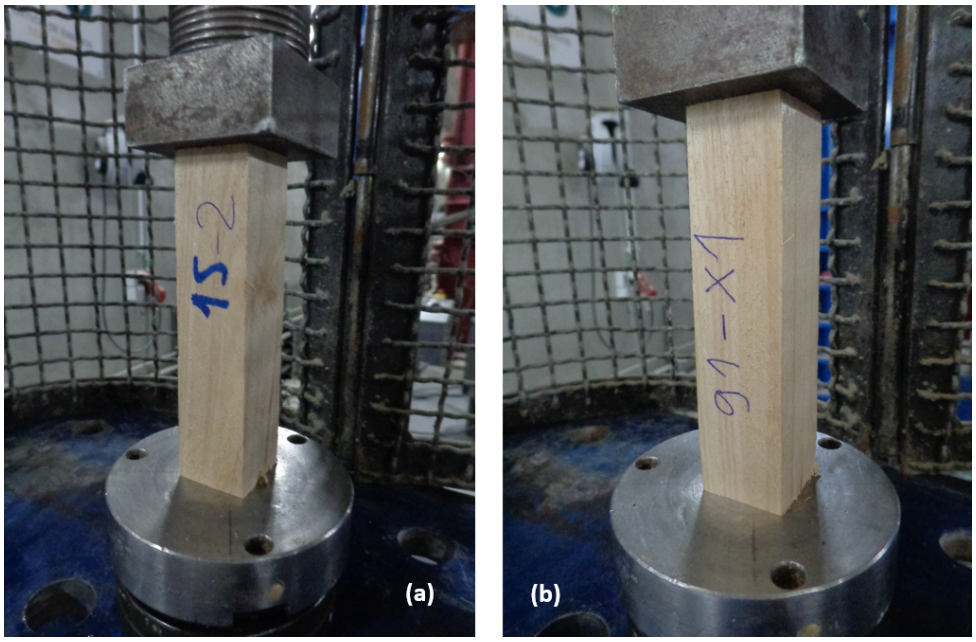

Figure 41: Parallel compression of small clear samples. (a), (b) View the set-up with a couple of samples before testing.

3.4.6 Analysis of Results on Free-defect Small Samples

An additional objective of the defect-free sample tests was to compare the observed trends in the differences between the two harvest groups (1st and 2nd), using a statistically more robust sample size. This approach aimed to isolate variables that could have influenced the mechanical performance of the full-size logs, such as moisture content, defects (e.g., knots or tapered edges), and the presence of bark.

The small diameter of the logs influenced the selection characteristics of the specimens. After preparation, specimens with pith were discarded; however, some specimens with a high percentage of heartwood, reaching up to 100%, were included. The mean heartwood percentage for the 1st and 2nd groups was 34.4% (SD = 29.0%) and 33.0% (SD = 29.3%), respectively. Load application was oriented along the radial plane with the core positioned at the top, although the mean angle of the tangential plane relative to the horizontal was 19.5° (SD = 17.7°) for the 1st group and 18.8° (SD = 16.4°) for the 2nd group, with a maximum deviation of 45°. Some samples, exhibiting a fibre slope of up to 10 mm over 410 mm on one

of their faces, were also tested.

The samples were transported to the test area in groups and kept packed to minimise the impact of environmental conditions on the moisture content (MC). Bending tests were conducted at an average temperature of 24.9°C and relative humidity of 53.5%, while parallel compression tests were carried out at 24.7°C and 64.2%, respectively. After the bending tests, a 25 mm sample was extracted from the failure area to determine the moisture content. Figures 42a,b display the resulting curves from the bending tests.

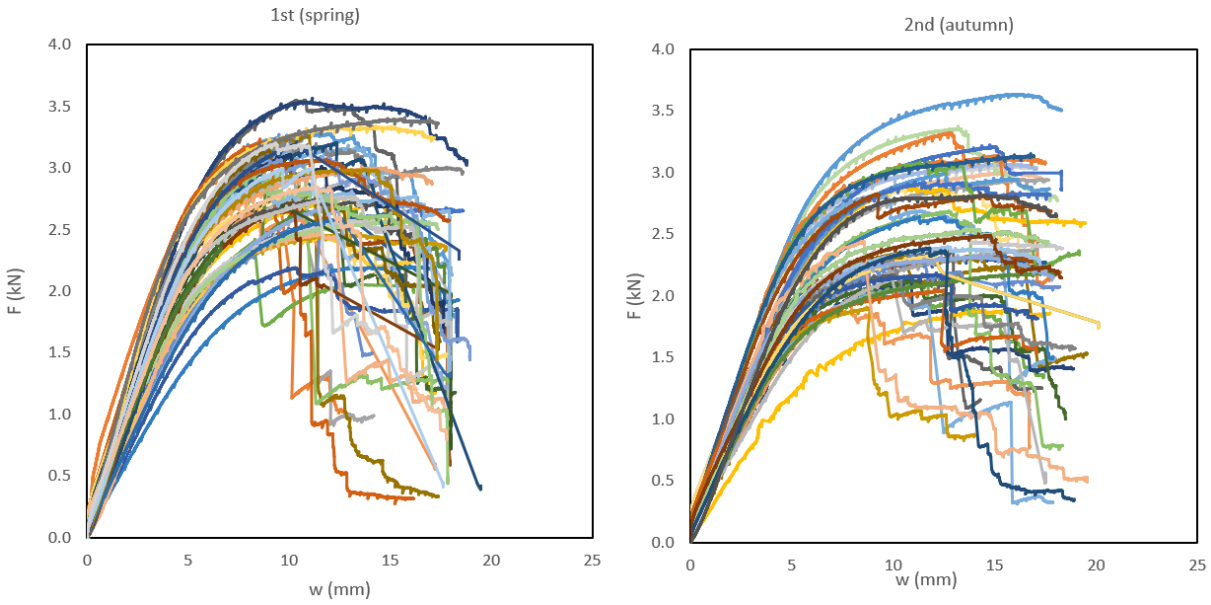

Figure 42: Bending force-displacement curves for free-defect small samples from 6 trees harvested in (a) spring (1st group) and 10 trees harvested in (b) autumn (2nd group).



Figure 43: Bending failure modes of free-defect small samples: (a) embedding failure; (b) typical brittle bending fracture; (c) and (d) splintering tension failure; and (e) slope fibre failure.

As observed in the full-size log tests, the bending curves exhibited post-elastic development with proto-ductility. However, a difference in the failure modes was noted, providing insight into the causes of this behaviour. While all samples ultimately failed by brittle fracture in tension, the majority of specimens (52.2% in the 1st group and 73.9% in the 2nd group) initiated failure with embedding of the upper fibres (see Figure 43a). This occurred due to the load head being embedded in the upper portion of the sample, leading to brittle fracture at the lower edge, which resulted in the sample being divided into two straight segments (see Figure 43b). In contrast, full-size logs did not exhibit this behaviour, as the interface between the load and the log allowed stress distribution over a larger area. Other failure modes were predominantly tensile, including brittle fracture of the tension edge (10.9% in the 1st group and 2nd group) and splintering tension, which affected a larger area in tension (13.0% in the 1st group and 2nd group, see Figures 43c,d). Failures due to fibre slope were also observed in both groups, at rates of 21.7% for the 1st group and 6.5% for the 2nd group (see Figure 43e)

Figures 44a,b display the curves obtained from the parallel compression tests. These curves exhibit linear development up to the maximum load, after which they experience a substantial reduction in strength without any post-elastic behaviour. Failures predominantly occurred along a shear plane at the center or in the upper or lower quarters of the specimen height, where the fibers within the plane buckled (Figure 45a). It was observed that this failure was influenced by surface cracks, such as checks (Figure 45b), or by eccentricity in strength distribution, particularly when the specimen contained both sapwood and heartwood, resulting in the crushing of the weaker side (Figure 45c,d).

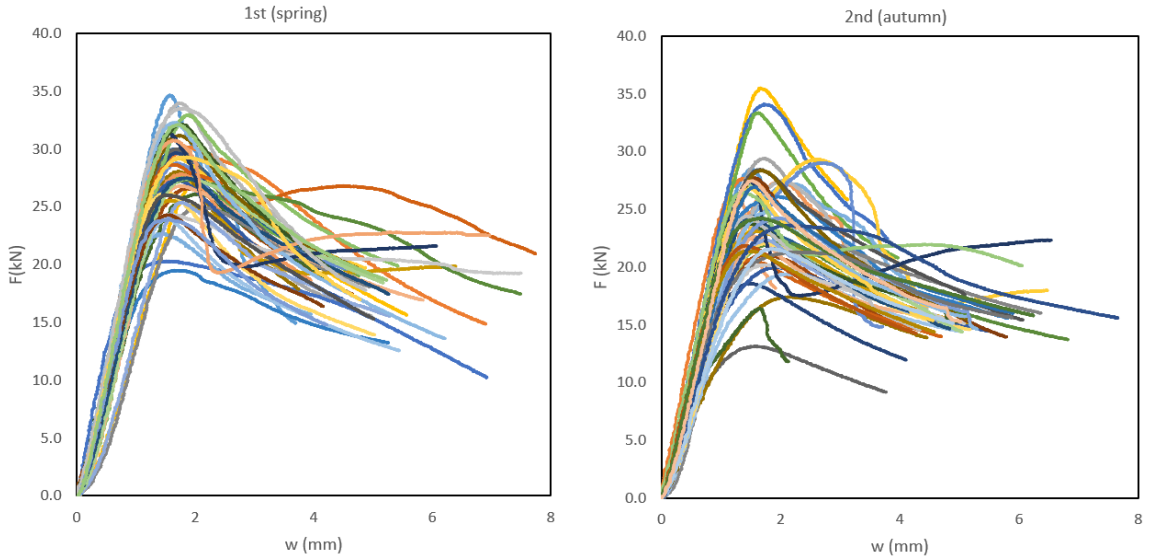

Figure 44: Parallel compressive force-displacement curves for free-defect small samples from 6 trees harvested in (a) spring (1st group) and 8 trees harvested in (b) autumn (2nd group).

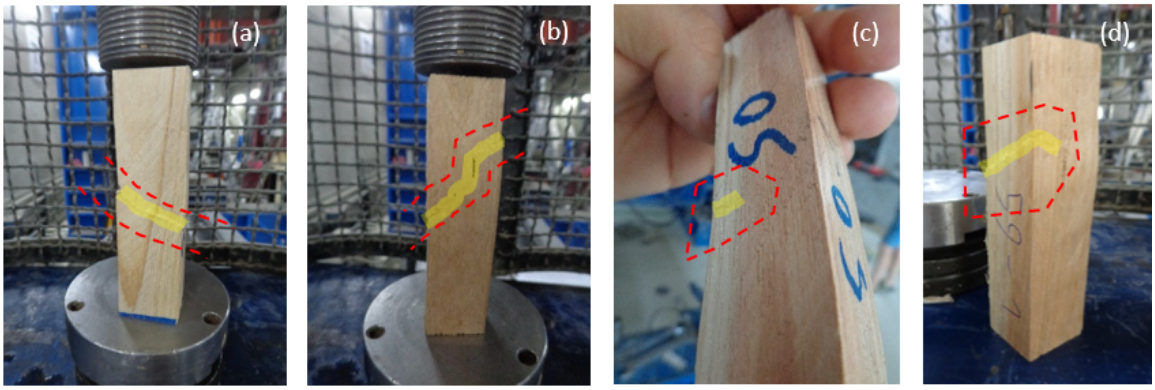

Figure 45: Parallel compressive failure modes of free-defect small samples: (a) shear failure in the middle; (b) failure associated with checks; (c) and (d) sapwood side failure.

Excluding the outliers from the analysis, Table 6 presents the descriptive statistics for the test results of each group. The moisture content (MC) of the samples during the tests was 12.3% (SD = 1.2%) for the 1st group and 12.5% (SD = 1.1%) for the 2nd group in the bending tests, and 11.3% (SD = 1.7%) and 10.8% (SSD = 1.8%) in the parallel compression tests, respectively. These values are close to the 12% reference, with coefficients of variation of 10.16% and 8.87% for bending tests, and 15.14% and 16.86% for parallel compression tests in the 1st and 2nd groups, respectively. Another difference is that the coefficients of variation (cov) for the defect-free small samples are lower when comparing each variable.

Table 6: Statistical summary for mechanical properties and density of free-defect small samples (1st and 2nd groups).

	$\rho_{small,12}$ kg/m^3		$E_{small,12}$ GPa		$f_{small,m}$ MPa		$f_{small,c,0}$ MPa	
	1st (s)	2nd (a)	1st (s)	2nd (a)	1st (s)	2nd (a)	1st (s)	2nd (a)
Mean	647.69	628.05	15.12	15.08	107.11	100.67	45.94	41.79
SD	46.77	59.51	1.99	2.18	10.49	15.80	5.14	7.79
cov (%)	7.22	9.48	13.18	14.46	9.79	15.69	11.20	18.64
Max	766.94	747.27	20.17	20.88	125.63	136.19	56.00	59.57
Min	524.11	520.12	10.06	9.59	83.15	69.80	31.24	21.39
n	43	40	43	40	43	40	45	48

Compared to other hardwood species tested using small samples without defects [183, 184], the mean values obtained in this study are relatively close. In terms of density (ρ_{12}), Iroko (*Milicia excelsa*), a tropical hardwood, exhibits higher values, reaching 743.12 kg/m³ [184]. The modulus of elasticity (E) of *Acacia dealbata* falls between that of Iroko, at 9.95 GPa [184], and *Eucalyptus globulus*, at 22.27 GPa [183]. The bending strength (f_m) is comparable to Iroko (105.30 MPa, [184]) but lower than that of Eucalyptus (124.1 MPa, [183]). Finally, the compressive strength parallel to the grain ($f_{c,0}$) is substantially lower than that of Eucalyptus, which reaches 73.6 MPa [183].

3.4.7 Comparison Between Full-Size Logs and Defect-Free Small Specimens

As shown in Table 7, the correlations between the mechanical properties obtained from the destructive tests on the defect-free small specimens were all highly significant ($p < 0.001$). Their values were also higher than those of the full-size samples (Table 3), although some variations were observed.

For density ($\rho_{small,12}$), the correlation with the modulus of elasticity by small samples (E_{small}) was moderate in both groups, close to the correlations between density (ρ_{12}) and the local (E_{local}) and global (E_{global}) moduli of elasticity in the full-size log samples, where the correlations were also moderate but lower ($r = 0.48$ and $r = 0.51$, respectively). The correlation between density ($\rho_{small,12}$) and bending strength ($f_{small,m}$) was moderate for the 1st group and very high for the 2nd group, whereas the full-size logs exhibited moderate but lower correlations ($r = 0.41$) between ρ_{12} and f_m. Although higher correlation values were observed (except for bending strength in the 2nd group), density did not show a strong relationship with the mechanical properties, similarly to what was found in the full-size samples. As expected, and as presented in Table 6, the variability (cov) of all parameters was lower in the small-specimen tests. Density exhibited relatively low variability (cov = 7.22% / 9.48%) compared to the mechanical properties, which presented cov values exceeding 10%.

For the 1st group, high correlations were found between bending strength (f_{small}) and the modulus of elasticity (E_{small}), in contrast to the medium correlations observed between bending strength (f_m) and the local (E_{local}) and global (E_{global}) moduli of elasticity ($r = 0.65$ and $r = 0.77$, respectively). For the 2nd group, moderate correlations between $f_{small,m}$ and E_{small} were found, whereas lower correlations were observed between f_m and E_{local} ($r = 0.48$), and non-significant correlations between f_m and E_{global} ($r = 0.37$). These results highlight the influence of natural defects in the full-size log samples, which increased the variability of the results and reduced the strength of the correlations.

Table 7: Pearson correlation coefficients between density ($\rho_{small,12}$), modulus of elasticity (E_{small}) and bending strength ($f_{small,m}$) for 1st (spring) and 2nd (autumn) harvest groups of free-defect small samples.

	1st (Spring)		2nd (Autumn)	
	$f_{small,m}$	E_{small}	$f_{small,m}$	E_{small}
$\rho_{small,12}$	0.68***	0.54***	0.91***	0.61***
E_{small}	0.83***	—	0.69***	—

ns: no significance level; * $p < 0.05$; ** $p < 0.01$; *** $p < 0.001$

Table 8 presents the results of the t-test comparing the mean values of each group for each variable of the small samples without defects. Figures 46, 47, 48, and 49 show boxplot graphs comparing the full-size logs (in orange colour box) with the free-defect small samples (in white box), including the MCs associated with each test (except for parallel compression). As observed in Table 6, higher values were consistently found for the 1st group across all parameters. However, statistically significant differences were only observed for bending and parallel compression strength. No significant differences were found for density or MOE.

Table 8: Means comparison (t-test) between the 1st and 2nd groups of free-defect small samples for different mechanical properties

	$\rho_{small12}$	E_{small}	$f_{small,m}$	$f_{small,c,0}$
t-statistic	1.68	0.09	2.17	3.05
p-value	ns	ns	*	**

ns: no significance level; * p < 0.05 ; ** p < 0.01; *** p < 0.001

In the free-defect small samples, no significant differences were observed between the densities of the spring (1st) and autumn (2nd) samples. Although the mean density of the 1st group (647.7 kg/m³) was higher than that of the 2nd group (628.1 kg/m³), statistical analysis revealed no significant differences between the groups in terms of density (p > 0.05). However, as illustrated in the boxplots in Figure 46, differences in density were found between full-size logs and defect-free small samples. This can be attributed to the anatomical structure of the logs, which includes higher-density zones such as the outwood region adjacent to the bark or the core heartwood. Due to the small diameter of the logs, the cleaned specimens were restricted to sections from less dense intermediate zones.

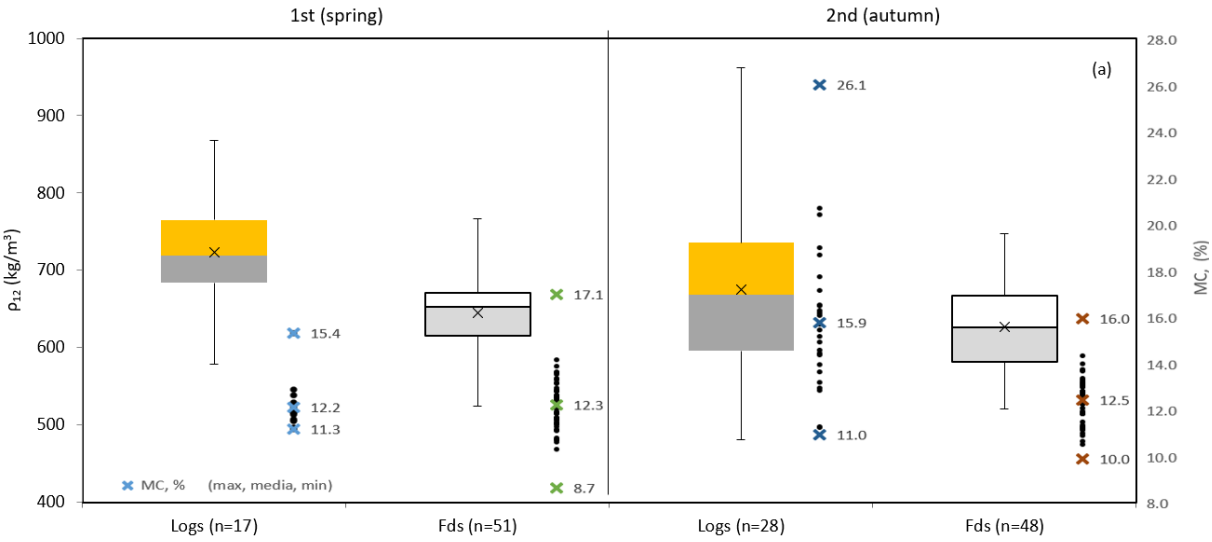

Figure 46: Box-plot comparing density adjusted according to EN 384:2016+A2:2022 (for moisture content, MC) and excluding outliers. The orange and grey colours without contours represent the full-size logs, while the white and grey colours with bold outlines correspond to the free-defect small samples. Dots on the left side of each box represent MC, with crosses indicating the lowest, middle, and highest values.

Regarding the modulus of elasticity (Figure 47), a distinction must be made between the local and global modulus when comparing the free-defect small samples with the full-size logs. As previously observed, the local modulus of elasticity in the full-size logs exhibits significant differences between the 1st and 2nd groups, a phenomenon attributed to the lack of shear influence on deformation. In contrast, no statistically significant differences were observed between the two groups for the global modulus of elasticity in either the full-size logs or the defect-free small samples. Thus, at the entire piece level, it can be inferred that the elastic moduli of the two groups do not differ.

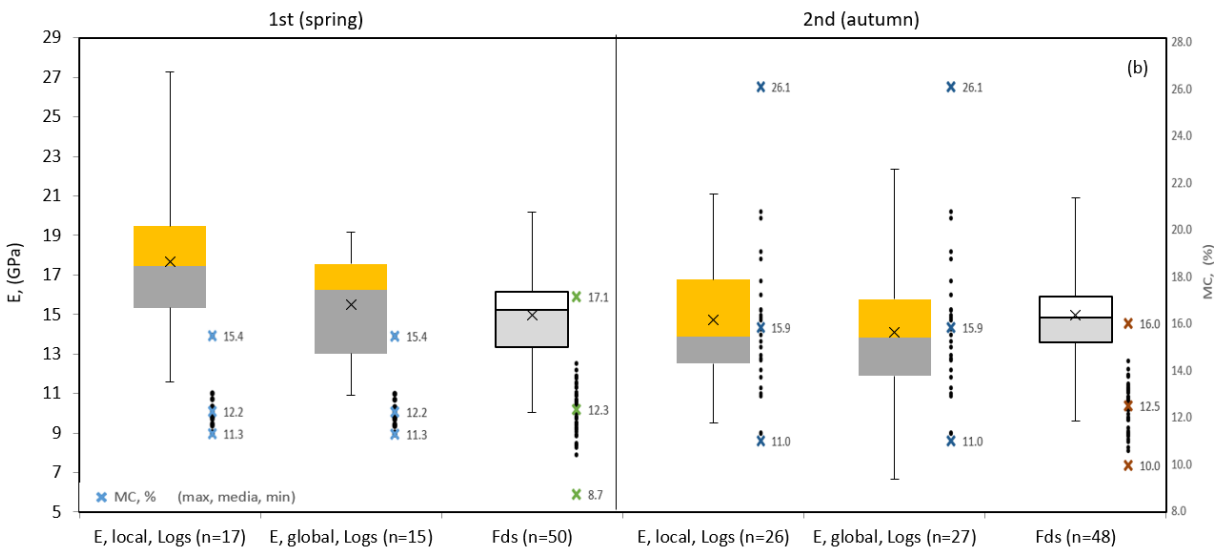

Figure 47: Box-plot comparing the Modulus of Elasticity adjusted according to EN 384:2016+A2:2022 (for MC) and excluding outliers. The orange and grey colours without contours represent the full-size logs for local modulus (E_{local}) and global modulus (E_{global}). In contrast, the white and grey colours with bold outlines correspond to the free-defect small samples. Dots on the left side of each box represent MC, with crosses indicating the lowest, middle, and highest values.

Table 8 further demonstrates that, similar to the full-size logs, there are significant differences in bending strength between the defect-free samples of both groups. However, the level of significance is lower ($p = 0.03$) when compared to the full-size logs, where the significance level is $p < 0.00$. As noted above and observed in the boxplots in Figure 48, the difference in strength between the logs from the 2nd group and those from the 1st group is highly significant. This difference is also evident in the defect-free samples, with values approximately one-third higher in the 1st and 2nd groups compared to the full-size logs. This contrasts with the difference in bending strength between the full-size logs from the 1st group and the defect-free small samples, which is approximately 6% for the 1st group and 12% for the 2nd group. This finding is consistent with literature reports, which suggest that logs with minimal processing exhibit greater strength relative to defect-free rectangular pieces.

As discussed earlier, one explanation for the lower performance of logs from the 2nd group is related to differences in moisture content (MC), which account for approximately 10–15% of the observed variation. In addition, environmental temperature conditions may have contributed to this outcome. Although temperature was not directly recorded during the tests, the literature suggests that it can partly influence reductions in mechanical resistance [140]. The temperature values previously mentioned are indicative, although those of the 1st group correspond to open-field conditions. It should be noted, however, that the group harvested in autumn (2nd group) was tested in August 2023, i.e., during midsummer, when higher temperatures prevailed. In contrast, the group harvested in spring (1st group) was tested in November, i.e., in autumn, under lower temperature conditions. The remaining differences in performance remain unexplained and may be attributed to multiple factors, including sample size, site of origin, or the presence of bark, which could have induced the development of internal moisture gradients.

Parallel compression tests on the defect-free samples revealed significantly higher values for the 1st

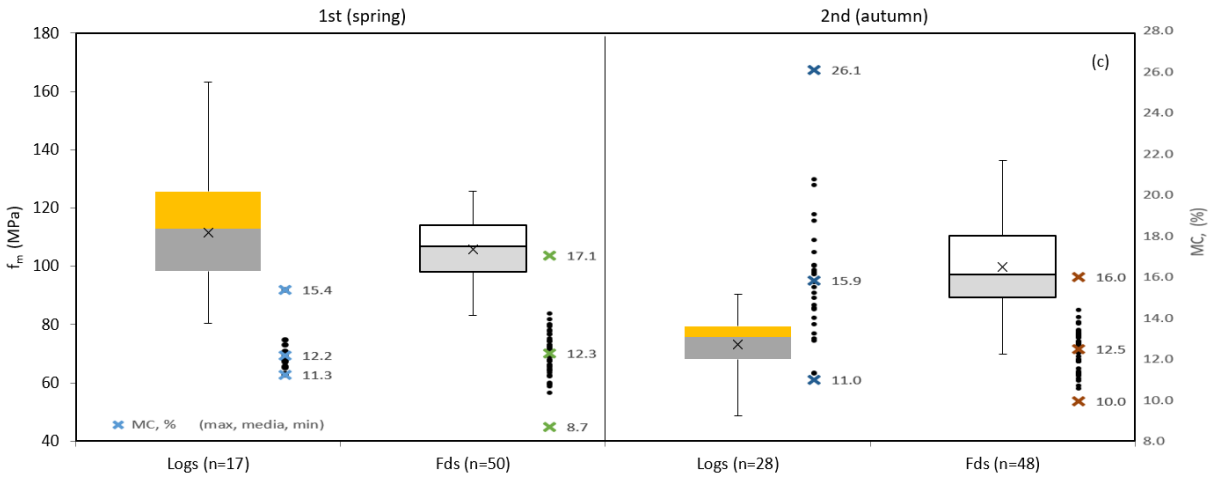

Figure 48: Box-plot comparing bending strengths, excluding outliers. The orange and grey colours without contours represent the full-size logs, while the white and grey boxes with bold outlines correspond to the free-defect small samples. Dots on the left side of each box represent MC, with crosses indicating the lowest, middle, and highest values.

group compared to the 2nd. This contrasts with the full-size samples, which exhibited no significant differences. Furthermore, as shown in the boxplots in Figure 49, the full-size samples had lower mean values than the defect-free small samples. These results suggest that defects in the full-size samples, such as curvature and knottiness, had a significant impact on their parallel compressive strength, thus influencing their overall mechanical performance. However, when these defects were controlled for, the difference in strength between the two groups became more apparent.

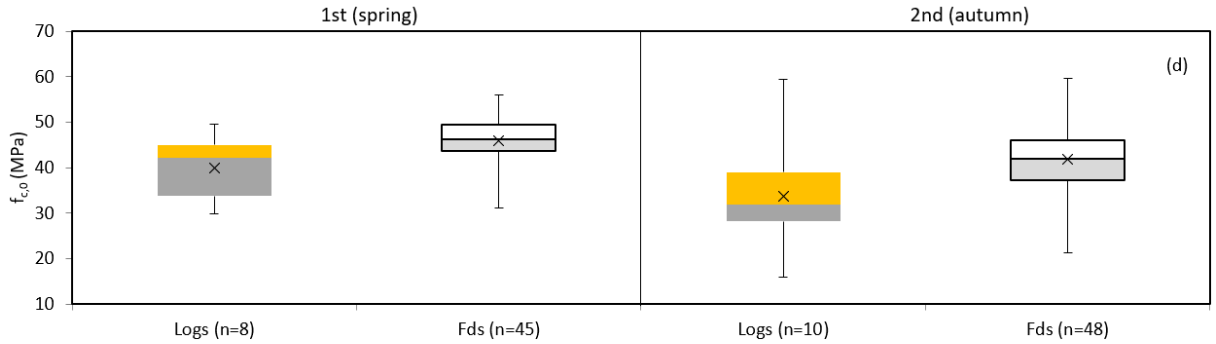

Figure 49: Box-plot comparing parallel compressive strengths, excluding outliers. The orange and grey boxes without outlines represent the full-size logs, while the white and grey boxes with bold outlines correspond to the free-defect small samples.

Additionally, the data indicate that the harvest season is a variable that affects the mechanical properties of the logs, and the defect-free samples support this conclusion. The samples harvested in the spring (1st group) exhibited significantly higher values for the local modulus of elasticity (a measure of material stiffness), as well as for bending and parallel compression strength, compared to those harvested in the autumn (2nd group). In contrast, no significant differences were found in density or the global modulus of elasticity (an indicator of the log's overall stiffness), suggesting that these variables can be considered consistent across all samples. This finding aligns with the conclusions drawn from dynamic tests, such as

wave velocity or log density [190], for similar tree species. This observation, however, is not widely referenced in the literature and appears to contradict previous studies. For example, Dimou et al. [201] studied the influence of blue stain on the strength of Scots Pine (*Pinus sylvestris*) and Norway Spruce (*Picea abies*) from Greek forests. They found that samples harvested in autumn (November) exhibited higher bending and parallel compression strength compared to those harvested in the summer (June–July). Similarly, Möttönen et al. [202] compared the characteristic hardness values of *Betula pendula* wood harvested in summer and winter, observing higher values in the winter samples. In light of these findings, the analyses conducted in the following sections will systematically differentiate between the two groups: those harvested in the spring (1st group) and those harvested in the autumn (2nd group).

3.5 Chapter conclusions

The experimental results demonstrate that, despite their juvenile nature and minimal processing, *Acacia dealbata* logs exhibit mechanical behaviour comparable to that of other hardwoods with performance levels consistent with structural applications.

- Destructive tests conducted on full-size logs revealed moderate and statistically significant correlations between density and both local and global moduli of elasticity. However, these correlations do not match those reported in the literature, which are higher, suggesting that density would not be a good predictor of mechanical properties for small round wood with minimal processing. Higher, highly significant correlations were found between local and global moduli of elasticity, and higher mean values for the spring-harvested logs (the 1st).

- Based on the data, strength classes according to EN 338:2016 [198] can be assigned within the ranges D50–D60 for the modulus of elasticity and D45–D75 for bending strength. In contrast, parallel compressive strength and density do not meet the requirements for classification into any strength class when all samples, including both sub-samples, are considered together. However, differences emerge when the data are analysed separately by group. Parallel compressive strength corresponds to class D35 for the spring group (1st) and D18 (the lowest class) for the autumn group (2nd). Similarly, density is classified as D45 for the 1st group, whereas the 2nd group does not satisfy the requirements for classification.

- The systematic comparison between the spring (1st) and autumn (2nd) harvest groups (in full-size specimens and defect-free specimens) revealed that logs collected in spring showed better mechanical performance than those harvested in autumn. Although these differences can be partially explained by variations in moisture content and temperature conditions during testing, the data also suggest possible seasonal effects on the mechanical performance of the wood—a finding that runs counter to what has been previously reported in the literature.

- The methodologies employed for determining moisture content and density, based on relatively simple and practical procedures, proved to be reliable and statistically consistent when properly calibrated. This allows mechanical results to be adjusted to standardized reference conditions (12% MC).

Overall, the results confirm that small-diameter, minimally processed *Acacia dealbata* logs, when carefully selected and properly air-dried, can achieve stiffness and strength levels sufficient to justify their investigation as a structural material.

These findings provide the empirical foundation for the development of predictive models based on non-destructive evaluation techniques, which will be addressed in the following chapter.

Chapter 4

Prediction of the Physical and Mechanical Properties of *Acacia dealbata* Logs Using Non-Destructive Techniques

A comprehensive protocol for the mechanical characterization and grading of logs for structural purposes should include the following stages: (1) a pre-selection phase based on visual evaluation criteria; (2) an air-drying process until the moisture content (MC) falls below the fiber saturation point (FSP); (3) characterization through non-destructive testing (NDT); and (4) a final kiln-drying process to reach the target MC.

This chapter contributes to the development and implementation of such a protocol by correlating the results presented in the previous chapter with those obtained using non-destructive techniques. The applicability and scope of the visual grading criteria proposed by Ranta-Maunus which served as the framework for this study are critically examined. Moreover, based on the correlations between visual grading variables and dynamic properties, predictive models are proposed to support a grading protocol for *Acacia dealbata* logs.

4.1 Non-Destructive Techniques

Non-destructive evaluation is defined as *the science of identifying the physical and mechanical properties of a piece of material without altering its end-use capabilities, and subsequently using this information to make decisions about its appropriate applications* [203].

In addition to visual grading, a wide range of NDT methods are currently available to support predictive models of the physical and mechanical behavior of standing trees, logs, sawn timber, and various wood-derived by-products [28]. Beyond preserving specimen integrity, these techniques allow for the early pre-selection of suitable logs during the initial stages of processing.

Acoustic tools, for example, have been shown to be effective in determining the dynamic modulus of elasticity (E_{dyn}). Moore et al. [204] demonstrated that such tools enable the segregation of unsuitable trees and logs prior to industrial processing. Measuring acoustic velocity in trees or logs is also relatively simple and inexpensive [154], which is particularly advantageous when working with residual logs from logging, thinning, or forest control operations in overpopulated stands [29]. Larson et al. [11] further emphasize that proper log classification can enhance economic value, facilitating the development of dedicated supply chains for these forest by-products.

4.2 Visual Grading

The earliest method of non-destructive evaluation is *visual grading*, which was initially based on local traditions and orally transmitted experiences. Over time, these practices were progressively formalized into standardized grading protocols, first in the United States and later in Europe [23].

Despite these advances, the standardization of visual grading remains challenging due to the wide diversity of species and construction traditions. For instance, Llana et al. [205] demonstrated that the grading of *Pinus radiata*, *P. sylvestris*, *P. laricio*, and *P. pinaster* is more accurate under the Spanish standard UNE 56544 compared to the German DIN 4074-1, since the former was specifically developed for the characteristics of these species.

In the context of hardwood logs, Hassler et al. [206] highlight the complexity of establishing standardized protocols in the North American timber industry, where even market pricing is directly influenced by visual grading. Blaß and Sandhaas [23] further stress that visual grading is inherently subjective, as it depends on the individual judgment and experience of the grader.

Another limitation is that visual grading does not provide direct information on critical mechanical parameters such as density or the modulus of elasticity, both of which are strongly correlated with strength. Consequently, undergrading often leads to overly conservative values, resulting in the underutilization of the material.

Several studies have confirmed these shortcomings. Vega et al. [13] evaluated machined chestnut (*Castanea sativa* Mill.) logs according to EN 1310 [207], and subsequently graded them under UNE EN 1927 [208, 209] and DIN 4074 [210]. Their comparison with destructive testing results showed that visual grading alone does not provide adequate segregation with respect to mechanical properties or density. Similarly, Vestøl and Høibø [211] demonstrated for *Pinus sylvestris* that variables such as taper, knots, grain inclination, and annual ring width are not reliable predictors of structural performance. Instead, they found that static MOE provided a more robust predictive parameter. However, some researchers have reported improved performance by comparing different visual grading standards. Fernández-Golfín et al. [27] evaluated 445 logs of black pine (*Pinus nigra* subsp. *Salzmannii*) using the "Optimal Grading" methodology described in EN 14081-2 to benchmark several standards. They concluded that the Finnish Voluntary Product Standard-Small Round Wood (VPS-SRT-2 [25]) outperformed the German DIN 4074 [210] and the European prEN 14544 [212], although it tended to over- or underestimate intermediate grades. Accordingly, they recommended the complementary use of non-destructive techniques to improve grading reliability. Morgado et al. [26] visually classified Portuguese *Pinus pinaster* logs into two groups, based on the Portuguese standard NP4305 [213] and the VPS-SRT-2 [25], and achieved grading efficiencies above 80% for strength and density, and over 70% for modulus of elasticity. Building on this work, Morgado et al. [26] reported slight improvements in regression models when visual parameters were combined with dynamic test results (dynamic MOE), showing the benefits of multiple regression over simple regression.

A wide range of national standards exists for the visual strength grading and qualitative classification of timber elements, most of which are primarily oriented toward rectangular cross-sections. The upper part of Table 9 summarises key reference standards for the grading of roundwood intended for structural use. Among these, the Finnish VPS-SRT-2 is the only voluntary standard specifically developed for small-diameter roundwood. It is based on an extensive study of logs obtained from thinning operations, reported and compiled by Alpo Ranta-Maunus from VTT Building Technology [25]. This work focused on northern European coniferous species (Norway spruce, Sitka spruce, Scots pine, larch, and Douglas fir),

Table 9: Standards related to visual strength grading and qualitative classification of round timber.

Source	Number	Year	Name
Visual strength grading for roundwood			
VPS-SRT	2	1999	Voluntary Product Standard – Small Round Wood
prEN	14544	2002	Timber structures – Strength graded structural timber with round cross-section – Requirements
EN	14229	2011	Structural timber – Wood poles for overhead lines
UNE	56547	2019	Visual classification for wood overhead poles
ASTM	D3957	2020	Standard Practices for Establishing Stress Grades for Structural Members used in log buildings
DIN	4074	2021	Strength grading of wood – Part 2: Structural round timber (coniferous species)
Qualitative classification for round timber			
EN	1927-1/2/3	2008	Qualitative classification of softwood round timber – Part 1: Spruces and firs; Part 2: Pines; Part 3: Larches and Douglas fir
EN	1316-1/2/3	2012	Hardwood round timber – Qualitative classification – Part 1: Oak and beech; Part 2: Poplar; Part 3: Ash, maples and sycamore
EN	1309-3	2018	Round and sawn timber – Method of measurement of features
ANSI	O5.1	2017	Wood poles – Specifications and dimensions

with the objective of evaluating their potential as construction materials. The prEN 14544 standard specifies requirements for the visual grading of structural timber with round cross-sections, whether barked or debarked. In contrast, EN 14229 is primarily focused on the grading of utility poles. Similarly, UNE 56547:2019 establishes a visual classification system for utility poles made from Spanish coniferous species, specifically *Pinus sylvestris* L. and *Pinus nigra* Arnold subsp. *salzmannii*, and includes corresponding characteristic mechanical properties. In North America, ASTM D3957 defines four grades and explicitly includes unsawn roundwood logs intended for use as beams or truss members. Although this standard allows relatively large knot sizes (up to half the diameter) and slope of grain (1:15), it is associated with comparatively high allowable properties. The German standard DIN 4074:2021 applies to the visual grading of coniferous timber based on strength-related criteria.

The lower part of Table 9 summarises key standards for the qualitative classification of round timber. The European EN 1927-1/2/3 defines four structural grades based on visual parameters (e.g., knot size and growth rate) for specific coniferous species such as spruce, fir, and pine. The EN 1316-1/2/3:2012 series addresses hardwood round timber classification, covering: Part 1 (oak and beech), Part 2 (poplar), and Part 3 (ash, maple, and sycamore). In addition, EN 1309-3 provides methodologies for recording physical characteristics (singularities) in both sawn and round timber. Finally, in North America, ANSI O5.1 primarily addresses specifications and dimensions for utility poles.

A wide range of national standards exist for visual characterization and grading of timber elements, most of them primarily oriented toward rectangular cross-sections. Table 9 summarizes key reference standards for roundwood grading for structural use. The American ASTM D3957 establishes four grades

and explicitly includes unsawn roundwood logs intended for beams or truss members. Although this grade imposes restrictions on knot size (up to half the diameter) and slope of grain (1:15), it is associated with the highest allowable properties [12]. In North America, ANSI O5.1 and the European EN 14229 focus mainly on grading utility poles. The European EN 1927-1/2 [208, 209] defines four structural grades based on visual parameters (e.g., knot size and growth rate) for specific conifers such as spruce, fir, and pines. EN 1310 [207] provides the methodology for recording physical characteristics (singularities) in both sawn and roundwood timber. The prEN 14544 [212] standard specifies requirements for visual grading of structural timber with round cross-sections, barked or debarked. The Finnish VPS-SRT-2 [25] is the only voluntary standard designed explicitly for small roundwood. It was developed from an extensive study of small-diameter logs obtained from thinning operations reported and edited by Alpo Ranta-Maunus from VTT Building Technology [25]. This work focused on northern European conifers (Norway spruce, Sitka spruce, Scots pine, Larch, and Douglas fir) with the objective of evaluating their potential use as a construction resource. Other more specialized standards, such as EN 14251, establish test methodologies for roundwood—including rustic logs—defining parameters such as ovality, taper, and sweep.

Several studies demonstrate that combining visual grading with non-destructive (or destructive) techniques significantly enhances predictive capacity (see Figure 50). Vestøl and Høibø [211] proposed models to predict the modulus of elasticity and bending strength of *Pinus sylvestris* round timber from southern Norway. Although predictive performance improved when visual characteristics were included, the authors warned about site effects and recommended the use of simple models based on machine grading. Aira et al. [214], working with small-diameter machined round logs of *Pinus sylvestris* and *Pinus nigra* subsp. *Salzmannii*, reported regression models with coefficients of determination of R^2 = 0.42 for MOE and R^2 = 0.43 for MOR when using dynamic MOE as the sole predictor. In multiple regression models, the inclusion of fiber deviation, density, and knottiness increased the adjusted coefficient of determination to R^2_{adj} = 0.53 for static MOE, and the addition of maximum knots per perimeter raised it to R^2_{adj} = 0.49 for MOR. Similarly, Wang et al. [24] showed that combining acoustic wave velocity with geometric parameters of *Pseudotsuga menziesii* logs improved MOE prediction (R^2 = 0.50), compared to simple linear correlations using velocity alone (R^2 = 0.40).

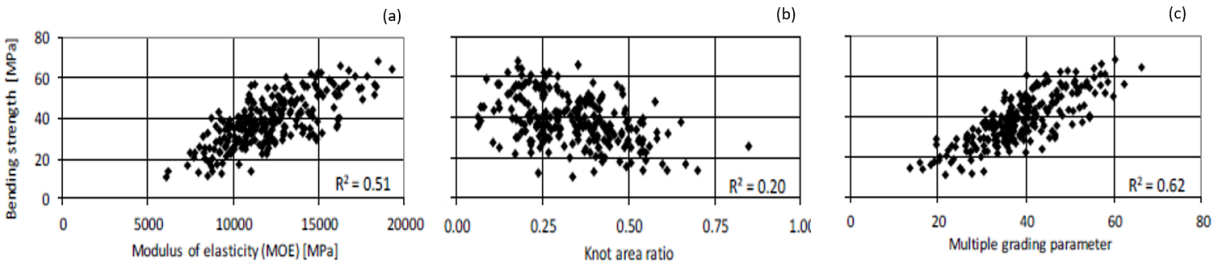

Figure 50: (a) Correlation between bending strength and MOE (softwood). (b) Correlation between bending strength and knot area ratio (softwood). (c) Correlation between bending strength and a combination of several grading parameters. Image from Blaß and Sandhaas & [23].

4.3 Influence of Visual Characteristics on Mechanical Performance

Several authors have demonstrated that certain microanatomical characteristics decisively influence the mechanical performance of wood, such as the microfibril angle in the S2 layer of the cell wall [140]. However, these properties require highly specialized equipment for their determination, making them impractical in forest management. In contrast, some macroanatomical characteristics such as the presence of knots or stem curvature are relatively easy to measure and, consequently, have been widely studied in relation to the mechanical performance of minimally processed logs.

These so-called *defects* are associated with tree growth and adaptation to environmental conditions, which in turn affect the distribution of structural tissue and the mechanical properties of the wood. Examples include Ovality in trees with asymmetrical crowns, or the formation of reaction wood on sloping terrain [158]. According to the literature, the visual characteristics that most strongly affect the structural behavior of logs are knottiness, growth rate, and grain inclination.

4.3.1 Knots

During tree growth, branch formation causes fiber deflection in the stem, resulting in knots [23]. If the branch cambium remains active, a live knot forms with continuity of fibers; conversely, if the branch is dead, a dry knot develops with discontinuity [140]. Numerous studies have documented the negative influence of knots on the strength and stiffness of sawn timber [160, 215].

At the log level, research is less abundant, although several authors have indicated that knots exert a relatively minor effect on minimally processed logs [11, 12], since the abrupt fiber discontinuities typical of sawing are absent. Nevertheless, knots still play a critical role in structural performance. For example, Martins et al. [216] reported that 86% of failures in destructive tests of utility poles under cantilever loading occurred near knots.

The effects of knottiness are difficult to quantify. Morgado et al. [26] found correlations of r = -0.66 and r = -0.51 in *Pinus pinaster* logs between the percentage of maximum knottiness and, respectively, bending strength and local modulus of elasticity (MOE). However, when multiple regression models included knottiness alongside dynamic parameters (E_{dyn}), the improvement in coefficients of determination was marginal (<1%). Vestøl and Høibø [211] obtained slightly higher correlations in their studies on *Pinus sylvestris*: r = -0.53 between MOE and knottiness relative to diameter, and r = -0.67 between bending strength and knottiness. Despite these results, they concluded that grading based solely on visual inspection is unreliable due to site effects, and recommended the use of automated machine grading techniques instead.

4.3.2 Sweep

Sweep is defined as the deviation of the stem axis from an ideal straight line. Excessive curvature, together with other geometric characteristics such as taper and ovality, can negatively affect the structural performance of logs for two principal reasons: (i) a direct reduction in usable wood volume [217], and (ii)

the introduction of initial eccentricities that increase the likelihood of second-order instabilities, such as buckling under axial compression.

The literature addressing the relationship between sweep and the physical–mechanical properties of wood remains limited. Xu et al. [218] reported that severe sweep reduced the mechanical performance of *Liriodendron tulipifera*, although it did not significantly affect the propagation of acoustic waves. Similarly, Suazo-Uribe et al. [190] found no significant correlation between the dynamic modulus of elasticity and sweep in *Acacia dealbata* logs. Hofmann et al. [136] and Schober et al. [137], investigating minimally processed oak logs with single and multiple curvatures, also reported no statistically significant relationships between sweep and bending strength.

4.3.3 Grain Angle

The inclination of the grain in structural elements distributes strength into two directions: one parallel and the other perpendicular to the stem axis. According to Dinwoodie [140], the tensile strength parallel to the grain in defect-free *Douglas fir* specimens at MC = 12% is 47.6 times greater than the tensile strength perpendicular to the grain, whereas in compression this ratio decreases to 7.19 (See Figure 51). This pronounced anisotropy explains why ultimate strength decreases substantially when the grain angle deviates between 0° and 45° from the principal axis, particularly under tensile loading.

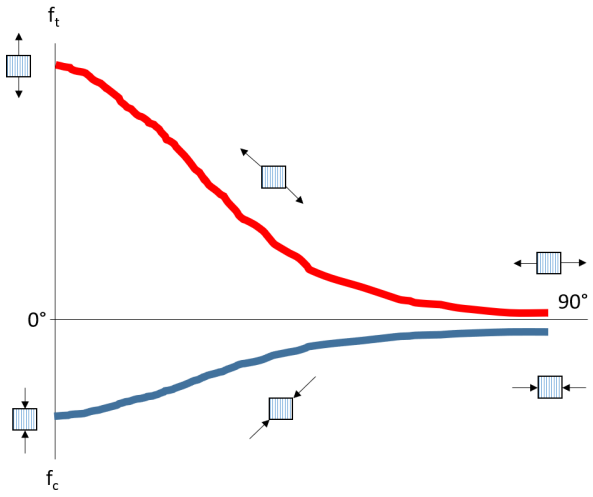

Figure 51: Schematic comparison of tensile and compressive strengths as a function of fibre angle relative to load, for small defect-free specimens of Douglas fir (*Pseudotsuga menziesii*) at MC = 12%. Adapted from Dinwoodie [140].

4.4 Non Destructive Methods

4.4.1 Acoustic Methods

When a solid medium is subjected to a dynamic or vibratory load, three main types of waves are generated: (i) longitudinal or primary waves (P), (ii) transverse or secondary waves (S), and (iii) surface or Rayleigh

waves. P waves propagate in the same direction as particle motion, can travel through any medium, generate normal stresses, and are the fastest of the three. By contrast, S waves propagate only in solids, generating stresses perpendicular to the direction of propagation and traveling at lower speeds. Finally, surface waves affect only the outer layers of the material [219].

The propagation of these waves depends on several factors, including the excitation source, the test configuration, the characteristics of the measured signal, and the processing applied [219]. Of particular importance is the propagation velocity, which is directly related to the elastic properties and density of the medium. In heterogeneous materials such as wood, this behavior is especially complex due to additional influences such as anisotropy, moisture content (MC), and specimen geometry.

Given the hygroscopic nature of wood, its dynamic properties are strongly influenced by MC. Acoustic velocity decreases as MC increases and slows further when the fiber saturation point (FSP) is exceeded [38, 220]. To account for this effect, numerous authors have proposed correction factors [221, 222]. Density also decreases with moisture loss, but at a different rate, which explains why the increase in modulus of elasticity (MOE) associated with drying is not strictly proportional [220].

The size and shape of the specimen also influence dynamic properties. For example, Wang et al. [223] reported that increasing the diameter of *Pinus resinosa* trunks reduced both static and dynamic MOE, although the same trend was not consistently observed in other conifers. Other studies have shown that dynamic tests can also facilitate the detection of defects such as knots [30]. Mvolo et al. [224] compared the results of dynamic tests and the SilviScan technology in *Picea glauca* (white spruce) and *Pinus contorta* (lodgepole pine), concluding that the determination coefficients depend both on the species and the technique applied.

At present, acoustic methods represent a consolidated category of non-destructive testing (NDT), successfully applied to standing trees, logs, and sawn timber for the estimation of stiffness properties [29]. In this study, two techniques were selected due to their instrumental availability: longitudinal stress waves (lsw) and transverse vibration (tv).

4.4.1.1 Longitudinal Stress Waves (LSW)

In an idealized, homogeneous, slender body, a longitudinal stress wave initiated at one end propagates at a constant velocity along its length. The propagation velocity is directly dependent on the stiffness of the material and inversely proportional to its density, allowing the dynamic modulus of elasticity ($E_{dyn,lsw}$) to be estimated from the velocity (v) and density (ρ).

$$v = \sqrt{\frac{E_{dyn,lsw}}{\rho}} \tag{43}$$

Although logs partially satisfy slenderness criteria, they are not homogeneous media, which introduces complexity into their analysis. Even so, the lsw technique has proven useful in a wide range of contexts, from assessing the condition of historic structures [203] to predicting the mechanical properties of small-diameter logs harvested from dense stands. Wang et al. [29] reported coefficients of determination of R^2 = 0.60 in *Pinus banksiana* and R^2 = 0.75 in *Pinus resinosa* between $E_{dyn,lsw}$ and static MOE.

Other studies have confirmed the applicability of this technique across different species. Rais et al. [152] observed correlations of R^2 = 0.37 between velocity in standing trees and dynamic MOE in *Pseudotsuga menziesii* logs, and R^2 = 0.70 between dynamic MOE in short logs and static MOE in planks. In *Castanea sativa*, Vega et al. [13] reported R^2 = 0.64 between dynamic and static MOE, while Llana et al. [15] found R^2 = 0.58 in Irish hardwood species, emphasizing that species-specific effects were decisive in model performance.

In general, coefficients of determination are more consistent for MOE than for bending strength (f_m). Llana, Íñiguez-González et al. [32] compiled research conducted in Spain, reporting R^2 values ranging from 0.45 to 0.92 for MOE, and between 0.20 and 0.61 for f_m.

4.4.1.2 Transverse Vibration (TV)

In a structural system resembling a beam with defined boundary conditions, a low-energy impact or ambient vibrations can excite natural resonant frequencies. The fundamental frequency (f_1) of the first transverse vibration mode, together with the geometry and support conditions of the member, enables the estimation of a dynamic MOE using analytical expressions derived from Euler–Bernoulli beam theory:

$$E_{dyn,tv} = \left(\frac{2 f_n \pi}{\gamma_n}\right)^2 \frac{m\, L^3}{I} \tag{44}$$

Where $E_{dyn,tv}$ is the dynamic modulus of elasticity in GPa, f_n is the natural frequency (Hz) of vibration in bending with n is modus (when n = 1, is basic or fundamental mode), m is the mass in kg, L is the length of the log in mm, γ_n is the constant and I is the second moment of area o moment of Inertia, in mm^4.

Larsson et al. [225] reported high coefficients of determination (R^2 = 0.7 – 0.9) in *Picea abies* using TV. In *Eucalyptus nitens*, Opazo-Vega et al. [30] obtained R^2 = 0.95 between static and dynamic MOE in edgewise orientation, according to ASTM D6874. Similar findings were reported by França et al. [31] in *Southern Pine* lumber, with R^2 values close to or above 0.80 for MOE, and lower values for f_m (0.21–0.43).

For *Pinus pinaster* logs intended for utility poles, Martins et al. [216] found relatively low correlation values (R^2 = 0.34 for TV and R^2 = 0.31 for lsw). In contrast, other studies have reported stronger performances: Wang et al. [14] observed R^2 = 0.85 in *Pinus banksiana* and R^2 = 0.95 in *Pinus resinosa*, while Carreira et al. [226] reported R^2 = 0.92 in *Corymbia citriodora*. Although irregularities in wood (e.g., knots, cracks) can distort the vibration signal, recent studies suggest that TV can also detect structural defects. Opazo-Vega et al. [30], for example, demonstrated that incorporating the analysis of the second and third transverse vibration modes allows for the detection of critical defects such as knots and cracks in boards of *Eucalyptus nitens*.

4.4.2 Resistance Drilling

Resistance drilling technology was developed in the 1980s as a semi-destructive tool for evaluating growth rings, diagnosing the health of urban trees, and detecting cavities or areas of decay. Initially conceived for

arboriculture and urban tree management [227], this technique employs a thin, flattened metal needle that penetrates the wood, recording the resistance to torque through the consumption of electrical energy. Resistance is electronically measured at small intervals (≈0.1 mm), generating a graphic profile of relative amplitude (0–100%). In species with well-defined growth rings, the profile typically reflects the alternation between earlywood (valleys) and latewood (peaks). From the integral of the curve area and the penetration depth, an average resistance (R_m) can be calculated and used as a reference parameter.

The device allows adjustment of two key variables: feed rate (cm/min) and needle rotation (RPM). Gendvilas et al. [228] reported that IML-RESI drills can operate with feed rates ranging from 15 to 200 cm/min and rotation speeds of 1500 to 5000 RPM. Proper adjustment of these parameters is essential to species-specific calibration and to improving measurement accuracy.

Numerous studies have shown significant correlations between penetration resistance (R_m) and fundamental wood properties. Henriques et al. [33], using small defect-free specimens of *Pinus pinaster* and *Pinus sylvestris*, obtained coefficients of determination of R^2 = 0.87 with density and R^2 = 0.70 with parallel compressive strength. Barría et al. [229] demonstrated the utility of resistography for detecting vertical density variations in *Pinus radiata*, observing a systematic decrease with stem height. Gao et al. [230], in a comparative study with traditional methods (Pilodyn, torsiometer, nail withdrawal), concluded that resistance drilling offers clear advantages: minimal damage to the tree, rapid operation, and high measurement sensitivity, making it comparable to more sophisticated techniques such as X-ray densitometry.

Extensive literature reviews corroborate these findings. Llana, Íñiguez-González et al. [32] compiled eight studies conducted in Spain, reporting R^2 values ranging from 0.39 to 0.85 depending on the species and equipment used. Low values were recorded for *Pinus pinaster* using an IML Resi-B1280 (R^2 = 0.39; Morales-Conde & Machado, 2017), while the highest values corresponded to *Pinus sylvestris* using an IML Resi F300 (R^2 = 0.85; Mariño et al., 2002). These findings confirm that both species density and device configuration (RPM, feed rate) decisively influence predictive performance.

Beyond density estimation, resistance drilling has proven valuable for the evaluation of existing timber structures, particularly in heritage restoration contexts. Sousa et al. [231], for instance, combined resistography with Pilodyn and ultrasound to assess old *Castanea sativa* beams affected by decay, demonstrating a correspondence between resistographic signals and the loss of mechanical capacity.

The method has also been applied to dendrochronology. Guller et al. [232] and Xu et al. [34] demonstrated its applicability for age determination in various species, although with limitations in very narrow rings ($<$1 mm). Similarly, Oh et al. [233, 234] confirmed its effectiveness in species such as *Pseudotsuga menziesii* and *Zelkova serrata*, including century-old trees, while noting resolution constraints in fine-ringed specimens.

Like all techniques, resistography presents operational limitations. Schimleck et al. [28] highlighted issues of needle wear and possible deviations within the borehole due to limited rigidity, while Wang [235] identified friction as a significant source of measurement error. Despite these limitations, resistance drilling remains a highly valuable technique for estimating density and identifying internal defects, providing an effective complement to both destructive and non-destructive methods in mechanical wood

characterization protocols.

4.5 Visual Grading and Mechanical Properties

For the visual characterization, two main references were adopted. The first is the EN 14251:2003 standard, which specifies test methods for determining the mechanical properties of structural roundwood and it establishes some specific definitions for *srw* [18]. The second is the classification framework proposed by Ranta-Maunus (1999) in the Voluntary Product Standard, Small Round Timber (VPS-SRT [25]). This grading system establishes three structural grades—A, B, and Reject—as summarized in Table 10 [25].

4.5.1 Ovality

The EN 14251 standard [18] defines it as *the difference between the maximum and minimum diameter at a cross-section, expressed as a percentage of the minimum diameter*. A section at 1 meter in height from the base was considered, and the following is defined.

$$Ovality = \frac{d_{max} - d_{min}}{d_{min}} \times 100\% \tag{45}$$

Where $Ovality$ is the ovality expressed as a percentage (%); d_{max} is the maximum diameter in mm, and d_{min} is the minimum diameter in mm.

4.5.2 Tapered

EN 14251 [18] defines it as a *gradual change in diameter along the length*. The maximum and minimum diameters at each end (top and bottom) were averaged and divided by the length. It is defined as:

$$Tapered = \frac{d_{media,down} - d_{media,up}}{l} \tag{46}$$

Where $Tapered$ is the taper expressed in mm/m; $d_{media,down}$ is the lower average diameter and $d_{media,up}$ the upper average diameter in mm, and l is the length of the log in m.

4.5.3 Sweep

EN 14251 [18] defines it as *deviation of the longitudinal axis from a straight line*. For this measurement, each log was placed and temporarily fixed on a flat surface, and the difference between the curvature and the reference plane was measured with a tape measure. Some logs had partial curvatures (crook) or even double curvatures, but in all cases, the most unfavourable deviation was selected.

$$Sweep = \frac{desv_{max}}{l} \tag{47}$$

Where $Sweep$ is the sweep value expressed in mm/m; $desv_{max}$ is the maximum deviation from the plane, and l is the log length in m.

4.5.4 Knots all/central, KS

Each knot in the log was identified, and its maximum diameter was measured in the section containing it. As Figure 52 shows, to determine the percentage of knotting, the knot with the largest diameter was selected, and the diameter of the section containing it was measured. If there were two or more knots within 150 mm of each other in the same section, their diameters were added together. The knotness percentage is expressed as:

$$Knot, all, cen/KS = \frac{d_{knot}}{d_{section-knot}} \times 100\% \quad (48)$$

Where $Knot, all$ considers the entire length of the log, $Knot, cen$ only considers the central third and KS describes knots sum; d_{knot} is the diameter of the knot on the section, and $d_{section-knot}$ is the diameter of the section.

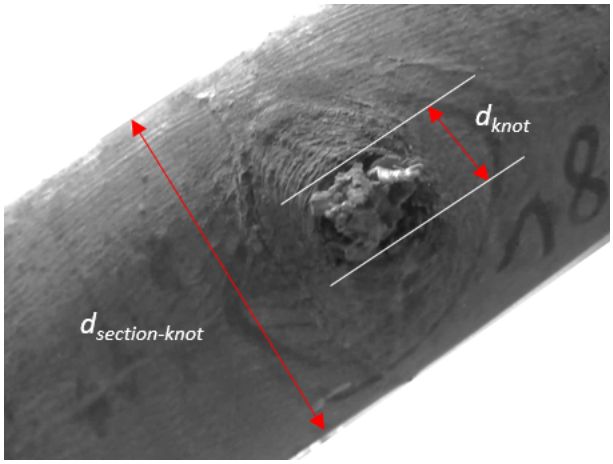

Figure 52: Graphical definition of the parameters used to determine knot percentage, $Knot, all, cen$: including d_{knot} (knot diameter) and $d_{section-knot}$ (sectional diameter of log).

4.5.5 Cracks

Before each destructive bending test, all visible cracks were identified and classified according to their type and severity. A check was defined as a crack that extended no further than the log's radius, while a splitting referred either to a full-diameter crack or to two non-coplanar cracks that intersected at the core. Each crack was described in terms of its longitudinal extent from the log ends (<25%, <50%, <75%, or 100%) and its principal orientation relative to the loading plane (vertical, horizontal, or diagonal). A qualitative assessment of these characteristics was conducted to examine their association with observed failure modes.

4.5.6 Allowable characteristics

In the analysis of visual characteristics, several variables commonly reported in the literature were excluded from consideration. For instance, ring growth rate was omitted because the macroanatomical structure of *Acacia dealbata*, characterised by its diffuse porous, prevents reliable ring counting (as seen in Figure 12a). Likewise, variables such as grain angle and the occurrence of checking or splitting were qualitatively assessed in connection with the destructive testing of logs.

Visual characterisation was carried out in the Civil Engineering Laboratory before kiln drying (January 2023). Based on the adopted definitions, a second selection process was performed, yielding a total of 45 logs: 17 from the 1st harvest and 28 from the 2nd. A summary of the allowable values proposed by Ranta-Maunus (R-M) for visual grading [25] is presented in Table 10.

Table 10: Allowable visual characteristics values grading to Ranta-Maunus. [25]

Characteristic	unit	Grade "A"	Grade "B"
Tapered	mm/m	$\leq$5	$\leq$10
Ovality	%	$\leq$10	$\leq$20
Sweep	deviation over 1m, in mm	$\leq$2.5	$\leq$5.0
Knot, all*	%	$\leq$25	$\leq$30
Knot, centre*	%	$\leq$25	$\leq$30
KS (knot sum)*	%	$\leq$75	$\leq$100
Single crack depth	%	$\leq$50	$\leq$50
Single crack length	%	not limited	not limited
Sum of any two cracks	%	$\leq$75	$\leq$75

* the $\%_{knot}$ is expressed in terms of the actual diameter of the log, unlike the R-M approach, which defines it based on the nominal dnom.

4.5.7 Visual Characteristics and Mechanical Properties of *Acacia dealbata* Logs

After visual measurements, to evaluate potential differences between the two groups of logs harvested in different seasons (spring and autumn), independent samples t-tests were conducted for nominal and apparent diameter, ovality, taper, sweep, and knotiness in bending tests, and for sweep and knotiness in compression parallel to the grain (all data review appendix E and F, table 24 and 25). The analysis showed no statistically significant differences ($p > 0.05$) for most variables. However, knotiness in bending exhibited significant differences. Given the non-normal distribution of these variables ($Knot, all$ and $Knot, cen$), a non-parametric Mann–Whitney U test was applied, revealing significant differences between the two groups ($p < 0.05$). The descriptive statistics of the visual characteristics for the logs selected for bending tests are presented in Table 11, while those for the logs tested in compression parallel to the grain are provided in Table 12.

Table 11: Visual characteristics of bending specimens.

	d_{app}	Ovality	Tapered	Sweep	Knots, all*		Knots, cen*		KS*	
Unit	mm	%	mm/m	mm/m	% (1st)	% (2nd)	% (1st)	% (2nd)	% (1st)	% (2nd)
mean	106.4	8.7	6.7	16.6	17.3	11.1	16.2	10.7	15.0	8.8
SD	8.7	5.8	2.1	7.0	9.1	4.6	9.0	2.4	6.3	2.9
cov (%)	8.2	66.7	30.6	42.0	52.6	41.4	55.5	22.5	41.9	33.1
max	123.6	20.0	10.4	35.5	36.8	19.6	36.8	17.2	28.4	16.3
min	89.6	0.0	2.3	4.9	5.5	4.7	9.0	8.7	6.8	4.5
n	45	45	45	45	15 *	27 *	12 *	21 *	10 *	19 *

* Logs without knots were discarded.

Table 12: Visual characteristics of parallel compression specimens.

	Apparent diameter	Sweep	Knot/diameter*
Unit	mm	mm/m	%
mean	103.0	15.6	17.7
SD	6.5	10.7	7.6
cov	6.3	68.4	42.9
max	119.7	40.1	27.8
min	94.5	2.6	10
n	29	29	7*

* Logs without knots were discarded.

Another geometric difference observed between the bending groups was the log length: logs from the 1st group measured 2.0 m, while those from the 2nd group measured 2.4 m. Aside from diameter, the data exhibited considerable variability, attributable to the intrinsic characteristics of unmanaged forests. In such environments, trees grow under high competition for light and water, leading to morphological adaptations that influence their geometry and mechanical performance (see Figure 20 c). However, a high density of the stands can positively affect the mechanical properties of the wood. Simic et al.[150] demonstrated that higher stand density in *Picea sitchensis* (Sitka spruce) improves the dynamic modulus of elasticity (E_{dyn}) and, citing previous studies, noted that higher tree spacing is associated with increased knot formation and size. Similarly, Rais et al. [152] reported that high-density managed stands of *Pseudotsuga menziesii* (Douglas fir) produce sawn timber with higher density and strength and lower knot content. This trend is consistent with observations in the present study: a proportion of logs were free of knots along their full length (knot, all), with 11.7% in the 1st group and 3.6% in the 2nd group and in the central third (knot, cen), 29.4% and 25.0%, respectively.

To contextualise these findings, Figure 53 presents the visual characteristics of the tested logs with the threshold values defined for visual grade B classification, as proposed by R-M (see Table 10). Most variables aligned closely with reference values (ratios near 1), except sweep, which exceeded the threshold by approximately a factor of three, indicating that these logs would be rejected under the R-M classification criteria. Only a limited number of studies have directly examined the influence of curvature on mechanical performance. Hofmann et al. [136, 137] investigated minimally processed Oak logs exhibiting both single and multiple curvatures. Their analysis reported average sweep values of 1.9% (±0.8%), corresponding to

approximately 19 mm over a 1 m length, which are comparable to those observed in the present study (blue bar in Figure 53).

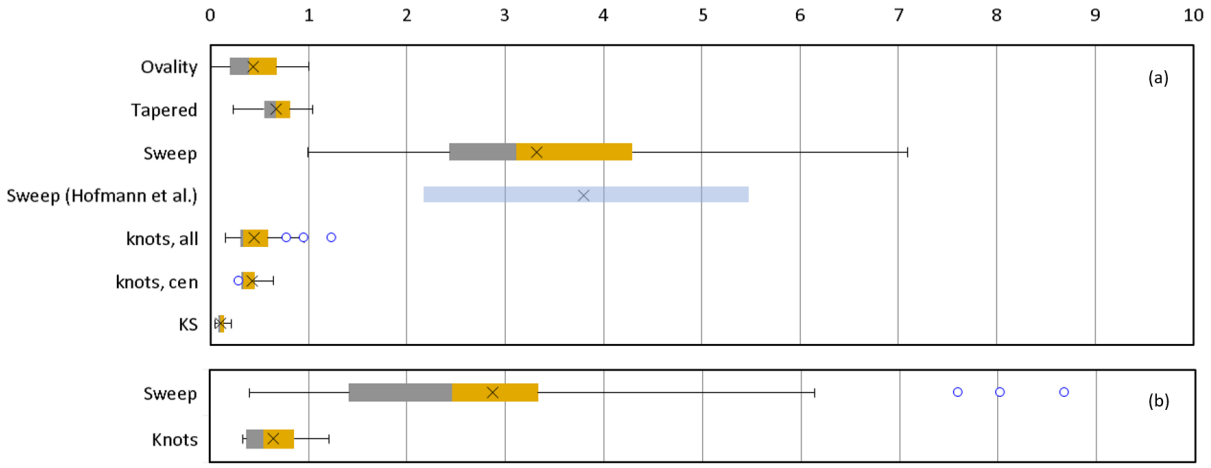

Figure 53: Relationship between the reference values of R-M and those of this study, for the visual characteristics of logs tested in (a) bending and (b) in parallel compression.

4.5.7.1 Sweep Influences

Figure 54 presents the relationship between sweep and mechanical performance metrics for both groups: bending strength (a), local (c) and global (d) modulus of elasticity, and compressive strength parallel to the grain (b). Although no statistically significant differences in sweep were observed between spring (1st) and autumn (2nd) groups, significant differences were found in mechanical properties, possibly attributable to differences in harvest season, drying conditions, or the higher mean and greater dispersion of moisture content (MC) in the 2nd group.

Sweep and knottiness analyses were performed independently for each group. For the spring group (1st), a slight but non-significant negative trend was found between sweep and bending strength (Figure 54 a). In contrast, statistically significant negative moderate correlations were observed for local ($r = -0.48$) and global ($r = -0.62$) modulus of elasticity (Figures 54 c and 54 d, respectively; $p < 0.05$). For compressive strength parallel to the grain, a significant negative correlation was also observed ($r = -0.41$; $p < 0.05$; Figure 54 b). No significant correlations were identified in the autumn group (2nd).

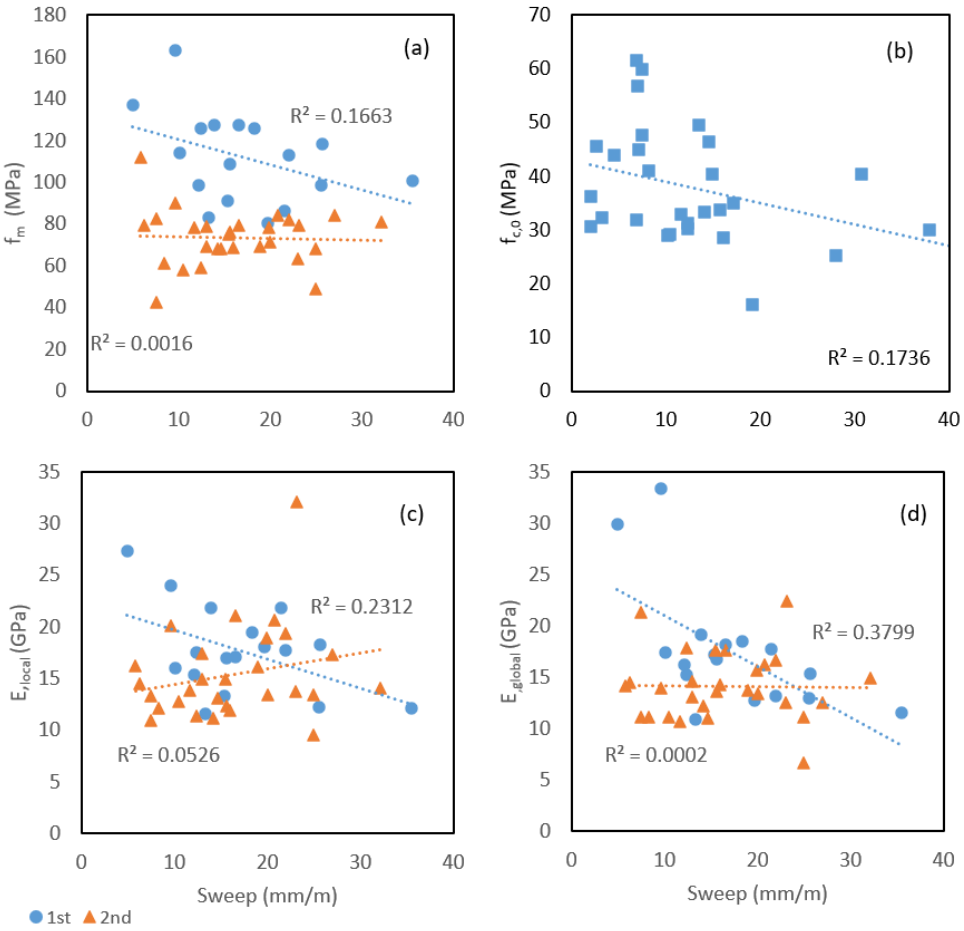

Figure 54: Relationship between Sweep and: (a) bending strength, (b) parallel compression, (c) local and (d) global modulus of elasticity, for 1st (spring) and 2nd (autumn) group.

These findings suggest that curvature has a significant impact on bending stiffness (E_{local} and E_{global}) and compressive strength ($f_{c,0}$) in spring-harvested logs. To explore this further, Figure 55-a categorises sweep ranges concerning local and global modulus of elasticity for the spring group. ANOVA and Tukey post hoc tests were performed to compare group means. The results indicate that logs with sweep below 10 mm/m exhibit significantly higher stiffness values, particularly for E_{global}. Although the 15–20 mm/m group did not differ significantly from the 5–10 mm/m group based on ANOVA, the narrow dispersion of the latter group suggests practical differentiation. In contrast, sweep groups of 10–15 mm/m and >20 mm/m exhibited significantly lower stiffness values ($p < 0.05$), supporting the consideration of a conservative sweep threshold for bending applications, consistent with the observations of Hofmann et al. [136].

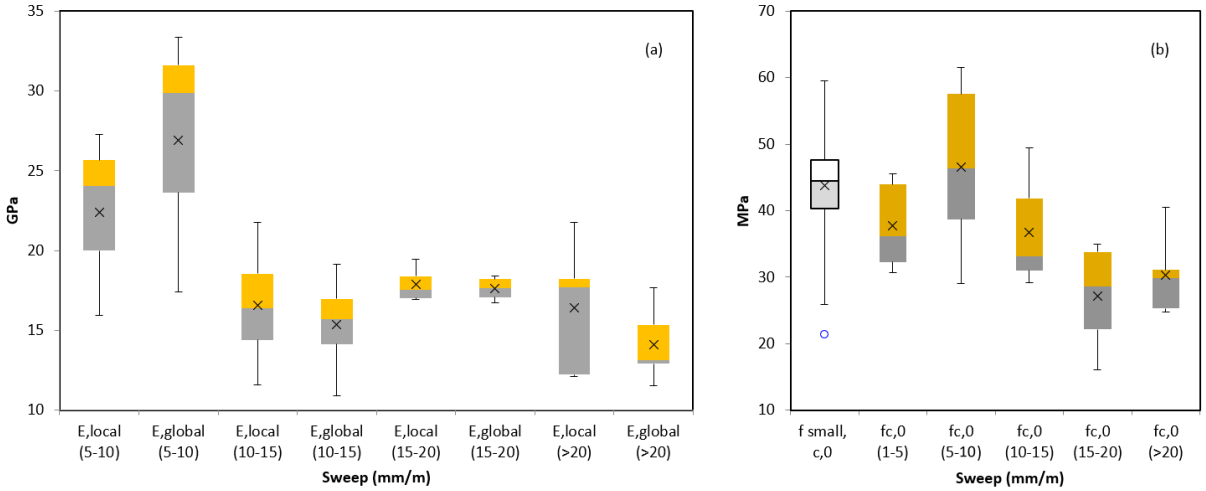

Figure 55: Relationship between different Sweep ranges in mm/m, and (a) local and global Modulus of Elasticity, and (b) parallel compression strength (note: The uncolored boxes correspond to the results of the defect-free samples).

In the case of compression parallel to the grain, initial eccentricity promotes global buckling of the element, making curvature a critical parameter for structural performance. To analyse this effect, the compressive strength of full-size logs was compared with that of small samples without defects, which were free of sweep and exhibited short-intermediate slenderness ($\lambda \approx 14$). Figure 55-b presents this comparison in logs categorised by sweep levels. Although the first sweep category (1-5 mm/m), which falls below the R-M classification threshold, yielded compressive strengths lower than those of the reference defect-free specimens, a progressive decrease in compressive strength is observed beginning with the 5–10 mm/m sweep category. According to the ANOVA, there are no statistically significant differences in compressive strength between the defect-free group and the first three curvature categories (1–5, 5–10, and 10–15 mm/m). However, from the 15–20 mm/m category onward, the reduction in compressive strength becomes highly significant ($p < 0.001$) when compared with both the 5–10 mm/m group and the defect-free reference specimens. This result supports the threshold previously inferred in the bending analysis.

Ultimately, in alignment with the findings of Hofmann et al.[136], the results of this study suggest that the sweep limits proposed by R-M may be conservative for minimally processed logs and that a slight upward revision of acceptable sweep thresholds may be feasible without compromising mechanical performance. In this regard, although not explicitly analyzing the influence of curvature, R-M [25] evaluated the buckling behaviour of French Douglas fir (*Pseudotsuga menziesii*) logs with varying slenderness ratios. The study, which included 48 logs grouped by lengths of 1500, 2000, and 3000 mm, concluded that the critical buckling loads—both those defined by EN 338 (those inferred from experimental results—were conservative for circular, slender elements). Nevertheless, further investigation is warranted. A statistically robust study that integrates slenderness, curvature, and other key variables—such as knot content and distribution—would be necessary to refine predictive models and design criteria for minimally processed roundwood elements.

4.5.7.2 Knotness Influences

Figures 56 and 57 illustrate the correlations between knotness in the central section ($Knot, cen$) and across the full length of the log ($Knot, all$) with the mechanical properties determined from destructive testing: Local modulus of Elasticity E_{local}, bending strength (f_m), and parallel compression strength ($f_{c,0}$). As can be seen in table 11, because the sum of knots (KS) yielded values well below the lowest allowable value (75% of the diameter per A grade), it was discarded from the analysis. In the 1st group, a moderate but statistically significant negative correlation was observed between $knot_{all}$ and f_m ($r = -0.62$; $p < 0.05$), as well as with E_{local} ($r = -0.64$; $p < 0.01$). No significant correlations were found for the 2nd group; however, the average values of both $Knot, all$ and $Knot, cen$ fell below the threshold proposed by R-M, suggesting that this classification limit is adequate for these specimens.

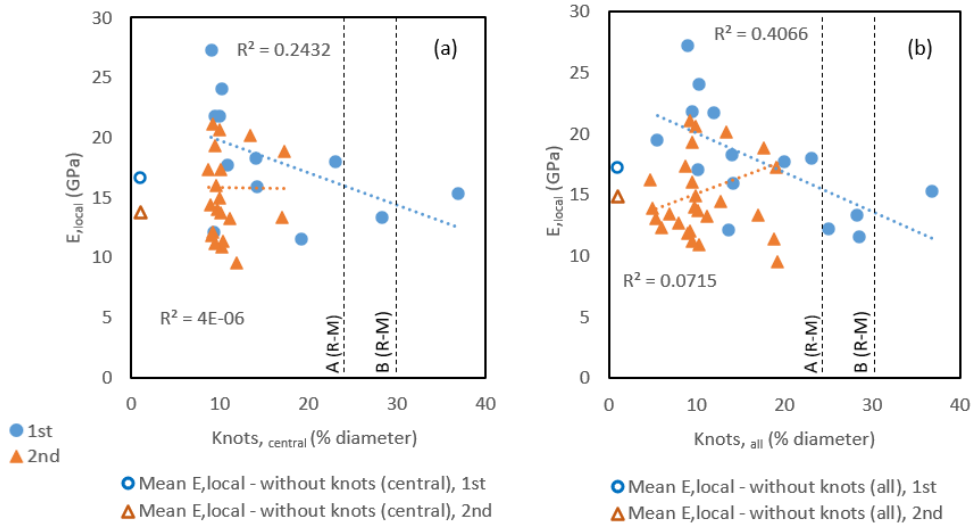

Figure 56: Knotness of the (a) central zone, $Knot, cen$, and of (b) the whole log, $Knot, all$, in relation to the Local Modulus of Elasticity , E_{local}.

In the parallel compression tests, 74% of the specimens showed no visible knots. A strong negative correlation was found between the presence of the knot and the compressive strength ($r = -0.73$; $p < 0.05$). While the detrimental impact of knottiness on the mechanical properties of sawn rectangular timber is well-documented [160, 215] Morgado [133] also demonstrated that in logs of Portuguese *Pinus pinaster*, knots are the primary strength-reducing defects. Their presence reduces the effective cross-sectional area, introduces eccentricities, creates stress concentrations, and alters fiber orientation—factors that collectively diminish mechanical performance.

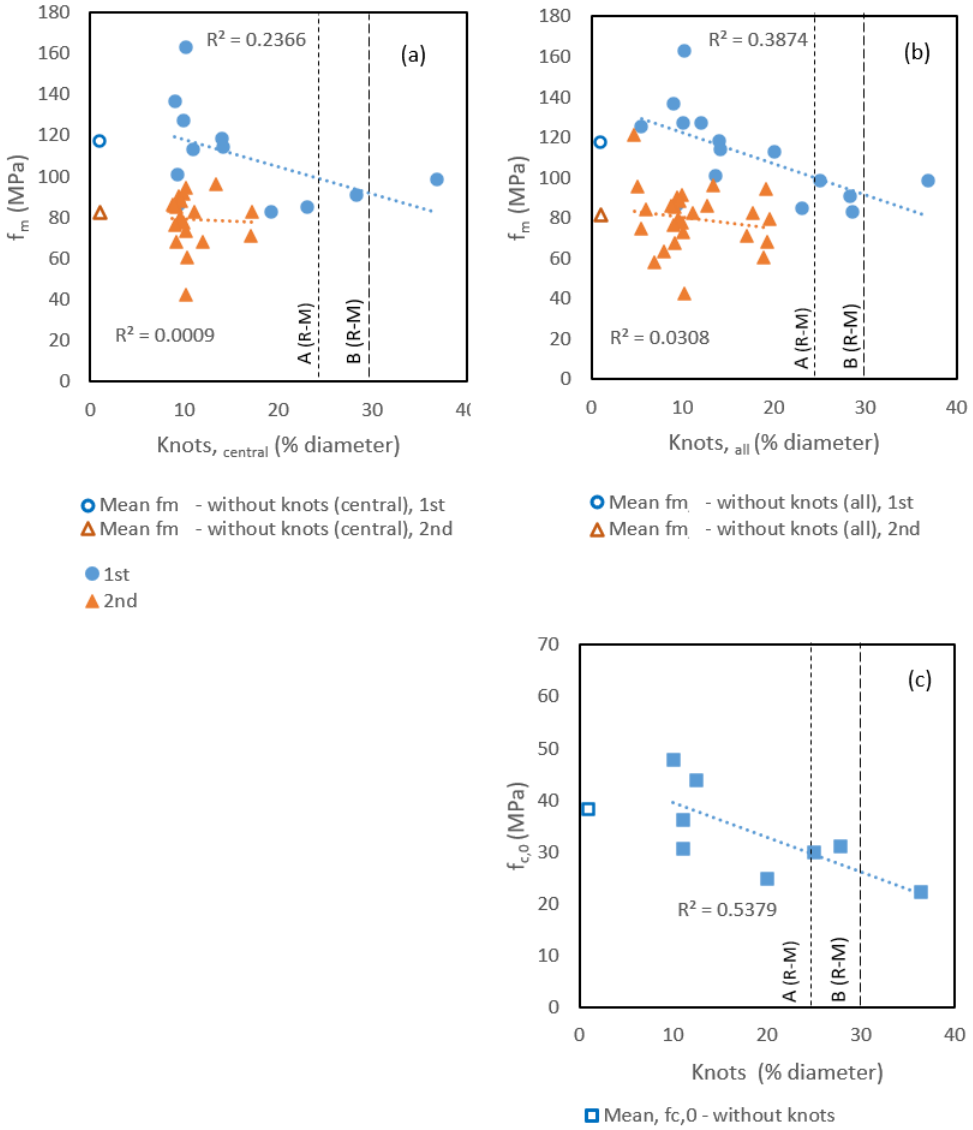

Figure 57: Knotness of the (a) central zone, $Knot, central$, and (b) the whole log, $Knot, all$, in relation to the bending strength, f_m; (c) Knotness in relation to the parallel compression strength, f_m

This influence is consistent with fracture modes observed in the current study. In bending, failure in knotted logs frequently did not initiate immediately at the knot. Instead, rupture occurred in the adjacent zone, where fibers—having deviated around the knot—returned to alignment with the longitudinal axis. In this zone of significant fiber deviation, the combined effect of tensile stress parallel to the grain and a secondary component perpendicular to the grain promotes brittle fracture at the tension edge (Figure 58).



Figure 58: Typical brittle failure adjacent to the log knot subjected to bending (log 1 and 2): parallel and perpendicular tension.

4.5.7.3 Ovality and Taper Influence

To assess potential relationships between the remaining visual characteristics and log mechanical performance, correlation analyses were conducted for all additional variables. No statistically significant correlations ($p > 0.05$) were found between either ovality or taper and bending strength (f_m). From an analytical standpoint, high ovality implies non-uniform cross-sectional performance. Therefore, if the intended application involves isotropic behavior—such as in active vector structures (e.g., truss systems)—the limits proposed by R-M appear to be appropriate.

With respect to tapered logs, the present study did not include machined specimens with uniform diameters that would allow a direct comparison of performance. Although a comparison between the bending strength of full-size logs (f_m) and small, defect-free specimens ($f_{small,m}$) was performed, the results varied across groups, preventing the identification of a consistent trend. Nonetheless, previous research has suggested that unprocessed tapered logs may outperform uniformly processed ones. Green et al. [12], for example, found that low-processed logs exhibited higher Modulus of Elasticity (MOE) and Modulus of Rupture (MOR) compared to those processed to achieve a constant diameter. Similarly, Vega et al. [13] observed that processing chestnut logs (*Castanea sativa* Mill.) into uniform diameters of 60, 80, and 100 mm resulted in decreased MOE, MOR, and density. This reduction was attributed to a higher proportion of juvenile wood in smaller-diameter specimens.

4.5.7.4 Cracking Influence

R-M recommends restricting the presence of checking (longitudinal cracks) to no more than 50% of the log's diameter along its entire length. However, the current dataset did not reveal any correlation between checking and mechanical performance. For instance, two logs with severe checking along their whole length (100%) exhibited above-average bending strength values. They failed under an initial compression of the central part of the log (e.g., logs 4 and the number 25 of Figure 32 g), suggesting that checking did not contribute to their failure mechanisms.

R-M is more conservative concerning end splitting, proposing that the sum of two end splits should not exceed 75% of the log's diameter. In this study, splitting was associated with horizontal shear failure in some cases, observed in 11% of the 1st group and 7% of the 2nd group. For example, log 3 of the 1st group, which had splitting at both ends extending up to 25% of the log length, failed abruptly with a combination of tensile rupture and a horizontal shear crack originating from the split (Figure 59 a–c). Similar failures were observed in logs 45 and 60 of the 2nd group (Figure 59 f-g). Notably, log 33, which exhibited severe end splitting at 25% and 75% of its length, experienced a pure shear failure with longitudinal sliding along the entire span, initiated at the split. Figure 59d illustrates the displacement at the end of the log, showing the initial (δ_0) and final (δ_f) slip positions. This behavior is consistent with findings by Zhang et al. [171], who reported that greater crack depth in solid rectangular beams of *Pinus sylvestris* reduces resistance to parallel shear.

Nevertheless, not all logs with similar degrees of splitting exhibited shear failure. In the 1st group, 4 of 17 logs had splitting at one or both ends (up to 25% of their length), yet failure occurred in the central third of the span, unrelated to the splitting defect. In the 2nd group, 11 of 28 logs presented the same level of splitting, and only 2 exhibited longitudinal shear failure. These results suggest that failure location relative to the applied load may also play a role. Shear failures were associated with horizontal or diagonal cracks and, in some cases, were coupled with steep grain inclination, as illustrated in Figure 59. However, the qualitative nature of this analysis precludes the establishment of conclusive trends—an observation consistent with findings by Esteban et al. [236].

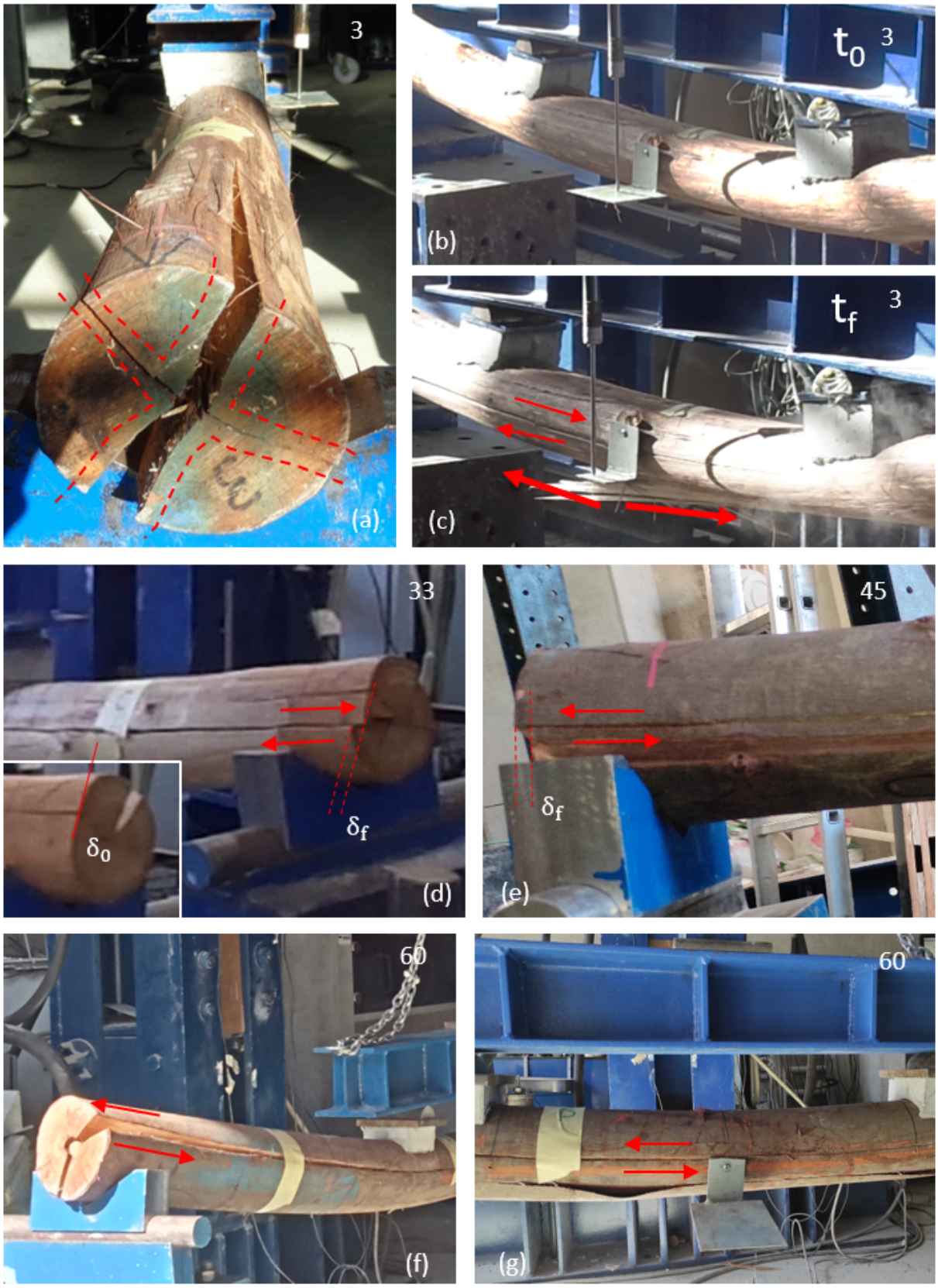

Figure 59: All images: Horizontal shear failure modes (the log number is indicated in the upper right corner).

4.5.7.5 Grain Angle Influence

As illustrated in Figure 60a–d, two of the 17 logs from the 1st group and three of the 28 from the 2nd group exhibited grain angles exceeding the maximum threshold defined by R-M (i.e., one grain deviation per seven units, corresponding to the lower bound for Grade B). These logs failed either in pure tension or in splintering tension, both characteristic of brittle behaviour. Except for one specimen, they also recorded the lowest bending strength (f_m) values within their respective groups. Regarding stiffness, the lowest E_{local} and E_{global} values in 1st group were likewise associated with logs presenting grain angle deviations. These findings are consistent with previous studies, which have demonstrated the detrimental effect of grain inclination on the mechanical performance of timber [140].



Figure 60: Logs with fibre deviation (the log number is indicated in the upper left corner).

4.5.8 Evaluation of Ranta-Maunus Visual Grading as a Pre-selection Tool

To assess its utility as a pre-selection method, the 45 selected logs were classified based on the criteria defined in Table 10, following the thresholds proposed by R-M. These criteria categorize logs into two quality grades: Grade A (superior) and Grade B (inferior). Given the previously discussed, the sweep and cracking variables were excluded from the analysis for bending tests, and logs tested in parallel compression were not considered.

Figure 61 presents the distribution of classification outcomes for each visual characteristic, both individually and as an overall (TOTAL) grade. For ovality, 60% of the logs met Grade A criteria, while 40% were assigned to Grade B. Tapered showed a more pronounced disparity, with only 20% of logs qualifying for Grade A and the remaining 80% categorized as Grade B. Knot-related characteristics exhibited the least impact on grading: over 80% of the logs were classified as Grade A for both total knot area ($Knot, all$)

and knot density in the central third ($Knot, cen$). No knot clustering was observed; therefore, for KS, all samples were classified as A; consequently, this variable was discarded from the analysis. When the TOTAL grade was considered, i.e. the most restrictive grade assigned among the evaluated characteristics, 7 logs (16%) were classified as Grade A, and 38 logs (84%) as Grade B.

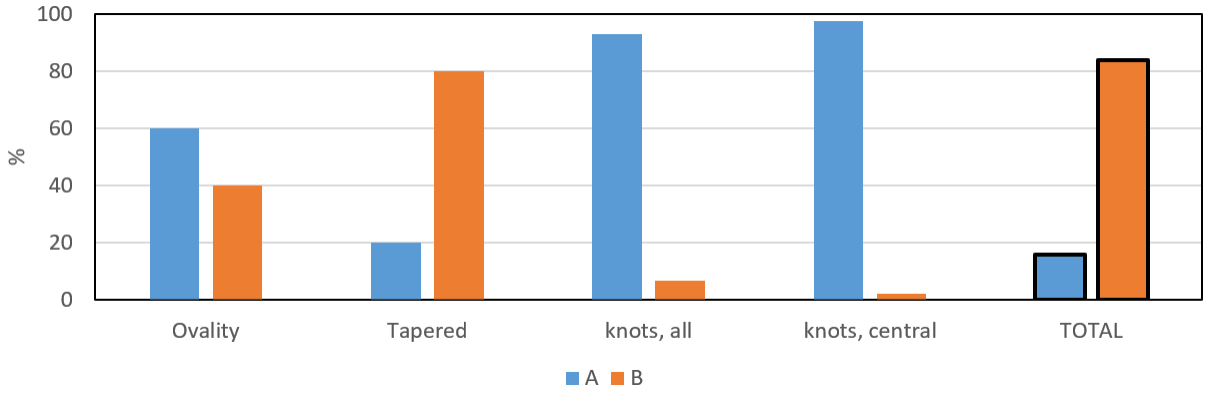

Figure 61: Grading of logs, A or B, according to the allowed values of R-M for each visual characteristic (see table 10). TOTAL considers the threshold of the most unfavorable classification.

When stratified by harvest period, the 1st group (spring) yielded 4 Grade A logs (24%) and 13 Grade B logs (76%). In the 2nd group (autumn), only 3 logs (10%) were assigned to Grade A, while 25 logs (90%) were classified as Grade B. To compare mean values across grading groups (all, 1st, and 2nd), non-parametric Mann–Whitney U tests were applied due to the small sample sizes and the non-normal distribution of some variables. The U test statistics and associated significance levels are summarized in Table 13. Figure 62 displays the corresponding boxplots, comparing mechanical properties between Grade A and Grade B for all samples.

Table 13: Comparison of means between groups A and B including U values and significance level.

	E_{local}			E_{global}			f_m		
	knot, all	tapered	R-M	knot, all	tapered	R-M	knot, all	tapered	R-M
1st	49	40	44	39	43	47	46	41	45
p-value	*	ns	*	ns	ns	*	*	ns	*
2nd		69	69		71	58		163	65
p-value		ns	ns		ns	*		**	ns
all		231	198		242	213		220	206
p-value		ns	*		*	*		ns	*

ns: no significance level; * p < 0.05 ; ** p < 0.01

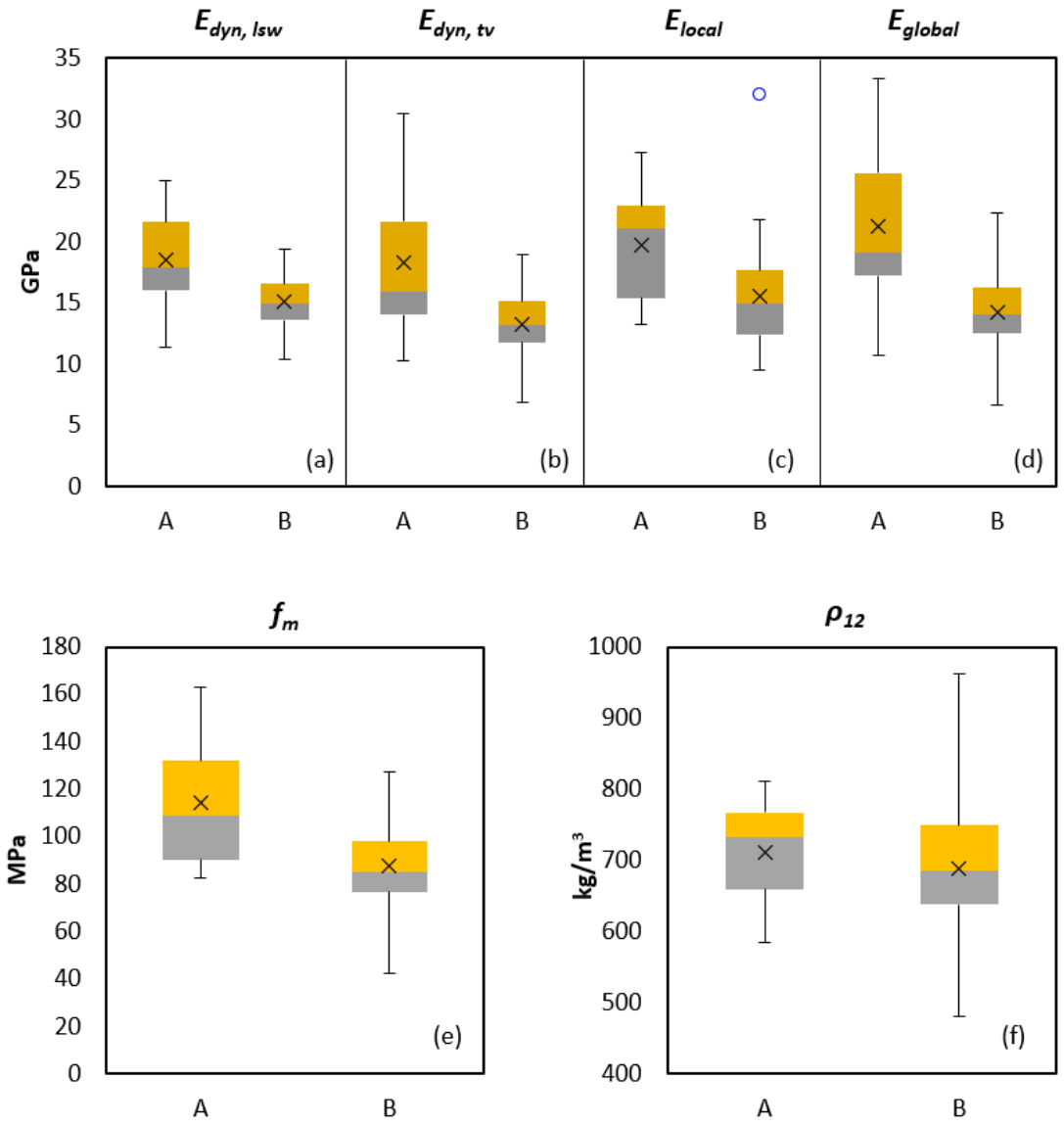

Figure 62: Comparison between grade A and B according to R-M for different physical-mechanical properties: dynamic Elasticity modulus for (a) longitudinal stress wave and (b) transversal vibration, static Elasticity modulus (c) local and (d) global, (e) bending strength and (f) density.

As reported by Suazo-Uribe et al. [190], although a slight trend toward higher dynamic modulus values was observed in Grade A (see Figure 62-a and 62-b), the R-M classification did not correlate significantly with the dynamic moduli for Longitudinal stress wave ($E_{dyn,lsw}$) and transversal vibration tests ($E_{dyn,tv}$). In contrast, the destructive tests revealed statistically significant differences between the two visual grades, with Grade A logs consistently exhibiting higher values. For the complete sample set (n = 45), significant differences were found for E_{local}, E_{global}, and f_m, but not for density (ρ_{12}). When analyzed by harvest group, similar patterns were observed: in both the 1st and 2nd groups, differences between Grades A and B were significant for E_{global} and ρ_{12}. However, for E_{local} and f_m, grade A and B were not different in the 2nd group. Although the trends are less pronounced, Table 13 presents disaggregated values to further examine the influence of knottiness ($knot_{all}$) and taper on the R-M grading. For knottiness, focusing exclusively on the 1st group (since all specimens in the 2nd group met the criteria for Grade A), 76% of

the specimens were classified as Grade A and 24% as Grade B. Statistically significant differences were observed in E_{local} and f_m, consistent with previous observations: lower knottiness (Grade A) is associated with significantly higher stiffness and bending strength.

In the case of taper, no significant differences in E_{local} were found between Grades A and B—whether analyzed separately by group or as a combined dataset. However, a significant difference was observed in E_{global} when considering all samples. A particularly strong difference was also observed in f_m for the 2nd group, which may suggest an interaction effect with log length—recalling that the 2nd group comprised logs that were 40 cm longer, potentially influencing the a coefficient in Equation 13.

This initial analysis supports a critical evaluation of the R-M visual classification method as a pre-selection tool for small-diameter logs. While the studied visual characteristics do not appear to influence the dynamic properties of the logs, they do impact the mechanical properties assessed through destructive testing. Among these, curvature and knottiness appear to be the most relevant, followed—though to a lesser extent—by taper.

The classification thresholds proposed by Ranta-Maunus for grades A and B appear adequate for most parameters, which is consistent with the results of Morgado et al. [26]. The data suggest that the Sweep value may be overestimated and that a threshold of 10 mm/m (twice the value originally proposed by R-M) remains a conservative limit. However, the limited sample size affects the statistical robustness of this conclusion.

4.6 Experimental Campaign to Predict the Mechanical Performance of *Acacia dealbata* Logs Using Non-Destructive Techniques

4.6.1 Transversal Vibration Testing

The tests were conducted in the Civil Engineering Laboratory of University of Minho, in a closed and isolated chamber. Due to the availability of equipment, measurements for logs with moisture content (MC) greater than 12% (MC > 12%) were performed at different times. The difference in harvest time and air-drying duration led to unequal MC values between both groups.

For the 1st group, which comprised 17 of the 34 specimens, tests with moisture content (MC) greater than 12% were conducted in August 2022, approximately 90 days after harvest. The 2nd group, consisting of 28 of the 31 logs, was tested in two phases: 18 logs in January 2023, 30 days after harvest, and the remaining 10 logs in March 2023, 60 days after harvest. MC measurements obtained with an electrical resistance meter indicated an average of 22.55% (SD = 6.31%) for the 1st group and 30.45% (SD = 7.39%) for the 2nd group. Subsequently, all 45 logs (17 from the 1st group and 28 from the 2nd) were kiln-dried in July 2023 to reach the reference MC of ≈12% for testing. The resulting values were close to the target, though with slight variations in magnitude and dispersion, likely due to the presence of strongly adherent bark in the 2nd group. The MC recorded during testing was 10.03% (SD = 0.50%) for the 1st group and

11.91% (SD = 1.98%) for the 2nd. The following devices were used for the tests:

- Accelerometers: PCB 393B12 (Figure 63b) for MC > 12% tests, with a sensitivity of 10000 mV/g (±10%); PCB 352B (Figure 63c) for MC ≈ 12% tests, with a lower sensitivity of 1000 mV/g (±5%). Both models were from PCB Piezotronic;
- Data acquisition cards: from National Instrument Dynamic Signal Acquisition (Figure 63d);
- Laptop and connection wires (Figure 63e4).

Logs were suspended using spring supports and 2-meter-long plastic wires (Figure 63a) to decouple the system from external frequencies, simulating free boundary conditions (Figure 63e). Five aluminium plates were screwed at specific distances along each log. Accelerometers were mounted on each plate to measure modal shapes and relevant resonant frequencies. These were connected to the data acquisition device and then to the laptop. After setting up each log, the chamber was sealed, and an 1800-second recording was initiated in 3 consecutive series, capturing the signal with National Instruments' Measurement and Automation Explorer.

The excitation method varied depending on the accelerometer model: ambient vibration was used for the high-sensitivity model, while little hits were applied to the log at 600 seconds for the lower-sensitivity model.

Data were analyzed using ARTemis Modal 4.0 to determine each log's first vertical resonance frequency (f_1). Before each test, MC was measured at 3 points using an electronic resistance meter, as outlined in section 3.2.4. Two pairs of measurements—mass and cross-sectional geometry—were taken: one before kiln-drying (MC > 12%) and one afterwards (MC ≈ 12%). Each log was weighed using an electronic scale. The inertia (I) was calculated using the apparent diameter, d_{app}, averaged over the five sections shown in Figure 5 and multiplied by the length (L).

The dynamic modulus of elasticity ($E_{dyn,tv}$) was calculated using an expression derived from the Euler-Bernoulli beam theory applied to the natural frequency of the first bending mode of a beam under free boundary conditions. The equation in GPa is:

$$E_{dyn,tv} = \frac{4\pi^2 f_1^2 m L^3}{4.73^4 I} \tag{49}$$

Where f_1 is the first longitudinal stress wave resonant frequency in Hz,m is the mass in kg, L is the length of the log in mm and I is the second moment of area (the mean of the apparent diameters d_{app}) in mm to the fourth power mm^4.

Finally, the dynamic modulus of elasticity ($E_{dyn,tv}$) was adjusted to a reference MC of 12%, following the moisture content adjustment formulas proposed by Unterwieser et al. [221] for values below or above the fibre saturation point (FSP = 28%).

$$E_{dyn,tv,MC\leq FSP} = \frac{E_{dyn,tv}}{1 - 0.00825(MC - 12)} \tag{50}$$

$$E_{dyn,tv,MC>FSP} = \frac{E_{dyn,tv}}{0.868} \tag{51}$$

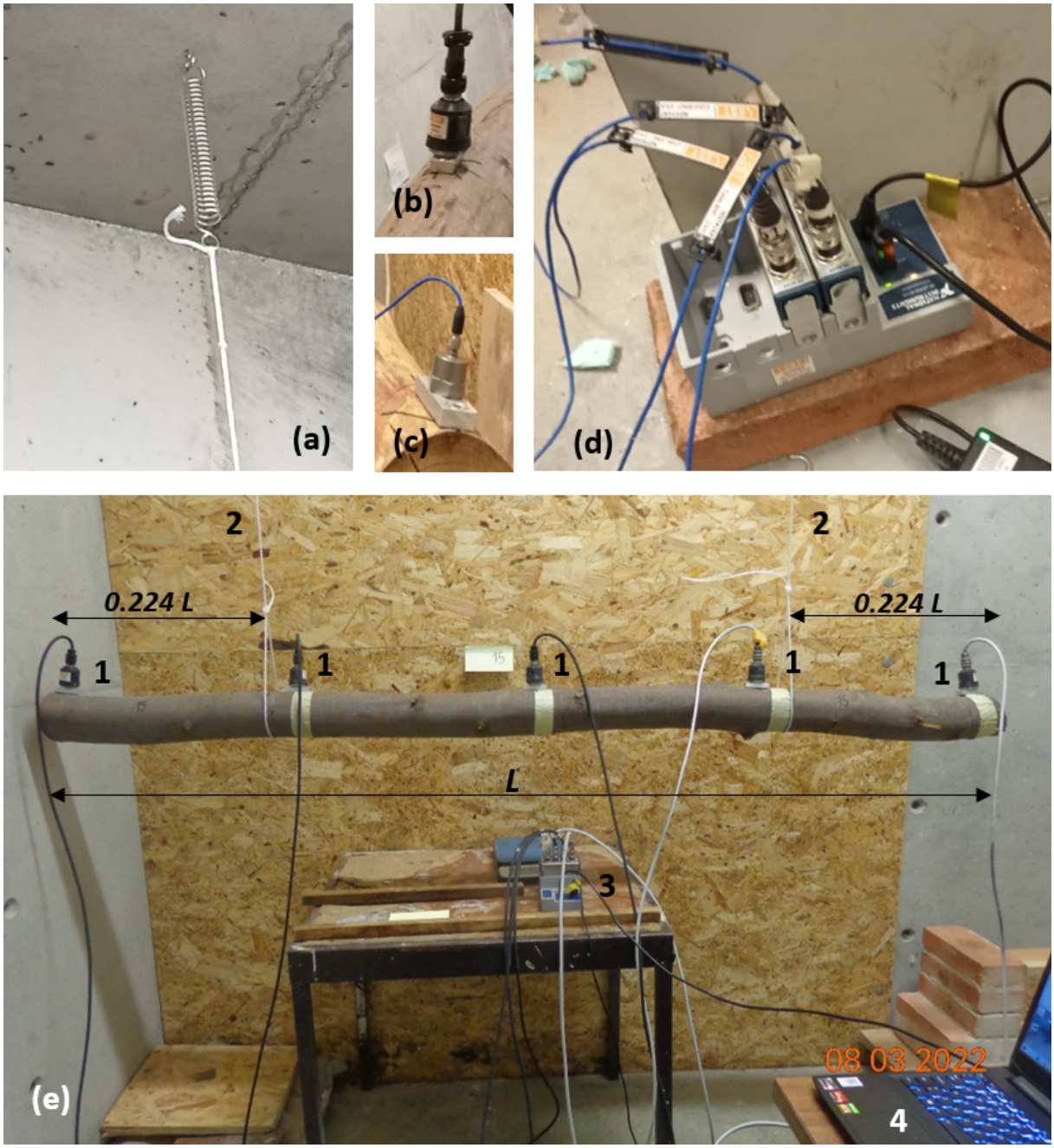

Figure 63: Transverse vibration testing. (a) Spring supports and 2-meter-long plastic wires, (b) accelerometer model PCB 393B12, (c) accelerometer model PCB 352B, (d) data acquisition cards, and (e) test setup showing the five accelerometers (1), wire supports (2), data acquisition system (3), and laptop (4). Note the geometric arrangement for free-free boundary conditions.

4.6.2 Longitudinal Stress Wave Testing

Due to equipment availability, longitudinal stress wave tests for specimens with MC > 12% were conducted at different times in the IBS-S main laboratory. The 1st group (17 specimens) was tested 180 days after harvest, in late November 2022, while the 2nd group (28 specimens) was tested 30 days after harvest, in early January 2023. MC measurements obtained with an electrical resistance meter indicated an average of 16.15% (SD = 2.21%) for the 1st group and 41.47% (SD = 7.39%) for the 2nd group.

After kiln drying in July 2023, all 45 specimens were retested at a target MC of 12%. As with the transverse vibration tests, slight differences in magnitude and dispersion were observed: 10.44% (SD = 0.58%) for the 1st group (debarked logs) and 13.17% (SD = 1.90%) for the 2nd group (logs with bark).The following equipment was used in all tests:

- Accelerometer: PCB 352B by PCB Piezotronic (Figure 64a2 and b2);
- Hammer: 1.1 kg model 086D20, PCB Piezotronic (Figure 64a1 and b1);
- Data acquisition card: NI USB-4431 Dynamic Signal Acquisition from National Instrument (Figure 64b3);
- Laptop and connection wires (Figure 64b4 and b5).

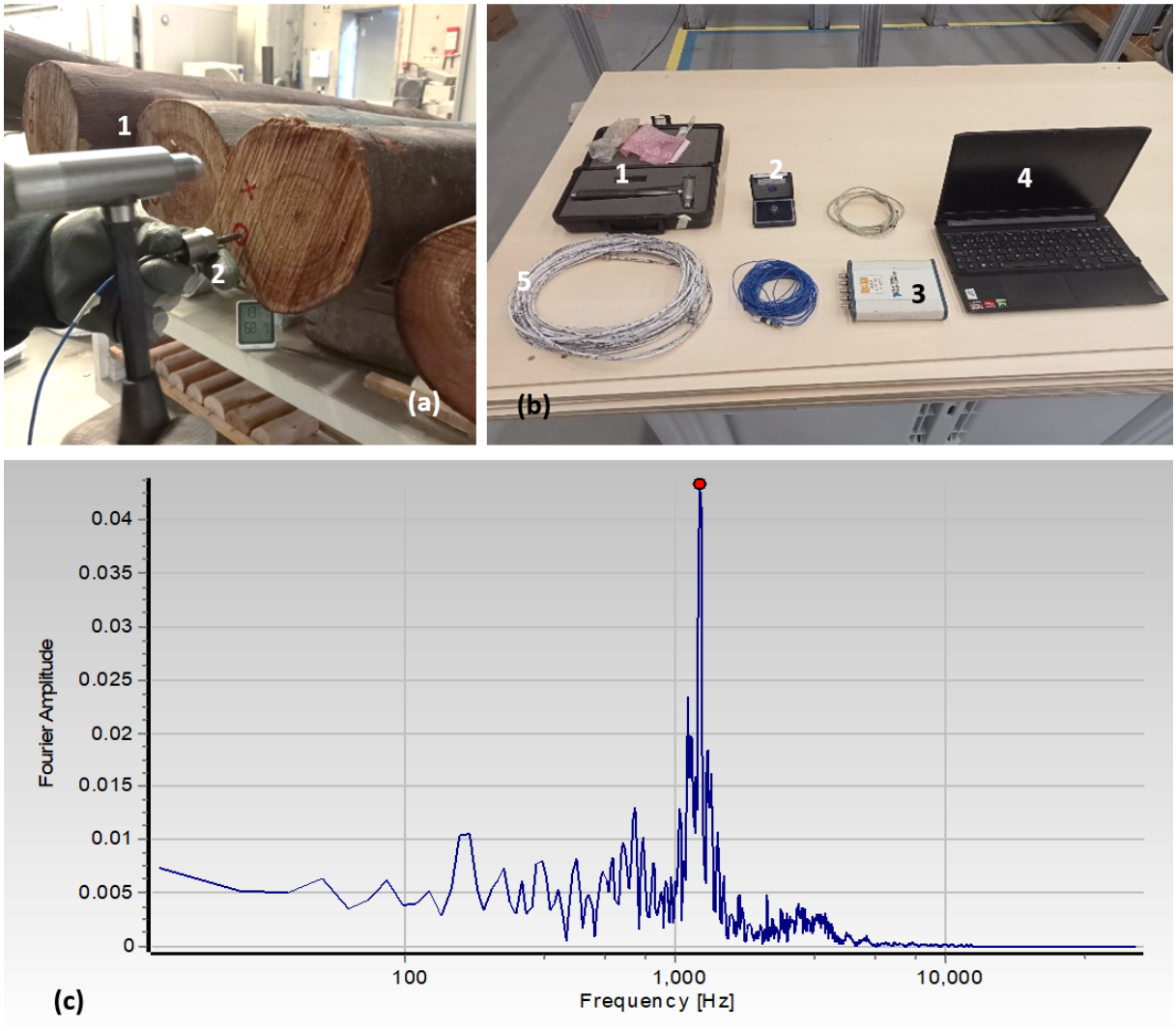

Figure 64: Longitudinal stress wave testing. (a) The test setup shows hammer model 086D20 (1) and accelerometer model PCB 352B (2), and the input-output points are marked on the log ends; (b) Devices: hammer (1), accelerometer (2), data acquisition card (3), laptop (4), and connection wires (5); and (c) Fourier amplitude spectrum showing the resonance frequency of the first longitudinal stress wave (f_{lsw}).

To introduce an acoustic wave through the length of each log, the accelerometer was first attached to a fixed point at the bottom end of the log. Using the hammer, 3 series of 5 impacts, spaced approximately 1 second apart, were delivered. The hammer (Figure 64a1 and b1) and accelerometer (Figure 64a2 and b2) were connected to the data acquisition card, and the signal was transmitted to the laptop. Instruments were calibrated, and data were recorded using National Instruments software (c). The data were analyzed using a Fourier transform in SeismoSignal v2022 to determine the resonance frequency of the first longitudinal stress wave (f_{lsw}) in Hz (Figure 64c). Including the log length (L) in mm, the longitudinal wave velocity (v) in mm/s was calculated based on the following equation, in mm/s is:

$$v = 2Lf_{lsw} \tag{52}$$

Where L is the length of the log in mm and f_{lsw} is the first longitudinal stress wave resonant frequency in Hz.

Following the moisture content adjustment formulas by Unterwieser et al. [221], the longitudinal wave velocity was adjusted to a reference MC of 12%, providing an adjusted velocity value both before (MC > 12%) and after kiln-drying (MC ≈ 12%):

$$v_{MC \leq FSP} = \frac{v_{MC}}{1 - 0.0061(MC - 12)} \tag{53}$$

$$v_{MC > FSP} = \frac{v_{MC}}{0.902 - 0.0017(MC - 28)} \tag{54}$$

After each test, each log was weighed, and its MC was measured following the procedure in section 3.4.2.1. To determine the density ($\rho_{fb,12}$), two pairs of mass and volume measurements were taken: one before kiln-drying (MC > 12%) and one after (MC = 12%). Volume was calculated using the average apparent diameter (d_{app}) and length (L). The EN 384:2016+A2:2022 [192] adjustment adjusted the density to a reference MC of 12%, providing adjusted density values for pre- and post-kiln drying. Finally, the dynamic modulus of elasticity ($E_{dyn,lsw}$) in GPa was inferred using the generic expression:

The equation gives the dynamic modulus of elasticity for longitudinal stress wave testing, $E_{dyn,lsw}$, in GPa is:

$$E_{dyn,lsw} = v^2 \rho_{fb,12} \tag{55}$$

Where $\rho_{fb,12}$ is the full body density, in kg/m^3.

4.6.3 Resistance Drilling Testing

Before conducting the bending tests, drill penetration resistance (R_m) was measured using a Resistance drilling tool, Resistograph IML-RESI PD Series (Germany) (Figure 65a). For this procedure, each log was positioned on supports, and three sections, labelled A, B, and C, were marked (Figure 65c). Sections A and C corresponded to areas near both ends of the log, between 5 and 10 cm from the edge, at the lower

and upper ends, respectively. Section B corresponded to the central portion of the log (S3 in Figure 28). The instrument was applied perpendicularly along each of the three diameters, ensuring that the testing areas were free of cracks or knots. A needle rotation speed of 2500 r/min was used, along with two needle feed speeds: 25 cm/min for 1st group and 50 cm/min 2nd.

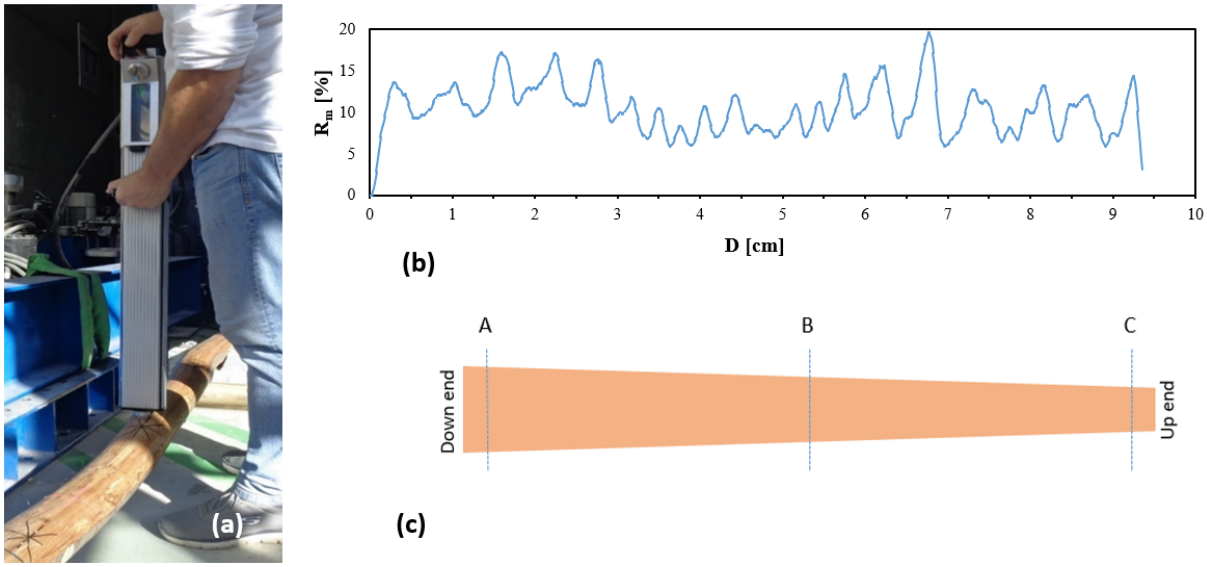

Figure 65: (a) Use of the Resistance drilling tool (Resistograph) on the central area of a log before the bending test; (b) result graph of resistance to drill penetration in %; (c) Indication of the sections of the log where the test is applied: A, B and C.

The data obtained were processed using IML's PD-Tools software, which generated a Resistance (R_m) versus Penetration Depth (D) curve (Figure 65b). Subsequently, each curve was analyzed in Microsoft Excel® 2021 to extract resistance values at intervals of 0.1 mm. The mean Resistance value, R_m, expressed as a percentage (%), was calculated according to the following equation:

$$R_m = \frac{\int_0^D A}{D} \tag{56}$$

Corresponding to the integral of the area A under the curve, between 0 and the needle's penetration length D.

4.6.4 Results of NDT for Physical-Mechanical Properties Prediction of Logs

4.6.4.1 NDT Results at MC > 12% and MC = 12%

As described in Suazo-Uribe et al. [190], for moisture content (MC) measurements during NDT, both before (MC > 12%) and after (MC ≈ 12%) oven-drying, the calibrated mean value of the three records obtained with the electrical resistance meter was used for each test. These values were then used to determine the adjustment factors according to equations 50, 51, 53, and 54.

All data obtained from the longitudinal stress wave non-destructive tests (for MC > 12 % and MC ≈ 12 %) are presented in Appendix G, H, I, and J, together with their corresponding Tables 26, 27, 28, and 29.

Likewise, the results from the transversal vibration non-destructive tests (for MC > 12 % and MC ≈ 12 %) are provided in Appendix K, L, M, and N, along with their respective Tables 30, 31, 32, and 33. The key findings from the non-destructive testing of logs with moisture content (MC) higher than 12% (MC > 12%) and those closer to the reference 12% (MC ≈ 12%) are presented in *Preliminary Study of Acacia dealbata Logs for Use in Construction: Visual Characterization and Non-Destructive Testing* [190]. The conclusions include:

- The dynamic modulus of elasticity (E_{dyn}) values obtained from longitudinal stress wave (lsw) and transverse vibration (tv) tests were comparable to those of reference species. Based on these results, the spring-harvested logs met the D40 classification for structural use as per EN 338: 2003.

- The results also suggest that the harvest season (spring versus autumn) may be a relevant parameter for log preselection in forest management. Logs harvested in spring demonstrated higher dynamic modulus of elasticity (MOE) values, faster air drying, and easier debarking, all of which offer economic and environmental benefits.

- While no significant correlations (p > 0.05) were found between visual grading and dynamic properties, previous studies suggest that defects such as knots and curvature can influence mechanical performance. Therefore, further validation through destructive testing is recommended.

- The MOE values for lsw were approximately 10% higher than those for tv, with a strong correlation observed between the two methods (r = 0.89; p > 0.05).

High correlations were observed between pre and post drying MOE values, with r > 0.90 for lsw and r > 0.70 for tv, suggesting that non-destructive techniques can estimate dynamic MOE at a standardized moisture content of 12% from higher MC measurements. However, due to instrumental limitations, it is advised to take measurements below the fiber saturation point.

4.6.4.2 Relationship Between NDT and DT Results at 12% MC

Table 14 presents the descriptive statistics for all tests conducted, encompassing both dynamic and static evaluations: dynamic elastic moduli $E_{dyn,lsw}$ and $E_{dyn,tv}$ and static elastic moduli (E_{local} and E_{global}), as well as bending strength (f_m), compressive strength parallel to the grain ($f_{c,0}$), and density. With the exception of f_m, all values were adjusted to a moisture content (MC) of 12% according to standardised procedures: the Unterweiser formulations for dynamic modulus adjustment (Equations 50, 51, 53, 54) and EN 384:2016+A2:2022 for static results (Equations 12).

Table 14: Descriptive statistics with results of dynamic and static tests and resistograph on full-scale logs(1st and 2nd groups).

	$E_{dyn,lsw}$ GPa	$E_{dyn,tv}$ GPa	E_{local} GPa	E_{global} GPa	f_m MPa	$E_{c,0}$ GPa	$f_{c,0}$ MPa	ρ_{12} kg/m^3	R_m %
1st									
mean	18.29	14.77	17.67	15.52	113.40	16.78	40.02		13.53
SD	3.32	2.33	4.30	2.66	21.74	6.56	7.27		2.02
cov (%)	18.12	15.75	24.33	17.15	19.17	39.08	18.17		14.95
max	25.91	17.93	27.27	19.16	163.18	27.96	49.50		16.64
min	12.90	9.52	11.59	10.90	80.50	8.77	29.92		9.36
n	17	15	17	15	17	8*	9*		17
2nd									
mean	14.00	12.69	14.75	14.11	71.01	13.57	33.92		16.41
SD	2.70	2.70	3.17	3.32	13.39	5.43	11.65		2.70
cov (%)	19.28	21.25	21.51	23.55	18.86	40.00	34.34		16.44
max	20.17	18.98	21.10	22.34	112.14	25.41	59.41		22.81
min	7.85	6.82	9.53	6.69	42.32	6.89	16.04		10.82
n	28	28	27	28	28	19*	20*		28
All									
mean	15.62	13.41	15.88	14.60	87.89	14.97	36.63	692.80	15.32
SD	3.59	2.74	3.88	3.15	25.17	5.97	10.16	97.87	2.82
cov (%)	23.00	20.40	24.42	21.57	28.64	39.85	27.75	14.13	18.40
max	25.91	18.98	27.27	22.34	163.18	27.96	59.41	962.14	22.81
min	7.85	6.82	9.53	6.69	42.32	6.89	16.04	481.44	9.36
n	45	43	44	43	43	27*	29*	45	45

*This number corresponds to the logs tested (some of the specimens tested correspond to the same tree).

Overall, the results confirm the distinction between the logs harvested in spring (1st) and those harvested in autumn (2nd). The spring-harvested logs exhibited higher mean values across all parameters, although substantial internal variability was observed (for example, cov reached 40.00% for $E_{c,0}$ in Relationship Between NDT and DT Results at 12% 2nd Group). Such variability reflects the intrinsic heterogeneity of the material, consistent with findings from a comparable study on 66 small-diameter Oak logs with minimal processing, which reported a cov of 48.98% for static MOE [138].

Excluding $E_{dyn,tv}$ and E_{global}, the variability of the remaining elastic moduli was closer to that reported in reference studies. For example, Vestøl & Høibø [211] obtained a cov of 24.87% in a sample of 533 Scots pine logs, while Morgado et al. [26] reported a cov of 17.98% for 80 Portuguese maritime pine logs. At the hardwood level, albeit with smaller sample sizes, Llana et al. [15] reported cov values ranging from 14.0% in Birch (5 specimens) to 24.2% in Sycamore (8 specimens) harvested in Ireland.

To statistically compare the mean values of the static and dynamic moduli of elasticity for all specimens and for each harvest group (1st and 2nd), Figure 66 presents the results in boxplot form. Given the high variability of the data, independent-samples t-tests were applied. For both the total dataset and the individual groups, no statistically significant differences were found between $E_{dyn,lsw}$ and E_{local}. Despite a slight difference in mean values ($E_{dyn,lsw}$ = 15.62 GPa; E_{local} = 15.88 GPa), the two parameters can be considered statistically equivalent. A similar trend was observed between $E_{dyn,tv}$ and E_{global}, although

in this case the difference in mean values was greater ($E_{dyn,tv}$ = 13.41 GPa; E_{global} = 14.60 GPa).

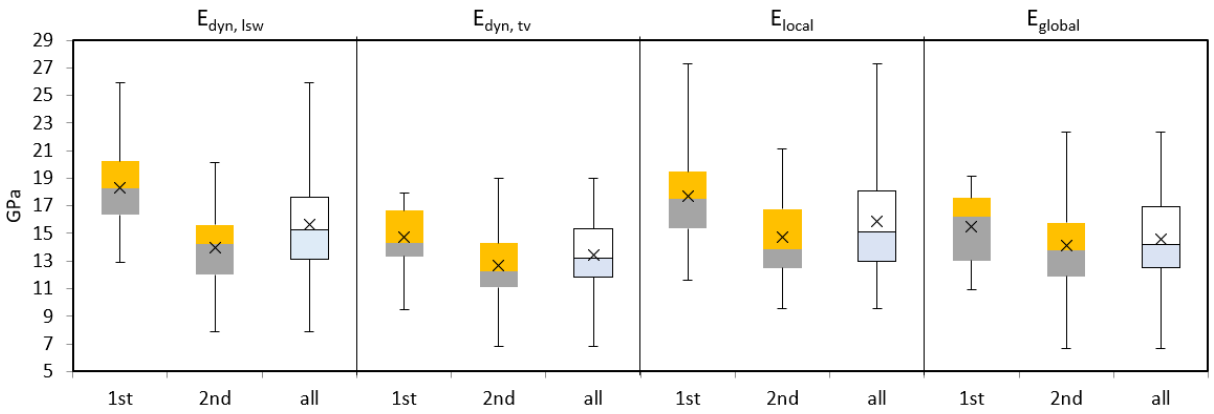

Figure 66: Boxplot comparing dynamic ($E_{dyn,lsw}$ and $E_{dyn,tv}$) and static (E_{local} and E_{global}) elastic moduli. "1st" refers to the spring harvest, "2nd" to the autumn harvest, and "all" to the combined dataset.

This outcome may be explained by the variables involved in calculating each modulus. $E_{dyn,lsw}$ incorporates density, a parameter independent of log geometry, while E_{local} reflects the central portion of the log ($5d_{nom}$), which typically exhibits lower variability and excludes the effects of shear deformation. In contrast, both $E_{dyn,tv}$ and E_{global} incorporate geometric characteristics of the entire log: length (L), the moment of inertia (I, based on the average apparent diameter) in the former, and, in the second, total deformation over $18d_{nom}$.

Regarding bending strength (f_m), variability was within the range of reference studies, with cov values of 19.17% for Relationship Between NDT and DT Results at 12% 1st Group and 18.86% for 2nd Group. For the complete dataset, cov reached 28.64%, largely explained by the significant difference in mean bending strength between groups (113.40 MPa for 1st group vs. 71.01 MPa for 2nd). Comparable studies include Vestøl & Høibø [211], who reported a cov of 21.96% in Scots pine logs; Llana et al. [15], who obtained cov values between 11.8% (Ash) and 22.2% (Alder) for Irish hardwood logs; and Morgado et al. [26], who reported a cov of 21.8% for Portuguese maritime pine.

The results of the compression tests ($E_{c,0}$ and $f_{c,0}$) revealed particularly high variability. This is partly attributable to the strong influence of specimen geometry on compression outcomes, which limits the robustness of the data. For instance, pronounced sweep increases the likelihood of buckling failures (Figure 55). Finally, density exhibited slightly higher variability than that reported in reference studies. Vestøl & Høibø [211] recorded a cov of 9.39% in Scots pine logs, while Morgado et al. [26] reported 9.90% in Maritime pine logs.

4.6.4.3 Correlations

Table 15 presents the correlations between predictors studied —visual characteristics, dynamic properties, dynamic modulus of elasticity and Resistograph measurements—, and the results of destructive bending tests: density, local and global modulus of elasticity, and bending strength. Based on the mean comparison results (t-test) presented in Tables 5 and 8 (full-size and defect-free specimens, respectively), the

grouping of samples was defined. Since no significant differences were observed in density, all specimens were analysed together for this parameter. For the elastic moduli (local and global), the significance levels were close to the confidence threshold (p ≈ 0.05); therefore, correlations were conducted both on the full dataset and separately for each harvest group (1st and 2nd) and due to the significant differences identified in bending strength, the two harvest groups were analysed independently.

Table 15: Correlation results for various mechanical properties.

		Tapered	Sweep	Knots$_{all}$	v	ρ_{fb}	E$_{dyn,lsw}$	E$_{dyn,tv}$	R$_m$
ρ_{12}	all	0.07 ns	0.11 ns	0.02 ns	0.24 ns	0.87 ***	0.67 ***	0.63 ***	0.59 ***
E$_{local}$	all	-0.24 ns	-0.02 ns	-0.06 ns	0.58 ***	0.44 **	0.67 ***	0.68 ***	0.27 ns
	1st	-0.27 ns	-0.48 *	-0.50 *	0.71 ns	0.42 **	0.79 ***	0.63 **	0.56 *
	2nd	-0.17 ns	0.23 ns	0.25 ns	0.43 *	0.36 ns	0.60 ***	0.70 ***	0.44 *
E$_{global}$	all	-0.17 *	-0.28 ns	-0.08 ns	0.59 ***	0.49 ***	0.75 ***	0.72 ***	0.21 ns
	1st	-0.36 ns	-0.62 **	-0.35 ns	0.90 ***	0.28 ns	0.91 ***	0.91 ***	0.54 *
	2nd	-0.19 ns	-0.02 ns	0.13 ns	0.12 ns	0.55 **	0.50 **	0.63 ***	0.50 **
f$_m$	1st	-0.30 ns	-0.41 ns	-0.57 *	0.78 ***	0.22 ns	0.76 ***	0.41 ***	0.39 ns
	2nd	0.05 ns	-0.04 ns	-0.03 ns	0.29 ns	0.34 ns	0.48 **	0.44 *	0.48 ns

ns: no significance level; * p < 0.05 ; ** p < 0.01 ; *** p < 0.00

As discussed previously (Figure 26), a strong and highly significant correlation was found between densities measured in full-size logs and in small slice samples. Table 15 also shows moderate, highly significant correlations of density with both dynamic elastic moduli and Resistograph measurements.

For both static elastic moduli (E$_{local}$ and E$_{global}$), correlations were generally stronger in the 1st group across most variables, which is consistent with the literature. For example, Morgado et al. [26] reported correlation coefficients of r = 0.77 and r = 0.90 between bending strength (f$_m$) and results from the longitudinal vibration method in maritime pine logs, values comparable to the r = 0.76 observed for E$_{dyn,lsw}$ in the 1st group of this study. Two notable exceptions were identified: (i) E$_{local}$ with E$_{dyn,tv}$, where correlations increased from moderate in the 1st group (r = 0.63) to high in the 2nd group (r = 0.79); and (ii) E$_{local}$ with ρ_{fb}, which was low and non significant in the 1st group but moderate and highly significant (p < 0.01) in the 2nd group.

Visual characteristics showed negligible or low correlations, with no significant values in the 2nd group. In the 1st group, slightly higher and statistically significant correlations were observed: E$_{local}$ with sweep (r = –0.48, p < 0.05) and with knot ratio (r = –0.50, p < 0.05), and E$_{global}$ with sweep (r = –0.62, p < 0.01). These findings are broadly comparable to previous studies on conifer logs with larger and more

statistically robust sample sizes. For bending strength, Morgado et al. [26] reported similar correlations with taper (r = –0.32), lower correlations with sweep (r = –0.10), and knots (r = –0.36 to –0.52). Vestøl & Høibø [211] reported higher correlations between E_{local}, E_{global}, f_m, and ρ_{12} with taper, with coefficients of r = –0.49, r = –0.59, and r = –0.41, respectively. By contrast, in minimally processed Oak hardwood logs, Hofmann et al. [136] observed only very weak negative correlations between bending strength (f_m) and knot-related features (r = –0.24, p < 0.05).

4.6.5 Regression Models

Based on the results obtained, several simple and multiple regression models were analysed to predict the mechanical properties of *Acacia dealbata* logs using visual characteristics and/or non-destructive testing results as predictors. The regression models were developed and statistically evaluated using the Real Statistics Excel add-in, and their performance was further compared with results obtained through Artificial Intelligence approaches.

The dependent variables (Y) considered in the models were density (ρ_{12}), local modulus of elasticity (E_{local}), global modulus of elasticity (E_{global}), and bending strength (f_m). All predictor variables (X_1, X_2...) listed in Table 15 were included in the analyses. The regression coefficients were estimated following the general form of Equation 57:

$$Y = \beta_0 + \beta_1 X_1 + \beta_2 X_2 ... + \epsilon \tag{57}$$

Where β_0 is the intercept, β_1 is the coefficient associated with variable X_1, β_2 with X_2... and ϵ is the random error.

The goodness-of-fit of the simple regression models was assessed using the coefficient of determination (R^2), where 0 indicates no correlation and 1 indicates a perfect correlation. For multiple regression models, the adjusted coefficient of determination (R^2_{adj}), calculated as (R^2_{adj} = 1-(n-1)/(n-k-1) [1-R^2]) was used to account for the number of predictors in the model.

4.6.5.1 Density

The Resistograph proved to be a reliable predictor of density [32, 228]. A Tukey ANOVA performed on the three penetration resistance measurements per log revealed no significant differences among the three R_m readings: A, B, and C in Figure 65c (all data resistograph measurements are in Appendix O and P and their respective tables 34 and 35). Figure 67a illustrates the relationship between mean drilling resistance (R_m) and mean density (ρ_{12}) for the 45 specimens, showing a moderately positive correlation (r = 0.59), which was statistically significant (p < 0.000). However, when comparing mean R_m values across harvest groups, significant differences were detected (p < 0.000): the spring-harvested group (1st) yielded a mean of 13.53 (SD = 2.02), whereas the autumn-harvested group (2nd) yielded a mean of 16.41 (SD = 2.70), representing an increase of 21.3%. Figure 67b further demonstrates an improved fit of the linear model when both groups are considered, with a correlation coefficient of r = 0.85.

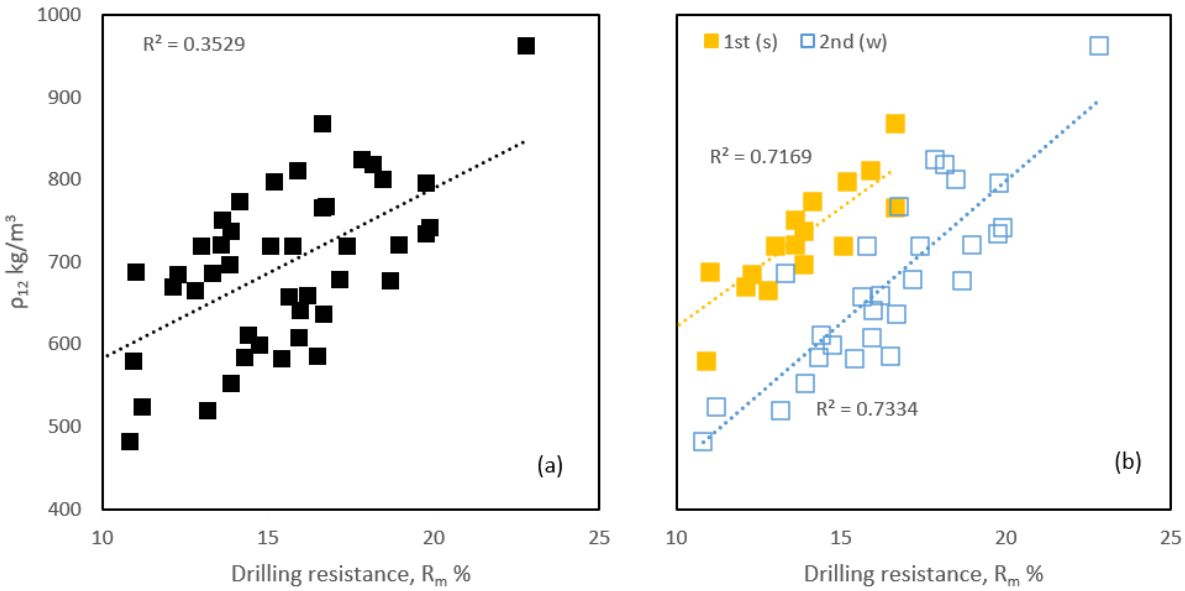

Figure 67: Relationship between drilling resistant (R_m) and density (ρ_{12}) considering (a) all specimens, and (b) separated into the 1st and 2nd groups.

The reasons for these group differences remain unclear. One possible explanation relates to moisture content (MC), which—as noted in the bending strength analysis—can influence mechanical performance. External environmental factors may also play a role. For example, Sharapov et al. [165], in a study on *Pinus sylvestris*, demonstrated that reductions in temperature below the fiber saturation point increase penetration resistance, consistent with the observations of this study.

Beyond these considerations, incorporating R_m as a predictor across all specimens increases statistical robustness and improves model performance. Table 16 presents two models, with Model 3 (which includes both whole-log density and the three Resistograph measurements) achieving the highest adjusted coefficient of determination (R^2_{adj} = 0.825). Figure 68 illustrates this model. However, these models should be interpreted with caution, since, as observed in the destructive tests, density does not exhibit high correlation values.

Table 16: Linear regression models for density, ρ_{12}.

Model	NDT	n	R^2	R^2_{adj}	Linear Regression Model
ρ_{12}					
1	ρ_{fb}	45	0.756	-	$\rho_{12} = 88.56 + 0.93\rho_{fb}$
2	R_m	45	0.353	-	$\rho_{12} = 376.83 + 20.62R_m$
3	ρ_{fb} + R_m	45	-	0.825	$\rho_{12} = 10.03 + 0.81\rho_{fb} + 10.4419R_m$

$$\rho_{12} = 10.03 + 0.81\rho_{fb,12} + 10.44\,R_m$$
$$R^2_{adj} = 0.825$$
$$n = 45$$

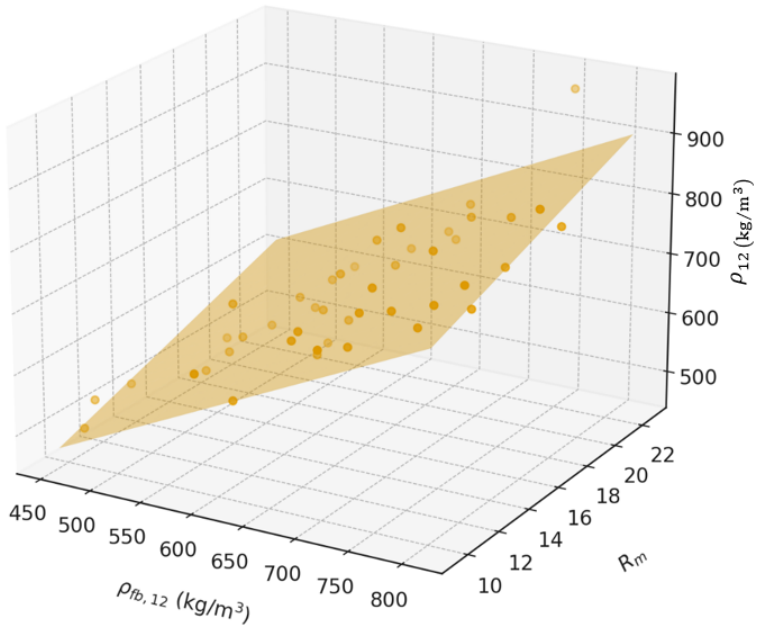

Figure 68: Model 3: regression model with full-body density ρ_{fb} and Resistograph resistance R_m as predictors, and density at 12% MC, ρ_{12} as the response variable.

4.6.5.2 Local Modulus of Elasticity

Table 17 presents the models with the best predictive performance. When both groups are considered, Model 6 (Figure 69a), derived from the 1st group, emerges as the most statistically robust. This model appears less affected by MC or environmental factors such as temperature, although its application should be restricted to MC levels similar to those of the trials (MC ≈ 12%). These results are consistent with the observation that no significant differences exist between $E_{dyn,lsw}$ and E_{local}. $Knot_{all}$ exhibited a moderate determination coefficient (R^2 = 0.41) in the 1st group (Figure 56b), yet this variable did not contribute significantly in the multiple regression models analysed.

For the 2nd group, the most reliable model is Model 9 (Figure 69b), albeit with a lower coefficient of determination.

Table 17: Linear regression models for local modulus of elasticity, E_{local}.

Model	NDT	n	R^2	Linear Regression Model
$E_{local,all}$				
4	$E_{dyn,lsw}$	44	0.576	$E_{local,all} = 3.22 + 0.81E_{dyn,\,lsw}$
5	$E_{dyn,tv}$	42	0.463	$E_{local,all} = 4.28 + 0.84E_{dyn,\,tv}$
$E_{local,1st}$				
6	$E_{dyn,lsw}$	17	0.628	$E_{local,1st} = -1.13 + 1.03E_{dyn,\,lsw}$
7	$E_{dyn,tv}$	15	0.395	$E_{local,1st} = 3.72 + 0.87E_{dyn,\,tv}$
$E_{local,2nd}$				
8	$E_{dyn,lsw}$	27	0.422	$E_{local,2nd} = 4.07 + 0.77E_{dyn,\,lsw}$
9	$E_{dyn,tv}$	27	0.433	$E_{local,2nd} = 4.42 + 0.83E_{dyn,\,tv}$

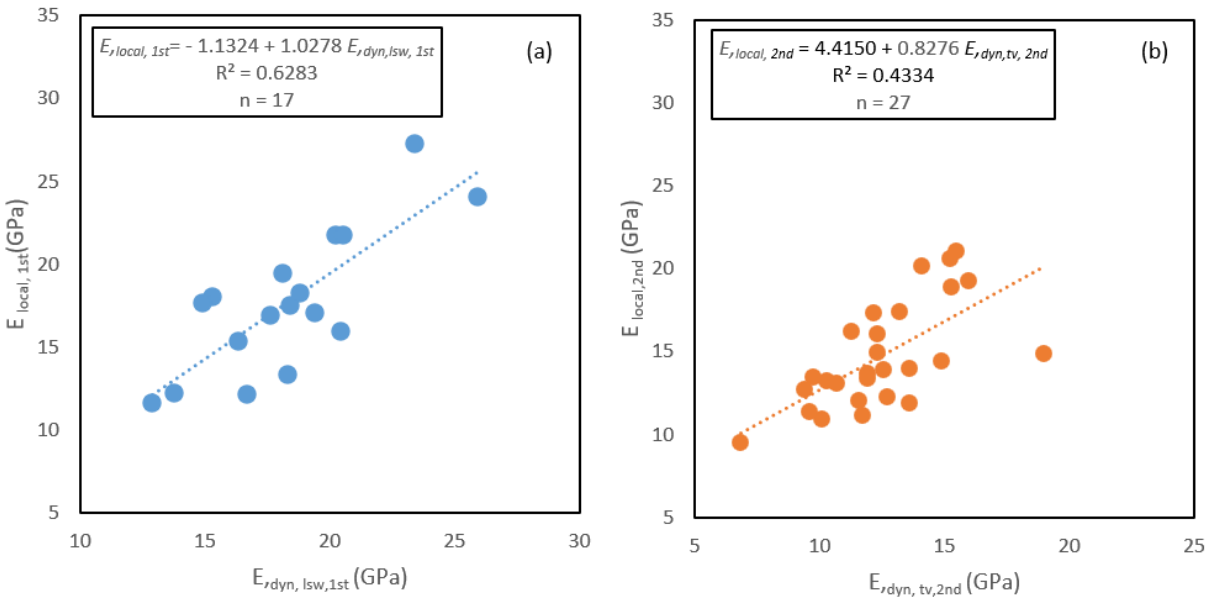

Figure 69: (a) Model 6: relationship between dynamic modulus of elasticity $E_{dyn,lsw}$ and local modulus of elasticity E_{local} in the 1st group. (b) Model 9: relationship between dynamic modulus of elasticity $E_{dyn,tv}$ and local modulus of elasticity E_{local} in the 2nd group.

4.6.5.3 Global Modulus of Elasticity

Table 18 summarizes the models with the highest coefficients of determination. Model 11 (Figure 70a), which includes all logs (excluding outlier values), achieved an R^2 of 0.51. This is consistent with previous analyses indicating no significant differences between $E_{dyn,tv}$ and E_{global} (Figure 66). These findings suggest that the model is valid over a broader MC range (MC < 20%), encompassing both groups. Models 12 (Figure 70b) and 13 produced high R^2 values, but t-tests indicated no significant group differences for E_{global}; thus, models incorporating all samples (Models 10 and 11) would be the most appropriate.

Comparable studies provide supporting reference values: Llana et al. [15] reported R^2 = 0.51 for various Irish hardwood log species using a longitudinal wave capture device (MTG), while in Oak logs, Huber et al. [138] reported a markedly lower R^2 = 0.16 between dynamic and static MOE.

Table 18: Linear regression models for global modulus of Elasticity, E_{global}.

Model	NDT	n	R^2	Linear Regression Model
$E_{global,all}$				
10	$E_{dyn,lsw}$	43	0.367	$E_{global,all} = 5.12 + 0.62E_{\text{dyn, lsw}}$
11	$E_{dyn,tv}$	43	0.512	$E_{global,all} = 3.48 + 0.83E_{\text{dyn, tv}}$
$E_{global,1st}$				
12	$E_{dyn,lsw}$	15	0.718	$E_{global,1st} = -0.81 + 0.94E_{\text{dyn, lsw}}$
13	$E_{dyn,tv}$	15	0.837	$E_{global,1st} = 0.07 + 1.05E_{\text{dyn, tv}}$
$E_{global,2nd}$				
14	$E_{dyn,lsw}$	28	0.254	$E_{global,2nd} = 5.43 + 0.62E_{\text{dyn, lsw}}$
15	$E_{dyn,tv}$	28	0.399	$E_{global,2nd} = 4.24 + 0.78E_{\text{dyn, tv}}$

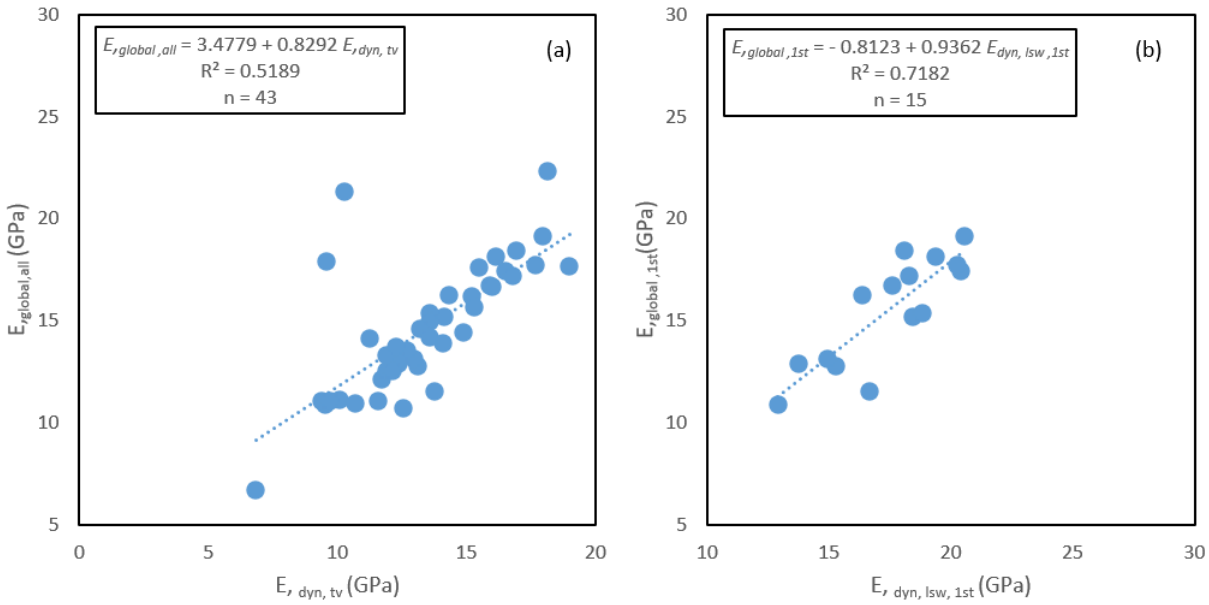

Figure 70: (a) Model 11: relationship between dynamic modulus of elasticity $E_{dyn,tv}$ and global modulus of elasticity E_{global} for all specimens.(b) Model 12: relationship between dynamic modulus of elasticity $E_{dyn,lsw}$ and global modulus of elasticity E_{global} in the 1st group.

4.6.5.4 Bending Strength

Table 19 presents Model 16 for the 1st group (Figure 71a), which uses velocity v, as a predictor and achieved R^2 = 0.60. A close value, slightly lower, is using a multiple regression that includes density and velocity with R^2_{adj} = 0.57. $Knot, all$, in the same group, showed a determination coefficient of R^2 = 0.39 (Figure 57b), though it did not significantly enhance the performance of the multiple regression models.

For the 2nd group (Figure 71b), several simple and multiple regression models were tested, producing results comparable to one another but without substantial improvements in predictive robustness. In related research, Llana et al. [15] reported R^2 = 0.53 for similar tests on hardwood logs, while Huber et al. [138] found lower correlations (R^2 = 0.26) for dynamic tests.

Table 19: Linear regression models for bending strength, f_m.

Model	NDT	n	R^2	Linear Regression Model
$f_{m,\ 1st}$				
16	v	17	0.601	$f_{m,1st} = -104.57 + 0.04v$
$f_{m,2nd}$				
17	$E_{dyn,\ lsw}$	26	0.372	$f_{m,2nd} = 39.18 + 2.25E_{dyn,\ lsw}$

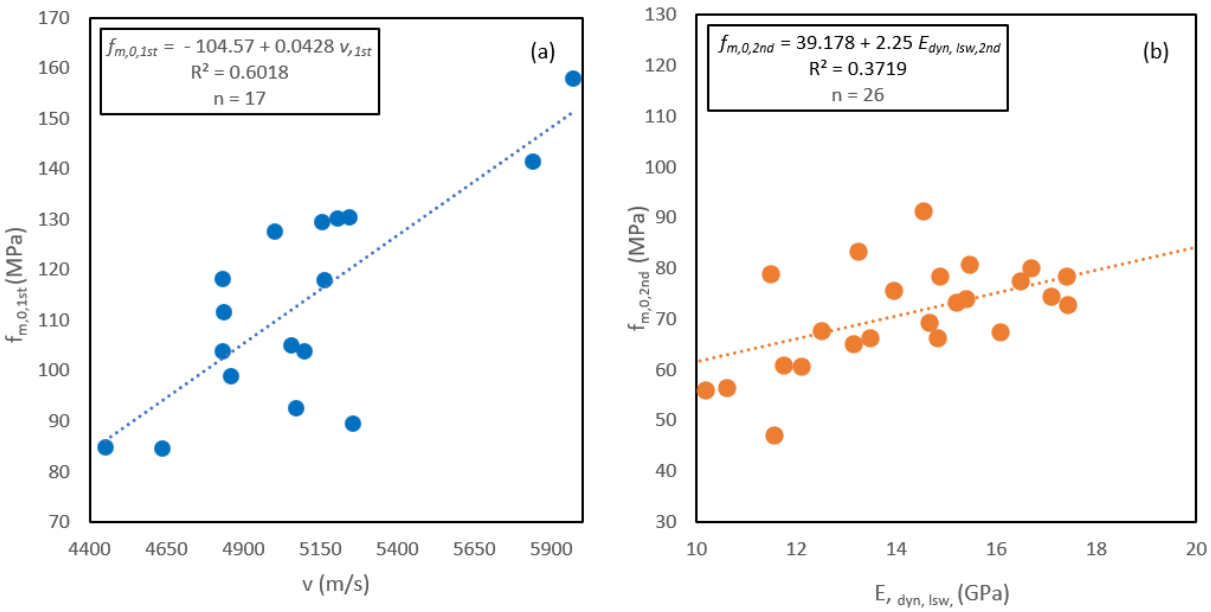

Figure 71: Model 16: relationship between wave velocity v and bending strength f_m in the 1st group.(b) Model 17: relationship between dynamic modulus of elasticity $E_{dyn,lsw}$ and bending strength f_m in the 2nd group.

Although the visual classification variables did not provide sufficient statistical robustness to support multiple regression models, the analysis of their individual influence on strength and stiffness, as well as the correlations obtained—some of which were relatively high (e.g., Sweep vs. E_{global}, r = -0.62)—indicates that these variables warrant further investigation in subsequent studies.

With respect to the regression models and their practical implications, the density-based model, while statistically robust, has limited applicability due to the weak correlations observed between ρ_{12} and the mechanical properties (f_m, E_{local}, and E_{global}). By contrast, the models for the local and global modulus of elasticity yielded slope values close to unity, suggesting only minor differences between static and dynamic MOE.

4.7 Chapter conclusions

This chapter establishes a methodological framework for predicting the physical and mechanical properties of minimally processed *Acacia dealbata* logs based on visual characterisation and NDT results.

- Visual characteristics such as knots, sweep, and taper exhibited no significant correlations with dynamic properties and only weak correlations with mechanical properties obtained from destructive testing. Nevertheless, within the scope of the validated protocol, the visual classification system presented in Table 10 proved to be an effective pre-selection tool for small-diameter logs. The analysis further indicated that sweep thresholds could be increased to approximately 10 mm/m without compromising structural performance. It should be noted, however, that the low occurrence of knots in the analysed samples may have limited the ability to capture their actual influence, an aspect that should be addressed in future studies. Despite these limitations, the findings support the use of visual grading as a practical and reliable field tool for preliminary log selection.

-The comparison among acoustic (longitudinal stress wave, lsw), vibrational (transverse vibration, tv), and drilling-resistance (R_m) techniques revealed strong relationships with the results obtained from destructive tests presented in the previous chapter. No statistically significant differences were observed between the mean values of the dynamic modulus of elasticity obtained using the longitudinal stress wave method ($E_{dyn,lsw}$) and the local modulus of elasticity (E_{local}). Similarly, no significant differences were found between the global modulus of elasticity (E_{global}) and the dynamic modulus derived from transverse vibration ($E_{dyn,tv}$); however, the correlation was weaker, likely due to the greater influence of the overall log geometry on the measurements. Among the evaluated techniques, the LSW method demonstrated greater potential in terms of predictive capacity and practical applicability, as it is also the most straightforward to implement in field conditions. Nevertheless, a larger dataset is required to improve the statistical robustness and to further validate these findings.

- The wave velocity (v) measured in debarked, 12% of moisture content logs demonstrated strong predictive capacity for bending strength.

- The drilling-resistance technique (R_m) was confirmed as a reliable indicator of wood density. However, as observed in the previous chapter, density itself did not exhibit strong correlations with the mechanical properties of the material.

Finally, consistent with the results of the destructive tests, the non-destructive evaluations conducted at different moisture contents (MC > 12% and MC = 12%) confirm the influence of the harvesting season on the mechanical performance of this material, highlighting the need for further research in this field.

Chapter 5

Formation and Control of End Cracks in *Acacia dealbata* Logs During Drying

Solid wood elements are often affected by the formation of cracks, which may arise from growth stresses in young fast-growing trees or from moisture gradients in larger sections. These cracks can impact performance at multiple levels: at the material level, by accelerating degradation; and at the structural level, particularly in connection zones where linear elements are joined with fasteners.

This final chapter describes and critically analyses this phenomenon. It presents the main conclusions of the study contained in the article *Assessing Treatments to Mitigate End-Face Cracking in Air-Dried Acacia dealbata Logs* [237], whose objective was to control or reduce end cracks in wild *Acacia dealbata* logs through a combination of air drying and two tangential stress-relief treatments: longitudinal kerfing and central hollowing.

5.1 Crack Formation

Following felling, wood tissues are subject to ruptures caused by interactions with environmental conditions. These cracks not only compromise aesthetic qualities but also reduce durability by facilitating water accumulation, encouraging colonization by degrading agents, and increasing vulnerability to fire by exposing larger surface areas to combustion. Structural performance may also be compromised. For instance, Mergny et al. [170] reported a 10% reduction in stiffness in solid sections affected by cracking. In connection zones, particularly fasteners-type joints, tissue ruptures can further reduce joint effectiveness and may result in brittle failure [132].

In small roundwood (*srw*) logs, the propensity to crack is increased due to the high proportion of juvenile wood typically found in trees harvested before 20 years of age. Juvenile wood, as noted by Moore and Cown [44], is more susceptible to brittle failure and exhibits greater longitudinal shrinkage compared to mature wood.

Evans et al. [238] classify the effects of cracks on wood performance and service life into three main categories: (i) Deep cracks may penetrate preservative-treated surfaces, exposing untreated sapwood or non-durable heartwood and accelerating decay; (ii) Splits and checks can compromise the holding capacity of metal fasteners and reduce mechanical strength; and (iii) Large cracks may impair visual quality and present safety risks, particularly in applications such as playground equipment.

Wood ruptures can be further classified by location and nature into end checks, surface checks, end splits, collapse, and honeycomb (Figure 72). These phenomena are commonly associated with drying, which causes uneven internal shrinkage particularly in larger logs (moisture gradient). Surface checks often occur in sawn boards (Figure 72a) or where bark is missing, while end splits result when drying-induced fractures propagate through the log, dividing it into two parts. Boxed-heart splits may arise from the release of growth stresses or from differential tangential and radial shrinkage near the pith [239]. Collapse, in contrast, is a distinct defect characterized by cell wall distortion, flattening, or crushing (Figure 72d). This form of rupture is especially prevalent in species such as *Eucalyptus* [240, 241].

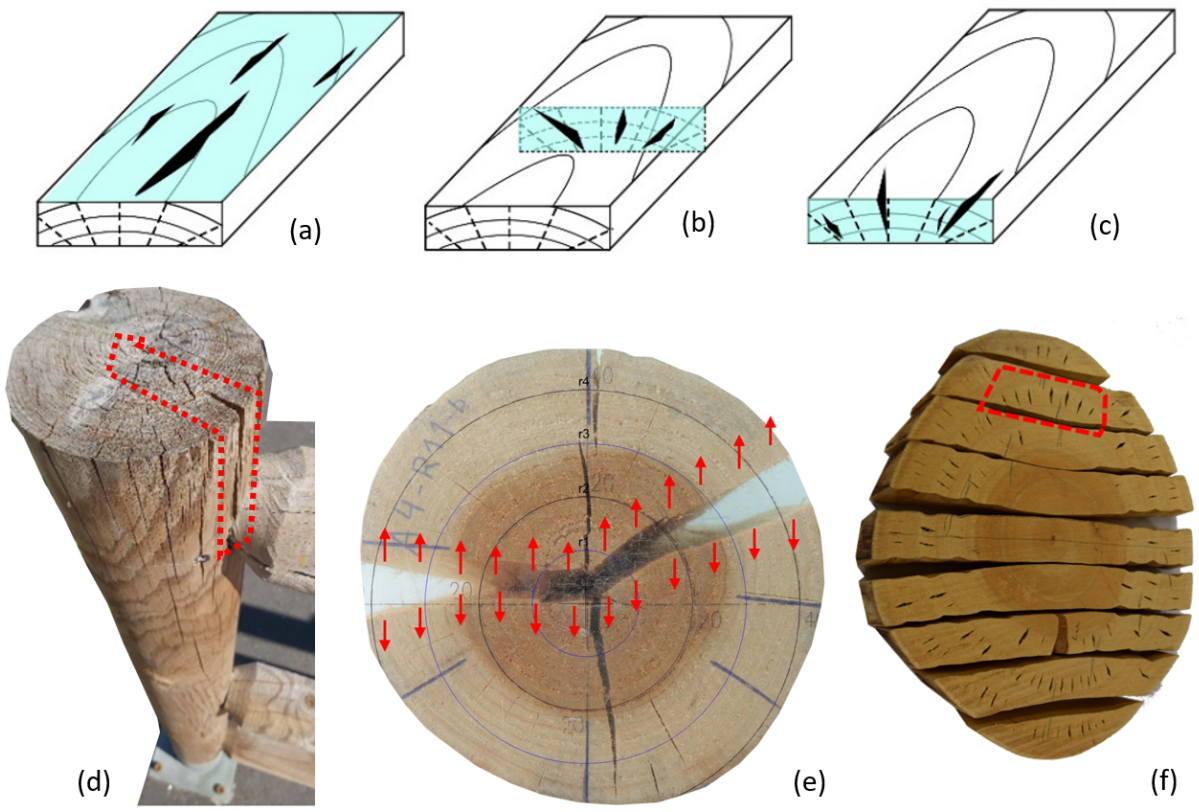

Figure 72: Examples of crack formation in wood. (a–c) Crack types according to Yin and Liu [242]: (a) surface checks, (b) internal checks, and (c) end checks. (d) Surface checks at the end of a log in service; (e) End splitting in a log due to the predominance of growth stresses; (f) Collapse in kiln-dried roundels (courtesy of Professor J.L. Louzada).

Given the viscoelastic nature of wood, the internal deformation mechanisms that lead to crack formation are complex. Yin and Liu [242] analytically described these deformations as a combination of free shrinkage (minimal), elastic deformation, delayed viscoelastic deformation (creep), and mechano-sorptive creep. Crack initiation and propagation are influenced not only by drying-induced stresses -the primary trigger- but also by growth-related stresses, as well as by the anatomical characteristics of the wood and the external drying environment [170].

5.1.1 Drying Stress

As soon as a tree is felled, new internal and external conditions trigger drying within the log. Water and water vapour in the cellular tissues are expelled from the interior to the surface through a complex intercellular hydraulic system driven by two main mechanisms: (i) capillary action, which moves free water through the cell lumen and via small pathways connecting adjacent cavities (pits), and (ii) bound-water diffusion, which drives vapour transport from regions of high to low concentration.

Logs, typically with an initial moisture content (MC) ranging from 30% to 200%, undergo drying in two phases: first, the movement of free water from the core to the surface, followed by evaporation. Over time, the process slows until the equilibrium moisture content (EMC) is reached, where the log's MC aligns with the ambient relative humidity [243].

In thicker elements such as beams or logs, surface moisture is lost more rapidly than moisture in the core, creating a moisture gradient (MG). This differential induces surface shrinkage and tangential stresses, which may cause cracks if the stresses exceed the wood's strength. Conversely, if the core dries more rapidly than the surface in later stages, internal ruptures or separations between annual rings can occur [243] (Figure 73). Yin and Liu [242] identify moisture gradients, temperature gradients, and anisotropic shrinkage as the main drivers of uneven shrinkage.

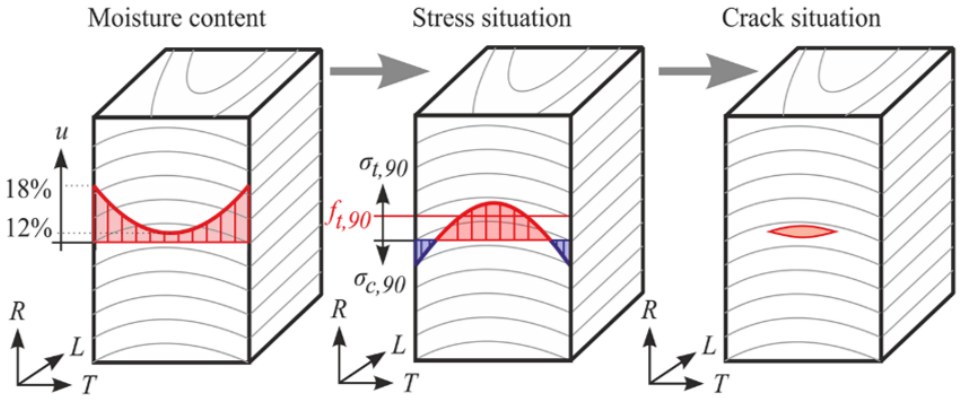

Figure 73: Schematic representation of moisture gradient and crack formation during drying [36].

Controlling the drying process is therefore essential to limit the impact of cracks on wood quality and mechanical performance. Variations in MC trigger dimensional changes, and if these variations are not moderated (e.g., by maintaining a more uniform moisture gradient), cracks are likely to form. Moreover, mechanical properties decrease as MC increases toward the fibre saturation point (25–30%). Wood with MC above 20% is also more vulnerable to biological degradation, while seasoned wood (8–20% MC) is lighter, easier to work, and more cost-effective to transport and prefabricate.

5.1.2 Growth Stresses

Growth stresses arise from the natural mechanical balance of standing trees, determined by their self-weight and metabolic processes [158]. Tensile stresses develop in the outer layers as new tissue forms at the cambium, while compressive stresses in the core counteract these forces, supporting the tree's structure. These stresses intensify when trees develop a type of reaction wood known as tension wood in hardwoods. Upon felling, the abrupt release of these internal stresses often results in cracking and degradation of wood quality. This effect is especially pronounced in juvenile trees (under 20 years old) and in fast-growing species, which typically present more severe stresses [244].

5.1.3 Internal and External Factors in Crack Formation

Crack formation is influenced by both internal and external factors that affect logs, green and dry wood, intermediate components, and final products. Cracks may develop at different stages of the wood's life cycle: during manufacturing, drying, storage, or in service [245].

The anisotropic mechanical properties of wood explain why cracks most frequently occur in the radial–longitudinal plane. Tangential shrinkage is significantly greater than radial shrinkage, while tensile strength in the tangential direction is approximately half that in the radial direction. Consequently, cracks generally form along the tangential plane.

Species variability also plays a significant role. The anatomical structure of wood influences its susceptibility to drying stresses, with vapour transport pathways being significant. For instance, Ananías et al. [93] and Rebolledo et al. [246] demonstrated that differences in anatomical characteristics strongly affect drying behaviour. Kang et al. [247] compared logs from two conifer species with control samples after applying polyethylene glycol (PEG) treatment, a method known to improve dimensional stability. While surface checking was observed in untreated controls, PEG-treated red pine logs showed only small, thin cracks, and treated Korean pine exhibited no checking at all. The authors attributed this to the higher permeability of Korean pine, which allowed for greater PEG absorption.

In most species, surface fibres quickly reach equilibrium moisture with the surrounding air, and temperature plays a decisive role in regulating evaporation rates. Some softwoods, such as Japanese cypress, are particularly prone to checking. Among hardwoods, susceptibility varies: oak, beech, and sycamore exhibit greater sensitivity, whereas sugar maple, yellow birch, and ash show intermediate levels of vulnerability [245].

Woods with large rays tend to be more prone to cracking than those with smaller rays [245], since the ray–fibre interface is particularly vulnerable to the formation of microcracks [248]. Ananías et al. [93] and Rebolledo et al. [246] studied the drying of *Acacia dealbata* and *Acacia melanoxylon* boards, observing a lower risk of collapse and checking due to their large, tylosis-free vessels, which facilitate water movement and exhibit relatively low transverse shrinkage anisotropy. In *Eucalyptus nitens*, however, Rebolledo et al. [246] found a higher incidence of cracks in lower-density areas, increasing radially from the pith to the bark and decreasing with tree height. At the cellular level, Dickson and Dawson (2020) observed significant positive correlations between shrinkage and collapse in *Eucaliptus nitens*, which they related to the distance between vessels and the cell perimeter.

Another important external factor influencing crack formation is the drying method. Despite its slower pace, air drying offers several advantages: it reduces moisture content naturally, saves energy, and decreases log weight, thereby lowering transportation costs. Consequently, it is often considered the logical first step in the drying process, provided that environmental conditions are adequately monitored and managed. For example, in experiments with cross-laid Finnish pine and spruce logs, Ranta-Maunus et al. [25] reported that an unusually wet summer extended the entire drying process, requiring adjustments to the initial schedule.

Air drying begins immediately after felling and stacking, ideally under protection from direct sunlight and rainfall, and in close proximity to the harvesting site to reduce transport costs. Elevated temperatures require particular attention, as they accelerate moisture transfer and can promote collapse or reduce mechanical strength. Several operational factors strongly influence air-drying performance, including stacking method, log length, and bark retention. Bark slows moisture loss by concentrating drying at the log ends—where splitting is most likely—but eventually detaches during prolonged storage, particularly under warm

conditions [249].

Artificial drying methods, such as kiln drying, provide greater control over critical variables including temperature, humidity, and airflow, enabling logs to reach target moisture content more efficiently. However, rapid drying at high temperatures or under low relative humidity can exacerbate end checking, since moisture loss is concentrated along the longitudinal axis of the log [245]. Relative humidity and airflow are also decisive: low humidity accelerates drying but increases the risk of cracking; insufficient airflow may lead to mould growth, whereas excessively fast airflow can cause surface defects and unnecessary energy consumption [250].

5.2 Description and Measurement

The literature presents various approaches to describe and measure the splitting phenomenon in solid wood, whether in sawn timber or logs, with applications in construction or in subsequent processes such as board sawing. Most studies are species-specific, which limits the possibility of broad generalization. Several investigations focus on the industrial use of sawn timber, where susceptibility to splitting can constrain its utility. For example, Rebolledo et al. [246] and Rocha-Sepúlveda et al. [251] studied hardwood species such as *Eucalyptus nitens* for solid wood products, while Wehrhausen et al. [252] examined softwood species such as spruce (*Picea abies*) and white fir (*Abies alba*) for construction purposes.

A common methodological approach is to analyze fracture in small, representative, defect-free samples under controlled conditions, which enables the isolation of specific variables or the testing of scalable measurement techniques (see Figure 74). For instance, Rostand et al. [253] examined 30 mm slices of water-saturated Douglas fir in controlled environments, using markers within a polar coordinate system to measure strain associated with moisture loss. Similarly, Fu et al. [254] studied small white birch specimens to quantify strain. Rocha-Sepúlveda et al. [251] employed advanced image analysis methods, using high-resolution scanned images (10,200 $\times$ 13,200 pixels) and open-source R software packages to measure shrinkage and collapse in *E. nitens* samples from Tasmania. In this study, kiln-dried wooden wedges were monitored using predefined reference points (polygons), enabling detailed comparisons of geometric changes between the initial and dried states.

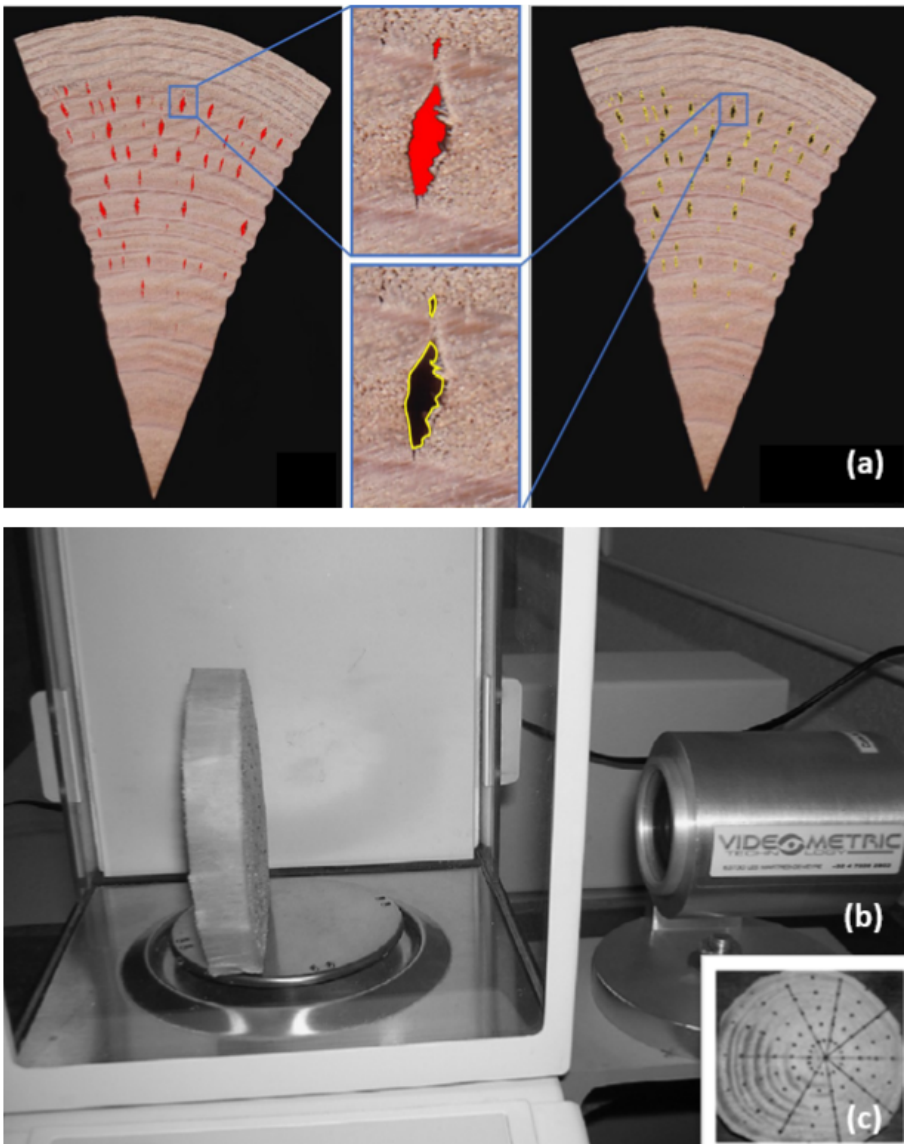

Figure 74: Examples of cracking measurement techniques in small samples: (a) Quantification of checking and shrinkage in *Eucalyptus nitens* wood wedges using open-source R-based image analysis algorithms [251]; (b) Analysis of deformation and fracture processes in Douglas-fir slice using vertical and horizontal deformation measurements with a video camera on a polar reference system (c) [253].

These approaches allow for a robust assessment of stress–strain relationships in both radial and tangential directions. Mugabi et al. [255] measured surface checks in 2.1 m *Eucalyptus grandis* logs after subjecting them to three different kiln-drying schedules. To determine moisture content, moisture gradients, and selected physical characteristics (sapwood depth and heartwood percentage), three 25 mm discs were extracted from each log. Results indicated that drying schedules had the greatest influence on crack formation, while the other variables had weaker effects. However, extrapolating these results to larger samples and assessing their practical applicability remain uncertain. Although Gonya et al. [240] did not directly measure checking, they evaluated collapse and shrinkage percentages in small wedge samples of *E. grandis* logs collected at different heights, comparing them with 25 mm thick, 4.8 m long boards from the same trees. Their findings revealed limited correlation between the two sample formats,

which they attributed to differences in geometry and methodology.

Other studies have employed larger-scale samples to evaluate crack-control treatments. Park et al. [48] investigated 140 mm diameter, 1.2 m long *Pinus rigida* logs to assess checking formation in hollowed specimens. Lee et al. [256] measured the number, length, and width of surface checks greater than 2 mm in rectangular red pine specimens (200 $\times$ 200 mm, 3.6 m long). Evans et al. [51] evaluated radiata pine posts (125/150 mm diameter, 3.6 m long), measuring the number, width, length, and depth of cracks after applying two treatments—kerfing and hollowing—under both air- and kiln-drying conditions.

5.3 Cracking Control

Once wood in service reaches its equilibrium moisture content (EMC) with the surrounding environment, it can stabilize dimensionally, thereby reducing its tendency to crack. However, fluctuating environmental conditions can cause the development of new cracks or the propagation of existing ones, particularly in large members with pronounced moisture gradients. While this issue has been extensively studied in sawn timber boards—the basis of many engineered wood products [242]—it has received comparatively less attention in solid wood intended for utilitarian uses, such as railroad ties [257] or utility poles [258]. Given the variability in wood's physical properties, even within the same tree, and the anatomical differences between species, it is essential to evaluate and combine different techniques (e.g., drying and treatments) to reduce and control cracking effectively.

5.3.1 Pretreatments

Pretreatments are applied prior to kiln or air drying, or to other conditioning methods such as microwave or radio-frequency heating. These processes exploit the elasticity and plasticity of wood to relieve growth stresses, thereby reducing the risk of overstressing and deformation and improving dimensional stability. Common media include water, steam, and microwaves, although other approaches or combined methods have also been explored [242]. For example, Moya and Tenorio [259] reported reductions in growth stresses in *Hieronyma alchorneoides* logs using a combination of steaming and heating treatments.

To minimize initial moisture content (MC) variation and prevent surface mould, Park et al. [48] stored hollowed log samples at low temperature (5.55 $\pm$ 0.46 °C) and high relative humidity (93.84 $\pm$ 5.01%) for two months, and also tested the effect of sealing logs with a polyethylene (PE) layer. Kang et al. [247] achieved significant reductions in both surface and internal checking in red pine and Korean pine logs by applying polyethylene glycol (PEG) treatment followed by a kiln-drying program.

Other studies have reported that high temperatures combined with low humidity can also help limit the occurrence of surface checks and splits [259, 260, 261]. Ranta-Maunus et al. [25] combined optimized kiln drying with hot-oil impregnation in 100 mm diameter Scots pine and Norway spruce logs, which minimized checking and improved external durability, although the treatment was less successful in improving the workability of Norway spruce.

5.3.2 Air-Drying Considerations

Although kiln drying under controlled programs generally provides more consistent results in minimizing cracking [51], air drying remains an important alternative for practical and economic reasons, particularly for roundwood logs. In industrial contexts, production capacity constraints often necessitate outdoor storage of logs for extended periods. Air drying is a passive process that requires little to no external energy, making it both cost-effective and environmentally sustainable.

The efficiency of air drying depends on several factors, including climate, season, storage method, log species, and log size. Simpson and Wang [262] demonstrated the seasonal variability of drying times by stacking ponderosa pine and Douglas-fir logs (102/203 mm diameter, 2.4 m long) at different times of the year. Ponderosa pine logs stacked in summer reached a 30% moisture content (MC) in as little as 10 days, whereas those stacked in autumn required more than 130 days under cooler and wetter conditions. Similarly, Visser et al. [263] found that *Pinus radiata* logs dried for fuel over a six-month period achieved significantly greater MC reduction during summer compared to winter.

In logs with intact bark, evaporation is concentrated at the ends, which slows overall drying and reduces steep moisture gradients. However, this also promotes end splitting, as observed by Tomczak et al. [249]. To optimize air drying directly at harvesting sites, Tomczak et al. [249] compared different techniques for Scots pine logs and found that logs stored in piles dried more efficiently than those subjected to transpirational drying (i.e., felled trees left on the ground with their crowns intact). Their study also highlighted log length as a critical factor influencing drying efficiency.

5.3.3 Techniques to Reduce Tangential Stresses in Logs

To control checking in large wooden elements such as logs, various methods have been developed to reduce tangential stresses, either by introducing cuts or incisions, or by decreasing the moisture gradient through internal hollowing. Evans et al. [51], in a comparative study of kerfing and hollowing against untreated control samples, reported significant reductions in cracking in conifer logs. Other variables, such as species (radiata pine or slash pine), diameter (125 or 150 mm), and drying type (air or kiln), had negligible or non-significant effects compared to the treatments applied.

Kerfing (Figure 75a,b) involves making longitudinal cuts along the entire length of the log to a limited depth. This technique is analogous to practices used in construction, such as slits in the back of exterior siding or in the underside of decking boards exposed to the elements [264]. The cuts relieve tangential stresses during drying, thereby reducing surface checking and improving preservative penetration in surface-treated posts [265, 51, 256, 266]. According to Lee et al. [267], kerfing is particularly effective during the early stages of drying. Larson et al. [11] further demonstrated that notches 12.5 mm deep in logs less than 127 mm in diameter, and 19 mm deep in larger logs, did not significantly reduce the bending strength of ponderosa pine.

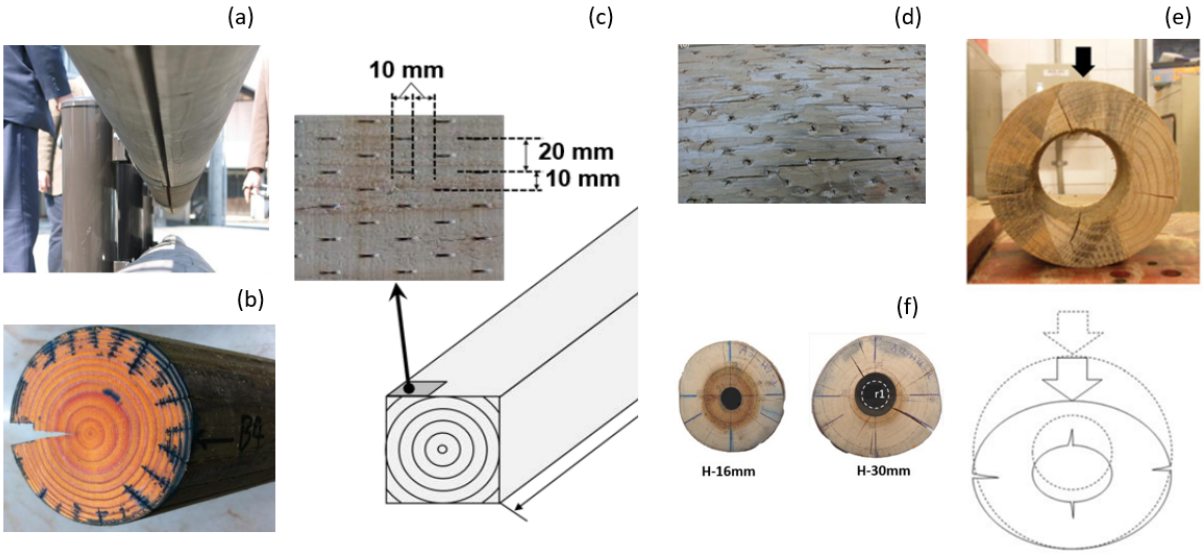

Figure 75: Examples of investigations employing techniques to reduce tangential stresses in logs. (a) Application of the kerfing technique on the lower part of a log in service [264]. (b) "Promoting" effect of kerfing (reagent colouration indicates treatment absorption levels) [265]. (c) Detail of the incision technique applied to a solid piece [268]. (d) Formation of larger cracks due to the interconnection of multiple incisions [238]. (e) Reduction in resistance to point loads in centrally hollowed logs [50]. (f) Partial central hollows of two diameters (16 mm and 30 mm) in *Acacia dealbata* logs [237].

Suazo-Uribe et al. [237] showed that in 450 mm long *Acacia dealbata* rustic logs, three kerfs approximately 15 mm deep significantly reduced outwood cracking compared to untreated samples. However, they also observed a tendency for cracks to initiate from the kerfs themselves (see Figure 75b). By contrast, Yeo et al. [49] reported that kerfing was less effective for controlling the moisture gradient in larch logs, as moisture was retained in the core, thereby limiting its overall effectiveness.

Incising (Figure 75c,d), a technique originally developed in the 19th century to improve preservative penetration [269], involves creating multiple parallel, thin, and deep incisions along the grain. Several studies have demonstrated that scoring can also reduce checking in certain species [238, 268]. For example, Lee and Eom [268] showed that combining longitudinal scoring in *Pinus densiflora* (red pine) posts significantly reduced surface checks. However, they also observed that numerous small incisions tended to interconnect, promoting the formation of larger cracks (Figure 75d).

Hollowing (Figure 75e,f) consists of removing material along the central axis of the log, thereby reducing its thickness and the differential moisture gradient that generates tangential stresses. In small-diameter logs, this procedure removes much of the juvenile core, while retaining the majority of mature wood and the more permeable sapwood, thus facilitating faster and more uniform drying. This approach reduces both the moisture gradient and energy consumption, while decreasing the likelihood of drying-related failures [48, 51, 261].

Yeo et al. [49] reported that hollowing improved drying uniformity and minimized cracking in larch logs. Park et al. [48], working with pitch pine (*Pinus rigida*) logs of 140 mm diameter and 1.4 m length, successfully reduced surface tension and moisture gradient variation through complete central hollowing (80 mm diameter), followed by cold storage, surface sealing with polyethylene wrapping, and a high-

temperature/low-relative-humidity kiln-drying program. This combined treatment led to a significant reduction in checks and splits.

However, excessive hollowing can compromise the structural performance of logs. Lim et al. [50] warned that over-hollowing may reduce load-bearing capacity, increasing the risk of failure under concentrated loads due to flattening effects (Figure 75e). Suazo-Uribe et al. [237] tested partial hollowing in 450 mm long *Acacia dealbata* logs, observing some reduction in surface checking, but the results were not statistically significant and proved less effective than kerfing.

5.4 Experimental campaign, article *Assessing Treatments to Mitigate End-Face Cracking in Air-Dried Acacia dealbata Logs*

All the aforementioned pre-treatments, treatments, and combined techniques have proven effective in reducing and controlling tissue rupture in thick timber elements, both at the surface and internal levels. Nevertheless, their applicability is not universal and may vary significantly among wood species.

Considering the limited amount of research in this field and the increasing need to evaluate alternative wood species for structural applications, the article *Assessing Treatments to Mitigate End-Face Cracking in Air-Dried Acacia dealbata Logs* [237] focuses on investigating this species to control or reduce end cracking. Descriptive statistics of the results, along with box plots comparing untreated and treated samples, are presented in Appendices Q, R, and S, together with their corresponding Tables 36 and Figures 37 and 38. The study analyses the combined effects of air drying and two specific treatments—longitudinal kerfing and central hollowing—applied to *Acacia dealbata* logs. The main conclusions drawn from this research are as follows:

- The results demonstrate that using air drying—a method that is easy to implement, economical, and environmentally friendly—along with destructive treatments such as kerfing and central hollowing can significantly reduce the formation of cracking at the ends of small logs of juvenile *Acacia dealbata* Link wood with minimal processing.

- More than two kerfs, each 15 mm deep along the entire log length, significantly reduce the total sum and number of surface cracks. During drying, the kerfs actively capture surface cracking triggered by environmental variations. However, the results at the center of the log ends do not show reductions different from the untreated samples and reveal a significant increase in the number of cracks, some of which may be large.

- Although less effective than the kerfing treatment, a 250 mm long perforation in the center of the log (in this case, 30 mm), which exposes the more permeable sapwood, facilitates moisture transport. This results in less surface tension around the perforation during air drying and thus fewer total cracks. However, the results indicate that it does not significantly reduce the number of interior cracks.

- This experimental design lacked greater differentiation between treatment variations, which could have provided clearer and more comparable results—for example, including four kerfs along the log and a complete hollowing. Additionally, a larger number of specimens with greater statistical weight could have improved the quality of the results.

This work is part of a broader study to evaluate the applicability of wild *Acacia dealbata* Link small-diameter logs as construction material in log structures as a by-product of control activities of an invasive species. It complements other studies that include, among other things, mechanical properties and the development of connection solutions. In this sense, advancing in studying the reduction in and/or control of cracking, especially at the ends of the logs, is a step towards the material's applicability for these uses.

Consequently, the further stage is based on these findings. It involves studying the formation of cracks at the ends of the logs by proposing two perpendicular cuts, as previously discussed. The cuts function as an artificial splitting, increasing the exposed area at the end of the log and theoretically capturing the tangential variation due to air drying. The experimental design and a few images of preliminary results are shown in Figure 76.

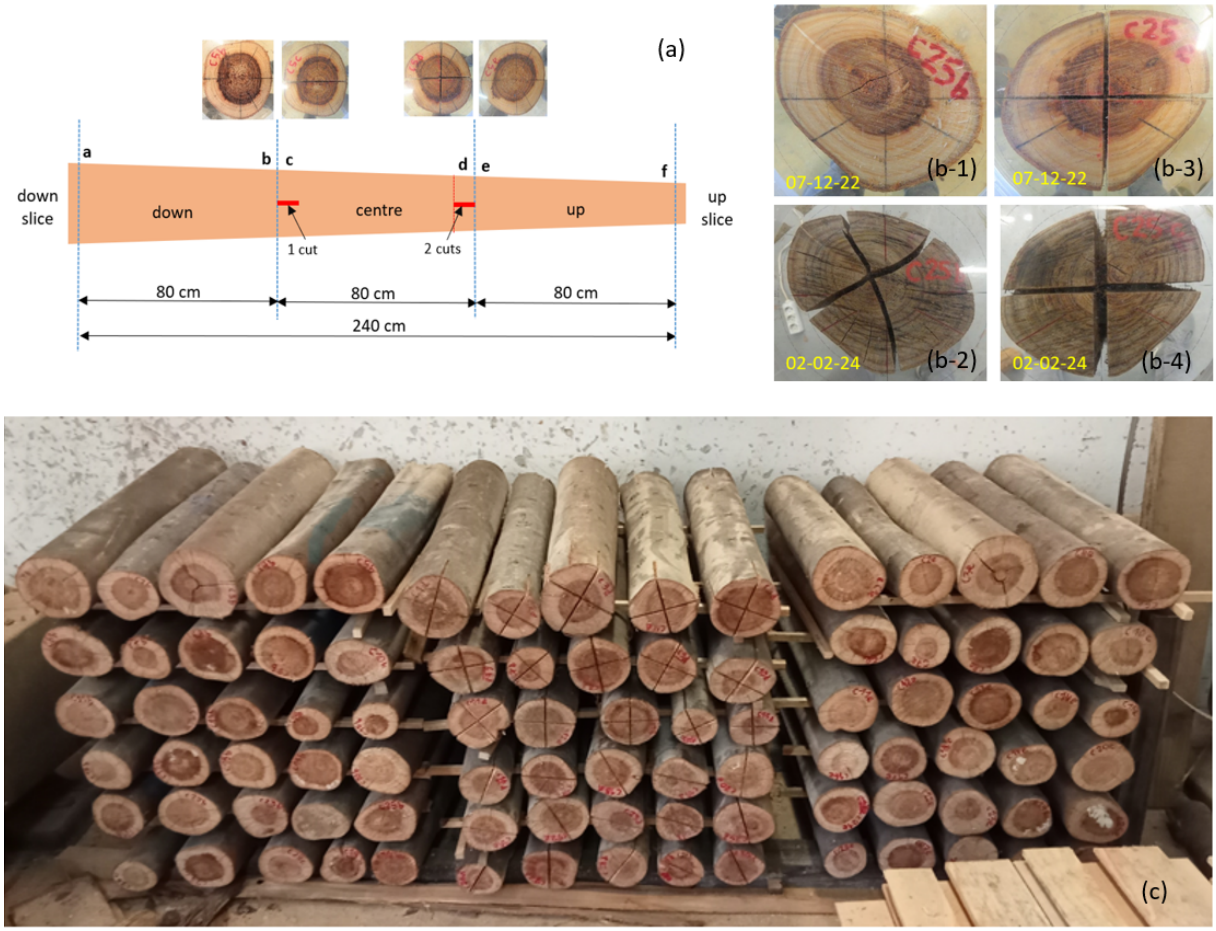

Figure 76: Preliminary results of an experimental campaign with air-dried logs. (a) Experimental design: 30 *Acacia dealbata* logs cut into three segments, the two control ends and the central one with one or two perpendicular cuts. (b) Preliminary view of log 25 dried for 14 months with the same cut on both sides: untreated (b-1 and b-2) and treated (b-3 and b-4). (c) View of the stack.

Chapter 6

Conclusions

The present work constitutes a comprehensive study on the physical, mechanical, and structural characterization of small-diameter *Acacia dealbata* Link logs, an invasive species that poses a significant threat to protected forests in Portugal and other parts of Europe (and other around the world). The main objective was to physically and mechanically assess the technical feasibility of using this species as a low-processed structural material within the framework of circular economy principles and sustainable forest management oriented toward invasive species control. The main findings and conclusions can be summarized as follows:

6.0.1 Context of the Study

Portuguese forests, particularly those with natural preservation value, face severe ecological pressure due to the spread of *Acacia dealbata*, a species that negatively impacts biodiversity and natural forest regeneration. Nevertheless, its anatomical properties as a hardwood species and its rapid growth position it as a potentially exploitable resource for various applications. The literature review highlighted a marked scarcity of research on its structural use, justifying the need to develop an experimental foundation to establish objective physical–mechanical performance values for potential structural applications, while remaining aligned with sustainable control strategies.

A relevant deontological consideration addressed in this work concerns the balance between valorizing a material with potential technical use and the ethical imperative to control an aggressively invasive species. This issue should guide any future management and utilization strategies involving *Acacia dealbata*.

6.0.2 Physical and Mechanical Characterization of Full-Size Logs

Destructive tests on full-size logs demonstrated that, despite their high proportion of juvenile wood, minimal processing, and absence of silvicultural management, *A. dealbata* logs exhibited stiffness and strength levels comparable to those of other hardwood species. High and statistically significant correlations were observed between local and global moduli of elasticity (with higher mean values for the former), revealing a competitive stiffness for structural purposes. The bending strength results ranged from high to very high according harvest season. Both in full-scale bending and compression tests, as well as in small clear specimen tests, logs harvested in spring showed superior mechanical performance compared to those harvested in autumn, suggesting a possible seasonal effect on the formation of mechanical properties—although in the opposite direction to that reported in the literature.

Other factors that could influence mechanical performance—such as moisture content, test temperature, presence or absence of bark, and sample geometry, particularly the high-misaligned stemp (sweep)—were also considered. Their influence was found to be either limited or insufficiently quantifiable due to constraints in data recording.

The destructive (and non-destructive) tests at full scale were conditioned by logistical factors such

as transportation capacity or equipment availability, resulting in a limited and statistically less robust sample size. In addition, the natural variability of the material condition the generalization of the results. Nonetheless, the findings establish strong trends, fill an initial knowledge gap regarding this species, and provide a consolidated protocol for its mechanical characterization that may be validated and extended to other contexts.

6.0.3 Evaluation through Visual Grading and Non-Destructive Techniques (NDT)

Analyses of visual characteristics in relation to mechanical properties confirmed trends reported in the literature regarding parameters such as knot ratio and grain slope and their influence on mechanical performance. In compression parallel to the grain, sweep proved to be a highly significant parameter due to its impact on instability (buckling), although the proposed threshold values may still allow room for adjustment.

The visual grading system proposed by Ranta-Maunus was verified as a reliable tool for on-site pre-selection of logs, facilitating its practical application. However, at a global level, statistical analysis revealed weak and mostly insignificant correlations for visual characteristics, limiting their effectiveness for structural grading purposes.

Conversely, the non-destructive techniques applied longitudinal stress wave (LSW), transverse vibration (TV), and drilling resistance (Rm), showed strong and statistically significant correlations with the destructive test results, enabling the development of predictive models supporting structural classification. Among these, the longitudinal stress wave method stands out as a simple, practical, and highly consistent technique, particularly in relation to the local modulus of elasticity. This method also yielded high correlations with bending strenght for debarked logs with moisture content close to 12%.

6.0.4 Control of Cracking and Air Drying

Air drying combined with the use of kerfing and central hollowing techniques, proved effective in reducing and controlling end cracking in logs. Together, these represent simple, low-energy, and low-cost alternatives for maintaining the structural integrity of logs.

Longitudinal kerfing was found to be highly effective and statistically significant in reducing surface cracks in the outerwood of logs, especially when applying three kerfs instead of two, as tangential stresses responsible for cracks tend to concentrate along the sawn lines. Although the total cracked area was significantly reduced, the number of cracks decreased only slightly. A secondary “propagation effect” from the kerf cuts was observed and warrants further analysis.

Partial central hollowing reduced internal cracking around the perforation zone, though not significantly, and was ineffective in mitigating outerwood cracking. While the total cracking width near the perforation tended to decrease, the number of cracks remained unchanged. Due exist of maior percentage of more permeability sapwood large perforation diameters exhibited a tendency toward further reduction, suggesting a possible optimization path.

6.0.5 General Implications

The results obtained demonstrate the technical feasibility of using minimally processed *Acacia dealbata* logs as structural elements in lightweight constructions or truss-type systems that do not require long members. In addition to providing original scientific knowledge about this species in the Iberian context and a methodological framework for physical and mechanical characterization applicable to other cases, this research offers a practical valorization pathway contributing to invasive species control, reduction of forest residues, and the transition toward a circular bioeconomy.

In summary, this investigation confirms that *Acacia dealbata* possesses an undervalued structural potential that can be sustainably exploited, provided its use remains subordinated to ecological control strategies. Moreover, the interdisciplinary approach of this thesis integrating structural engineering, wood science, and forest management offers a replicable model for the valorization of other invasive species, fostering a direct link between scientific research, environmental conservation, and innovation in timber construction.

6.1 Future Developments

As indicated at the end of Chapter 5, forthcoming work includes the processing and analysis of an air-drying study on 80 cm *Acacia dealbata* logs. This study compares untreated reference logs with others treated through single and double transverse end cuts, with the objective of controlling and reducing end cracking during the drying process. Additional research directions are outlined as follows:

- *Silvicultural aspects:* Given the specific characteristics of the material, a multidisciplinary study is recommended to address silvicultural variables not yet examined, such as the influence of soil properties and stand density. Moreover, due to the intrinsic variability of the material, it is crucial to calibrate both the number and the provenance of specimens to enhance statistical robustness, particularly for specific regions such as central–southern Chile, where *Acacia dealbata* is also an invasive species.

- *Anatomical characterization:* At the species level, a microscopic anatomical analysis is proposed in order to identify features that, according to the literature, may influence macroscopic mechanical performance. These include the area and distribution of vessels, as well as the microfibril angle in the S2 layer of the cell wall. Furthermore, there is a lack of studies addressing the influence of anatomical characteristics on critical aspects of structural performance, such as durability, including parameters such as permeability and the sapwood-to-heartwood ratio.

- *Mechanical performance assessment:* From a mechanical perspective and for a more statistically robust approach, the following full-scale tests are suggested, to be complemented by small defect-free specimens as in the bending tests carried out in this research:

- *Modulus of elasticity and bending strength:* to confirm the observed seasonal effects on mechanical properties and to provide greater statistical robustness through a larger sample size.
- *Compression parallel to the grain strength:* to be performed on full-size members adjusted to the admissible limits defined by visual classification, including elements with different slenderness ratios (low, medium, and high) to refine stress and critical buckling load estimates.
- *Tension parallel to the grain strength:* to evaluate the influence of geometry and natural defects in logs through a dedicated experimental design, followed by comparison with defect-free specimens under standardized geometric and loading conditions.
- *Embedding strength:* Parallel and radial-tangential (half-log specimen).

Connections and structural modelling: Based on these results, further studies on fastener-type connections are recommended, beginning with simple configurations and gradually increasing complexity. The outcomes may also serve as input for convergence studies and finite element modelling (FEM) simulations.

Geometric description and digital modelling: Another promising line of research concerns the geometric characterization and control of irregular bodies, such as minimally processed logs. Consistent with prior literature, this study showed that such low-processing logs exhibit greater stiffness than defect-free samples (though the results regarding strength are less conclusive). New geometric description techniques—such as photogrammetry and 3D scanning combined with CAD–CAM integration, represent a growing field of development that broadens the potential of wood-based materials.

Prototype development: As the culmination of the proposed research stages, the design and construction of a full-scale prototype structure composed of *Acacia dealbata* logs such as a truss system or a beam assembly is proposed to validate the structural feasibility of this material under real-world conditions.

Table 20: A: Reproduction of the questionnaire administered to Mr. Henrique José Morais Fernandes Reis, Head of the Northern Coastal Forestry Management Division of the Portuguese ICNF, concerning specific aspects of the *Acacia dealbata* invasion in the Peneda–Gerês National Park, northern Portugal.

QUESTIONÁRIO (Novembro de 2024)

Valorização do potencial económico de troncos de *Acacia dealbata* Link (mimosa) provenientes do Parque Nacional da Peneda-Gerês

A. A *Acacia dealbata* Link (mimosa) no parque:

1. Existe alguma estimativa da percentagem de área atual do parque (702,9 km², segundo https://riominho.org/pt-pt/ruta-espazo/parque-nacional-peneda-geres) ocupada por esta espécie?

Não temos uma estimativa atual que possa ser indicada como fidedigna. A última referencia a tal indica uma área ocupada com Acácia de cerca de 1350 hectares.

2. Existe alguma estimativa da taxa de crescimento da espécie? (ver Referência 1)

3. Em povoamentos de mimosa, existe alguma estimativa da densidade de ocupação?

4. Como descreveria a forma de ocupação da espécie no parque?

5. Quais são os impactos associados à invasão desta espécie observados nos últimos 10 anos, a nível de:

a. espécies nativas,
b. biodiversidade,
c. qualidade do solo,
d. ciclo hidrológico.

Referência 1: Existe um estudo sobre o potencial de ocupação da espécie no Parque Nacional da Peneda-Gerês, que abrange uma área central de 53,5 km² (ver Apêndice 1). Neste, Monteiro et al. (2017) estimaram uma ocupação potencial de aproximadamente dois terços da área estudada, deduzindo para a data do estudo um percentual de ocupação da espécie de 62,5% desta área.

B. Controlo da espécie:

6. Quais estratégias de controlo foram utilizadas para combater a espécie no parque? (ver Referência 2)

A nossa atuação visa em primeiro lugar procurar controlar os exemplares isolados, posteriormente as pequeñas manchas e nas manchas maiores intervir do exterior para o interior. As formas de combate são esencialmente intervenções macânicas ou por ação do ensombramento com outras espécies.

7. Quais estratégias apresentaram os melhores resultados? E as piores?

A melhor estratégia é a preventiva, isto é, a atuação nos exemplares isolados logo que detetados. Exigem um menor esforço e a taxa de sucesso é elevada poise m muitos casos ainda não estão a produzir sementes.

8. Quais têm sido as principais dificuldades no controlo?

A maior dificuldade é a falta de recursos humanos, a orografia do terreno que dificulta muito os trabalhos de campo e sempre ocorrem incendios pois como estes favorecem esta espécie em detrimento de outras.

9. Em campanhas de controlo de um ou mais povoamentos de mimosa situados em condições favoráveis (terrenos planos e relativamente acessíveis), existe alguma estimativa do custo em horas de trabalho por pessoa ou custos unitários do controlo? (ver Referência 3)

Os custos podem varia muito em função dos meios que temos de utilizar: mecânicos ou manuais e se apenas queremos cortar a árvore totalmente, se queremos arrancar a planta com a raiz ou se queremos descascar. Não temos referências adequadas.

10. Existe alguma estimativa sobre o intervalo de preços de venda de troncos de mimosa para utilização como lenha?

11. Poderia indicar, por ordem de maior para menor dificuldade, quais condições desfavoráveis aumentariam o custo de um eventual controlo da espécie?

Declive, tipo de intervenção, pedregosidade

Referência 2: A literatura científica sobre espécies invasoras (Paula Lorenzo & Maria Cristina Morais, 2023; Vieites-Blanco & González-Prieto, 2020) distingue três tipos principais de estratégias de controlo, que podem ser aplicadas isoladamente ou em combinação:

- **Mecânico** (remoção parcial, como descasque, ou total);
- **Químico** (uso de herbicidas, como o Triclopyr);
- **Biológico** (introdução de agentes bióticos externos que atuam na espécie).

Referência 3: Sobre os custos de remoção da espécie, Nunes et al. (2022) descrevem os seguintes valores em euros/tonelada (€ /t):

- Limpeza e corte de ramos: 10,00 a 60,00 €/t;
- Recuperação e extração: 10,00 a 45,00 €/t;
- Transporte (carga/descarga): 12,00 a 60,00 €/t.

C. Utilização dos resíduos do controlo:

12. Na sua opinião, além da utilização como lenha, existe alguma aplicação comercialmente viável para os resíduos provenientes do controlo da espécie? (ver Referência 4)

Desde que as utilizações não potenciem a utilização deste espécie como maior utilidade do que outras autóctones, todas as utilizações que possam ser feitas aos resíduos dos cortes que é necessário efetuar não me parecem mal.

Referência 4: Investigação abundante (Paula Lorenzo & Maria Cristina Morais, 2023) aponta para várias utilizações potenciais dos resíduos de mimosa com valor comercial, incluindo:

- Bioenergia;
- Herbicidas para controlo de pragas;
- Cosmética;
- Alimentação animal;
- Pasta de papel;
- Materiais de construção.

Apêndice 1

Figura retirada de Monteiro et al. (2017): Estimating invasion success by non-native trees in a national park combining worldview-2 very high resolution satellite data and species distribution models (https://doi.org/10.3390/d9010006)

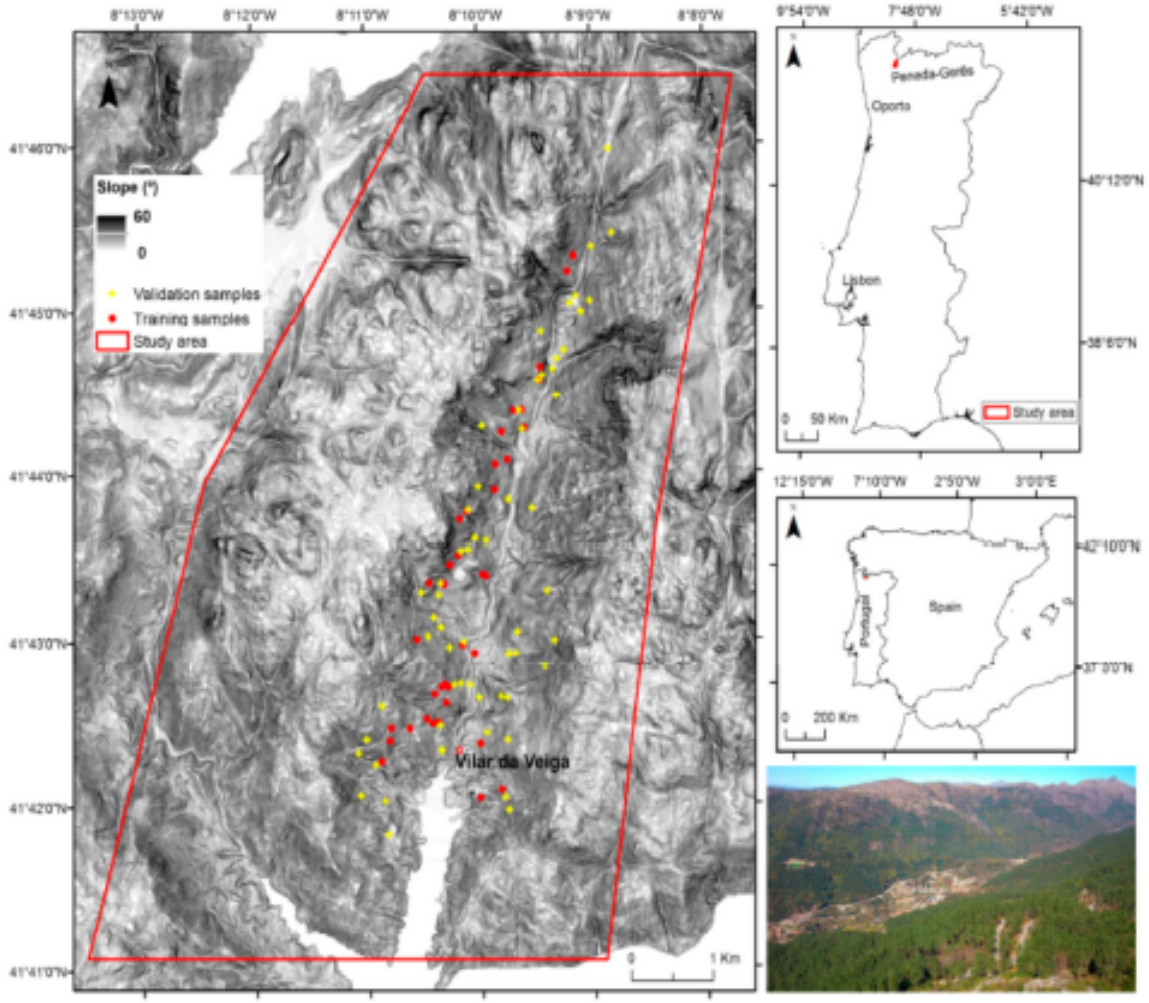

Table 21: B: Results for each specimen obtained from static bending tests, including nominal (d_{nom}) and apparent (d_{app}) diameter, oven-dry moisture content (MC), density adjusted to 12% moisture content (ρ_{12}), local modulus of elasticity (E_{local}), global modulus of elasticity (E_{global}), and bending strength (f_m).

Log	d_{nom} mm	d_{app} mm	MC %	Density, ρ_{12} kg/m^3	E_{local} GPa	E_{global} GPa	f_m MPa
1st							
1	120.0	122.9	15.4	774.9	18.0	12.8	80.5
2	105.6	92.8	11.3	751.2	15.3	16.2	98.4
3	117.4	102.1	12.7	718.6	16.0	17.4	114.1
4	102.0	94.3	11.7	765.0	17.1	18.1	127.3
6	90.0	89.6	11.3	719.3	16.9	16.8	108.7
15	100.0	96.6	12.1	670.3	17.7	13.1	113.0
19	123.1	109.9	12.0	644.5	12.2	12.9	98.4
20	109.7	99.8	12.0	579.1	11.6	10.9	82.9
21	114.0	109.2	12.1	688.1	17.5	15.2	125.7
22	115.0	109.6	11.9	684.1	12.1	11.5	100.7
24	109.0	105.9	12.2	720.2	13.4	17.2	91.1
25	114.0	118.5	13.0	664.5	19.5	18.4	125.7
29	101.0	99.5	11.4	868.5	18.3	15.3	118.5
30	116.0	109.7	12.1	696.3	21.8	17.7	86.4
31	111.0	98.2	11.6	737.4	21.8	19.2	127.2
32	106.2	94.5	12.4	798.0	24.0	33.4	163.2
33	131.7	109.5	12.3	811.2	27.3	29.9	136.7
2nd							
35	114.0	109.8	16.2	962.1	19.3	16.7	82.2
36	112.0	109.9	14.5	719.6	12.3	13.5	76.4
38	98.0	105.8	16.7	552.9	10.9	11.1	42.3
39	115.0	109.2	15.9	796.5	20.6	16.2	84.1
41	96.0	89.6	11.4	583.6	13.9	10.7	78.5
42	104.0	101.2	15.6	585.5	11.4	17.9	58.8
43	106.0	102.4	13.8	685.5	11.2	12.1	68.1
44	106.0	103.6	15.3	611.1	13.7	12.6	63.6
45	125.3	110.9	20.8	678.7	15.0	13.1	69.4
46	117.0	115.9	16.3	733.6	21.1	17.6	79.2
48	113.0	113.4	13.3	677.1	14.0	14.9	81.1
49	102.0	101.3	26.1	824.9	13.4	13.3	71.3
50	105.0	95.5	14.1	599.4	13.3	21.3	82.6

continued on the next page

Log	d_{nom} mm	d_{app} mm	MC %	Density, ρ_{12} kg/m^3	E_{local} GPa	E_{global} GPa	f_m MPa
51	115.0	121.1	14.7	481.4	12.7	11.1	57.9
52	122.8	111.6	16.6	636.2	12.1	11.9	61.0
53	110.0	103.6	11.0	524.3	13.5	11.0	48.8
54	94.0	103.6	13.1	519.3	9.5	6.7	68.2
55	122.0	118.7	15.0	582.2	13.1	10.9	68.2
56	110.0	106.8	11.3	608.0	16.2	14.1	112.1
57	122.0	111.9	17.3	657.3	17.4	14.6	79.0
58	122.1	100.7	14.5	658.8	17.3	12.5	84.0
59	106.0	102.6	20.5	800.3	16.1	13.7	69.2
60	113.0	113.1	16.4	742.4	14.9	17.7	75.0
61	142.5	123.6	15.8	641.1	18.9	15.6	78.0
62	105.0	112.7	13.0	718.7	14.4	14.5	79.3
63	97.0	96.6	17.9	767.1	32.1	22.3	79.5
64	130.7	119.0	18.8	720.4	20.1	13.9	90.3
65	110.0	109.8	19.1	818.1	11.9	14.2	68.5

Table 22: C: Summary of results obtained from static bending tests, including MC, ρ_{12}, E_{local}, E_{global}, and f_m.

Log	MC %	Density, ρ_{12} kg/m^3	E_{local} GPa	E_{global} GPa	f_m MPa
1st					
mean	12.2	722.9	17.7	17.4	111.7
SD	1.0	69.1	4.3	5.9	21.7
cov (%)	7.8	9.6	24.3	34.1	19.5
max	15.4	868.5	27.3	33.4	163.2
min	11.3	579.1	11.6	10.9	80.5
n	17	17	17	17	17
2nd					
mean	15.9	674.5	15.4	14.1	73.4
SD	3.2	108.9	4.5	3.3	13.4
cov (%)	20.3	16.1	29.4	23.6	18.2
max	26.1	962.1	32.1	22.3	112.1
min	11.0	481.4	9.5	6.7	42.3
n	28	28	28	28	28
All					
mean	14.5	692.8	16.2	15.4	87.9
SD	3.2	97.9	4.5	4.7	25.2
cov (%)	21.7	14.1	27.9	30.7	28.6
max	26.1	962.1	32.1	33.4	163.2
min	11.0	481.4	9.5	6.7	42.3
n	45	45	45	45	45

Table 23: D: Results for each specimen and summary obtained from compression parallel tests, including moisture content (MC), density adjusted to 12% moisture content (ρ_{12}), compression parallel modulus of elasticity ($E_{c,0}$) and compression parallel strength ($f_{c,0}$). The remaining columns expose visual characteristics of the samples: Apparent diameter, Sweep, and Knottness.

Log	MC %	Density ρ_{12} kg/m^3	$E_{c,0}$ GPa	$f_{c,0}$ MPa	App. diam. mm	Sweep mm/m	Knot/diam. %
1st							
5	12.7	552.9	10.9	43.9	103.0	4.5	12.5
6	12.7	616.8	21.1	45.6	103.0	2.6	–
11	13.2	615.7	17.4	40.4	103.8	14.9	–
16	12.2	601.7	28.0	31.1	106.3	40.1	27.8
19	13.5	491.9	13.1	29.9	103.0	37.9	25.0
20*	12.6	531.7	8.8	34.8	94.5	20.4	–
30	12.4	–	–	49.5	101.9	13.4	–
31	12.0	663.0	18.2	44.9	94.5	7.1	–
2nd							
38	15.3	493.1	–	25.3	107.9	28.0	–
40**	15.6	708.2	25.4	59.4	97.7	7.1	–
42	16.3	540.1	6.9	16.0	111.1	19.1	–
49***	27.1	667.3	16.7	33.0	97.9	6.3	11.1
50*	15.8	593.9	10.0	33.0	101.5	9.5	–
54**	13.3	501.5	9.4	28.1	98.9	22.0	20.0
58	14.6	562.8	12.4	41.0	98.7	8.2	–
59	18.4	642.8	12.9	33.0	98.7	11.6	–
62**	14.8	608.3	12.3	41.8	119.7	11.4	10.0
65	19.9	665.4	16.2	28.5	112.0	16.1	–
Summary all							
Mean	15.1	591.6	15.0	36.6	103.0	15.6	17.7
SD	3.7	66.3	6.0	10.2	6.5	17.9	7.6
COV (%)	24.4	11.2	39.9	27.8	6.3	115.2	42.9
Max	27.1	708.2	28.0	59.4	119.7	40.1	27.8
Min	12.0	491.9	6.9	16.0	94.5	2.6	10.0

* 2 specimens / 1 tree; ** 3 specimens / 1 tree; *** 4 specimens / 1 tree.

Table 24: E: Visual characteristics of each specimen and corresponding grading according to the Ranta-Maunus system (A: superior grade, B: intermediate grade, R: reject), evaluated for each individual parameter and globally. The assessed parameters include Ovality, Tapered, Sweep, Knots (all and central), and the Knot sum (KS). Note: For completeness, the KS factor was included, although the logs were unaffected, as indicated by the Ranta–Maunus classification.

Log	Ovality		Tapered		Sweep		Knots, all		Knots, cen		KS		R–M
	%	R–M	mm/m	R–M	mm/m	R–M	% d_{all}	R–M	% d_{cen}	R–M	% d_{nom}	R–M	
1st													
1	7.3	A	7.8	B	19.7	R	23.1	A	23.1	A	15.8	A	B
2	3.2	A	6.6	B	12.2	R	36.8	R	36.8	R	16.1	A	B
3	0.0	A	5.0	B	10.1	B	14.2	A	14.2	A	14.5	A	B
4	13.3	B	7.0	B	16.5	R	10.1	A	0.0	A	0.0	A	B
6	7.9	A	4.6	A	15.5	R	0.0	A	0.0	A	0.0	A	A
15	5.2	A	5.5	B	22.0	R	20.0	A	10.9	A	15.0	A	B
19	4.3	A	6.4	B	25.6	R	25.0	B	0.0	A	28.4	A	B
20	3.9	A	3.8	A	13.3	R	28.6	B	19.2	A	21.0	A	B
21	5.6	A	9.9	B	12.4	R	0.0	A	0.0	A	0.0	A	B
22	9.4	A	7.1	B	35.5	R	13.6	A	9.3	A	0.0	A	B
24	9.3	A	9.2	B	15.3	R	28.3	B	28.3	B	0.0	A	B
25	13.8	B	5.6	B	18.3	R	5.5	A	0.0	A	0.0	A	B
29	16.2	B	10.0	B	25.6	R	14.0	A	14.0	A	0.0	A	B
30	16.8	B	8.2	B	21.5	R	9.4	A	9.4	A	13.8	A	B
31	1.0	A	2.3	A	13.9	R	12.0	A	9.9	A	8.1	A	A
32	4.0	A	4.1	A	9.6	B	10.2	A	10.2	A	10.4	A	A
33	2.6	A	4.3	A	4.9	B	9.0	A	9.0	A	6.8	A	A
2nd													
35	10.1	B	7.1	B	22.0	R	9.4	A	9.4	A	9.6	A	B
36	18.5	B	10.0	B	15.6	R	6.0	A	0.0	A	0.0	A	B
38	20.0	B	6.9	B	7.5	B	10.2	A	10.2	A	16.3	A	B
39	10.1	B	7.7	B	20.7	R	9.9	A	9.9	A	7.8	A	B
41	3.2	A	3.1	A	11.7	R	5.0	A	0.0	A	0.0	A	A
42	8.7	A	7.5	B	12.4	R	18.9	A	10.3	A	7.7	A	B
43	6.7	A	7.7	B	14.2	R	9.4	A	9.4	A	0.0	A	B
44	5.8	A	6.5	B	23.0	R	10.1	A	10.1	A	7.5	A	B
45	4.3	A	5.6	B	13.0	R	9.9	A	9.9	A	5.6	A	B
46	5.1	A	3.9	A	16.6	R	9.2	A	9.2	A	0.0	A	A
48	15.2	B	7.4	B	32.1	R	9.7	A	9.7	A	6.2	A	B
49	17.0	B	5.2	B	20.0	R	17.0	A	17.0	A	0.0	A	B
50	1.0	A	4.4	A	7.5	B	11.1	A	11.1	A	4.8	A	A
51	19.3	B	5.6	B	10.4	R	7.9	A	0.0	A	8.7	A	B
52	0.9	A	5.6	B	8.4	B	9.2	A	9.2	A	9.0	A	B
53	11.3	B	5.8	B	24.9	R	6.9	A	0.0	A	8.2	A	B
54	6.7	A	8.1	B	24.9	R	19.2	A	11.9	A	9.6	A	B
55	12.1	B	8.3	B	14.6	R	5.4	A	0.0	A	0.0	A	B
56	9.2	A	5.8	B	5.8	B	4.7	A	0.0	A	4.5	A	B

continued on next page

Log	Ovality		Tapered		Sweep		Knots, all		Knots, cen		KS		R–M
	%	R–M	mm/m	R–M	mm/m	R–M	% d_{all}	R–M	% d_{cen}	R–M	% d_{nom}	R–M	
57	6.2	A	10.2	B	13.0	R	8.7	A	8.7	A	0.0	A	B
58	3.0	A	10.4	B	27.0	R	19.1	A	10.1	A	13.1	A	B
59	17.9	B	8.6	B	18.9	R	9.5	A	9.5	A	10.4	A	B
60	15.2	B	6.7	B	15.5	R	0.0	A	0.0	A	0.0	A	B
61	0.8	A	10.3	B	19.9	R	17.7	A	17.2	A	9.8	A	B
62	11.1	B	7.3	B	6.2	B	12.7	A	8.9	A	0.0	A	B
63	14.9	B	4.4	A	23.1	R	19.6	A	9.7	A	6.2	A	B
64	0.8	A	5.6	B	9.6	B	13.4	A	13.4	A	11.5	A	B
65	13.5	B	8.4	B	15.9	R	9.0	A	9.0	A	10.0	A	B

Table 25: F: Summary of visual characteristics, including Ovality, Tapered, Sweep, Knots (all and central), and Knotness sum (KS). The last columns present the mean values of nominal diameter (d_{nom}), apparent diameter (d_{app}), and length for each group.

Log	Ovality %	Tapered mm/m	Sweep mm/m	Knots, all $\%d_{all}$	Knots, cen $\%d_{cen}$	KS $\%d_{nom}$	d_{nom} mm	d_{app} mm	Length m
1st									
mean	7.3	6.3	17.2	15.3	11.4	8.8	110.9	103.7	2.0
SD	5.2	2.2	7.4	10.3	10.6	8.9	9.9	9.3	0.1
cov (%)	71.1	35.0	42.8	67.3	93.1	101.5	8.9	8.9	5.2
max	16.8	10.0	35.5	36.8	36.8	28.4	131.7	122.9	2.3
min	0.0	2.3	4.9	0.0	0.0	0.0	90.0	89.6	1.9
n	17	17	17	17	17	17	17	17	17
2nd									
mean	9.6	6.9	16.2	10.7	8.0	5.9	112.0	108.0	2.4
SD	6.1	1.9	6.8	5.0	5.1	4.8	11.1	8.0	0.0
cov (%)	63.6	28.1	42.2	46.5	64.2	80.6	9.9	7.4	0.5
max	20.0	10.4	32.1	19.6	17.2	16.3	142.5	123.6	2.4
min	0.8	3.1	5.8	0.0	0.0	0.0	94.0	89.6	2.4
n	28	28	28	28	28	28	28	28	28
All									
mean	8.7	6.7	16.6	12.4	9.3	7.0	111.6	106.4	
SD	5.8	2.0	7.0	7.7	7.8	6.7	10.5	8.7	
cov (%)	66.7	30.6	42.0	61.7	83.5	95.6	9.4	8.2	
max	20.0	10.4	35.5	36.8	36.8	28.4	142.5	123.6	
min	0.0	2.3	4.9	0.0	0.0	0.0	90.0	89.6	
n	45	45	45	45	45	45	45	45	45

Table 26: G: Results for each specimen obtained from Non-destructive test longitudinal stress wave (lsw) for MC > 12 %. Parameters include the MC obtained with the electrical resistance meter, Velocity (Vel), Density for full-body (ρ_{fb}), and the corresponding dynamic modulus of Elasticity ($E_{dyn,lsw}$) and its respective values, adjusted to 12 % of MC.

Log	MC %	Vel m/s	$Vel_{adj,12}$ m/s	Density kg/m^3	$Density_{adj}$ kg/m^3	E_{lsw} GPa	$E_{lsw,adj,12}$ GPa
1st							
1	16.7	4193.6	4318.5	932.8	910.7	16.4	17.0
2	16.6	4780.8	4918.4	812.1	793.5	18.6	19.2
3	23.1	4757.6	5103.5	873.7	873.7	19.8	22.8
4	14.7	4868.4	4950.9	855.9	844.2	20.3	20.7
6	15.5	4946.3	5055.1	770.9	757.3	18.9	19.4
15	14.0	4768.3	4826.1	761.2	753.7	17.3	17.6
19	15.0	4689.0	4777.6	662.9	652.8	14.6	14.9
20	14.7	4528.5	4603.4	680.4	671.3	14.0	14.2
21	16.1	5022.2	5150.3	776.8	760.9	19.6	20.2
22	14.9	4317.6	4395.7	731.0	720.4	13.6	13.9
24	19.7	4880.9	5121.2	825.5	825.5	19.7	21.6
25	15.8	4768.1	4881.0	777.8	763.0	17.7	18.2
29	16.5	4670.3	4801.4	974.1	952.3	21.2	22.0
30	14.9	5156.1	5248.6	815.4	803.6	21.7	22.1
31	15.0	5077.0	5170.9	847.7	835.1	21.9	22.3
32	16.4	5827.1	5986.5	777.9	760.9	26.4	27.3
33	15.0	5710.1	5816.5	780.5	768.8	25.4	26.0
2nd							
35	43.7	4084.5	4666.1	1240.7	1240.7	20.7	27.0
36	43.4	4170.6	4762.2	1039.8	1039.8	18.1	23.6
38	52.0	3618.9	4202.4	1020.9	1020.9	13.4	18.0
39	39.2	4471.7	5064.2	1236.6	1236.6	24.7	31.7
41	46.6	4268.4	4904.6	995.9	995.9	18.1	24.0
42	55.2	2987.0	3490.5	1296.1	1296.1	11.6	15.8
43	32.7	3797.5	4248.0	1049.9	1049.9	15.1	18.9
44	39.4	3735.9	4232.8	1029.8	1029.8	14.4	18.5
45	43.7	3824.5	4368.8	1066.7	1066.7	15.6	20.4
46	39.0	4001.0	4530.0	1176.0	1176.0	18.8	24.1
48	41.5	4386.5	4990.2	1066.9	1066.9	20.5	26.6
49	41.6	3574.2	4066.6	1386.7	1386.7	17.7	22.9
50	37.1	3457.0	3899.5	1106.5	1106.5	13.2	16.8
51	42.6	3750.0	4274.8	880.6	880.6	12.4	16.1
52	46.9	3625.2	4167.5	1050.9	1050.9	13.8	18.3
53	40.9	3878.5	4407.0	907.0	907.0	13.6	17.6
54	43.1	3115.8	3555.7	1093.4	1093.4	10.6	13.8
55	40.1	4043.0	4586.8	904.0	904.0	14.8	19.0
56	37.4	4043.0	4563.2	916.8	916.8	15.0	19.1

continued on the next page

Log	MC %	Vel m/s	$Vel_{adj,12}$ m/s	Density kg/m^3	$Density_{adj}$ kg/m^3	E_{lsw} GPa	$E_{lsw,adj,12}$ GPa
57	34.7	4043.0	4539.6	1037.9	1037.9	17.0	21.4
58	37.0	3883.3	4379.6	990.4	990.4	14.9	19.0
59	38.7	3556.3	4024.0	1304.5	1304.5	16.5	21.1
60	45.2	3867.2	4431.3	1227.6	1227.6	18.4	24.1
61	38.3	4191.4	4738.3	999.6	999.6	17.6	22.4
62	38.0	3932.3	4443.4	1064.6	1064.6	16.5	21.0
63	38.4	4074.2	4607.0	1166.0	1166.0	19.4	24.7
64	45.0	3920.9	4490.5	1109.7	1109.7	17.1	22.4
65	39.6	3734.4	4232.8	1229.0	1229.0	17.1	22.0

Table 27: H: Summary of results obtained from Non-destructive test longitudinal stress wave (lsw) tests for MC > 12 %. Including MC, Velocity, Density and dynamic modulus of elastic and its respective values, adjusted to 12 % of MC.

Log	MC %	Vel m/s	$Vel_{adj,12}$ m/s	Density kg/m^3	$Density_{adj}$ kg/m^3	E_{lsw} GPa	$E_{lsw,adj,12}$ GPa
1st							
mean	16.1	4880.1	5007.4	803.3	791.0	19.2	20.0
SD	2.2	415.9	426.5	79.7	78.0	3.6	3.8
cov (%)	13.7	8.5	8.5	9.9	9.9	18.6	19.0
max	23.1	5827.1	5986.5	974.1	952.3	26.4	27.3
min	14.0	4193.6	4318.5	662.9	652.8	13.6	13.9
n	17	17	17	17	17	17	17
2nd							
mean	41.5	3858.4	4388.1	1092.7	1092.7	16.3	21.1
SD	4.9	336.9	372.2	130.5	130.5	3.1	3.9
cov (%)	11.7	8.7	8.5	11.9	11.9	18.8	18.5
max	55.2	4471.7	5064.2	1386.7	1386.7	24.7	31.7
min	32.7	2987.0	3490.5	880.6	880.6	10.6	13.8
n	28	28	28	28	28	28	28
All							
mean	31.9	4244.4	4622.1	983.4	978.7	17.4	20.7
SD	13.1	619.3	493.3	181.4	185.8	3.5	3.9
cov (%)	40.9	14.6	10.7	18.4	19.0	20.3	18.6
max	55.2	5827.1	5986.5	1386.7	1386.7	26.4	31.7
min	14.0	2987.0	3490.5	662.9	652.8	10.6	13.8
n	45	45	45	45	45	45	45

Table 28: I: Results for each specimen obtained from Non-destructive test longitudinal stress wave (lsw) for MC = 12 %. Parameters include the MC obtained with the electrical resistance meter, Velocity (Vel), Density for full-body (ρ_{fb}), and the corresponding dynamic modulus of Elasticity ($E_{dyn,lsw}$) and its respective values, adjusted to 12 % of MC.

Log	MC %	Vel m/s	$Vel_{adj,12}$ m/s	Density kg/m^3	$Density_{adj}$ kg/m^3	E_{lsw} GPa	$E_{lsw,adj,12}$ GPa
1st							
1	11.1	4476.3	4450.6	768.8	772.4	15.4	15.3
2	9.7	4925.7	4858.4	692.8	692.8	16.8	16.4
3	11.0	5194.6	5163.4	761.8	765.6	20.6	20.4
4	10.2	5057.4	5003.0	767.9	774.8	19.6	19.4
6	10.8	5090.4	5053.7	685.6	689.7	17.8	17.6
15	9.2	4915.8	4834.6	637.8	637.8	15.4	14.9
19	10.4	4878.4	4831.7	583.8	588.4	13.9	13.7
20	10.8	4671.5	4636.6	596.2	599.9	13.0	12.9
21	10.3	5256.8	5204.4	674.8	680.4	18.6	18.4
22	10.8	5133.2	5095.5	637.8	641.7	16.8	16.7
24	10.4	5120.1	5071.1	705.7	711.2	18.5	18.3
25	10.6	5197.2	5153.6	676.9	681.6	18.3	18.1
29	11.0	4860.9	4831.1	802.4	806.5	19.0	18.8
30	10.7	5299.3	5256.3	727.5	732.4	20.4	20.2
31	11.2	5266.8	5241.5	744.4	747.4	20.6	20.5
32	9.7	6051.3	5968.7	727.3	727.3	26.6	25.9
33	9.5	5927.7	5839.8	685.5	685.5	24.1	23.4
2nd							
35	13.3	4668.0	4706.6	759.4	754.3	16.5	16.7
36	12.4	4934.2	4947.5	630.4	629.0	15.3	15.4
38	13.4	4508.8	4547.3	527.9	524.3	10.7	10.8
39	12.8	5354.2	5381.1	699.4	696.5	20.0	20.2
41	11.4	5320.9	5301.0	539.6	541.2	15.3	15.2
42	14.5	4041.3	4104.2	612.8	605.1	10.0	10.2
43	13.7	4790.7	4840.2	566.1	561.4	13.0	13.2
44	11.8	4611.5	4606.0	552.8	553.3	11.8	11.7
45	14.1	4883.5	4947.4	605.7	599.3	14.4	14.7
46	16.9	4765.9	4913.2	699.7	682.5	15.9	16.5
48	15.6	5275.7	5393.8	609.2	598.2	17.0	17.4
49	18.5	4277.3	4454.6	810.9	810.9	14.8	16.1
50	10.6	4335.9	4298.4	617.3	621.7	11.6	11.5
51	11.3	4863.3	4842.5	450.5	452.1	10.7	10.6
52	13.0	4502.3	4530.4	592.5	589.5	12.0	12.1
53	11.2	5053.8	5028.1	455.0	456.9	11.6	11.6
54	12.7	4115.2	4133.6	461.2	459.6	7.8	7.9
55	11.3	4921.9	4900.8	519.0	520.8	12.6	12.5
56	9.9	4863.3	4801.3	557.9	557.9	13.2	12.9

continued on the next page

Log	MC %	Vel m/s	$Vel_{adj,12}$ m/s	Density kg/m^3	$Density_{adj}$ kg/m^3	E_{lsw} GPa	$E_{lsw,adj,12}$ GPa
57	12.0	4921.9	4921.9	614.1	614.1	14.9	14.9
58	12.1	4765.9	4767.8	582.3	582.1	13.2	13.2
59	15.2	4256.0	4340.0	727.4	715.9	13.2	13.5
60	13.5	5039.1	5087.0	679.0	673.8	17.2	17.4
61	13.4	4899.8	4941.6	638.0	633.6	15.3	15.5
62	10.8	4636.6	4602.0	654.2	658.2	14.1	13.9
63	16.0	5005.5	5131.1	663.1	649.8	16.6	17.1
64	13.6	4681.6	4728.1	655.9	650.6	14.4	14.5
65	13.7	4376.2	4422.6	765.1	758.5	14.7	14.8

Table 29: J: Summary of results obtained from Non-destructive test longitudinal stress wave (lsw) tests for MC = 12 %. Including MC, Velocity, Density and dynamic modulus of elastic and its respective values, adjusted to 12 % of MC.

	MC %	Vel m/s	$Vel_{adj,12}$ m/s	Density kg/m^3	$Density_{adj}$ kg/m^3	E_{lsw} GPa	$E_{lsw,adj,12}$ GPa
1st							
mean	10.4	5136.7	5087.9	698.7	702.1	18.6	18.3
SD	0.6	389.2	377.8	61.6	61.9	3.4	3.3
cov (%)	5.5	7.6	7.4	8.8	8.8	18.5	18.1
max	11.2	6051.3	5968.7	802.4	806.5	26.6	25.9
min	9.2	4476.3	4450.6	583.8	588.4	13.0	12.9
n	17	17	17	17	17	17	17
2nd							
mean	13.2	4738.2	4772.2	615.9	612.5	13.9	14.0
SD	2.0	344.9	341.5	92.1	90.0	2.6	2.7
cov (%)	15.1	7.3	7.2	15.0	14.7	18.7	19.3
max	18.5	5354.2	5393.8	810.9	810.9	20.0	20.2
min	9.9	4041.3	4104.2	450.5	452.1	7.8	7.9
n	28	28	28	28	28	28	28
All							
mean	12.1	4888.7	4891.4	647.2	646.4	15.6	15.6
SD	2.1	407.8	384.0	90.7	91.0	3.7	3.6
cov (%)	17.2	8.3	7.9	14.0	14.1	23.7	23.0
max	18.5	6051.3	5968.7	810.9	810.9	26.6	25.9
min	9.2	4041.3	4104.2	450.5	452.1	7.8	7.9
n	45	45	45	45	45	45	45

Table 30: K: Results for each specimen obtained from Non-destructive test transversal vibration (tv) for MC > 12 %. Parameters include the MC ⊣ obtained with the electrical resistance meter, first vibration mode (f_1), mass, length, moment of inertia and modulus of Elasticity ($E_{dyn,lsw}$) with it respective value, adjusted to 12 % of MC.

Log	MC %	f * Hz	mass N	length mm	inertia $10^3 \times mm^4$	E_{tv} GPa	$E_{tv,adj,12}$ GPa
1st							
1	19.3	108.7	230.3	1930.0	9742.7	16.1	17.2
2	20.1	83.0	117.4	1978.0	3121.3	16.1	17.3
3	23.7	94.0	162.6	1988.5	5086.3	17.9	20.5
4	25.6	94.1	125.1	1936.0	3590.3	18.0	20.7
6	27.7	82.0	101.5	1967.0	2796.9	14.9	17.2
15	27.5	83.9	111.3	2013.5	3414.6	15.1	17.3
19	13.2	105.4	111.4	1940.0	6198.2	11.7	11.8
20	24.9	83.1	110.9	1952.5	4181.3	11.0	12.6
21	24.7	108.7	151.7	1922.5	6198.8	16.5	19.0
22	19.0	106.8	136.7	1965.0	5968.0	15.9	16.9
24	38.5	94.8	155.0	1960.0	5639.5	15.0	17.2
25	30.5	111.1	190.8	1953.0	8785.0	16.1	18.5
30 **	-	-	-	-	-	-	-
30	17.4	113.6	167.3	1955.5	6495.6	20.0	20.9
31	19.2	99.0	134.3	1943.5	4054.7	19.2	20.4
32	18.6	95.6	141.4	2295.0	3649.9	34.4	36.4
33	19.0	109.0	181.9	2227.5	6555.4	29.3	31.1
2nd							
35 **	-	-	-	-	-	-	-
36	18.1	66.7	189.3	2406.0	5213.9	18.1	19.1
38	21.1	57.9	161.8	2430.0	4401.3	14.2	16.2
39	31.2	65.4	220.6	2410.0	5053.8	21.0	24.5
41	35.8	52.2	112.3	2395.0	2211.6	15.3	14.6
42	29.1	49.4	196.6	2399.0	3911.8	13.6	15.7
43	17.5	67.3	159.4	2393.0	3773.5	21.1	22.1
44 **	-	-	-	-	-	-	-
45	30.2	65.5	203.0	2410.0	5644.2	17.4	19.8
46	31.8	67.9	236.3	2410.0	6366.9	19.3	22.4
48	39.6	66.9	213.8	2428.0	6410.1	17.2	19.8
49 **	-	-	-	-	-	-	-
50	29.6	52.6	147.1	2400.0	2943.1	15.4	17.4
51	34.9	66.8	182.4	2400.0	7487.2	12.1	14.0
52	33.8	61.2	192.7	2395.0	5460.9	14.6	17.1
53	43.2	58.2	148.6	2407.0	4684.9	12.0	15.5
54	21.1	48.7	144.2	2408.0	3012.8	12.8	15.0
55	31.4	68.8	180.9	2400.0	6694.7	14.2	16.3
56	27.7	63.1	158.4	2400.0	4806.8	14.6	16.5

continued on the next page

Log	MC %	f * Hz	mass N	length mm	inertia $10^3 \times mm^4$	E $_{tv}$ GPa	E $_{tv,adj,12}$ GPa
57	15.7	69.2	189.3	2400.0	5469.1	18.4	19.0
58	32.2	58.3	148.1	2410.0	3643.0	15.5	17.6
59	37.9	48.6	206.3	2388.0	3720.5	14.4	17.5
60	40.4	65.9	239.3	2400.0	6197.1	18.6	22.0
61	36.1	78.9	237.3	2418.0	8479.9	19.8	23.1
62	31.4	64.0	204.0	2404.0	5694.3	16.4	19.1
63	34.0	55.8	160.8	2384.0	3029.2	18.0	20.6
64	34.9	72.1	232.4	2397.0	7028.9	19.0	21.6
65	22.7	62.4	220.6	2390.0	5007.0	18.9	21.4

* first mode of vibration; ** not data.

Table 31: L: Summary of results obtained from Non-destructive test transversal vibration (tv) for MC > 12 %. Including MC, first vibration mode (f_1), mass, length, moment of inertia and modulus of Elasticity ($E_{dyn,lsw}$) with it respective value, adjusted to 12 % of MC.

Log	MC	f *	mass	length	inertia	E_{tv}	$E_{tv,adj,12}$
	%	Hz	N	mm	$10^3 \times mm^4$	GPa	GPa
1st							
mean	23.1	98.3	145.6	1995.5	5342.4	18.0	19.7
SD	6.2	11.1	35.0	106.9	2001.6	6.0	6.1
cov (%)	26.7	11.3	24.0	5.4	37.5	33.3	31.2
max	38.5	113.6	230.3	2295.0	9742.7	34.4	36.4
min	13.2	82.0	101.5	1922.5	2796.9	11.0	11.9
n	16	16	16	16	16	16	16
2nd							
mean	30.5	62.2	187.4	2403.3	5053.9	16.5	18.7
SD	7.4	7.8	34.6	11.0	1559.7	2.7	2.9
cov (%)	24.3	12.5	18.5	0.5	30.9	16.3	15.7
max	43.2	78.9	239.3	2430.0	8479.9	21.1	24.5
min	15.7	48.6	112.3	2384.0	2211.6	12.0	14.0
n	25	25	25	25	25	25	25
All							
mean	27.6	76.3	171.1	2244.1	5166.5	17.1	19.1
SD	7.8	20.0	40.1	212.0	1726.9	4.3	4.4
cov (%)	28.2	26.3	23.4	9.4	33.4	25.1	23.1
max	43.2	113.6	239.3	2430.0	9742.7	34.4	36.4
min	13.2	48.6	101.5	1922.5	2211.6	11.0	11.9
n	41	41	41	41	41	41	41

* first mode of vibration.

Table 32: M: Results for each specimen obtained from Non-destructive test transversal vibration (tv) for MC = 12 %. Parameters include the MC obtained with the electrical resistance meter, first vibration mode (f), mass, length, moment of inertia and modulus of Elasticity ($E_{dyn,lsw}$) with it respective value, adjusted to 12 % of MC.

Log	MC %	f * Hz	mass N	length mm	inertia $10^3 \times mm^4$	E_{tv} GPa	$E_{tv,adj,12}$ GPa
1st							
1	11.4	125.5	162.0	1930.0	11210.4	13.2	13.1
2	9.7	101.1	83.4	1978.0	3633.5	14.6	14.3
3	10.6	112.2	111.6	1988.5	5323.8	16.7	16.5
4	10.4	107.4	94.1	1936.0	3878.9	16.3	16.1
6	10.5	104.3	76.6	1967.0	3168.8	16.1	15.9
15	9.5	98.8	88.6	2013.5	4281.3	13.3	13.0
19	10.2	126.8	95.0	1940.0	7155.7	12.5	12.3
20	10.1	99.6	79.3	1952.5	4873.9	9.7	9.5
21	10.1	126.0	110.7	1922.5	6991.3	14.4	14.1
22	9.6	120.9	111.4	1965.0	7089.6	14.0	13.8
24	10.2	124.2	112.9	1960.0	6181.6	17.1	16.8
25	9.3	144.9	133.2	1953.0	9691.9	17.3	16.9
29	9.8	101.1	108.8	1952.0	4812.0	13.8	13.6
30	9.9	132.8	120.5	1955.5	7106.1	18.0	17.7
31	9.9	119.8	98.2	1943.5	4558.6	18.2	17.9
32	9.7	112.2	99.2	2295.0	3910.4	31.0	30.5
33	9.6	125.9	129.7	2227.5	7056.7	25.9	25.4
2nd							
35	12.3	78.6	167.3	2390.0	7122.6	15.9	16.0
36	12.4	76.2	139.4	2406.0	7172.3	12.7	12.7
38	13.0	69.8	109.4	2430.0	6152.0	10.0	10.1
39	10.8	78.9	152.8	2410.0	6975.0	15.4	15.2
41	10.4	67.6	79.6	2395.0	3159.9	12.7	12.6
42	11.2	62.4	115.0	2399.0	5153.2	9.6	9.6
43	12.4	72.5	108.9	2393.0	5390.6	11.7	11.7
44	9.8	75.9	108.3	2391.0	5663.8	12.1	11.9
45	16.8	75.4	137.0	2410.0	7424.8	11.8	12.3
46	14.8	82.9	173.1	2410.0	8866.0	15.1	15.5
48	10.7	82.0	144.2	2428.0	8130.6	13.7	13.6
49	13.9	59.7	152.6	2400.0	5166.2	11.7	11.9
50	9.8	60.9	103.6	2400.0	4081.8	10.5	10.3
51	11.2	85.9	121.2	2400.0	10551.9	9.4	9.4
52	12.9	76.4	135.8	2395.0	7614.1	11.5	11.6
53	11.7	74.0	89.8	2407.0	5663.8	9.7	9.7
54	10.2	61.9	91.3	2408.0	5663.8	6.9	6.8
55	11.5	83.4	135.2	2400.0	9754.5	10.7	10.7
56	8.8	75.2	117.3	2400.0	6392.3	11.5	11.2
57	9.2	81.3	141.6	2400.0	7701.3	13.5	13.2
58	10.5	71.0	109.2	2410.0	5050.3	12.3	12.1
59	15.5	65.1	139.6	2388.0	5430.9	11.9	12.3
60	12.7	92.5	159.4	2400.0	8039.7	18.9	19.0
61	10.4	92.8	181.0	2418.0	11444.4	15.5	15.3
62	9.8	83.7	153.5	2404.0	7931.7	15.2	14.9

continued on the next page

Log	MC %	f * Hz	mass N	length mm	inertia $10^3 \times mm^4$	E $_{tv}$ GPa	E $_{tv,adj,12}$ GPa
63	14.4	78.7	112.6	2384.0	4270.0	17.8	18.1
64	12.6	85.4	171.1	2397.0	9859.5	14.0	14.1
65	13.7	71.7	169.0	2390.0	7122.6	13.4	13.6

* first mode of vibration.

Table 33: N: Summary of results obtained from Non-destructive test transversal vibration (tv) for MC = 12 %. Including MC, first vibration mode (f), mass, length, moment of inertia and modulus of Elasticity ($E_{dyn,lsw}$) with it respective value, adjusted to 12 % of MC.

Log	MC %	f * Hz	mass N	length mm	inertia $10^3 \times mm^4$	E $_{tv}$ GPa	E $_{tv,adj,12}$ GPa
1st							
mean	10.0	116.7	106.8	1992.9	5936.7	16.6	16.3
SD	0.5	13.4	21.7	104.0	2197.1	5.1	5.0
cov (%)	5.0	11.5	20.3	5.2	37.0	30.6	30.4
max	11.4	144.9	162.0	2295.0	11210.4	31.0	30.5
min	9.3	98.8	76.6	1922.5	3168.8	9.7	9.5
n	17	17	17	17	17	17	17
2nd							
mean	11.9	75.8	132.8	2402.3	6891.1	12.7	12.7
SD	2.0	8.9	27.8	10.9	2003.8	2.7	2.7
cov (%)	16.7	11.8	20.9	0.5	29.1	20.9	21.3
max	16.8	92.8	181.0	2430.0	11444.4	18.9	19.0
min	8.8	59.7	79.6	2384.0	3159.9	6.9	6.8
n	28	28	28	28	28	28	28
All							
mean	11.2	91.2	123.0	2247.6	6530.5	14.2	14.1
SD	1.8	22.7	28.4	210.5	2106.7	4.2	4.1
cov (%)	16.4	24.9	23.1	9.4	32.3	29.4	29.0
max	16.8	144.9	181.0	2430.0	11444.4	31.0	30.5
min	8.8	59.7	76.6	1922.5	3159.9	6.9	6.8
n	45	45	45	45	45	45	45

* first mode of vibration.

Table 34: O: Results for each specimen obtained from Resistograph tests performed on sections A, B, and C, including the corresponding mean value (R_m).

Log	A (%)	B (%)	C (%)	R_m (%)
1st				
1	15.6	14.0	12.8	14.1
2	14.7	12.8	13.4	13.6
3	14.4	15.4	15.4	15.1
4	16.9	18.0	15.0	16.6
6	14.0	12.3	12.8	13.0
15	11.8	12.6	12.0	12.1
19	9.5	9.0	9.5	9.4
20	11.5	10.4	10.9	10.9
21	12.9	10.4	9.8	11.0
22	12.6	11.7	12.5	12.3
24	12.7	13.7	14.4	13.6
25	13.7	11.6	13.1	12.8
29	17.7	15.5	16.7	16.6
30	13.7	13.7	14.2	13.9
31	14.3	14.1	13.3	13.9
32	15.8	14.8	15.0	15.2
33	17.7	14.4	15.6	15.9
2nd				
35	26.5	20.4	21.5	22.8
36	15.9	15.9	15.5	15.8
38	13.8	11.7	16.1	13.9
39	21.3	19.2	18.8	19.8
41	15.6	13.0	14.3	14.3
42	15.0	17.7	16.8	16.5
43	14.8	13.0	12.1	13.3
44	16.4	14.3	12.5	14.4
45	17.8	17.2	16.5	17.2
46	18.8	17.8	22.7	19.8
48	20.9	17.4	17.7	18.7
49	16.7	18.2	18.5	17.8
50	15.5	14.0	14.8	14.8
51	12.2	10.0	10.2	10.8
52	18.9	15.6	15.6	16.7
53	11.9	10.1	11.6	11.2
54	14.9	12.0	12.7	13.2
55	16.4	14.6	15.2	15.4
56	16.1	15.6	16.2	15.9
57	18.5	14.2	14.2	15.6
58	16.8	15.7	16.1	16.2
59	19.5	16.9	19.0	18.5
60	22.6	19.7	17.3	19.9
61	16.9	16.1	14.9	16.0
62	18.8	16.5	16.9	17.4
63	17.6	15.7	16.9	16.7

continued on the next page

Log	A (%)	B (%)	C (%)	R_m (%)
64	18.9	18.7	19.2	18.9
65	18.6	17.3	18.5	18.2

Table 35: P: Summary of Resistograph Results tests and its mean values (R_m).

Log	A (%)	B (%)	C (%)	R_m (%)
1st				
mean	14.1	13.2	13.3	13.5
ds	2.2	2.2	2.0	2.0
cov (%)	15.7	16.8	15.1	15.0
max	17.7	18.0	16.7	16.6
min	9.5	9.0	9.5	9.4
n	17	17	17	17
2nd				
mean	17.4	15.7	16.2	16.4
ds	3.1	2.7	2.9	2.7
cov (%)	17.7	17.3	17.8	16.4
max	26.5	20.4	22.7	22.8
min	11.9	10.0	10.2	10.8
n	28	28	28	28
All				
mean	16.2	14.7	15.1	15.3
ds	3.2	2.8	2.9	2.8
cov (%)	19.8	18.9	19.3	18.4
max	26.5	20.4	22.7	22.8
min	9.5	9.0	9.5	9.4
n	45	45	45	45

Table 36: Q: Descriptive statistics of end-face crack measurements across each concentric ring (from pith: r_1, r_2, r_3, r_4, and r_p, corresponding to the log perimeter) after the air-drying campaign. Parameters include the relative crack ratio (c_r), defined as the percentage of the total crack length over each ring, and the number of cracks (n_r). Reported statistics comprise the mean, standard error (S.Error), standard deviation (SD), maximum (Max), minimum (Min), and count (Count).

	c_r (%)					n_r° (n° dm^{-1})				
	r1	r2	r3	r4	rp	r1	r2	r3	r4	rp
Reference										
Mean	5.36	3.75	3.68	3.79	3.36	6.86	4.18	3.68	2.93	2.37
S.Error	0.47	0.27	0.24	0.20	0.18	0.32	0.26	0.21	0.19	0.14
SD	2.55	1.48	1.34	0.75	0.96	1.83	1.49	1.21	0.73	0.79
Max	10.76	6.82	6.94	4.82	5.73	11.14	7.16	6.90	3.98	3.81
Min	1.03	0.84	1.13	2.63	1.01	4.77	1.59	1.59	1.99	0.77
Count	30	30	30	14	30	32	32	32	14	32
K–2k										
Mean	4.61	3.31	1.99	1.24	0.74	6.57	5.17	4.05	2.29	1.39
S.Error	1.50	0.75	0.64	0.33	0.18	0.87	0.54	0.55	0.59	0.20
SD	3.97	1.98	1.70	0.67	0.49	2.47	1.53	1.55	1.19	0.57
Max	11.55	6.54	5.48	1.84	1.52	9.55	7.16	6.90	3.98	2.44
Min	0.64	1.25	0.45	0.28	0.28	1.59	3.18	2.65	1.19	0.52
Count	7	7	7	4	7	8	8	8	4	8
K–3k										
Mean	4.28	3.54	2.15	1.08	0.70	6.17	5.17	3.65	2.92	1.16
S.Error	1.00	0.60	0.62	0.22	0.38	0.47	0.50	0.80	0.13	0.40
SD	2.82	1.70	1.76	0.38	1.07	1.33	1.41	2.28	0.23	1.14
Max	9.23	6.25	5.13	1.37	3.20	7.96	7.16	6.90	3.18	3.06
Min	0.89	1.45	0.33	0.66	0.00	4.77	3.18	0.53	2.79	0.00
Count	8	8	8	3	8	8	8	8	3	8
H–16 mm										
Mean	3.78	3.31	3.22	3.33	3.03	6.68	5.25	4.24	4.24	2.36
S.Error	0.89	0.63	0.49	0.56	0.42	0.62	0.38	0.36	0.87	0.13
SD	2.68	1.88	1.48	0.97	1.26	1.96	1.20	1.15	1.51	0.41
Max	8.57	6.37	6.10	4.43	5.53	9.55	7.16	5.84	5.97	3.12
Min	0.65	1.08	1.71	2.62	1.75	4.77	3.98	2.65	3.18	1.66
Count	9	9	9	3	9	10	10	10	3	10
H–30 mm										
Mean	–	2.55	2.94	3.11	3.11	–	4.51	4.16	3.28	2.61
S.Error	–	0.52	0.36	0.43	0.25	–	0.34	0.59	0.25	0.38
SD	–	1.28	0.87	0.85	0.61	–	0.82	1.44	0.50	0.93
Max	–	4.47	4.15	4.21	4.02	–	5.57	6.90	3.98	4.21
Min	–	0.92	2.03	2.20	2.38	–	3.18	2.65	2.79	1.79
Count	–	6	6	4	6	–	6	6	4	6

Reference: untreated samples (control); K–3k and K–2k correspond to kerfing treatments with three and two longitudinal kerfs, respectively; H–30mm and H–16mm represent central hollowing with drill diameters of 30mm and 16mm, respectively.

Table 37: R: Comparative performance of relative cracking (c_r) on the peripheral ring, r_p (a), and ring 2, more central, r_2 (b). The boxplots comparing untreated (samples in black/white), R, with their respective other treated faces, K-2k, K-3k, H-16 mm, and H-30 mm (in gray). In the top left corner, the significance level for the t-test is indicated, with * = p < 0.05; ** = p < 0.001; ns = not significant. The cross on each box indicates the mean value.

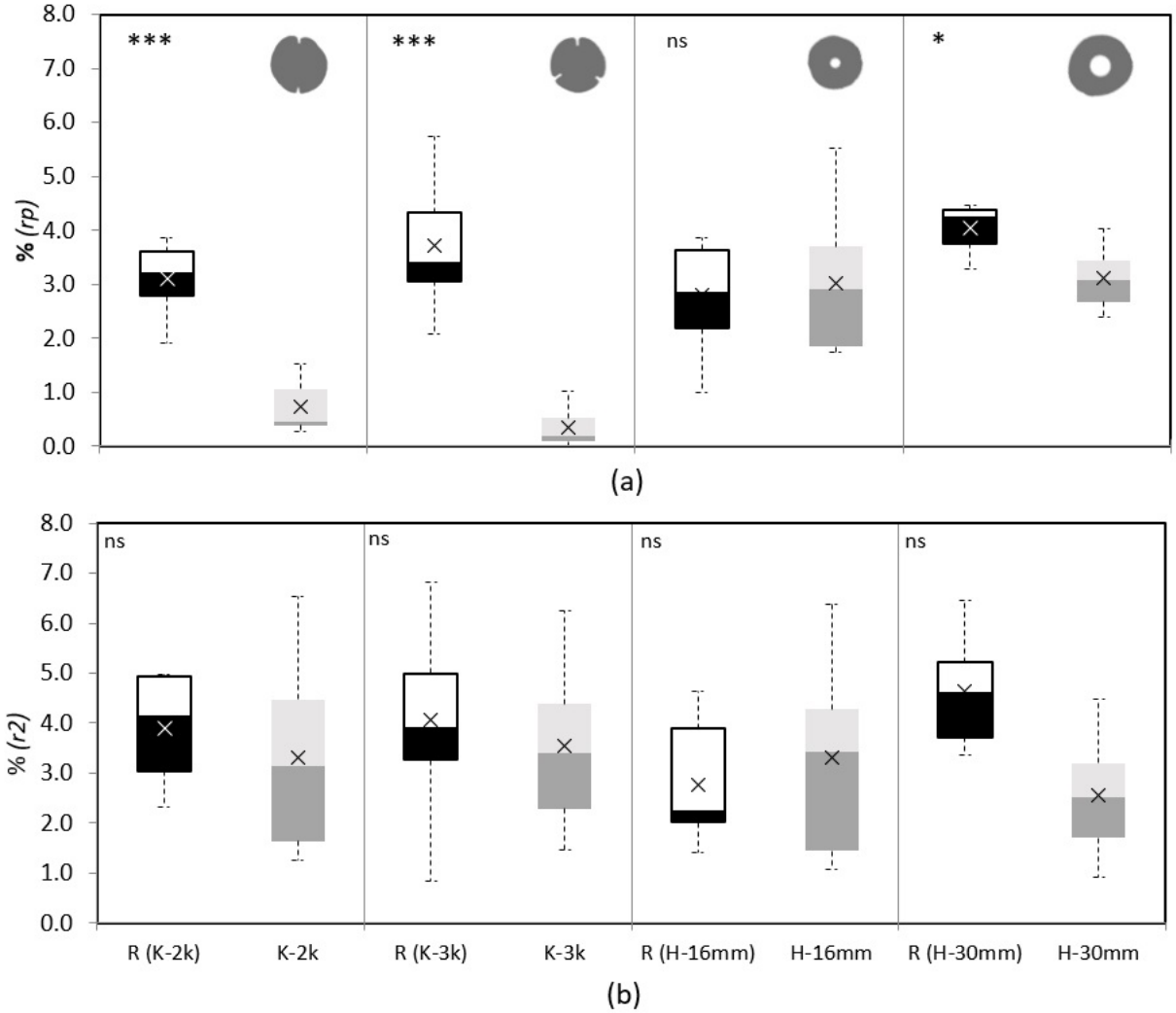

Table 38: S: Comparative performance of the number of cracks ($n°_r$) on the peripheral ring, r_p (a), and ring 2, more central, r_2 (b). The boxplots comparing untreated (samples in black/white), R, with their respective other treated faces, K-2k, K-3k, H-16 mm, and H-30 mm (in gray). In the top left corner, the significance level for the t-test is indicated, with * = p < 0.05; ** = p < 0.001; ns = not significant. The cross on each box indicates the mean value.

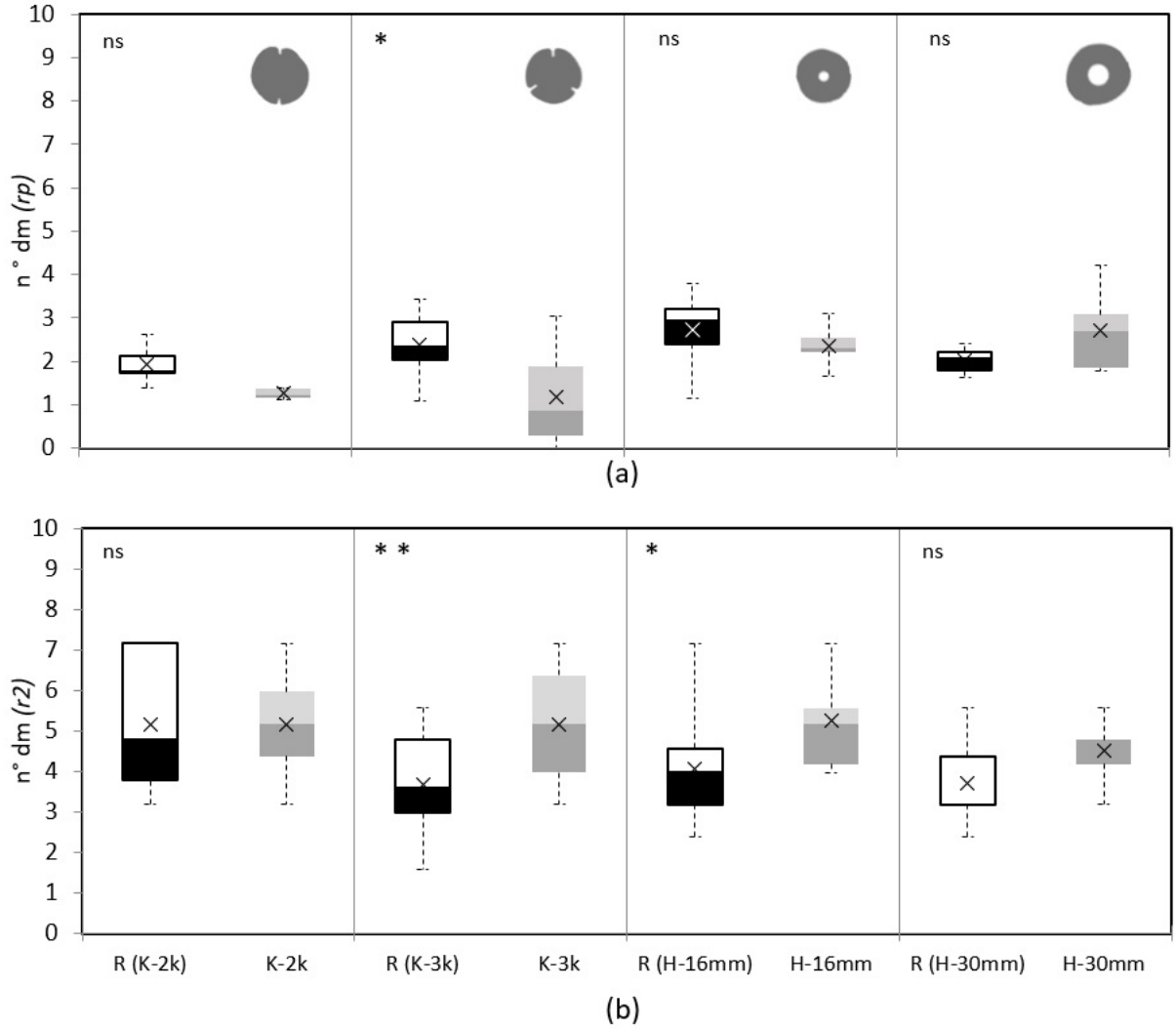

References

[1] Michael H Ramage, Henry Burridge, Marta Busse-Wicher, George Fereday, Thomas Reynolds, Darshil U Shah, Guanglu Wu, Li Yu, Patrick Fleming, Danielle Densley-Tingley, et al. The wood from the trees: The use of timber in construction. *Renewable and sustainable energy reviews*, 68:333–359, 2017.

[2] Yan Yang, Shozo Nakamura, Baochun Chen, and Takafumi Nishikawa. Mechanical behavior of chinese woven timber arch bridges. *Engineering Structures*, 195:340–357, 2019.

[3] Haifei Zhou, Jiawei Leng, Man Zhou, Qing Chun, Mostafa Fahmi Hassanein, and Wenzhou Zhong. China's unique woven timber arch bridges. In *Proceedings of the Institution of Civil Engineers-Civil Engineering*, volume 171-3, pages 115–120. Thomas Telford Ltd, 2018.

[4] Olga Popovic Larsen. *Reciprocal frame architecture*. Routledge, 2007.

[5] PVs plus Timber: The Earth Centre's Solar Canopy. https://www.fourthdoor.org/annular/archive/323-annular-archive-pvs-plus-timber/. (Accessed: 2026-03-05).

[6] Aurimas Bukauskas, Paul Mayencourt, Paul Shepherd, Bhavna Sharma, Caitlin Mueller, Pete Walker, and Julie Bregulla. Whole timber construction: A state of the art review. *Construction and Building Materials*, 213:748–769, 2019.

[7] Ron Wolfe. Research challenges for structural use of small-diameter round timbers. *Forest Products Journal*, 50(2):21–29, 2000.

[8] E George Stern. Construction with small-diameter wood. *Forest products journal*, 51(4), 2001.

[9] PJ Verkerk, M Hassegawa, J Van Brusselen, M Cramm, X Chen, Y Imparato Maximo, M Koç, et al. *Forest products in the global bioeconomy: Enabling substitution by wood-based products and contributing to the Sustainable Development Goals*. Food & Agriculture Org., 2021.

[10] FJ Ezquerra and LA Gil. Wood anatomy and stress distribution in the stem of *Pinus pinaster* ait. *Forest Systems*, 10(1):165–177, 2001.

[11] Debra Larson, Richard Mirth, and Ronald Wolfe. Evaluation of small-diameter ponderosa pine logs in bending. *Forest products journal. Vol. 54, no. 12 (Dec. 2004): Pages 52-58*, 2004.

[12] David William Green. *Mechanical Grading of 6-inch-diameter Lodgepole Pine Logs for the Traveler's Rest and Rattlesnake Creek Bridges*, volume 297. US Department of Agriculture, Forest Service, Forest Products Laboratory, 2005.

[13] Abel Vega, Laura González, Isabel Fernández, and Pablo González. Grading and mechanical characterization of small-diameter round chestnut (*Castanea sativa* mill.) timber from thinning operations. *Wood Material Science & Engineering*, 14(2):81–87, 2019.

[14] Xiping Wang, Robert J Ross, Michael McClellan, R James Barbour, John R Erickson, John W Forsman, and Gary D McGinnis. Nondestructive evaluation of standing trees with a stress wave method. *Wood and fiber science*, pages 522–533, 2001.

[15] Daniel F Llana, Ian Short, and Annette M Harte. Use of non-destructive test methods on irish hardwood standing trees and small-diameter round timber for prediction of mechanical properties. *Annals of forest science*, 77:1–13, 2020.

[16] Karlo Simic, Vilius Gendvilas, Conor O'Reilly, and Annette M Harte. Predicting structural timber grade-determining properties using acoustic and density measurements on young sitka spruce trees and logs. *Holzforschung*, 73(2):139–149, 2019.

[17] Mohammad Derikvand, Nathan Kotlarewski, Michael Lee, Hui Jiao, and Gregory Nolan. Flexural and visual characteristics of fibre-managed plantation *Eucalyptus globulus* timber. *Wood Material Science & Engineering*, 2020.

[18] Standard published by European Committee for Standardisation (CEN). En 14251- Structural round timber - Test methods. Standard published by European Committee for Standardisation (CEN), 2003. EN 14251:2003.

[19] American Society for Testing and Materials (ASTM). Standard test methods of static tests of wood poles. ASTM. West Conshohocken, PA, USA, 2017. ASTM D1036-99.

[20] Everette D Rast, David L Sonderman, and Glenn L Gammon. A guide to hardwood log grading. *Gen. Tech. Rep. NE-1. Upper Darby, PA: US Department of Agriculture, Forest Service, Northeastern Forest Experiment Station. 32 p.*, 1, 1973.

[21] Eugene M Wengert and Dan A Meyer. Guidelines for grading hardwood logs. Technical report, Departament of Forest Ecology and Management, University of Wisconsin-Madison, 1994.

[22] E Macdonald, S Mochan, and T. Connolly. *Protocol for stem straightness assessment in Sitka spruce*, 2001.

[23] Hans Joachim Blaß and Carmen Sandhaas. *Timber engineering-principles for design*. KIT scientific publishing, 2017.

[24] Xiping Wang, Steve Verrill, Eini Lowell, Robert J Ross, and Vicki L Herian. Acoustic sorting models for improved log segregation. *Wood and Fiber Science, Volume 45, Number 4, 2013; pp 343–352*, 45(4):343–352, 2013.

[25] Alpo Ranta-Maunus et al. Round small-diameter timber for construction. *Final report of project FAIR CT*, pages 95–0091, 1999.

[26] Telmo FM Morgado, Alfredo MPG Dias, José S Machado, João H Negrão, and André FS Marques. Grading of portuguese maritime pine small-diameter roundwood. *Journal of Materials in Civil Engineering*, 29(2):04016209, 2017.

[27] Juan I Fernández-Golfín, MR Diez Barra, E Hermoso, and R Mier. Mechanical characterization of visually classified, small-diameter laricio pine round timber. *Spanish Journal of Agricultural Research*, 5(3):304–311, 2007.

[28] Laurence Schimleck, Joseph Dahlen, Luis A Apiolaza, Geoff Downes, Grant Emms, Robert Evans, John Moore, Luc Pâques, Jan Van den Bulcke, and Xiping Wang. Non-destructive evaluation techniques and what they tell us about wood property variation. *Forests*, 10(9):728, 2019.

[29] Xiping Wang, Robert J Ross, James A Mattson, John R Erickson, et al. Nondestructive evaluation techniques for assessing modulus of elasticity and stiffness of small-diameter logs. *Forest Products Journal*, 52(2):79, 2002.

[30] Alexander Opazo-Vega, Víctor Rosales-Garcés, and Claudio Oyarzo-Vera. Non-destructive assessment of the dynamic elasticity modulus of *Eucalyptus nitens* timber boards. *Materials*, 14(2):269, 2021.

[31] Frederico JN França, R Daniel Seale, Robert J Ross, Rubin Shmulsky, and Tâmara SF Amorim França. Using transverse vibration nondestructive testing techniques to estimate stiffness and strength of southern pine lumber. *Res. Paper FPL-RP-695. Madison, WI: US Department of Agriculture, Forest Service, Forest Products Laboratory. 8 p.*, 695, 2018.

[32] Daniel F Llana, Guillermo Íñiguez-González, M Rafael Díez, and Francisco Arriaga. Nondestructive testing used on timber in spain: A literature review. *Maderas. Ciencia y tecnología*, 22(2):133–156, 2020.

[33] Dulce Franco Henriques, Lina Nunes, José Saporiti Machado, and Jorge de Brito. Timber in buildings: Estimation of some properties using pilodyn and resistograph. In *Proceedings of the International Conference on Durability of Building Materials and Components, Porto, Portugal*, pages 12–15, 2011.

[34] Pengfei Xu, Zhang Houjiang, Xin Zhenbo, Liu Fenglu, Song Haiou, and Yuan Jiangyu. Determining ages of conifer trees with resistance microdrilling. *Canadian Journal of Forest Research*, 54(3):268–277, 2023.

[35] Beatrice Faggiano, Maria Rosaria Grippa, Anna Marzo, and Federico M Mazzolani. Experimental study for non-destructive mechanical evaluation of ancient chestnut timber. *Journal of Civil Structural Health Monitoring*, 1(3):103–112, 2011.

[36] Philipp Dietsch, Steffen Franke, Bettina Franke, Andreas Gamper, and Stefan Winter. Methods to determine wood moisture content and their applicability in monitoring concepts. *Journal of Civil Structural Health Monitoring*, 5(2):115–127, 2015.

[37] Mohammad Kherais, Anikó Csébfalvi, Adél Len, Attila Fülöp, and Judit Pál-Schreiner. The effect of moisture content on the mechanical properties of wood structure. *Pollack Periodica*, 19(1):41–46, 2024.

[38] MJ Montero, Jaime de La Mata, Miguel Esteban, and Eva Hermoso. Influence of moisture content on the wave velocity to estimate the mechanical properties of large cross-section pieces for structural use of scots pine from spain. *Maderas. Ciencia y tecnología*, 17(2):407–420, 2015.

[39] Richard Burton, Michael Dickson, and Richard Harris. The use of roundwood thinnings in buildings–a case study. *Building Research & Information*, 26(2):76–93, 1998.

[40] Niels Martin Larsen, Anders Kruse Aagaard, and Lynn Hyun Kieffer. Digital workflows for natural wood in constructions. In *Proceedings of the 25th International Conference of the Association for Computer-Aided Architectural Design Research in Asia (CAADRIA) 2020*, 2020.

[41] Pradeep Devadass, Farid Dailami, Zachary Mollica, and Martin Self. Robotic fabrication of non-standard material. In *ACADIA*, volume 2016, pages 206–213, 2016.

[42] Anders Kruse Aagaard and Niels Martin Larsen. Developing a fabrication workflow for irregular sawlogs. *International Journal of Architectural Computing*, 18(3):270–283, 2020.

[43] Hua Chai, Xinjie Zhou, Xiaofan Gao, Qinhui Yang, Yanmin Zhou, and Philip F Yuan. Integrated workflow for cooperative robotic fabrication of natural tree fork structures. *Automation in Construction*, 165:105524, 2024.

[44] John R Moore and Dave J Cown. Corewood (juvenile wood) and its impact on wood utilisation. *Current Forestry Reports*, 3:107–118, 2017.

[45] Forest Service United States Department of Agriculture. *Wood Handbook. Wood as an Engineering Material*. Forest Products Laboratory, Madison, Wisconsin, 2010.

[46] Graham Barnard. *Engineering with small roundwood-Its mechanical and physical characteristics*. University of Surrey (United Kingdom), 2001.

[47] Mark L. Batchelar. Innovative use of timber rounds in high-performance structure. In *World Conference on Timber Engineering 2012*, volume Session 45, Design 15, page 557. Auckland New Zealand, 2012.

[48] JH Park, Y Park, Y Han, JW Choi, IG Choi, JJ Lee, and H Yeo. Effect of outer surface sealing treatment on the reduction of surface check occurrence during the drying of center-bored round timber. *Drying technology*, 32(2):236–243, 2014.

[49] Hwanmyeong Yeo, Chang-Deuk Eom, William B Smith, Kug-Bo Shim, Yeonjung Han, Jung-Hwan Park, Do-Sik Lee, Hyoung-Woo Lee, Moon Jae Park, Joo-Saeng Park, et al. Effects of center boring and kerf treatment on kiln-drying of larch square and round timbers. *Forest products journal*, 57(11), 2007.

[50] Jinah Lim, Jung-Kwon Oh, Hwanmyeong Yeo, and Jun-Jae Lee. Behavior of center-bored round timber beams in center-point bending test. *Journal of wood science*, 59:389–395, 2013.

[51] Philip D Evans, Robin Wingate-Hill, and Simon C Barry. Effects of different kerfing and center-boring treatments on the checking of acq treated pine posts exposed to the weather. *Forest products journal*, 50(2), 2000.

[52] Pieter Huybers. Timber pole space frames. *International Journal of Space Structures*, 2(2):77–86, 1987.

[53] ICNF. 6° inventário florestal nacional (ifn6) - 2015 relatório final. Technical report, ICNF, 2015.

[54] Konrad Merz, Anne Niemann, and Stefan Torno. *Building with Hardwood*. Detail, 2021.

[55] Carlos Martins, Sandra Monteiro, Sofia Knapic, and Alfredo Dias. Assessment of bending properties of sawn and glulam blackwood in Portugal. *Forests*, 11(4):418, 2020.

[56] Juan Carlos Pinilla Suárez, V Vásquez, C Hernández, Karina Luengo Vergara, P Campos, M Elgueta, L Catalán, T Navarrete, et al. Tensiones admisibles de la madera aserrada de aromo (*Acacia dealbata* d. link.) clasificada visualmente. Technical report, Instituto Forestal, INFOR, 2019.

[57] Wolfgang Nentwig, Sven Bacher, Sabrina Kumschick, Petr Pyšek, and Montserrat Vilà. More than "100 worst" alien species in Europe. *Biological Invasions*, 20(6):1611–1621, 2018.

[58] Manuel Miranda Fernandes. Acácias errantes, acácias infestantes: Notas sobre a ascensão e queda de uma utopia florida. *Lucanus II*, pages 180–191, 2018.

[59] Pablo Souza-Alonso, Jonatan Rodríguez, Luís González, and Paula Lorenzo. Here to stay. recent advances and perspectives about acacia invasion in mediterranean areas. *Annals of Forest Science*, 74:1–20, 2017.

[60] M Raposo, CJP Gomes, and LJR Nunes. Evaluation of species invasiveness: A case study with *Acacia dealbata* link. on the slopes of cabeça (seia-portugal). sustainability 2021, 13, 11233. htps. *doi. org/10.3390/su132011233*, 2021.

[61] Fabián Guerrero, Carla Hernández, Mario Toledo, Lorena Espinoza, Yulian Carrasco, Andrés Arriagada, Ariel Muñoz, Lautaro Taborga, Jan Bergmann, and Camilo Carmona. Leaf thermal and chemical properties as natural drivers of plant flammability of native and exotic tree species of the Valparaíso region, Chile. *International journal of environmental research and public health*, 18(13):7191, 2021.

[62] Paula Lorenzo, Luís González, and Manuel J Reigosa. The genus acacia as invader: the characteristic case of *Acacia dealbata* link in Europe. *Annals of Forest Science*, 67(1):101, 2010.

[63] Marta Correia, Sílvia Castro, Victoria Ferrero, João A Crisóstomo, and Susana Rodríguez-Echeverría. Reproductive biology and success of invasive australian acacias in Portugal. *Botanical Journal of the Linnean Society*, 174(4):574–588, 2014.

[64] Paula Lorenzo and Maria Cristina Morais. Strategies for the management of aggressive invasive plant species. *Plants*, 12(13):2482, 2023.

[65] Miika Laitinen, Hüseyin Emre Ilgın, Markku Karjalainen, and Arto Saari. Low-carbon emissions and cost of frame structures for wooden and concrete apartment buildings: Case study from finland. *Buildings*, 14(5):1194, 2024.

[66] Mahboobeh Hemmati, Tahar Messadi, Hongmei Gu, Jacob Seddelmeyer, and Moein Hemmati. Comparison of embodied carbon footprint of a mass timber building structure with a steel equivalent. *Buildings*, 14(5):1276, 2024.

[67] Forest map of Europe. https://www.eea.europa.eu/en/analysis/maps-and-charts/forest-map-of-europe-1, 2001. (Accessed: 2026-03-05).

[68] FAO. Terms and definitions. Technical report, FOOD AND AGRICULTURE ORGANIZATION OF THE UNITED NATIONS, 2018.

[69] R Sathre and S González-García. Life cycle assessment (lca) of wood-based building materials. In *Eco-efficient construction and building materials*, pages 311–337. Elsevier, 2014.

[70] Francesco Maria Sabatini, Hendrik Bluhm, Zoltan Kun, Dmitry Aksenov, José A Atauri, Erik Buchwald, Sabina Burrascano, Eugénie Cateau, Abdulla Diku, Inês Marques Duarte, et al. European primary forest database v2. 0. *Scientific data*, 8(1):220, 2021.

[71] F. Droppelmann, H. Grosse, and A. Laroze. Contribución de los bosques nativos y plantados a la mitigación de los impactos del cambio climático en Chile en un contexto de desarrollo sustentable. *Ciencia & Investigación Forestal*, pages 7–36, 2019.

[72] Kamalakanta Sahoo, Richard Bergman, Sevda Alanya-Rosenbaum, Hongmei Gu, and Shaobo Liang. Life cycle assessment of forest-based products: A review. *Sustainability*, 11(17):4722, 2019.

[73] Susan L LeVan-Green and Jean M Livingston. Uses for small-diameter and low-value forest thinnings. *Ecological Restoration*, 21(1):34–38, 2003.

[74] Moonil Kim, Woo-Kyun Lee, Yoo-Seoung Kim, Chul-Hee Lim, Cholho Song, Taejin Park, Yowhan Son, and Yeong-Mo Son. Impact of thinning intensity on the diameter and height growth of *Larix kaempferi* stands in central korea. *Forest science and technology*, 12(2):77–87, 2016.

[75] Jonathan Vallejos, Roger Moya, and Rafael Serrano. Effects of thinning on diameter, heartwood, density and drying defects of *Gmelina arborea*. *Maderas. Ciencia y tecnología*, 17(2):365–372, 2015.

[76] Andrew David Cameron. Importance of early selective thinning in the development of long-term stand stability and improved log quality: a review. *Forestry*, 75(1):25–35, 2002.

[77] Hangfeng Qu, Xibin Dong, Hui Liu, Baoshan Zhang, Tong Gao, Yuan Meng, Yunze Ren, and Ying Zhang. Effect of thinning intensity on the carbon sequestration of natural mixed coniferous and broadleaf forests in Xiaoxing'an Mountains, China. *Journal of Forestry Research*, 35(1):115, 2024.

[78] Julia A Sohn, Somidh Saha, and Jürgen Bauhus. Potential of forest thinning to mitigate drought stress: A meta-analysis. *Forest Ecology and Management*, 380:261–273, 2016.

[79] Leonel JR Nunes, Catarina IR Meireles, Carlos J Pinto Gomes, and Nuno MC Almeida Ribeiro. *Acacia dealbata* link. aboveground biomass assessment: sustainability of control and eradication actions to reduce rural fires risk. *Fire*, 5(1):7, 2022.

[80] David C Le Maitre, Mirijam Gaertner, Elizabete Marchante, Emilie-Jane Ens, Patricia M Holmes, Aníbal Pauchard, Patrick J O'Farrell, Andrew M Rogers, Ryan Blanchard, James Blignaut, et al. Impacts of invasive australian acacias: implications for management and restoration. *Diversity and Distributions*, 17(5):1015–1029, 2011.

[81] Cristina Vieites-Blanco and Serafín J González-Prieto. Invasiveness, ecological impacts and control of acacias in southwestern europe–a review. *Web Ecology*, 20(2):33–51, 2020.

[82] E. Muçat. Impact of forest fires on the trees and wood quality—a case study for a beech stand. *fire*, 7(9), 2024.

[83] G Bortoletto and C. Moreschi. Physical–mechanical properties and chemical composition of pinus taeda mature wood following a forest fire. *Bioresource technology*, 87(3):231–238, 2003.

[84] JM Linton, HM Barnes, RD Seale, PD Jones, EC Lowell, and SS Hummel. Suitability of live and fire-killed small-diameter ponderosa and lodgepole pine trees for manufacturing a new structural wood composite. *Bioresource technology*, 101(15):6242–6247, 2010.

[85] G. Rojas, J. Vergara, F. Navarrete, and M. Nuñez-Decap. Caracterización de madera aserrada proveniente de árboles siniestrados de *Pinus radiata* d.don. In *III Congreso Ibero-Latinoamericano de La Madera en la Construcción*, 2024.

[86] Mehmet Akgül, Nadir Ayrilmis, Osman Çamlıbel, and Süleyman Korkut. Potential utilization of burned wood in manufacture of medium density fiberboard. *Journal of Material Cycles and Waste Management*, 15:195–201, 2013.

[87] Laura Moya, Jerrold E Winandy, William TY Tze, and Shri Ramaswamy. Use of fire-impacted trees for oriented strandboards. *Forest products journal*, 58(6):45, 2008.

[88] Eva Hermoso Prieto, Juan I Fernández-Golfín Seco, M Rafael Díez Barra, and Rafael Mier Pérez. Aplicación de los ultrasonidos a la evaluación de las propiedades mecánicas de la madera en rollo de pequeño diámetro. *Informes de la Construcción*, 59(506):87–95, 2007.

[89] Ian D Underhill, Benoit P Gilbert, Henri Bailleres, Robbie L McGavin, and Dale Patterson. Structural veneer based composite products from hardwood thinning–part i: Background and manufacturing. In *Materials and Joints in Timber Structures: Recent Developments of Technology*, pages 577–588. Springer, 2014.

[90] Antonio JA Santos, Ofelia MS Anjos, and Rogerio MS Simoes. Papermaking potential of *Acacia dealbata* and *Acacia melanoxylon*. *Appita: Technology, Innovation, Manufacturing, Environment*, 59(1):58–64, 2006.

[91] Leonel JR Nunes, Mauro AM Raposo, Catarina IR Meireles, Carlos J Pinto Gomes, and Nuno MC Almeida Ribeiro. Control of invasive forest species through the creation of a value chain: *Acacia dealbata* biomass recovery. *Environments*, 7(5):39, 2020.

[92] Leonel JR Nunes, Abel M Rodrigues, Liliana MEF Loureiro, Letícia CR Sá, and João CO Matias. Energy recovery from invasive species: Creation of value chains to promote control and eradication. *Recycling*, 6(1):21, 2021.

[93] Rubén A Ananías, Linette Salvo, Ricardo Estrada, and Rodrigo Briones. Estudio experimental del secado a temperaturas convencionales de acacias. *Maderas. Ciencia y tecnología*, 10(2):151–162, 2008.

[94] Susan L LeVan-Green and Jean Livingston. Exploring the uses for small-diameter trees. *Forest products journal*, 51(9):10–21, 2001.

[95] Roland Hernandez, David W Green, David E Kretschmann, and Steven P Verrill. Improved utilization of small-diameter ponderosa pine in glued-laminated timber. Technical report, US Department of Agriculture, Forest Service, Forest Products Laboratory, 2005.

[96] Yuchao Liao, Dengyun Tu, Jianhui Zhou, Haibin Zhou, Hong Yun, Jin Gu, and Chuanshuang Hu. Feasibility of manufacturing cross-laminated timber using fast-grown small diameter eucalyptus lumbers. *Construction and Building Materials*, 132:508–515, 2017.

[97] John Rusty Dramm. Small-diameter utilization issues and opportunities. In *Conference proceedings: Wood Technology Clinic & Show... Portland, Oregon, USA, March 24-26, 1999.[San Francisco]: Wood Technology,[1999?]: pages 30-38.*, 1999.

[98] Justin Dewey, Rabin Tuladhar, and Nagaratnam Sivakugan. Review of design methods for round notched timber sections subjected to flexure and shear. *Journal of Building Engineering*, 18:130–141, 2018.

[99] Ronald Wolfe and Cassandra Moseley. Small-diameter log evaluation for value-added structural applications. *Forest Products Journal*, 2000.

[100] Mauro Bernabei, Nicola Macchioni, Benedetto Pizzo, Lorena Sozzi, Simona Lazzeri, Luigi Fiorentino, Elisa Pecoraro, Gianluca Quarta, and Lucio Calcagnile. The wooden foundations of rialto bridge (ponte di rialto) in venice: Technological characterisation and dating. *Journal of Cultural Heritage*, 36:85–93, 2019.

[101] A. Numata, T. Murata, and T. Hara. Ground stabilization using wood to minimize liquefaction damage and mitigate climate change. In *World Conference on Timber Engineering 2021*, 2021.

[102] G. Wu, E. Zhu, Y Zhong, and H Ren. Development and investigation of a hybrid built-up column made of small diameter logs originating from juvenile trees. *Journal of Wood Science*, 64(4):356–363, 2018.

[103] GF Wu, EC Zhu, HJ Zhou, and JL Pan. Testing and modelling of shearwalls studded with small-diameter round timber under cyclic lateral load. *Construction and Building Materials*, 77:288–296, 2015.

[104] Thomas Gorman, Brad Miller, and DE Kretschmann. Wood i beams manufactured from small diameter logs. In *Proceedings of World Conference on Timber Engineering (WCTE 2016). August*, pages 22–25, 2016.

[105] Susana Gómez-González, Fernando Ojeda, and Paulo M Fernandes. Portugal and chile: Longing for sustainable forestry while rising from the ashes. *Environmental Science & Policy*, 81:104–107, 2018.

[106] Roundwood NZ. https://www.permapine.co.nz/, 2022. (Accessed: 2026-03-05).

[107] P. Devadass, F. Dailami, Z. Mollica, and M. Self. Robotic fabrication of non-standard material. In *ACADIA 2016: Posthuman Frontiers: Data, Designers, and Cognitive Machines - Proceedings of the 36th Annual Conference of the Association for Computer Aided Design in Architecture*, 2016.

[108] Zachary Mollica and Martin Self. Tree fork truss. *Advances in architectural geometry*, 2016:138–153, 2016.

[109] Martin Steinmetz, Pierre Latteur, and Luca Sgambi. Optimal log floor patterns. *Engineering Structures*, 297:116970, 2023.

[110] George Fereday, Nick Meech, Guy Nevill, Dougal Driver, and Harri Lewis. Coppiced sweet chestnut in uk construction–challenges and opportunities for design development of hardwood building products. *International Wood Products Journal*, 14(2):87–93, 2023.

[111] Amelia Baxter. The future of structural round timber, 2020. https://www.structuremag.org/article/the-future-of-structural-round-timber/.

[112] N González-Muñoz, M Costa-Tenorio, and T Espigares. Invasion of alien *Acacia dealbata* on spanish quercus robur forests: impact on soils and vegetation. *Forest Ecology and Management*, 269:214–221, 2012.

[113] Antonio Vazquez de la Cueva. Case studies of the expansion of *Acacia dealbata* in the valley of the river miño (galicia, spain). *Forest systems*, 23(1):3–14, 2014.

[114] Antonio T Monteiro, João Gonçalves, Rui F Fernandes, Susana Alves, Bruno Marcos, Richard Lucas, Ana Claúdia Teodoro, and João P Honrado. Estimating invasion success by non-native trees in a national park combining worldview-2 very high resolution satellite data and species distribution models. *Diversity*, 9(1):6, 2017.

[115] Elisabeth Pötzelsberger, Heinrich Spiecker, Charalambos Neophytou, Frits Mohren, Anna Gazda, and Hubert Hasenauer. Growing non-native trees in european forests brings benefits and opportunities but also has its risks and limits. *Current Forestry Reports*, 6(4):339–353, 2020.

[116] Maria Conceição Colaço, Ana Catarina Sequeira, and Iryna Skulska. Genus acacia in mainland portugal: Knowledge and experience of stakeholders in their management. *Land*, 12(11):2026, 2023.

[117] Jonatan Rodríguez, Paula Lorenzo, and Luís González. Different growth strategies to invade undisturbed plant communities by *Acacia dealbata* link. *Forest Ecology and Management*, 399:47–53, 2017.

[118] Parlamento Europeo. Regulation (eu) no 1143/2014 of the european parliament and of the council of 22 october 2014 on the prevention and management of the introduction and spread of invasive alien species. Official Journal of the European Union, 2014. Document 32014R1143.

[119] Ambiente e Transição Energética. Decreto-lei n.º 92/2019, de 10 de julho. Presidência do Conselho de Ministros, 2019. Decree-Law N°92/2019.

[120] Alimentación y Medio Ambiente Ministerio de Agricultura. Real decreto 630/2013, de 2 de agosto, por el que se regula el catálogo español de especies exóticas invasoras. BOE, 2013. BOE-A-2013-8565.

[121] ICNF. Portugal market report 2023. Technical report, ICNF, 2023.

[122] INE. Contas económicas da silvicultura 2022. Technical report, INE, 2024.

[123] Parque Nacional Peneda-Gerês. https://riominho.org/pt-pt/ruta-espazo/parque-nacional-peneda-geres. (Accessed: 2026-03-05).

[124] Christopher G Bousfield, Oscar Morton, and David P Edwards. Climate change will exacerbate land conflict between agriculture and timber production. *Nature Climate Change*, pages 1–7, 2024.

[125] Narciso Aguilera, Jose Becerra, Lubia M Guedes, Cristobal Villasenor-Parada, Luis Gonzalez, and Victor Hernandez. Allelopathic effect of the invasive *Acacia dealbata* link (fabaceae) on two native plant species in south-central chile. *Gayana Botánica*, 72(2):231–239, 2015.

[126] Paula Lorenzo, Jonatan Reboredo-Durán, Luís Muñoz, Helena Freitas, and Luís González. Herbicidal properties of the commercial formulation of methyl cinnamate, a natural compound in the invasive silver wattle (*Acacia dealbata*). *Weed Science*, 68(1):69–78, 2020.

[127] Paagiotis Kanatas. Potential role of *Eucalyptus spp.* and *Acacia spp.* allelochemicals in weed management. *Chilean journal of agricultural research*, 80(3):452–458, 2020.

[128] T Uushona, OC Chikwanha, T Tayengwa, CLF Katiyatiya, PE Strydom, and C Mapiye. Nutraceutical and preservative potential of *Acacia mearnsii* and *Acacia dealbata* leaves for ruminant production and product quality enhancement. *The Journal of Agricultural Science*, 159(9-10):743–756, 2021.

[129] Ricardo Correia, Maria Paula Duarte, Elisabete Muchagato Maurício, João Brinco, José Carlos Quintela, Marco Gomes da Silva, and Margarida Gonçalves. Chemical and functional characterization of extracts from leaves and twigs of *Acacia dealbata*. *Processes*, 10(11):2429, 2022.

[130] Teresa Linhares and Maria Teresa Pessoa de Amorim. Lca of textile dyeing with *Acacia dealbata* tree bark: a case study research. *Procedia engineering*, 200:365–369, 2017.

[131] Alessandra Ranesi, Paulina Faria, Maria Teresa Freire, Margarida Gonçalves, and M Rosário Veiga. Eco-efficient plastering mortars for improved indoor comfort- the influence of *Acacia dealbata* bark addition. *Construction and Building Materials*, 421:135572, 2024.

[132] Telmo FM Morgado, Alfredo MPG Dias, José S Machado, and João H Negrão. Structural connections for small-diameter poles. *Journal of Structural Engineering*, 139(11):2003–2009, 2013.

[133] T Morgado, AMPG Dias, J Saporiti Machado, and J Negrão. Simpole-simulation of wood poles mechanical behaviour. *BioResources*, 7(3), 2012.

[134] André Luiz Zangiácomo, André Luis Christoforo, and Francisco Antonio Rocco Lahr. Módulo de elasticidade aparente em vigas roliças estruturais de madeira pinus elliottii. *Ambiente Construído*, 14:7–13, 2014.

[135] André Luiz Zangiácomo. *Estudo de elementos estruturais roliços de madeira*. PhD thesis, Universidade de Sao Paulo, 2007.

[136] Nicolas Hofmann, Franka Brüchert, Udo H. Sauter, Kay-Uwe Schober, Beate Hörnel-Metzger, and Maximilian L Müller. Green oak building with high-tech methods, part 1: Characterisation of the raw material. In *World Conference on Timber Engineering (WCTE 2023)*, pages 711–716, 2023.

[137] Kay-Uwe Schober, Beate Hörnel-Metzger, Maximilian Leonhard Müller, Nicolas Hofmann, Franka Brüchert, and Udo H Sauter. Green oak building with high-tech methods, part 2: log bending tests for determination of strength and stiffness. In *Proceedings of the 17th World Conference on Timber Engineering (WCTE 2023), Oslo, Norway*, pages 19–22, 2023.

[138] Martin Huber, Franka Brüchert, Nicolas Hofmann, Kay-Uwe Schober, Beate Hörnel-Metzger, Maximilian Müller, and Udo H Sauter. Green oak building – small diameter logs for construction. In *11th Hardwood conference proceedings*, 2024.

[139] Reinhard Brandner. Properties of axially loaded self-tapping screws with focus on application in hardwood. *Wood Material Science & Engineering*, 14(5):254–268, 2019.

[140] John M Dinwoodie. *Timber: its nature and behaviour*. CRC Press, 2000.

[141] Andrés Fuentes-Ramírez, Aníbal Pauchard, Lohengrin A Cavieres, and Rafael A García. Survival and growth of *Acacia dealbata* vs. native trees across an invasion front in south-central chile. *Forest Ecology and Management*, 261(6):1003–1009, 2011.

[142] Marcos S Karlin and Ulf O Karlin. Ecology of acacieae. *Acacia: Characteristics, Distribution and Uses*, pages 27–81, 2018.

[143] Nigel WM Warwick, Luke Hailey, Kerri L Clarke, and Peter E Gasson. Climate trends in the wood anatomy of acacia sensu stricto (leguminosae: Mimosoideae). *Annals of botany*, 119(8):1249–1266, 2017.

[144] Heidi Hirsch, David M Richardson, Aníbal Pauchard, and Johannes J Le Roux. Genetic analyses reveal complex introduction histories for the invasive tree *Acacia dealbata* link around the world. *Diversity and Distributions*, 27(2):360–376, 2021.

[145] Claudia Giuliani, M Giovanetti, Bruno Foggi, and M Mariotti Lippi. Two alien invasive acacias in italy: differences and similarities in their flowering and insect visitors. *Plant Biosystems-An International Journal Dealing with all Aspects of Plant Biology*, 150(2):285–294, 2016.

[146] Luigi Minuto, Gabriele Casazza, Davide Dagnino, Maria Guerrina, Carmelo Nicodemo Macrì, Elena Zappa, and Mauro Giorgio Mariotti. Reproductive traits of the invasive species *Acacia dealbata* link. in the northern mediterranean basin. *Annali di Botanica*, 10:13–20, 2020.

[147] José Newton Cardoso Marchiori. Anatomia da madeira de *Acacia dealbata* link. *Balduinia*, 18:26–32, 2011.

[148] CABI Digital Library. https://www.cabidigitallibrary.org/. (Accessed: 2026-03-05).

[149] *Acacia dealbata*. https://es.wikipedia.org/wiki/Acacia-dealbata. (Accessed: 2026-03-05).

[150] Karlo Simic, VILIUS GENDVILAS, CONOR O'REILLY, Maarten Nieuwenhuis, and Annette M Harte. The influence of planting density on modulus of elasticity of structural timber from irish-grown sitka spruce. *International Journal of Design & Nature and Ecodynamics*, 12(4):438–447, 2018.

[151] Andreas Rais, Andriy Kovryga, Martin Bacher, Hans Pretzsch, and Jan-Willem van de Kuilen. Timber strength variation due to establishment density—can grading cope with it? *Forestry: An International Journal of Forest Research*, 95(5):647–658, 2022.

[152] Andreas Rais, Werner Poschenrieder, Hans Pretzsch, and Jan-Willem G van de Kuilen. Influence of initial plant density on sawn timber properties for douglas-fir (*Pseudotsuga menziesii* (mirb.) franco). *Annals of Forest Science*, 71(5):617–626, 2014.

[153] Bárbara Langdon, Aníbal Pauchard, and Ramiro O Bustamante. *Acacia dealbata* invasion in chile: Surprises from climatic niche and species distribution models. *Ecology and evolution*, 9(13):7562–7573, 2019.

[154] Carolin Fischer, Geir I Vestøl, Audun Øvrum, and Olav A Høibø. Pre-sorting of norway spruce structural timber using acoustic measurements combined with site-, tree-and log characteristics. *European Journal of Wood and Wood Products*, 73(6):819–828, 2015.

[155] Ron Wolfe and Joe Murphy. Strength of small-diameter round and tapered bending members. *Forest products journal. Vol. 53, no. 3 (Mar. 2005): Pages 50-55*, 2005.

[156] A. G Glukhikh, V. N.and Chernykh. Reasoning of tree cross sections oval shaping while growing with an inclination. *Lesnoy Zhurnal (Forestry Journal)*, 0(5 (377)):166–175, 2020.

[157] Mississippi State University Extension. *Grading Hardwood Trees: A Guide to Identifying Stem Quality in Hardwood Stands*, 2021.

[158] Joseph Gril, Delphine Jullien, Sandrine Bardet, and Hiroyuki Yamamoto. Tree growth stress and related problems. *Journal of Wood Science*, 63:411–432, 2017.

[159] Francisco Arriaga, Xiping Wang, Guillermo Íñiguez-González, Daniel F Llana, Miguel Esteban, and Peter Niemz. Mechanical properties of wood: A review. *Forests*, 14(6):1202, 2023.

[160] Khaled Saad and András Lengyel. A parametric investigation of the influence of knots on the flexural behavior of timber beams. *Periodica Polytechnica Civil Engineering*, 67(1):261–271, 2023.

[161] Jean Luc Sandoz. Form and treatment effects on conical roundwood tested in bending. *Wood Science and Technology*, 25(3):203–214, 1991.

[162] Forest Service U.S.Department of Agriculture. *Wood handbook—Wood as an engineering material. General Technical Report FPL-GTR-190*. Forest Products Laboratory, 2010.

[163] Edward J Angus. *Robust CT scanning of logs with feature-tailored voxels*. PhD thesis, University of British Columbia, 2015.

[164] American Society for Testing and Materials. Standard test methods for density and specific gravity (relative density) of wood and wood-based materials. Standard published by American Society for Testing and Materials (ASTM), 2018. D2395-17.

[165] Evgenii Sharapov, Aleksandr Korolev, and Yury Demakov. The effect of temperature and moisture content on drilling resistance measurements in wood (*Pinus sylvestris* l.). *Wood Material Science & Engineering*, pages 1–7, 2024.

[166] Hirofumi Ido, Hirofumi Nagao, Hideo Kato, and Sachiko Miura. Strength properties and effect of moisture content on the bending and compressive strength parallel to the grain of sugi (*Cryptomeria japonica*) round timber. *Journal of wood science*, 59(1):67–72, 2013.

[167] International Organization for Standardization. Wood - determination of moisture content for physical and mechanical tests. Standard published by International Organization for Standardization, 1975. ISO 3130-1975.

[168] Ester Garcia-Castillo, Thomas Gernay, and Ignacio Paya-Zaforteza. Probabilistic models for temperature-dependent compressive and tensile strengths of timber. *Journal of Structural Engineering*, 149(2):04022239, 2023.

[169] Miguel Esteban, Francisco Arriaga, Guillermo Íñiguez, Ignacio Bobadilla, and Raquel Mateo. The effect of fissures on the strength of structural timber. *Materiales de Construcción*, 60(299):115–132, 2010.

[170] Elke Mergny, Raquel Mateo, Miguel Esteban, Thierry Descamps, and Pierre Latteur. Influence of cracks on the stiffness of timber structural elements. In *Proceedings of the World conference on timber engineering, Vienna, Austria*, 2016.

[171] Baozhuang Zhang, Qifang Xie, and Jianyang Xue. Study on the flexural behavior evolution of timber beams with natural shrinkage cracks in historic timber structure. In *Structures*, volume 73, page 108429. Elsevier, 2025.

[172] CA Eckelman and JF Senft. Truss system for developing countries using small diameter roundwood and dowel nut construction. *Forest products journal*, 45(10):77, 1995.

[173] Tarick Chahade and Kay-Uwe Schober. Experimental investigations on the pull-out strength of steel rods bonded in douglas fir roundwood specimens with polymer concrete. *European Journal of Wood and Wood Products*, 81(2):439–450, 2023.

[174] Antonio Villasante, Alvaro Fernandez-Serrano, Lluis Puigdomenech, Jorge Lampurlanes, and David Moliner. Effect of a longitudinal cut on the mechanical properties of small-diameter roundwood of pinus nigra arnold. *BioResources*, 11(2):3587–3597, 2016.

[175] American Society for Testing and Materials (ASTM). Standard test methods of static tests of lumber in structural sizes. ASTM. West Conshohocken, PA, USA, 2022. ASTM D198-22.

[176] American Society for Testing and Materials. Standard methods of testing small clear specimens of timber. Standard published by American Society for Testing and Materials (ASTM), 1994. D143-94.

[177] American Society for Testing and Materials (ASTM). Standard practice for establishing allowable stresses for round timber piles. ASTM. West Conshohocken, PA, USA, 2017. ASTM D2899-12(2017).

[178] International Code Council. Standard on the design and construction of log structures. International Code Council, Inc., 2017. ICC 400-2017.

[179] American Wood Council. National design specification (nds) for wood construction. American National Standards INstitute & American Wood Council, 2018. 2018 NDS.

[180] Timber PIles and Poles Committee (P 3605). Timber structures standard, 1993. AS/NZS 1328.1:1998.

[181] Overhead line design, 2016. AS/NZS 7000:2016.

[182] Argüelles R. and Arriaga F. *Estructuras de Madera, diseño y calculo*. Aitim, 1996.

[183] Jorge Crespo, Almudena Majano-Majano, Antonio José Lara-Bocanegra, and Manuel Guaita. Mechanical properties of small clear specimens of *Eucalyptus globulus* labill. *Materials*, 13(4):906, 2020.

[184] Carlos Cunha, Marina Tenório, Daniel F Lima, Arthur Rebouças, Luís C Neves, and Jorge M Branco. Mechanical characterization of iroko wood using small specimens. *Buildings*, 11(3):116, 2021.

[185] Instituto chileno de normalización. Madera - determinación de las propiedades mecánicas - ensayo de flexión estática, 2018. NCh987:2018.

[186] Instituto chileno de normalización. Maderas - determinación de las propiedades mecánicas - ensayo de compresión paralela a la fibra, 2018. NCh973:2018.

[187] International Organization for Standardization. Physical and mechanical properties of wood — test methods for small clear wood specimens. Standard published by International Organization for Standardization, 2014. ISO 13061.

[188] Padilla-Reyes J., Catalán J., Campos R., Vásquez L., Reyes C., Hernández G., Mardones P., Elgueta P., Troncoso L., and Arriagada M. Mechanical characterization of visually graded sawn acacia lumber (*Acacia dealbata* link) grown in chile. In *World Conference on Timber Engineering 2020*. World Conference on Timber Engineering, 2020.

[189] Sofia Knapic Carlos Eduardo de Jesus Martins. Caracterização mecânica da madeira de acácia. Technical report, SerQ - Centro de Inovação e Competências da Floresta, Portugal, 2019.

[190] Manuel Suazo-Uribe, Alexander Opazo-Vega, Claudio Montero, Dante Marranzini, Beatrice Faggiano, José L Louzada, and Jorge M Branco. Preliminary study of *Acacia dealbata* logs for use in construction: Visual characterization and non-destructive testing. *Maderas. Ciencia y tecnología*, 27, 2025.

[191] Mavuto M Mukaka. A guide to appropriate use of correlation coefficient in medical research. *Malawi medical journal*, 24(3):69–71, 2012.

[192] Standard published by European Committee for Standardization (CEN). Structural timber - Determination of characteristic values of mechanical properties and density. Standard published by European Committee for Standardization (CEN), 2016+A1:2019. UNE EN 384:2016+A2:2022.

[193] Standard published by European Committee for Standardization (CEN). Timber structures - Structural timber and glued laminated timber - Determination of some physical and mechanical properties. Standard published by European Committee for Standardization (CEN), 2010. EN 408: 2011+A1:2012.

[194] Standard published by European Committee for Standardization (CEN). Timber structures - Calculation and verification of characteristic values. Standard published by European Committee for Standardization (CEN), 2016. EN 14358: 2016.

[195] September 2023 weather history in Guimarães, Portugal. https://weatherspark.com/h/m/32437/2023/9/Historical-Weather-in-September-2023-in-Guimar (Accessed: 2026-03-05).

[196] André L Christoforo, Túlio H Panzera, Fabiano B Batista, Paulo HR Borges, Francisco AR Lahr, and Claudenir F Franco. The position effect of structural eucalyptus round timber on the flexural modulus of elasticity. *Engenharia Agrícola*, 31:1219–1225, 2011.

[197] Robert J Ross. Wood handbook: wood as an engineering material. Technical report, Department of Agriculture, Forest Service, Forest Products Laboratory, Madison, WI: U.S., 2021.

[198] Standard published by European Committee for Standardization (CEN). Structural timber. Strength classess. Standard published by European Committee for Standardization (CEN), 2016. EN 338: 2016.

[199] Instituto Nacional de Normalización. Madera - determinación de las propiedades mecánicas - ensayos a flexión estática. Norma chilena oficial (NCh), 1986. NCh987.Of86.

[200] Instituto Nacional de Normalización. Madera - determinación de las propiedades mecánicas - ensayos de compresión paralela. Norma chilena oficial (NCh), 1986. NCh973.Of86.

[201] Vasiliki Dimou, Dimitrios N Kaziolas, Iordanis Zygomalas, and Nikolaos Avtzis. Influence of biotic factors on the mechanical properties of wood, taking into account the time of harvesting. *Wood Material Science & Engineering*, 12(3):140–148, 2017.

[202] Veikko Möttönen, Henrik Heräjärvi, Hannu Koivunen, and Jari Lindblad. Influence of felling season, drying method and within-tree location on the brinell hardness and equilibrium moisture content of wood from 27–35-year-old betula pendula. *Scandinavian Journal of Forest Research*, 19(3):241–249, 2004.

[203] Robert Jon Ross. *Stress wave timing nondestructive evaluation tools for inspecting historic structures: a guide for use and interpretation*, volume 119. US Department of Agriculture, Forest Service, Forest Products Laboratory, 2000.

[204] John R Moore, Andrew J Lyon, Gregory J Searles, Stefan A Lehneke, and Daniel J Ridley-Ellis. Within-and between-stand variation in selected properties of sitka spruce sawn timber in the uk: implications for segregation and grade recovery. *Annals of forest science*, 70(4):403–415, 2013.

[205] DF Llana, F Arriaga, M Esteban, and G Íñiguez-González. Comparison between wet and dry timber visual strength grading according to the spanish (une 56544) and german (din 4074-1) standards. *Materiales de construcción*, 69(336):e205–e205, 2019.

[206] Curt C Hassler, Jordan R Thompson, and Joseph F McNeel. Hardwood log grading in the united states—part iii: An assessment of the current status of log grading in the hardwood industry. *Forest Products Journal*, 71(2):133–143, 2021.

[207] Standard published by European Committee for Standardisation (CEN). En 1310:1997: Round and sawn timber - Method of measurement of features. Standard published by European Committee for Standardisation (CEN), 1997. EN 1310-1997.

[208] Standard published by European Committee for Standardisation (CEN). En 1927- 1: 2008 Qualitative classification of softwood round timbers - part 1: Spruces and firs. Standard published by European Committee for Standardisation (CEN), 2008. EN 1927-1:2008.

[209] Standard published by European Committee for Standardisation (CEN). En 1927- 2: 2008 Qualitative classification of softwood round timbers - part 2: Pines. Standard published by European Committee for Standardisation (CEN), 2008. EN 1927-2:2008.

[210] DIN 4074-1:2008-12: Strength grading of wood - Part 1: Coniferous sawn timber. Deutsches Institut für Normung, 2008. DIN 4074-1:2008.

[211] Geir I Vestøl and Olav Høibø. Bending strength and modulus of elasticity of pinus sylvestris round timber from southern norway. *Scandinavian Journal of Forest Research*, 25(2):185–195, 2010.

[212] Standard published by European Committee for Standardisation (CEN). prEN-2003: Timber structures - Strength graded structural timber with round cross-section - Requirements. Standard published by European Committee for Standardisation (CEN), 2003. prEN-2003.

[213] Instituto Português da Qualidade (IPQ). Madeira de pinheiro bravo para estruturas. IPQ, Lisbon, Portugal, 1995. NP4305.

[214] JR Aira, JL Villanueva, and E Lafuente. Visual and machine grading of small diameter machined round *Pinus sylvestris* and *Pinus nigra subsp. salzmannii* wood from mature spanish forests. *Materials and Structures*, 52(2):32, 2019.

[215] Szabolcs Koman, Sandor Feher, Jozsef Abraham, and Robert Taschner. Effect of knots on the bending strength and the modulus of elasticity of wood. *Wood Research*, 58(4):617–626, 2013.

[216] Carlos EJ Martins, AMPG Dias, André FS Marques, and André MA Dias. Non-destructive methodologies for assessment of the mechanical properties of new utility poles. *BioResources*, 12(2):2269–2283, 2017.

[217] Peter Hamner, Marshall White, and Philip Araman. The frequency and level of sweep in mixed hardwood saw logs in the eastern united states. *Forest Products Journal*, 57(9):23, 2007.

[218] Feng Xu, Xiping Wang, Ed Thomas, Yunfei Liu, Brian K Brashaw, and Robert J Ross. Defect detection and quality assessment of hardwood logs: Part 1—acoustic impact test and wavelet analysis. *Wood and Fiber Science. 50 (3): 291-309.*, 50(3):291–309, 2018.

[219] Guillermo Iñiguez Gonzalez. *Clasificación mediante técnicas no destructivas y evaluación de las propiedades mecánicas de la madera aserrada de coníferas de gran escuadría para uso estructural*. PhD thesis, Montes, 2007.

[220] Julian Moreno Chan, John C Walker, and Carolyn A Raymond. Effects of moisture content and temperature on acoustic velocity and dynamic moe of radiata pine sapwood boards. *Wood Science and Technology*, 45(4):609–626, 2011.

[221] Helene Unterwieser and Gerhard Schickhofer. Influence of moisture content of wood on sound velocity and dynamic moe of natural frequency-and ultrasonic runtime measurement. *European Journal of Wood and Wood Products*, 69(2):171–181, 2010.

[222] Llana D.F.and Iñiguez Gonzalez G.and Hermoso E.and Maynou V.and Arriaga F. Timber moisture content influence on non-destructive local measurements. In *WCTE 2016 - World Conference on Timber Engineering.*, 2016.

[223] Robert J Ross, Brian K Brashaw, John Punches, John R Erickson, John W Forsman, Roy F Pellerin, and Xiping Wang. Diameter effect on stress-wave evaluation of modulus of elasticity of logs. *Wood and fiber science*, pages 368–377, 2004.

[224] Cyriac S Mvolo, James D Stewart, and Ahmed Koubaa. Comparison between static modulus of elasticity, non-destructive testing moduli of elasticity and stress-wave speed in white spruce and lodgepole pine wood. *Wood Material Science & Engineering*, 17(5):345–355, 2022.

[225] D Larsson, S Ohlsson, M Perstorper, and J Brundin. Mechanical properties of sawn timber from norway spruce. *European Journal of Wood and Wood Products*, 56(5):331–338, 1998.

[226] Marcelo Rodrigo Carreira, Antonio Alves Dias, and Pedro Gutemberg de Alcântara Segundinho. Nondestructive evaluation of *corymbia citriodora* logs by means of the free transverse vibration test. *Journal of Nondestructive Evaluation*, 36(2):26, 2017.

[227] Brian K Brashaw. Sounding, probing, moisture content, and resistance drilling techniques. *Nondestructive Evaluation of Wood*, 100(300):59, 2015.

[228] Vilius Gendvilas, Geoffrey M Downes, Marco Lausberg, Jonathan J Harrington, and David J Lee. Predicting wood density using resistance drilling: The effect of varying feed speed and rpm. *Forests*, 15(4):579, 2024.

[229] Cristián Barría, Simón Sandoval, and Gerson Rojas. Uso del método de resistografía para la predicción de la densidad básica de la madera en árboles en pie de *Pinus radiata*. *Maderas. Ciencia y tecnología*, 19(3):349–362, 2017.

[230] Shan Gao, Xiping Wang, Michael C Wiemann, Brian K Brashaw, Robert J Ross, and Lihai Wang. A critical analysis of methods for rapid and nondestructive determination of wood density in standing trees. *Annals of Forest Science*, 74(2):27, 2017.

[231] Hélder S Sousa, Jorge M Branco, and Paulo B Lourenço. Characterization of cross-sections from old chestnut beams weakened by decay. *International journal of architectural heritage*, 8(3):436–451, 2014.

[232] Bilgin Guller, Adnan Guller, and Gökhan Kazaz. Is resistograph an appropriate tool for the annual ring measurement of *Pinus brutia*. *NDE for safety/Defektoskopie*, 2012:89–94, 2012.

[233] Jung OH, Jeong-Wook Seo, Byung-Ro Kim, et al. Determinate the number of growth rings using resistograph with tree-ring chronology to investigate ages of big old trees. *Journal of the Korean Wood Science and Technology*, 47(6):700–708, 2019.

[234] Jung-ae Oh, Jeong-Wook Seo, Byung-Ro Kim, et al. Verifying the possibility of investigating tree ages using resistograph. *Journal of the Korean Wood Science and Technology*, 47(1):90–100, 2019.

[235] Xiping Wang. Recent advances in nondestructive evaluation of wood: in-forest wood quality assessments. *Forests*, 12(7):949, 2021.

[236] Miguel Esteban Herrero, Francisco Arriaga Martitegui, Guillermo Íñiguez, Ignacio Bobadilla Maldonado, and Raquel Mateos Gil. Influencia de las fendas en la resistencia de la madera estructural. *Materiales de construcción*, 60(299):115–132, 2010.

[237] M Suazo-Uribe, L Salvo-Sepúlveda, V Rosales, C Montero, JL Louzada, and JM Branco. Assessing treatments to mitigate end-face cracking in air-dried *Acacia dealbata* logs. buildings 2024, 14, 2090, 2024.

[238] PD Evans. The effects of incising on the checking of wood: A review. *International Wood Products Journal*, 7(1):12–25, 2016.

[239] *Dry Kiln Operator's Manual*, 1991.

[240] NAS Gonya, Z Naghizadeh, and CB Wessels. An investigation into collapse and shrinkage behaviour of *Eucalyptus grandis* and *Eucalyptus grandis-urophylla* wood. *European Journal of Wood and Wood Products*, 80(1):139–157, 2022.

[241] Yi-Qiang Wu, Kazuo Hayashi, Yuan Liu, Yingchun Cai, and Masatoshi Sugimori. Relationships of anatomical characteristics versus shrinkage and collapse properties in plantation-grown eucalypt wood from china. *Journal of Wood Science*, 52:187–194, 2006.

[242] Qin Yin and Hong-Hai Liu. Drying stress and strain of wood: A review. *Applied Sciences*, 11(11):5023, 2021.

[243] Feng Xu, Yunfei Liu, Xiping Wang, Brian K Brashaw, Lon A Yeary, and Robert J Ross. Evaluating internal condition of hardwood logs based on ar-minimum entropy deconvolution combined with wavelet based spectral kurtosis approach. *Holzforschung*, 75(3):237–249, 2021.

[244] Carlos Rozas, Marcia Marcia, Patricia Vega, Arijit Sinha, and Claudio Montera. Investigating storage time to minimize end splitting in *Eucalyptus nitens* logs. *Wood and Fiber Science*, 55(3/4), 2023.

[245] Dian-Qing Yang and Dany Normand. Element 4: Hardwood initiative—development of new processes and technologies in the hardwood industry best practices to avoid hardwood checking part i. hardwood checking–the causes and prevention. *Transformative Technologies Program Project No. TT4. 3.03*, 201005167, 2012.

[246] Pamela Rebolledo, Linette Salvo, Helga Contreras, Alain Cloutier, and Rubén A Ananias. Variation of internal checks related to anatomical structure and density in *Eucalyptus nitens* wood. *Wood and Fiber Science*, pages 279–286, 2013.

[247] H Kang, W Lee, S Jang, and C Kang. Polyethylene glycol treatment of han-ok round wood components to prevent surface checking. *BioResources*, 12(2):4229–4238, 2017.

[248] Hiroki Sakagami, Junji Matsumura, and Kazuyuki Oda. In situ visualization of hardwood microcracks occurring during drying. *Journal of Wood Science*, 55:323–328, 2009.

[249] Karol Tomczak, Arkadiusz Tomczak, and Tomasz Jelonek. Effect of natural drying methods on moisture content and mass change of scots pine roundwood. *Forests*, 11(6):668, 2020.

[250] Rubén A Ananias, Sergio Vallejos, and Carlos Salinas. Estudio de la cinética del secado convencional y bajo vacío del pino radiata. *Maderas. Ciencia y tecnología*, 7(1):37–47, 2005.

[251] Manuel F Rocha-Sepúlveda, Mario Vega, Vilius Gendvilas, Dean Williams, Peter A Harrison, René E Vaillancourt, and Brad M Potts. R-based image analysis to quantify checking and shrinkage from wood wedges. *European Journal of Wood and Wood Products*, 79(5):1269–1281, 2021.

[252] Martin Wehrhausen, Norvin Laudon, Franka Brüchert, and Udo Hans Sauter. Crack detection in computer tomographic scans of softwood tree discs. *Forest Products Journal*, 62(6):434–442, 2012.

[253] Moutou Pitti Rostand, Frédéric Dubois, Nicolas Sauvat, and Eric Fournely. Strain analysis in dried green wood: Experimentation and modelling approaches. *Engineering Fracture Mechanics*, 105:182–199, 2013.

[254] Fu Zongying, Jingyao Zhao, Yangyi Lv, Siqi Huan, and Yingchun Cai. Stress characteristics and stress reversal mechanism of white birch (*Betula platyphylla*) disks under different drying conditions. *Maderas. Ciencia y tecnología*, 18(2):361–372, 2016.

[255] P Mugabi, T Rypstra, HF Vermaas, and DG Nel. Relationships between drying defect parameters and some growth characteristics in kiln-dried south african grown *Eucalyptus grandis* poles. *European Journal of Wood and Wood Products*, 68(3):329–340, 2010.

[256] Chang Jin Lee, Seung Won Oh, Nam Ho Lee, and Chun Won Kang. Effect of the knife-incising pretreatment on the surface checks occurrence of red pine heavy timber after drying. *European Journal of Wood and Wood Products*, 75:143–145, 2017.

[257] Terrance E Conners. *Producing and inspecting railroad crossties*. University of Kentucky, Cooperative Extension Service, 2008.

[258] André FS Marques, Carlos EJ Martins, AMPG Dias, Ricardo JT Costa, and Telmo FM Morgado. Assessment of reuse potential of maritime pine utility poles for structural applications after removal from service. *BioResources*, 11(4):9340–9349, 2016.

[259] Róger Moya and Carolina Tenorio. Reduction of growth stresses in logs of *Hieronyma alchorneoides* allemão from fast-growth plantations using steaming and heating: effects on the quality of lumber. *Annals of Forest Science*, 78(3):74, 2021.

[260] Masaya Nogi, Hiroyuki Yamamoto, and Takashi Okuyama. Relaxation mechanism of residual stress inside logs by heat treatment: choosing the heating time and temperature. *Journal of wood science*, 49:0022–0028, 2003.

[261] Nam-Ho Lee, Chengyuan Li, Xue-Feng Zhao, and Moon-Jae Park. Effect of pretreatment with high temperature and low humidity on drying time and prevention of checking during radio-frequency/vacuum drying of japanese cedar pillar. *Journal of Wood Science*, 56:19–24, 2010.

[262] William T Simpson and Xiping Wang. Estimating air-drying times of small-diameter ponderosa pine and douglas-fir logs. *Forest products journal. Vol. 54, no. 12 (Dec. 2004): Pages 24-28*, 2004.

[263] Rien Visser, Hamish Berkett, and Raffaele Spinelli. Determining the effect of storage conditions on the natural drying of radiata pine logs for energy use. *New Zealand Journal of Forestry Science*, 44:1–8, 2014.

[264] Kenneth Jenkye Cheng. *Reducing the surface checking of deck-boards exposed to natural weathering: effects of wood species and surface profiling*. PhD thesis, University of British Columbia, 2015.

[265] Sung Jun Pang, Jung Kwon Oh, Sang Joon Lee, Jun Ho Park, Sung Il Jang, and Jun Jae Lee. Surface checking reduction effect of preservative-treated korean larch round-woods with various physical treatments1. *Journal of the Korean Wood Science and Technology*, 45(1):107–115, 2017.

[266] Chung-Ho Kim, Chun-Won Kang, Seog-Goo Kang, and Ho-Yang Kang. Effect of pretreatments on reducing surface cracks of heat-treated western hemlock roundwoods. *Journal of the Korean Wood Science and Technology*, 40(5):343–351, 2012.

[267] Chang-Jin Lee et al. Effect of kerfing and incising pretreatments on high-temperature drying characteristics of cedar and larch boxed-heart timbers with less than 150 mm in cross section size. *Journal of the Korean Wood Science and Technology*, 48(3):345–363, 2020.

[268] Chang Jin Lee and C-D Eom. Effects of knife-incising and longitudinal kerfing pretreatments on high-temperature drying of red pine and pitch pine timbers. *BioResources*, 16(4):8184, 2021.

[269] Asghar Tarmian, Ismaeil Zahedi Tajrishi, Reza Oladi, and Davood Efhamisisi. Treatability of wood for pressure treatment processes: a literature review. *European Journal of Wood and Wood Products*, 78:635–660, 2020.